Cinder Cones of the Lyttelton Volcano

Banks Peninsula, New Zealand

A thesis

submitted in partial fulfilment

of the requirements for the degree

of

Master of Science in Geology

in the

University of Canterbury

by

ANDREW B. LIVERMORE

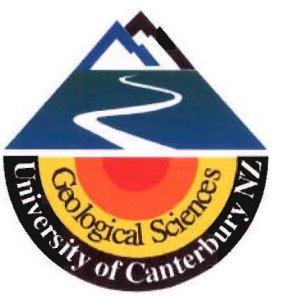

University of Canterbury

June 1999

FRONTISPIECE: Sunset over Lyttelton Harbour

ABSTRACT

Cinder cones are common on Banks Peninsula and this study concentrates on eleven sites situated on the Lyttelton Volcano. The study focuses on the structure, petrology and geochemistry of cinder cones and discusses their eruptive history.

Lyttelton volcanism began in the Miocene (10.8 Ma) with early (L1) activity centred near "Head of the Bay". Constant replenishment of the main chamber caused L1 lavas to be dominantly basaltic with limited differentiation. The development of a large cone resulted in distension which caused the development of horizontally fed radial dikes. Initial dike activity was low and lavas were dominantly fed from the central conduit with little flank activity. As L1 grew though, dikes became more common and so did cinder cone activity on the flanks. Cinder cones would have been fed by volatile rich magmas quickly reaching the surface via dikes and hence erupting explosively. The increase in dikes during L1 also caused the increasing development of more evolved magmas that fed lavas. Then during a quiescent period there was large-scale collapse of the eastern flank, followed by erosion and weathering of the L1 volcanic edifice during which activity shifted north-east to "Charteris Bay". Renewed (L2) activity after the quiescent period gave rise to more evolved lavas due to the large increase in dike activity, caused by the large amounts of stress acting on the edifice. Hence cinder cone activity on the flanks was also very common.

Cinder cone samples are dominated by phenocrysts of plagioclase, clinopyroxene, olivine and Ti-magnetite and show a wide range of mineral textures. This suggests that crystals have grown under a variety of temperatures and pressures and/or been derived from magmas of different compositions. Geochemically the cones are part of an alkaline basalt-hawaiite-mugearite-benmoreite-trachyte association.

The deposits in this study are all inferred to have formed by Strombolian and Hawaiian type eruptions due to their small dispersal areas. These eruptions formed cinder cones whose morphology depended on numerous factors, all of which contributed to their overall development. In this study the deposits have been classified into four facies based on welding, dip direction, block and bomb size, colour and the presence or absence of some clasts. The *Vent Facies* consists of densely welded grey/black fused spatter and represents vent and early formed products. Vesicularity is <20% with outcrops resembling massive lava; occasionally, however, dips towards the vent region can be found, establishing an origin within the vent. The *Proximal Facies* consists of >80% flattened clasts with deposits inferred to be welded due to their flattened nature. Spatter flows are common in the facies due to the rapid accumulation of spatter and its flowage. The *Medial Facies* consist of crudely bedded bomb, block and lapilli beds. Clasts are undeformed and non-welded. The *Distal Facies* consist of lapilli, ash, and crystals. Rare bombs occasionally occur and the deposits are generally well sorted and bedded. Overall, throughout each of the facies, clast size and welding decreases with increasing distance from the vent area.

TABLE OF CONTENTS

CHAPTER THREE – Petrology and Mineralogy

CHAPTER FOUR – Geochemistry

CHAPTER FIVE – Discussion and Interpretation

CHAPTER SIX – Conclusions

LIST OF FIGURES

CHAPTER ONE: Introduction

CHAPTER TWO: Site Descriptions

CHAPTER THREE: Petrology and Mineralogy

CHAPTER FOUR: Geochemistry

CHAPTER FIVE: Intrepretation and Discussion

CHAPTER SIX: Conclusions

LIST OF TABLES

CHAPTER ONE: Introduction

CHAPTER TWO: Site Descriptions

CHAPTER THREE: Petrology and Mineralogy

CHAPTER FIVE: Discussion and Interpretation

Chapter One

INTRODUCTION

"In examining the nature of the rocks of which the system under consideration is composed, we find with the exception of a small zone at the head of Lyttelton Harbour, the whole is composed of volcanic rocks; that the deep indentations are ancient crater walls, so-called calderas, into which a channel with precipitous walls, the barranco, leads; and that they consist of a series of lava-streams, with agglomerates consisting of scoriae, lapilli, ashes, and tufas interstratified with them." "The ashes, scoriae, and lapilli that were first thrown out formed agglomerate beds, then came streams of viscid basaltic lava pouring out and down the slopes of the remnant of the cone cooling in the ascent, or, as they flowed over the lip of the crater and passed over cold ground, converting the layer of soil or exposed agglomerate bed into laterite, a brick coloured rock."

Sir Julius von Haast describes the features of the Lyttelton Volcano in 1879.

1.1 PURPOSE AND SCOPE OF STUDY

"Little detailed attention has hitherto been paid to the pyroclastic deposits of Lyttelton Volcano. Nevertheless, thick deposits of scoriaceous material are very common, and probably represent cones built along radial fissures caused by radial dike activity" (Shelley 1992). The aim of this study is therefore to better understand the distribution of cinder cones on Lyttelton Volcano and how their size and shape may be related to mechanisms of eruption. To achieve this, geological mapping of previously known cinder cones and new cinder cones was undertaken, along with the collection of selected samples for petrographic and geochemical analysis.

1.2 LOCATION AND HISTORY

Banks Peninsula forms a 1200 km^2 promontory on the central East Coast of the South Island, New Zealand, at latitude 43° 40'S, longitude 172° 45'E (Figure 1.1). The peninsula was named by Captain James Cook, who in 1770 sailed along the coast of the South Island in the ship Endeavour. Cook mistook the landmass from 15 km out to sea for an island, and called it "Banks Island" after the expedition's botanist Sir Joseph Banks. Lyttelton Volcano is named after the Port of Lyttelton, which is in turn named after Lord Lyttelton of Hagley Park, Chairman of the Canterbury Association (Haast 1948).

The Maori name for the Peninsula is *Te Pataka a Te Rakaihautu* or "the storehouse of Rakaihautu". While the name for the Port Hills is *Te Whakatakanga o Te Ngarehu o Tamatea Pokai Whenua* or "the place where *Tamatea Pokai Whenua* left ashes of the fire he brought" (Brown & Weeber 1992).

Due to the scarcity of nearby timber, and the proximity to Banks Peninsula, early Christchurch builders took advantage of the numerous varieties of volcanic rocks available (Hayward 1987). One of the rocks commonly favoured due to its red colouration and ease of working, was the "Port Hills Tuff". However, due to its pyroclastic origin, the stone would fritter badly and often leaked when exposed to the weather. Nevertheless the stone can be seen around Christchurch and was used in the Towers of the Provincial Buildings (1861), Queen Victoria Diamond Jubilee clock tower (1897), the Information Technology Services Building at the University of Canterbury, and in numerous fences around the city. The major quarries of this stone were located at Redcliffs, Sumner and near Lyttelton Harbour (Brown & Weeber 1992).

1.3 TOPOGRAPHY AND STUDY AREA

Banks Peninsula comprises two Late Miocene stratovolcanoes, Lyttelton (in the north-west) and Akaroa (in the south-east). Originally an island, Banks Peninsula has been connected to the South Island by alluvial gravels deposited during extensive glaciation over 2.0 Ma from the Southern Alps (Sewell et al. 1992). The original heights above sea level of the two volcanoes has been estimated at 1500 m (Weaver & Smith 1989) and 2000 - 2500 m (Shelley 1992) for Lyttelton and 1800 m for Akaroa (Weaver & Smith 1989).

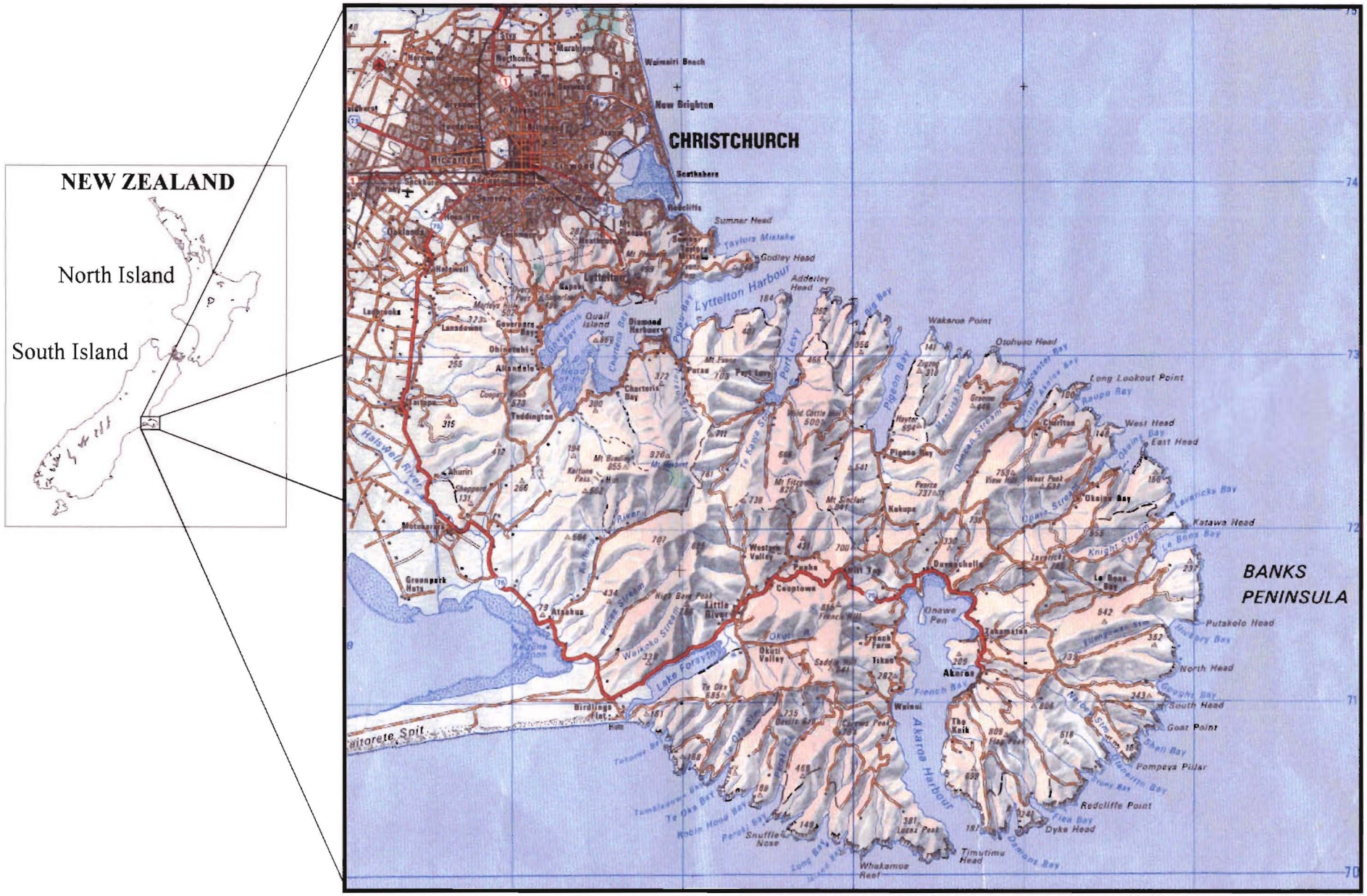

Figure 1.1. Location of Banks Peninsula. Topographic map taken from New Zealand Map Series 262, 1:250,000, Sheet 13, Christchurch.

The eroded and flooded craters of the Lyttelton and Akaroa volcanoes are the principle landforms. Within the basins, the crater rims and walls are the dominant features, while on the outer flanks, rolling to steep hills created from lava flows, radiate out to the sea. These lava flows are dissected by a series of very steep-sided narrow-bottomed valleys.

The study looks at eleven sites of pyroclastic deposits located on Lyttelton Volcano. The study areas are located in a semi-circular fashion, and all occur between 200 m and 500 m above current sea level (Figure 1.2). Areas are located either on the inside of the crater wall or outside on the flanks of dissected valleys.

1.4 VEGETATION AND GEOLOGICAL EXPOSURE

During the volcanic activity on the Banks Peninsula vegetation had a foothold on the land and with the cessation of activity, continuous vegetation developed on the fertile basaltic and loessic surface (Anon 1990). By the time humans first set foot on the Banks Peninsula 1000 years ago, forest would have been virtually covered the whole peninsula (Cox et al. 1994). The only exceptions would have been very steep, exposed sites (at all altitudes but very limited in extent) and areas too water logged to support trees. The landscape, however, changed quickly with many generations of Maori and Pakeha use, with tussock now common, after the previous vegetation was burned off to clear the way for farming (Anon 1990).

Early vegetation would have been podocarp forest, densest in the alluvial valleys. Vegetation patterns, however, varied according to altitude, aspect, soils and proximity to the coast (Cox et al. 1994). Less than 1% of the original forest cover remains, mainly in the form of scenic reserves, although significant remnants and individual forest trees remain on private land. Scrub may be second or even third generation, often consisting of species such as manuka, kanuka, fivefinger, Coprosma species, Fuchsia and often exotic weeds such as gorse and broom (Anon 1990).

The best rock exposure on the peninsula is found at the top of the crater rim on the inside of the 'caldera' walls, which are dominated by steep rocky outcrops. Exposure below the

Location of Study Sites and General Geology of Northern Banks Peninsula

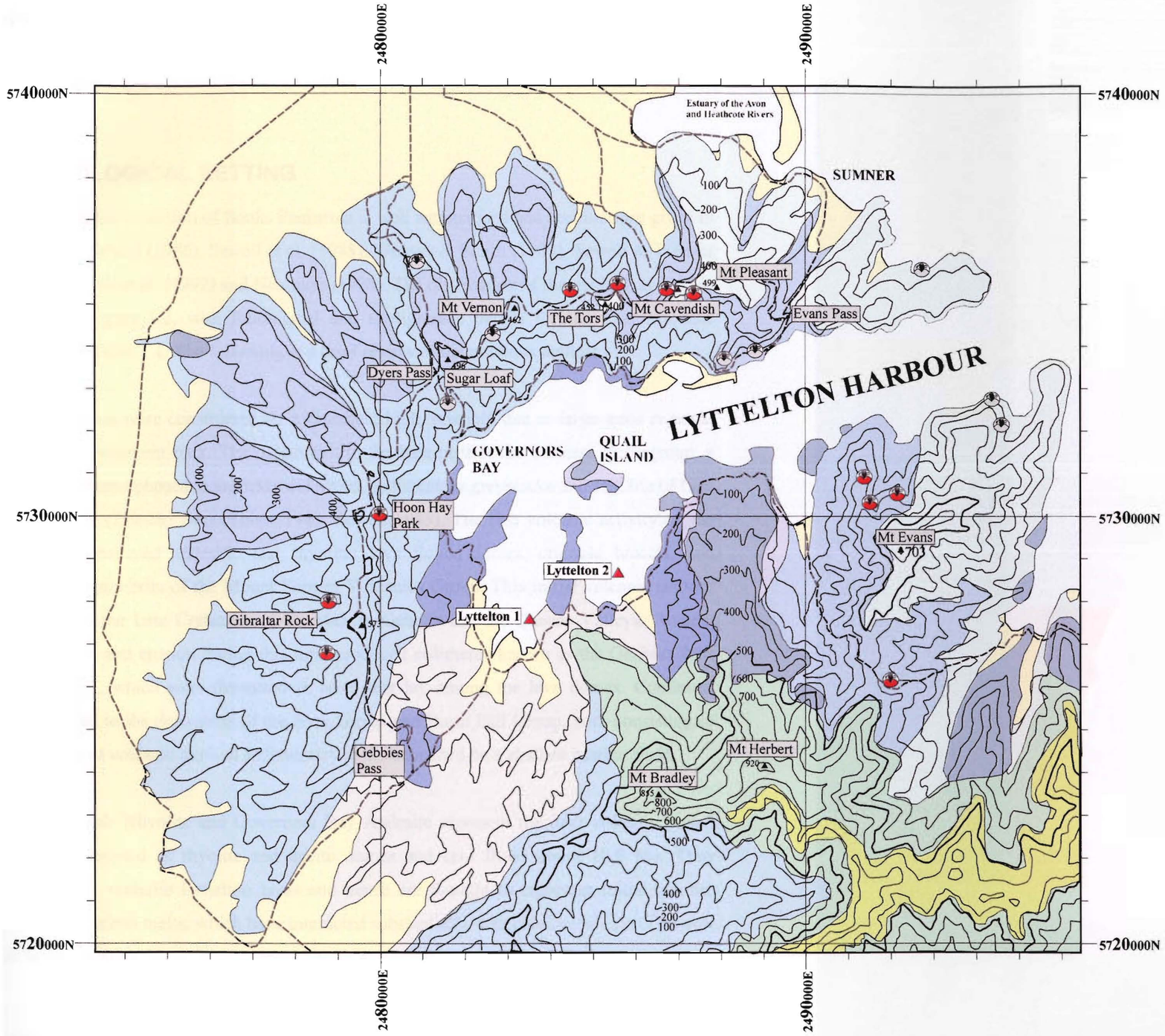

LOCALITY MAP

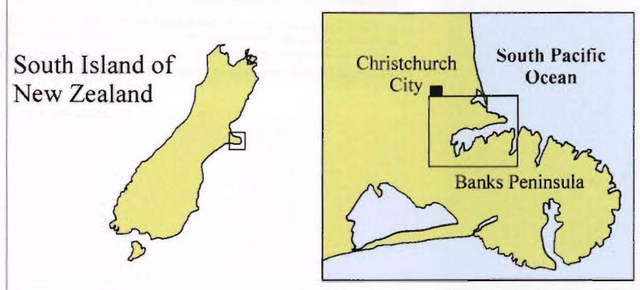

GEOLOGICAL LEGEND

- Quaternary sediments
- Diamond Harbour Volcanic Group
- 'Church-type' lavas
- Akaroa Volcanic Group
- Mount Herbert Volcanic Group
- L2b, L2a, L1 — Lyttelton Volcanic Group
- Governors Bay Volcanics *(informal)*
- Basement
- Other known pyroclastic deposits
- Studied pyroclastic deposits
- Trig points
- Roads
- Road passes
- Lyttelton eruptive centres

N

0 5km

NOTE: This map is drawn on the New Zealand Map Grid Projection, a minimum-error conformal projection. The grid is the New Zealand Map Grid, showing coordinates in metres in terms of the Geodetic Datum 1949, based on the International (Hayford Spheroid)

Figure 1.2. Location of study sites and general geology of northern Banks Peninsula (geology after Sewell et al. 1992, Slaughter 1995, and Neumayr 1998).

caldera walls becomes progressively poorer with decreasing altitude, except at sea level where exposure is best within the tidal zone and sea cliffs. The gently sloping quaquaversal spurs and ridges provide few outcrops, especially on northern slopes where thick loess mantles the landscape. However, where valleys cut the spurs outcrops can usually be found on the valley walls.

1.5 GEOLOGICAL SETTING

The geological evolution of Banks Peninsula is well summarised and accounts are given in Weaver & Sewell (1986), Sewell et al. (1988), Weaver & Smith (1989), Sewell & Weaver (1990), Sewell et al. (1992) and Neumayr (1998). The distribution of the geological units is shown in Figure 1.2, with lithological and stratigraphic details for the Late Miocene outlined in Table 1.1. The following is a brief review of the previous authors.

The volcanoes were constructed on a basement high, possibly due to large scale regional faulting of basement rock. The oldest unit in the basement is the Torlesse Supergroup, a slightly metamorphosed, complexly deformed, sedimentary greywacke and argillite of Late Triassic age (230-205 Ma) (Thiele 1983, Sewell 1985). The first volcanic activity on the peninsula produced andesitic and rhyolitic lava flows, domes, crumble breccia, and explosive ignimbrite of the Mount Somers Volcanics Group. This initial volcanic activity occurred in the Late Cretaceous (~80 Ma), in Gebbies and McQueens Valleys. Ancient scree slopes and erosion during this time produced sediments known as the Gebbies Pass 'plant beds', which were deposited in lakes that lay among the lava domes. Continued erosion lead to the deposition of the Eyre Group and Burnt Hill Group, both consisting of siliceous and volcanic-derived sedimentary rocks deposited on a shallow marine shelf.

The Allandale Rhyolite and Governors Bay Andesite represent the next volcanic period and were erupted as rhyolite and dacite domes and lava flows about 10.8 Ma. They immediately underlie Lyttelton lavas and hence are thought to represent initial mantle-derived Lyttelton melts, which have interacted substantially with continental crust (Weaver & Sewell 1986).

Table 1.1. Basic stratigraphy for the Late Miocene Volcanics of Banks Peninsula (Sewell 1988).

Group	Estimated Volume	Formation	K/Ar Age Range (Ma)	Lithology	Stratigraphic Relationships
Diamond Harbour Volcanic Group	20km^3	Stoddart Basalt	7.0 - 5.8	Fresh, columnar-jointed, olivine +/- clinopyroxene phyric basanites, olivine - basalts and olivine - hawaiites - rare olivine - basalt dikes	
		Kaioruru Basalt	6.9 - 6.8	Commonly weathered, vesicular, pale pink, olivine + clinopyroxene - phyric and aphyric olivine hawaiites	
"Church Type" Lavas	5km^3	Church Basalt	8.0 - 7.3	Fresh, columnar-jointed, olivine +/- clinopyroxene +/- plagioclase - phyric olivine - basalts	
		Chateau Intrusives	8.0	Grey columnar to knobbly - jointed aphyric hawaiites	
		Darra Basanitoid	8.1 - 7.7	Fresh, columnar - jointed olivine +/- clinopyroxene - phyric basanitoids - rare basanitoid dikes	
Akaroa Volcanic Group	1200km^3		9.0 - 8.0	Fresh, medium to fine -grained, olivine - clinopyroxene - plagioclase - phyric and grey, aphyric hawaiites - rare trachyte domes and dikes	
Mt Herbert Volcanic Group	100km^3	Herbert Peak Hawaiite	8.5 - 8.0	Grey, columnar-jointed, aphyric and rarely olivine - phyric olivine - hawaiites	
		Port Levy Formation	8.9 - 8.5	Grey-black, columnar-jointed, aphyric hawaiites - rare porphyritic basalts	
		Orton Bradley Formation	9.5 - 8.6	Black, fresh aphyric, olivine - hawaiites + olivine - phyric olivine - basalts	
		Kaituna Valley Hawaiite	9.7 - 9.5	Columnar-jointed, dark grey-black, fresh olivine - phyric olivine - basalts	
Lyttelton Volcanic Group	350km^3		11 - 9.7	Moderately weathered, plagioclase +/- olivine +/- clinopyroxene - phyric hawaiites - trachyte lava flows and domes - numerous trachyte and basaltic dikes	

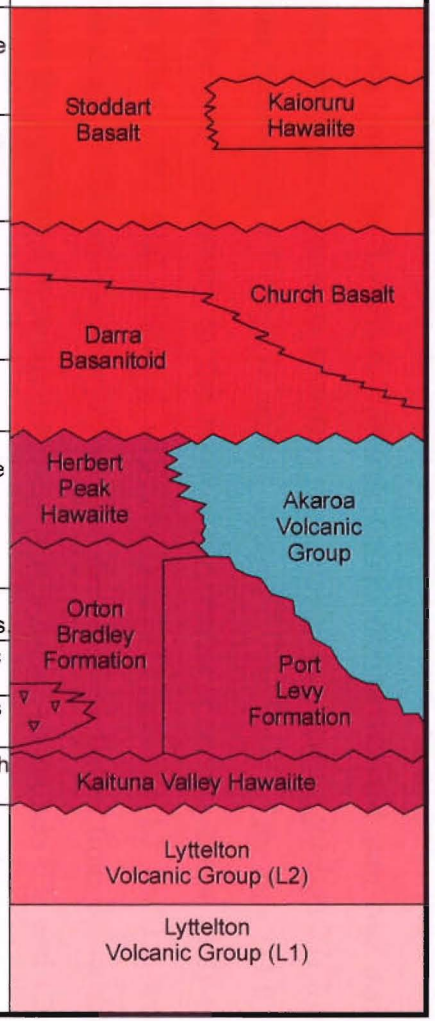

The development of the Lyttelton Volcanic Group occurred between 11.0 and 9.7 Ma (Figure 1.3A), which is composed of basalt, hawaiite, mugearite, benmoreite and trachyte lava flows, with interbedded sediments and pyroclastic deposits. Dikes were emplaced throughout the history of the volcano and occur in a radial fashion, ranging in composition from basalt to trachyte. The Lyttelton Volcanic Group can be divided into two main eruptive phases, which are commonly known as the Lyttelton 1 (L1) and Lyttelton 2 (L2 or Mount Pleasant Formation). L1 eruptive activity centred on the Head of the Bay (11.0 – 10.4 Ma) with a shift in activity to the north-east, forming a second centre (L2) on Charteris Bay (10.4 – 9.7 Ma) (Figure 1.3B). The boundary between L1 and L2 was defined by Neumayr (1998) as occurring between a lahar that he traced from below the Tors to just past the Lyttelton Township. He also divided the L2 phase into L2a and L2b based on further lahars that outcrop on the Summit Road between Mount Cavendish and Castle Rock. These lahars represent quiescence and were caused by erosion of the outer slopes. Following the activity on Lyttelton, erosion into the edifice caused deep excavation of the crater with breeches opening to the south-east (near what are now Mt Herbert and Port Levy), and possibly to the south-west (now Gebbies Pass).

The Mount Herbert Volcanic Group represents a shift in activity from the L2 centre to the south, and comprises mildly alkaline hawaiite, mugearite, and basalt dikes, plugs, lava flows, and epiclastic and pyroclastic deposits. Activity occurred on the south flanks of the Lyttelton Volcano between 9.5 and 8.3 Ma and in the eroded crater (Figure 1.3C). A lake developed on the floor of the crater that drained through the breech in the south-east, which was infilled by alkalic lavas and pyroclastics between 9.1 and 8.6 Ma (Figure 1.3D).

Activity continued to migrate south and activity between the Akaroa and Mt Herbert Volcanic occurred simultaneously (Figure 1.3E). Initial activity of Akaroa Volcano commenced with the eruption of the Tikao Trachyte dome, which was then overlain by alkaline basalt to trachyte lavas and intrusive rocks, tuffs, agglomerates and parasitic cinder cones. Akaroa activity ranged from 9.1 - 8.0 Ma and was centred on the Onawe Peninsula, based on the outcropping of plutonic rocks (eg Gabbro and Syenite) that are thought to represent magma which crystallised deep in the feeder pipe (Figure 1.3F).

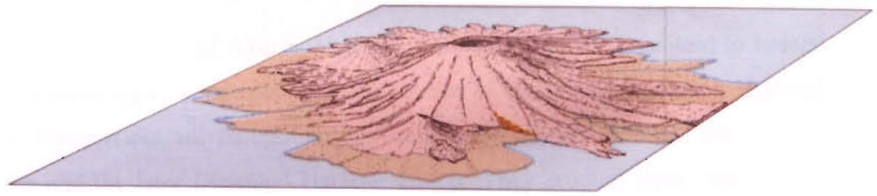

A **11.0-10.4 Ma.** Construction of main cone of Lyttelton Volcano (Lyttelton 1) by rocks of Lyttelton Volcanic Group. Minor strombolian flank activity.

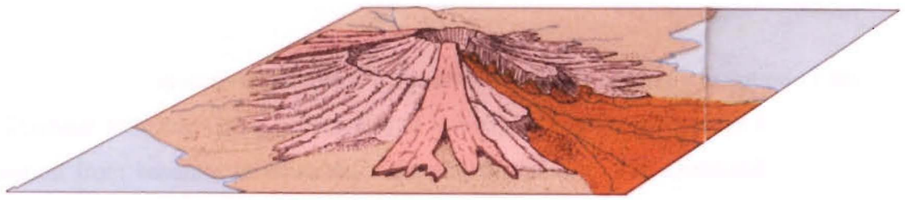

B **10.4-9.7 Ma.** Shift in focus of activity to Lyttelton 2 centre, accompanied by eruption of Mount Pleasant Formation lavas onto northern and southwestern flanks of the volcano from local vents. Crater area breached in the southeast during final stages of eruption.

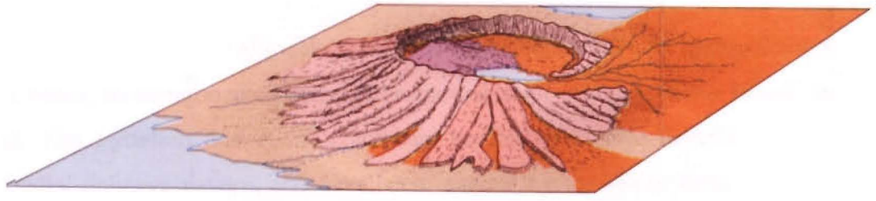

C **9.5-9.1 Ma.** Deep excavation of Lyttelton Volcano by erosion. Eruption of Mount Herbert Volcanic Group lavas within breached sector of Lyttelton crater area, and formation of lake on the crater floor. Development of volcaniclastic deposits in lake.

D **9.1-8.6 Ma.** Further eruptions of Mount Herbert lavas from vents close to breach in crater wall of the Lyttelton Volcano, and from Port Levy. Emplacement of oldest part of Akaroa Volcanic Group (Tikao Trachyte Dome), and construction of main cone of the Akaroa Volcano.

E **8.6-8.3 Ma.** Continued eruption of Mount Herbert Volcanic Group from vents near Mount Herbert. Further extrusion of Akaroa Group lavas from fissure vents in the vicinity of Mount Sinclair and Mount Fitzgearld,

F **8.3-8.0 Ma.** Final eruptions of Mount Herbert Volcanic Group. New breach in Lyttelton crater area opens along Gebbies Pass. Eruption of late phase Akaroa Volcanic Group lavas from central cone of Akaroa Volcano.

G **8.1-7.3 Ma.** Eruption of "Church-type" lavas on flanks and floor of eroded Lyttelton crater. Breach in crater wall to form main channel along which Lyttelton Harbour develops. Excavation of Akaroa Volcano.

H **7.0-5.8 Ma.** Eruption of Diamond Harbour Volcanic group lavas from numerous monogenetic cones on flanks of both Lyttelton and Akaroa volcanoes, and into eroded Lyttelton crater area.

Figure 1.3. Diagrams illustrating the history of Miocene volcanism on Banks Peninsula. Note not to scale, with colour key given in Table 1.1 (after Sewell et al. 1992).

Near the end of the formation of Akaroa Volcano, new eruptions of basanitoid to basalt, known as the "Church type" lavas, occurred in the area of the present Lyttelton Harbour (Figure 1.3G). These rocks are thought to represent the transition between the Akaroa Volcanic Group and the later Diamond Harbour Group. They erupted from vents in the upper Kaituna Valley, within the eroded Lyttelton crater towards Quail Island, and from vents south of Charteris Bay between 8.1 and 7.3 Ma. From about 8.0 Ma the Lyttelton Harbour was also being drained suggesting that a new breach had developed at the site of the present harbour entrance.

The last phase of volcanic activity occurred between 7.0 – 5.8 Ma with the eruption of the Diamond Harbour Volcanic Group, consisting of lava flows and volcanic plugs that range in composition from basanite to hawaiite, with rare nephelinite. The Diamond Harbour Volcanic Group lavas form valley infillings and flat sheets that were erupted from a number of vents mainly within the crater of Lyttelton Volcano, with isolated patches on Akaroa Volcano (Figure 1.3G). The group also forms a well known 5 km long dip-slope that dips northward from Mount Herbert.

Post-volcanic geology consists of alluvial gravels and sands deposited over approximately the last 2 Ma which, as mentioned earlier, were responsible for joining "Banks Island" to the mainland. The Lyttelton and Akaroa volcanic centres were also severely eroded producing a radial drainage pattern, and have been invaded by the sea to form Lyttelton and Akaroa Harbours. During the glacial periods, silt-sized glacial 'flour' was also transported and deposited by north-west winds producing an extensive mantle of loess covering much of Banks Peninsula. Deposits are thickest on the lower north facing slopes and have been the focus of many engineering geology investigations (eg. Bell 1978, Yetton 1986).

1.6 TECTONIC SETTING

Prior to the Cretaceous, New Zealand was located on the eastern side of Gondwana under a compressional regime, which peaked in the Rangitata Orogeny (Bradshaw et al. 1981). In the Late Cretaceous there was a period of extension and major rifting during which the Tasman Sea opened and New Zealand became separated from Gondwana (Sewell &

Gibson 1988). The Early Tertiary on southern continental New Zealand is thought to have been a period of relative tectonic quiescence. Renewed tectonism in the Late Eocene – Oligocene was marked by gentle warping and local basin subsidence, thought to be related to extensional tectonics, also causing widespread alkalic to tholeiitic volcanism in the Canterbury region (Sewell et al. 1988). In the Early Miocene there was a change to compressional tectonics (The Kaikoura Orogeny) with uplift in the west and an increase in sedimentation in the east, and the onset of alkalic to tholeiitic volcanism throughout the South Island, including Banks Peninsula (Adams 1981).

Since the end of volcanism, Banks Peninsula has commonly been thought to have been differentially subsiding. However, in a study of shore platforms on the northern flanks and southwestern flanks, Bal (1997) found that these contemporaneous features had been relatively stable for at least the last 120,000 years. He therefore concluded that Banks Peninsula has been tectonically stable since the mid-late Quaternary.

1.7 PREVIOUS WORK

Work on Banks Peninsula first began in the late 1800's by Haast (1860, 1879), Hutton (1885), Marshall (1893), and continued into the early 1900's with Speight (1908, 1917, 1924, 1940, 1944). These early workers recognised that the Lyttelton and Akaroa Harbours had been the eruptive centres during the development of Banks Peninsula, but generally they had a poor understanding of the stratigraphy and the exact eruptive centres.

Oborn & Suggate (1959) continued with Speight's idea of the Mount Herbert Volcanics being a separate group (due to their lighter colour and more alkaline character). Ligett & Gregg (1965) produced a geological map that distinguished the Diamond Harbour volcanics from the Lyttelton and Akaroa volcanics. Stipp and McDougall (1968), using K/Ar geochronology, later confirmed this stratigraphy.

Most of the recent work on Banks Peninsula has been done in the form of University of Canterbury unpublished theses and research projects (eg. Dorsey 1981, Falloon 1982, Sewell 1985, Shearer 1986, Dorsey 1989, Altaye 1989, Johnston 1990, Hobden 1990, Hibberd 1994, Mckenzie 1995, Slaughter 1995, Neumayr 1998, Guard 1999). There have

also been engineering geological and geophysical studies on the problems of 'tunnel gullies' and the stability of loess (eg Jones 1997, Harrison 1999). However, Sewell (1985, 1988) was the first to 'grasp' and define the Miocene stratigraphy, with numerous other papers (eg Weaver 1980, Shelley 1985a, 1987, 1988, Weaver et al. 1985, Weaver & Sewell 1986, Weaver & Smith 1989 and Sewell et al. 1992) on dikes, chemical characteristics and the evolution of Banks Peninsula. However the above reports only briefly mention or describe pyroclastic deposits (Figure 1.4), and only Johnston (1990) fully focused on pyroclastics, in the Pigeon Bay - Port Levy area of Akaroa.

1.8 RESEARCH METHODS

Preliminary fieldwork involved investigating possible field sites over two weeks in early December (1997). After initial field investigations, eleven sites were selected, based on the amount of exposure and accessibility, and also due to their location so as to give a wide variety of possible samples and to see if there was any variation in between sites. Once located, aerial photographs were used to map the sites (see Appendix 1 for air photo list and methods). Mapping took approximately 5 weeks from January to February 1998, and over 150 samples were collected, and many photos taken. A second period of fieldwork took place during December and January 1998/1999 and continued for approximately two weeks. During this time additional samples were collected, more photos taken, and maps drafted over the winter were tidied up and completed. Sample collection focused on pyroclastic material, dikes, and surrounding lava flows. 73 pyroclastic samples were then selected for thin section analysis and 112 dike, lava and pyroclastic samples were selected for geochemistry. From the analysis of samples and interpretation of field deposits, along with a discussion of relevant literature on mechanisms and deposits, a model for the generation of cinder cone eruptions on Lyttelton Volcano has been developed.

Location of Relevant Previous Studies on Northern Banks Peninsula

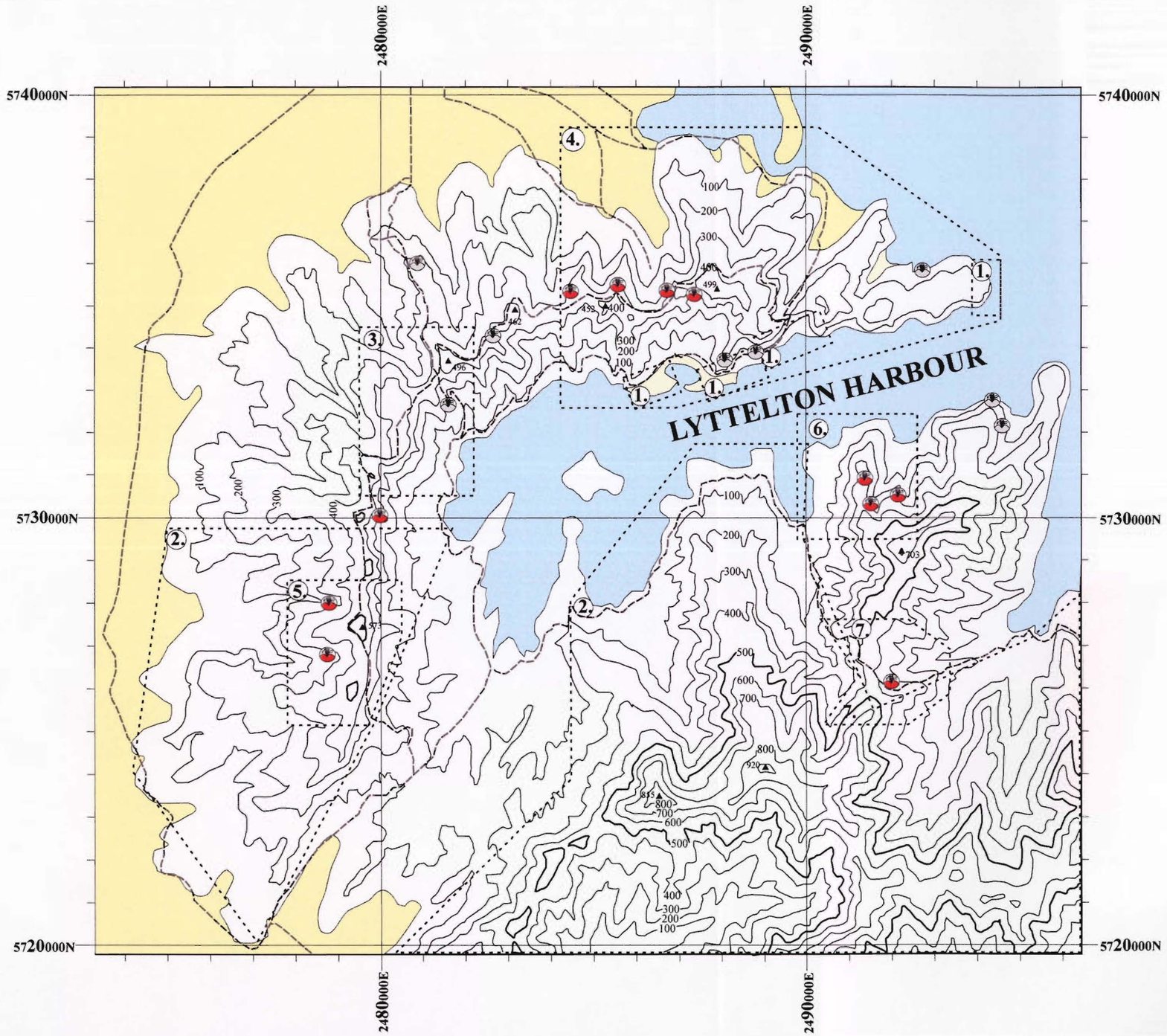

LOCALITY MAP

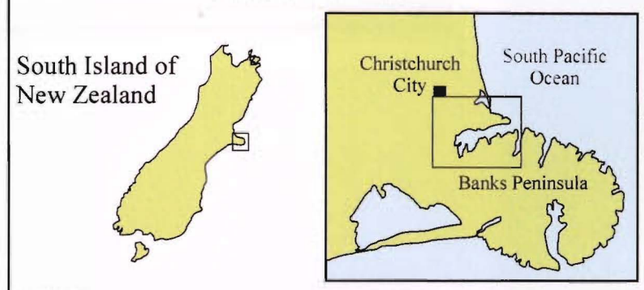

LIST OF PREVIOUSLY DESCRIBED CINDER CONE AND PYROCLASTIC DEPOSITS

Author	Deposit type and number
1. Coates (1976)	5 pyroclastic horizions
2. Sewell (1985)	3 cinder cones
3. Shearer (1986)	1 cinder cone
4. Altaye (1989)	3 cinder cones
5. Hibberd (1994)	2 cinder cones
6. Slaughter (1995)	3 cinder cones
7. Mckenzie (1995)	1 cinder cone

KEY

- Quaternary Sediments
- Pyroclastic deposits described in this study
- Other known pyroclastic deposits
- Roads

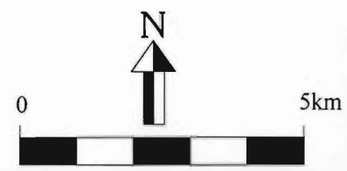

NOTE: This map is drawn on the New Zealand Map Grid Projection, a minimum-error conformal projection. The grid is the New Zealand Map Grid, showing coordinates in metres in terms of the Geodetic Datum 1949, based on the International (Hayford Spheroid)

Figure 1.4. Location of previous studies on Lyttelton relevant to this study (map after Sewell et al. 1992)

Chapter Two
SITE DESCRIPTIONS

2.1 INTRODUCTION

Pyroclastic rocks are composed of fragments that originate from explosive volcanic eruptions or form as a direct consequence of the eruption. Cinder cones are a direct consequence of Hawaiian and Strombolian eruptions and are dominantly composed of pyroclastic material (except for flank lava or spatter flows). The aim of this chapter is to describe the selected pyroclastic deposits that occur on the Lyttelton Volcano. Classification of pyroclastic deposits is covered first followed by site descriptions of each area.

2.2 CLASSIFICATION OF PYROCLASTIC DEPOSITS

Cas & Wright (1987) suggest that to describe pyroclastic deposits, two systems are needed. Firstly a *genetic classification* is needed to interpret the genesis of deposits, which can then be related to the history, eruptive pattern and mechanisms of the volcano or volcanic terrain. Secondly a *lithological classification* is needed, describing and documenting the major characteristics of a deposit, such as grainsize and constituent fragments.

2.2.1 Genetic Classification

The aim of a genetic classification is to deduce the origin of a pyroclastic deposit. Overall there are three types of deposit; pyroclastic surge, flow and fall deposits. Since cinder cones are built primarily by the falling of pyroclasts, only fall deposits are discussed in this section.

Walker (1973) was the first to describe and classify explosive volcanic eruptions producing pyroclastic fall deposits and he produced a classification based on characteristics of fall deposits in the field. This involved two parameters: dispersal (D) and fragmentation index or degree of fragmentation of the deposit (F). It was later amended by Wright et al. (1980) and the amended version is given in Figure 2.1. Such a classification scheme relies heavily

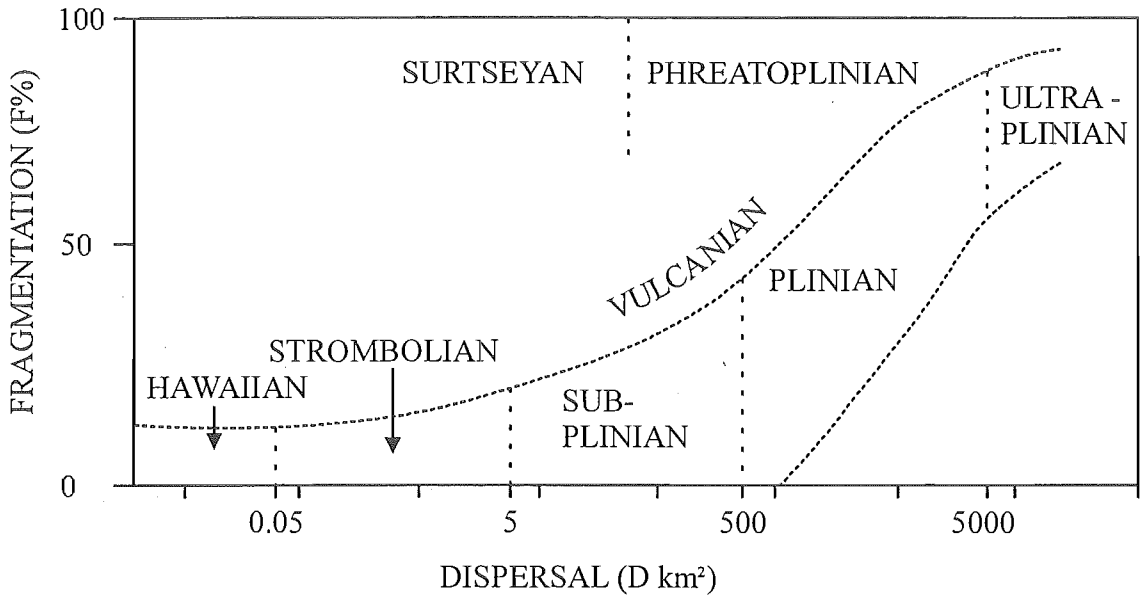

Figure 2.1. D - F plot used to characterise different types of pyroclastic fall deposits (after Walker 1973 and updated by Wright et al. 1980).

Table 2.1. Grain size limits for proven pyroclastic fragments and pyroclastic aggregates (after Fisher 1961 & 1966, Walker 1973).

Grainsize (mm)		Pyroclastic fragments		Name of unconsolidated aggregate	Lithified equivalent
		round and fluidally shaped	angular		
256	coarse	bombs	blocks	agglomerate (bombs) or pyroclastic breccia	agglomerate (bombs) or pyroclastic breccia
	fine				
64		lapilli		lapilli deposit	lapillistone
2					
1/16	coarse	ash		ash deposit	tuff
	fine				

on granulometry and therefore only works on very young and well exposed deposits. It is difficult to apply to lithified deposits like those on Lyttelton Volcano. All the deposits in this study however are classed as Hawaiian to Strombolian due to their small dispersal areas (all ≤ 1 km^2).

2.2.2 Lithological Classification

There are three main bases needed for a lithological classification.

1. Grain size. The grainsize limits of pyroclastic fragments are based on schemes by Fisher (1961, 1966). The distribution of the overall grainsize can also be important in distinguishing different types of deposits (Table 2.1).
2. Constituent fragments. There are three kinds of pyroclasts or components that make up pyroclastic deposits:

   I. Juvenile fragments. These represent samples of the erupting magma, and may be partially crystallised, or noncrystallised, depending on the pre-eruptive history of the magma. They include both scoria and spatter, where scoria is defined as "vesiculated basaltic fragments produced by explosive eruptions". The term spatter is used to describe coherent lumps of hot and fluidal magma, and can also be used as a collective term for fused material. Individual clasts of spatter can also accumulate in large enough amounts to produce flows called 'spatter flows'. Fragments that are ejected for longer distances cool and retain their inflight shape, and are called bombs. The term 'bomb' is defined as "a pyroclastic fragment larger than 64 mm that is viscous (wholly or partly) when ejected" (Macdonald 1972). A summary and description of the main types of bombs is given in Table 2.2, with illustrations given in Figure 2.2 and these terms will be adopted in this study.

   II. Crystals. Free crystals and angular fragments of crystals are released during the explosive disruption and breakage of porphyritic magmas and juvenile fragments, and form a discrete juvenile component from the vesiculated and non-vesiculated magmatic fragments in the pyroclastic deposit.

   III. Lithic fragments. These are the dense components in a pyroclastic deposit of which there are two types in a fall deposit, cognate and accessory

Table 2.2. A list of the different types and mechanisms for formation of volcanic bombs and lapilli, after Tsuya (1941), Brady & Webb (1943), Walker & Croasdale (1972), Macdonald (1967, 1972), Francis (1973), Williams & McBirney (1979), Cas & Wright (1987).

Pancake/ cowdung/ cowpat bombs. Caused by small blobs of very fluid magma that have low flight times and little cooling before emplacement, consequently causing them to flatten on impact.
Ribbon bombs. Caused by molten lava being ejected in long strings or ribbons. Commonly the ribbons are still sufficiently plastic to bend or twist on impact, and some ribbon bombs are looped and twisted. Short segments of ribbons occur when they break on impact and are sometimes referred to as *cylindrical bombs.* Ribbon and cylindrical bombs are generally marked by more or less continuous ridges or flutings parallel to their lengths.
Spheroidal bombs. Caused by low viscosity magma that has a sufficiently low surface tension causing the bombs to be drawn into shapes approaching spheres.
Almond/ spindle/ fusiform bombs. Viscous blebs are only partly drawn into a spherical shape and remain elongate causing *almond/ spindle/ fusiform bombs.* Some of them have been ejected by independent blobs while others come from broken up ribbon bombs. If from the middle of the ribbon they have two 'ears' on each side caused by the separation of the ribbon and these are called *bipolar.* If they come from the ends of the ribbon then they will only have one ear and are therefore called *unipolar.* The actual rotation of bombs through the air does not create the shape (as first thought) although twisting of the ears can occur by rotation through the air. Bombs however may have a smooth leading edge (stoss side) and rough following (lee side) edge.
Cored bombs. Are formed by the wrapping of solid nuclei in liquid lava or by re-ejecting falling cinders out of the vent again. Cored bombs may have any of the external features mentioned above.
Breadcrust bombs. Are notably less abundant among basaltic than among more silicic rocks. They are formed by continued vesiculation and swelling of the core after the outer skin has become too rigid to stretch.
Pele's hair and Pele's tears (achneliths). Finely spun glass threads (*Pele's hair)* are produced by explosions of gas-rich, extremely fluid basaltic lava fountains. Liquid droplets may be drawn into threads up to 2 m or more in length, that may drift in the wind for distances of 15 kilometres. Other liquid droplets, measuring a few millimetres across, chill quickly to glass beads with pendent threads (*Pele's tears or achneliths)*).

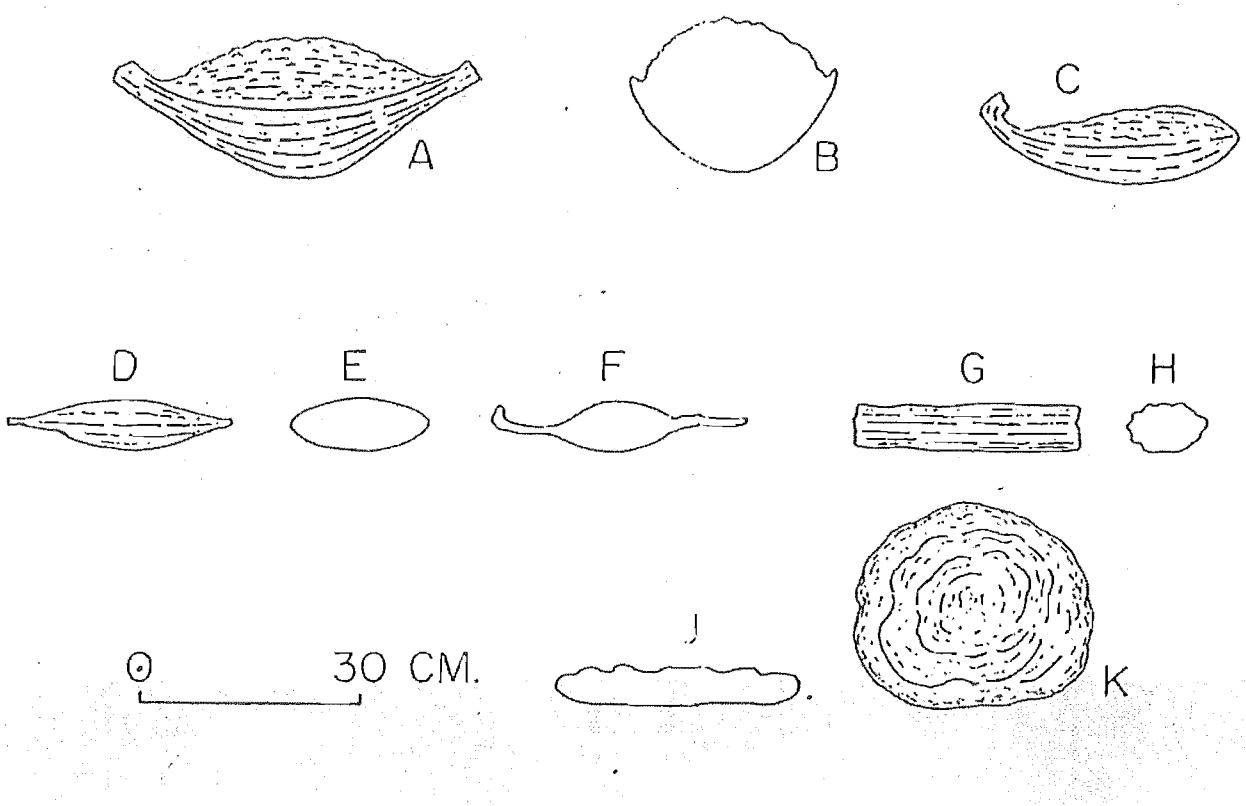

Figure 2.2. Sketches and cross sections of bombs (Macdonald 1972). **A)** bipolar fusiform bomb with stoss side at bottom and lee side at top; **B)** cross section of A, showing drawing of skin toward lee side by air resistance during flight; **C)** unipolar fusiform bomb; **D)** almond-shaped bomb; **E)** cross section of D; **F)** cross section of bomb with broad equatorial fin; **G)** cylindrical ribbon bomb; **H)** cross section of G; **J)** cross section of cow-dung bomb; **K)** cow-dung bomb.

lithics. Cognate are non-vesiculated juvenile magmatic fragments (blocks), and accessory lithics are country rock fragments that have been ejected during an eruption.

3. Welding. Cas & Wright (1987) give a definition of welding as "the sintering together of hot, glassy fragments, irrespective of shape and size, under the influence of a compactional lithostatic load. They go on to explain that "during welding the glassy fragments deform plastically, producing a bedding parallel fabric of flattened, elongate large pumice fragments (fiamme) and glass shards, known as eutaxtic texture". Cas & Wright (1987) restrict the use of the term 'agglutination' to describing the process of deformation and sintering of air-fall pyroclasts when they impact on an accumulating bed. Flattening is caused by the momentum of the falling pyroclasts, thus distinct from welding. When interpreting older deposits the distinction between welding and agglutination is difficult because of the need to decide whether lithostatic loading is involved. Johnston (1990) preferred to use the term welding for "any sintering together of pyroclastic material" and this usage will also be applied in this study. Johnston (1990) also found that modern pyroclastic welding terms are difficult to apply to old deposits due to post-eruption alteration. The devitrification of glass, alteration to clays, and secondary deposition of minerals, within the vesicles and between the clasts, leads to post-eruption lithification of much of the material. Therefore making it sometimes impossible to distinguish between cohesion produced by welding or secondary processes. Johnston (1990) in his study used the degree of flattening to make inferences into the degree of welding and this approach is also used in this study. The deposits are divided into three types;

   I. *Non-flattened.* Pyroclastic deposits with undeformed clasts.
   II. *Welded.* Deposits in which all or some pyroclasts are flattened out.
   III. *Densely welded.* Pyroclasts totally fused together and shapes are unrecognisable.

2.3 FACIES DESCRIPTIONS

The deposits that make up cinder cones can be classed into four gradational lithofacies, based on variations in welding, dip direction, block size, colour and the presence or absence of some clasts. Boundaries for each facies are drawn as sharp contacts on maps, but are gradational in the field. The following general descriptions are based on criteria used in other studies on similar areas (eg. Guest (1982) for Mt Etna, Houghton &

Schmincke (1989) for Rothenburg, Brown (1990) for Taupo, Johnston (1990), and Johnston et al. (1997) for Akaroa, Hibberd (1994), Slaughter (1995), and Mckenzie (1995) for Lyttelton), and will continue to be used throughout the text to describe similar deposits in the study areas. Clast size in all descriptions refers to the length of the longest axis in elongate bombs, or the diameter in spherical bombs and lapilli.

Vent facies: The facies is characterised by grey-black densely welded spatter and rare scoria fragments. In places these deposits can have the appearance of lava and may have dip directions inward toward the eruption centre.

Proximal facies (outer wall): The facies is welded, consisting of red, red-brown and grey, nonflattened and flattened bombs. Flattened bombs range in size from 50 – 80 cm in length, although some blocks and bombs can reach up to 3 m. The facies lack the characteristic ash layers of typical medial and distal facies, but usually has rheomorphic ('spatter') flows. The proportion of non-flattened to flattened bombs varies and the facies is defined as having > 20% flattened bombs.

Medial facies (outer wall): The facies consists of weakly bedded to massive ash, lapilli, bombs and blocks. Bombs and blocks up to 20 cm dominate with rare bombs ranging up to 2 m. The colour ranges from red to red-brown with deposits sometimes crudely bedded (20 - 30°) and dipping away from the eruption centre. Sorting is generally poor but thin bands of similar sized lapilli can occasionally be found. Pyroclasts are undeformed and are therefore inferred to be non-welded.

Distal facies (outer wall): The facies is distinguishable from the medial facies by its finer bedding and a dominant lapilli and ash sized fraction, better sorting and yellow to brown colour. Beds again dip (15 - 25°) away from the eruption centre and clasts are again undeformed and therefore inferred to be non-welded. Irregular clast shapes are most common, but some spindle and ribbon bombs and angular blocks are present.

2.4 SITE DESCRIPTIONS

2.4.1 Southern Mount Cavendish

Pyroclastic deposits cover 0.8 km^2 of the area (Figure 2.3) and are well exposed. Distal deposits outcrop on the eastern edge of the exposure and consist of well sorted, bedded (15° E) lapilli and ash (Figure 2.4A), with rare bombs up to 10 cm. Medial deposits outcrop at the northern and western margins of the area, with average bomb and block size decreasing away from the vent (~60 – 10 cm). Medial deposits consist of fusiform, round and spindle bombs and blocks (Figure 2.4B), set in a finer lapilli and ash matrix which are crudely bedded (~30°) in places (Figure 2.4C) (Appendix 2A). Along the base of the exposure the medial deposits grade into proximal deposits with a decrease in blocks and well-shaped bombs to more spatter and flattened clasts. Proximal deposits grade into the vent facies, with a complete loss of clast preservation causing an appearance like lava in places (Figure 2.4D). Vent material is very densely welded and from a distance appears highly fractured and jointed. Proximal deposits are 'cavernous' in appearance with medial and distal deposits weakly bedded. The exposure thins out both east and west with overlying lavas onlapping the cone. A small dike (1 m wide) located in the medial deposits appears related to the pyroclastics due to it striking towards the eruption centre, and probably represents a late stage feature. The eruption centre is located in the centre of the exposure, at the edge of the vent deposits, based on outcrop patterns and dips in the area (Figure 2.3).

2.4.2 Northern Mount Cavendish

Pyroclastic deposits cover an elongate area of 0.6 km^2 with outcrops found predominantly below the road (Figure 2.5). Distal deposits are found at the northeastern edge of the exposure (Figure 2.6A), and are bedded (27° E), very well sorted, ash-rich and lapilli-poor. Distal deposits grade into medial deposits directly below this outcrop, which is bedded (27° E), and contains fusiform and spindle bombs (< 15 cm) set in a finer matrix. Medial deposits outcropping in the south, consist of similar material, with dips (~20°) that define a radial pattern (Figure 2.5). At the outer margin of this southern exposure deposits start to become distal, with a decrease in clast size (Figure 2.6B). Proximal deposits dominate the area, which are 'cavernous' and made up of flattened bombs and spatter that range in size

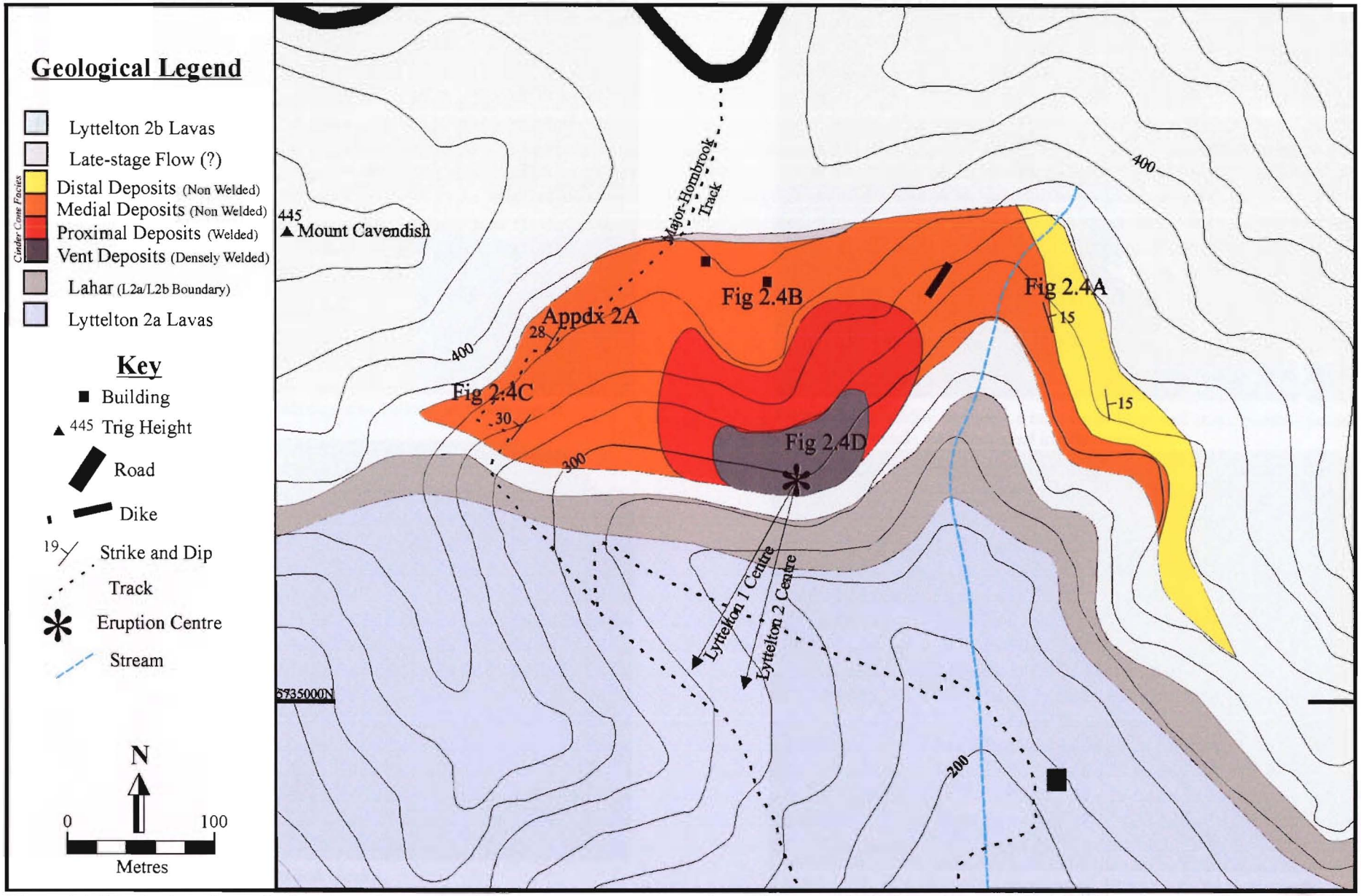

Figure 2.3. Distribution of pyroclastic units and general geology in the south-east Mount Cavendish area. Distribution of Lyttelton 2a & 2b lavas based on Neumayr (1998).

Figure 2.4A. Distal lapilli and ash deposits, bedded and well sorted.

Figure 2.4C. Well bedded bombs and blocks.

Figure 2.4B. Medial deposits, a mixture of large and small bombs (fusiform, spindle and round), and blocks, set in a finer matrix.

Figure 2.4D. Vent deposits, consisting of densely welded spatter.

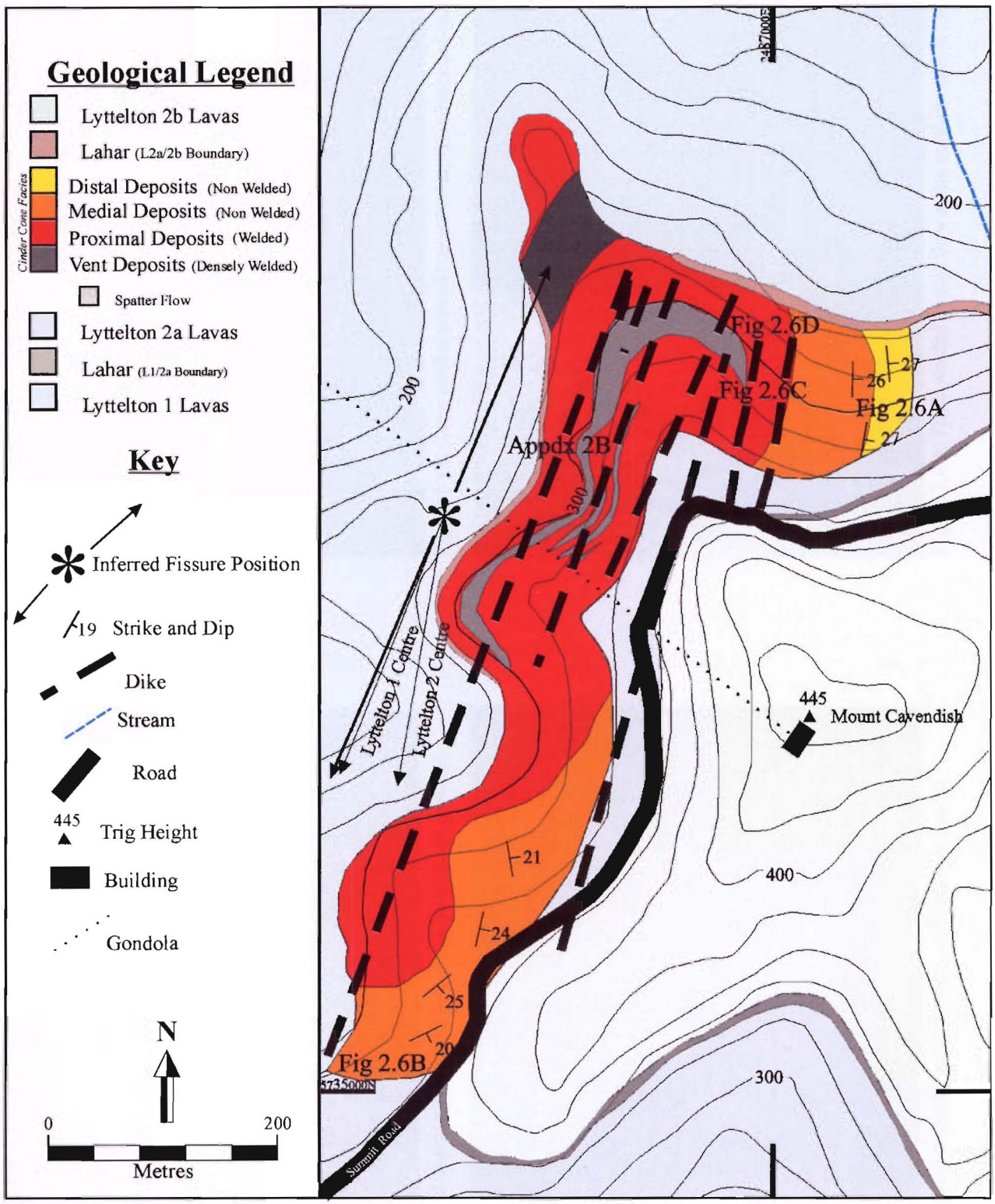

Figure 2.5. Distribution of pyroclastic units and general geology in the north-west Mt Cavendish area. Distribution of L2a and L2b lavas based on Neumayr (1998).

Figure 2.6A. Distal deposits, very well sorted and bedded ash material.

Figure 2.6B. Outer medial material, unsorted lapilli, with occasional bombs.

Figure 2.6C. Proximal deposits, welded spatter and flattened bombs.

Figure 2.6D. Thick welded spatter flow at the northern end of the area.

up to 30 cm (Figure 2.6C). Interbedded between the proximal deposits are four spatter flows that range in length between 40-300 m and are up to 5 m thick (Figure 2.6D) (Appendix 2B). The area is cut by seven dikes that range in thickness between 0.3-3 m, and vary in strike from between 195°-205°. Due to the elongate nature of the deposits in the area, and the large extent of proximal deposits, initial eruptions were located along a fissure. The fissure would have been located about 60 m from the limit of exposure, due to the proximity of the many spatter flows, and oriented sub-parallel to the dikes exposed at the site. Evidence for the fissure is provided on a small saddle where an elongate densely welded deposit outcrops and is interpreted as vent material (Figure 2.5). However, as eruptions proceeded, activity became localised in the south as shown by the arrangement of dips (Figure 2.5).

2.4.3 Castle Rock

A trachyte-benmoreite dome dominates the Castle Rock area with the pyroclastic deposits located on the western side (Figure 2.7). No pyroclastic material is exposed on the eastern side due to large amounts of fallen blocks and bush cover. No distal or vent deposits outcrop in the area, which is elongate and covers an area of 0.2 km^2. Medial deposits at the southern end consist of predominantly small (< 0.15 cm) bombs, set in a crudely bedded (24° SE) fine lapilli and ash matrix, with occasional flattened bombs (< 10 cm). The deposits grade northwards into proximal deposits with flattened bombs and blocks that range between 5 - 30 cm (Figure 2.8A), with rare large round bombs up to 45 cm. Heading north, the dominant material changes from pyroclastics to a thick spatter flow (~8 m), that is covered by proximal deposits. The spatter flow can be traced for 130 m and is underlain by a thin band of pyroclastics that is made up of rare flattened bombs (< 30 cm) and dominated by lapilli and ash. Along the base of the spatter flow, gradations and relatively sharp boundaries are seen with underlying pyroclastics (Figure 2.8B) (Appendix 2C). The flow is thickest on the west-side of Castle Rock thinning towards the north where it dips 25° north-east (Figure 2.8C). At the north end the pyroclastics become much finer grained and contain flattened clasts (15 – 45 cm) that are light grey (benmoreitic clasts) (Figure 2.8D). The eruption centre is difficult to locate with only two dips crudely defining a circular shape, however it would have been located about 50 m to the west of the exposure

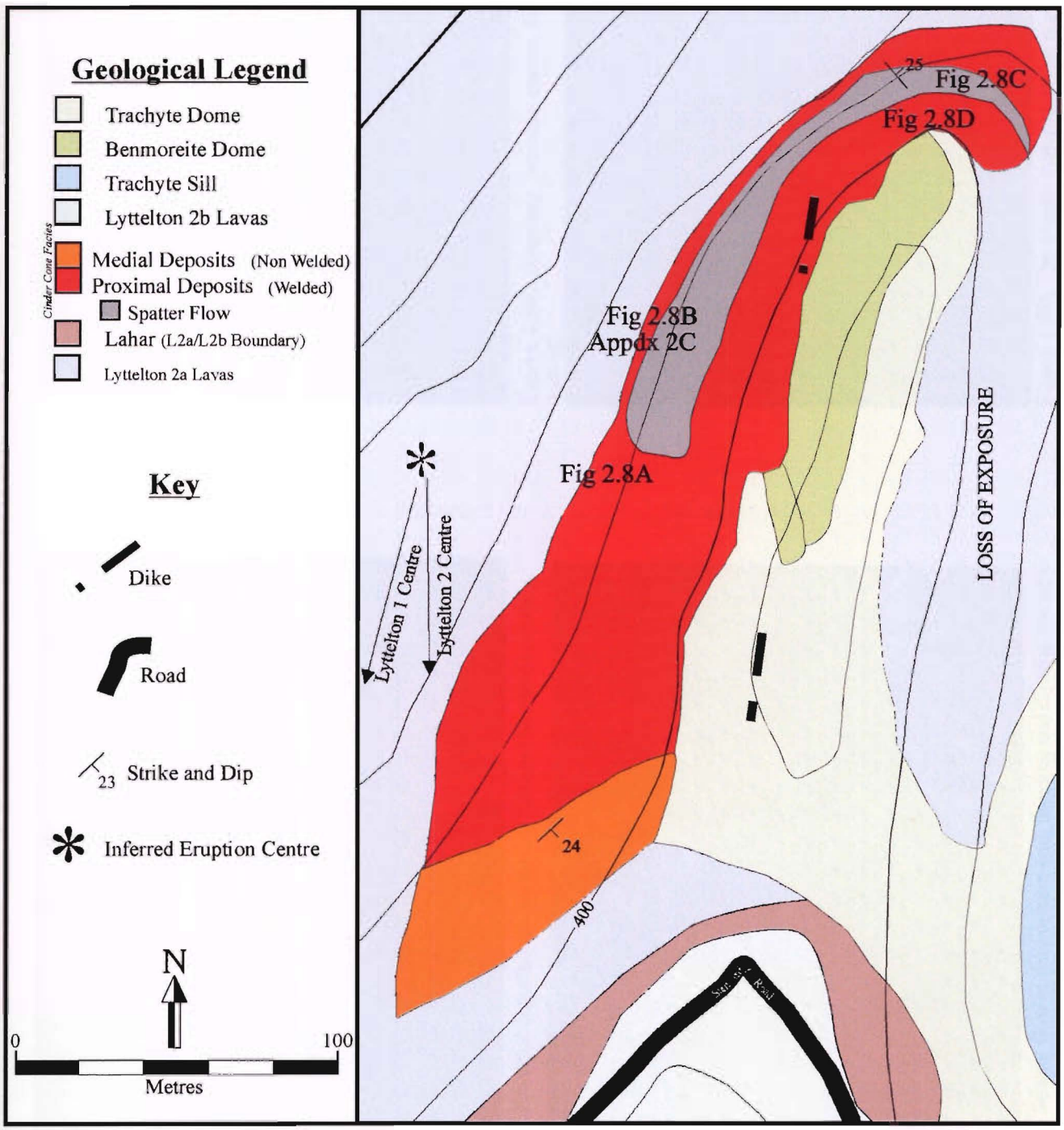

Figure 2.7. Distribution of pyroclastic units in the Castle Rock area (geology after Fitzgerald (1991) and Neumayr (1998).

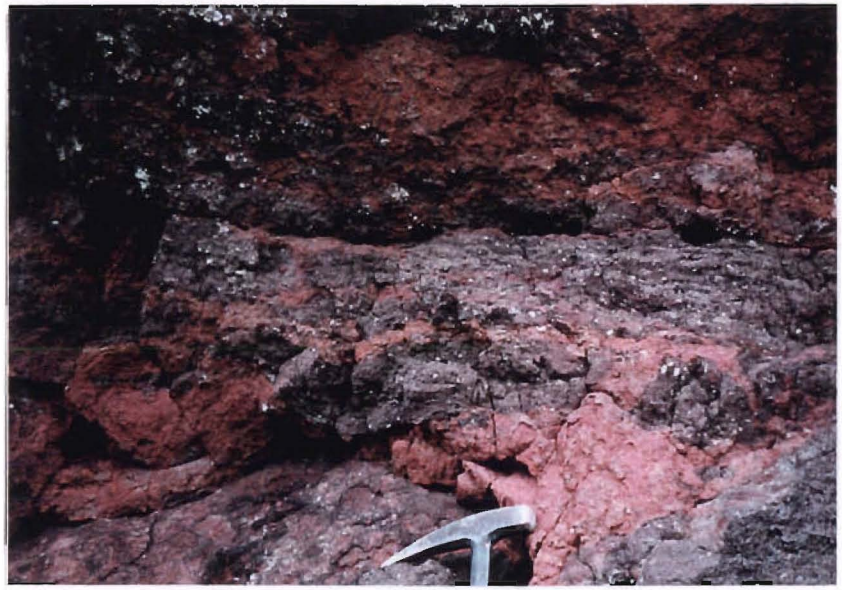

Figure 2.8A. Proximal deposits with spatter and flattened bombs dominating.

Figure 2.8C. Spatter flow at the northern end, thinning and dipping towards the north at 25°.

Figure 2.8B. Boundary between spatter flow and underlying pyroclastic material.

Figure 2.8D. Pyroclastic material at the northern end of the area, note the mingling of the benmoreite clasts from the dome structure.

(Figure 2.7). Eruption type was more effusive than explosive, creating a large spatter flow with little pyroclastics. Late stage interaction with the trachyte-benmoreite activity is evident with the presence of benmoreitic material in the pyroclastics.

2.4.4 Witch Hill Scenic Reserve

Pyroclastic deposits are exposed in two areas that are separated by a small valley and cover a total area of 0.5 km^2 (Figure 2.9). Distal deposits are only exposed at the northwestern limit of the area and are weakly bedded (20° NW), composed of fine ash, lapilli and crystals (Figure 2.10A). Medial deposits are found at the northeastern and southeastern edges, consisting of round bombs and blocks (30 cm) (Appendix 2D). Rare large bombs ranging up to 3 m (Figure 2.10B) are found at the top of medial deposits which are in places crudely bedded (22° SE). The proximal deposits contain flattened and non-flattened bombs that range up to 30 cm (Figure 2.10C) and are 'cavernous' (Figure 2.10D). A small spatter flow outcrops in the proximal deposits and dips at 25° to the north-east. The vent deposits are exposed in a small area on the western central edge and are black and densely welded. The area is cut by one dike that may be related to the pyroclastic activity due to its proximity to the vent material. The eruption centre here is not well exposed but can be inferred by dip directions and outcrop pattern, and would have been located approximately 50 m to the west of the vent deposits (Figure 2.9).

2.4.5 Hoon Hay Park

Hoon Hay Park 1

Pyroclastic deposits outcrop in a small area (0.09 km^2) above the track, with only medial deposits exposed (Figure 2.11). The deposits pinch out to the east but are not seen in the west due to extensive dense bush. However, rare fallen blocks on the track and a red discolouration suggest that the deposits also pinch out to the west. Outer medial material is found at the northern edge of exposure (Figure 2.12A) and consists of yellow, bedded (23° N) bombs (15 cm) and lapilli. To the west deposits change into an orange bomb-dominated unit with bomb layers crudely bedded in places (22° NW). Bombs vary in form with fusiform, flattened and round shapes, with an average size of about 25 cm (Figure 2.12B) (Appendix 2E). A dike (3 m wide) cuts the deposits and appears related to pyroclastic

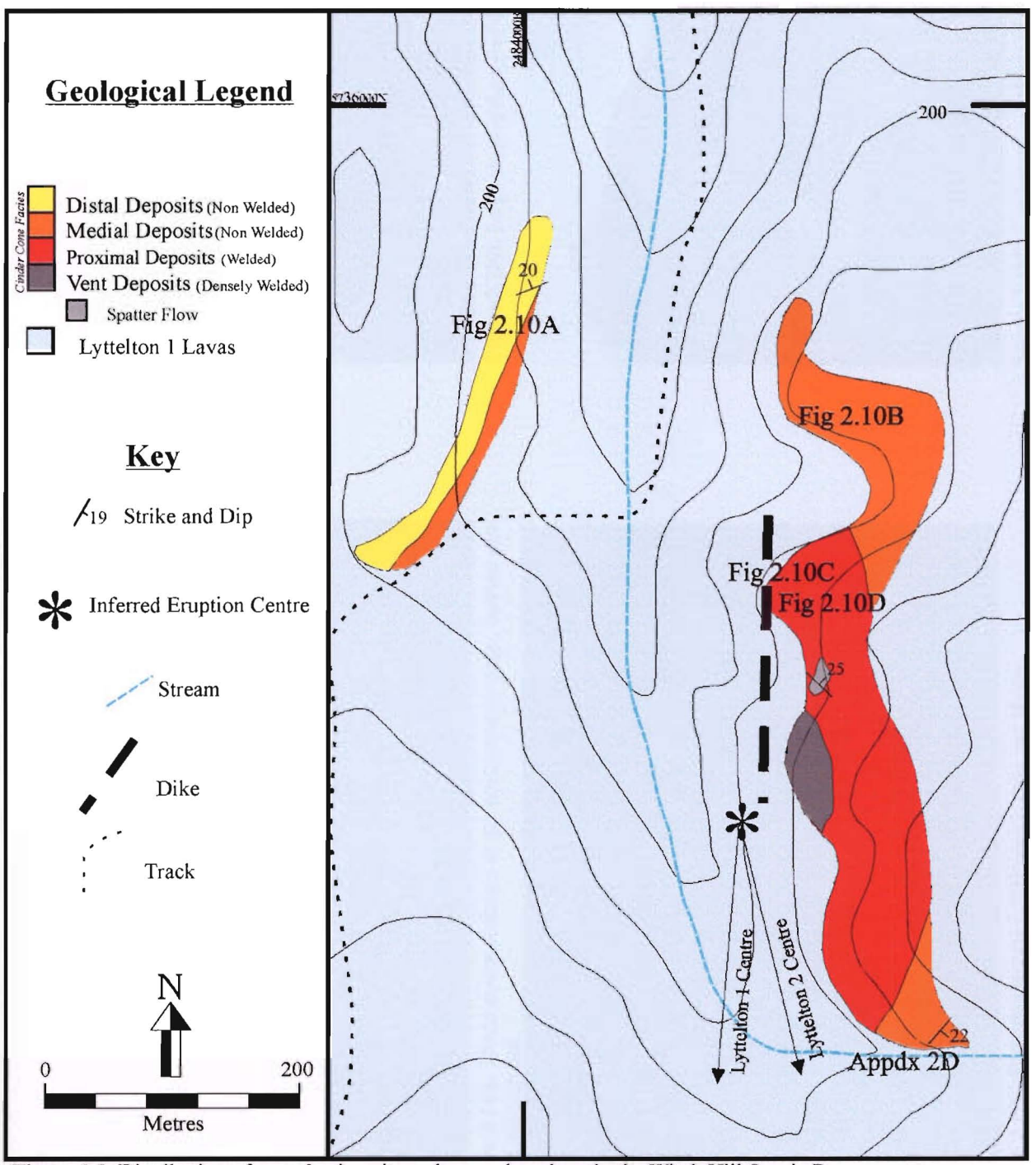

Figure 2.9. Distribution of pyroclastic units and general geology in the Witch Hill Scenic Reserve area.

Figure 2.10A. Distal material found at the northwestern edge, bedded and sorted ash material.

Figure 2.10C. Proximal material, flattened bombs and spatter.

Figure 2.10B. Large block at the top of the medial facies.

Figure 2.10D. Cavernous weathering in the proximal facies.

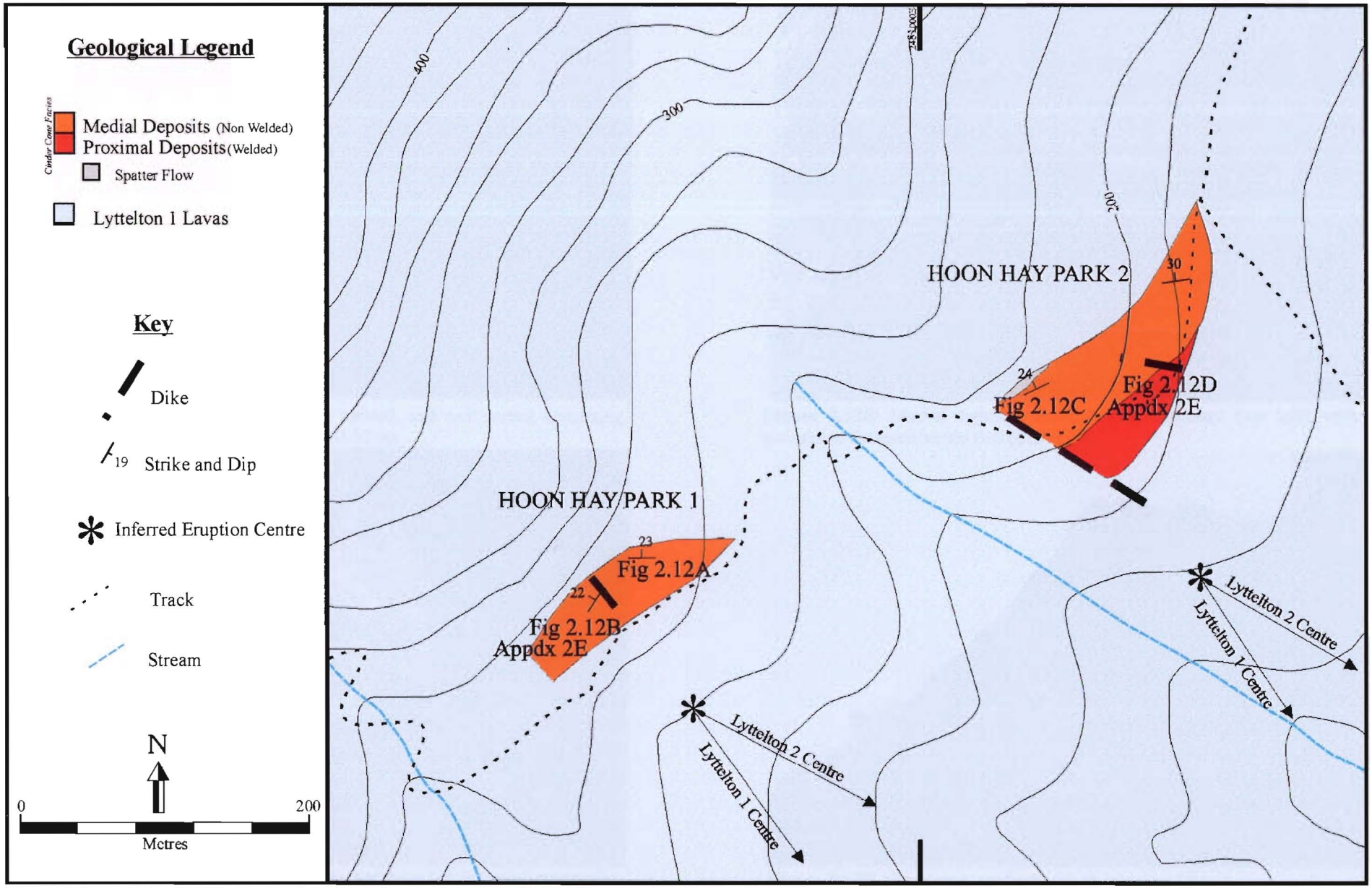

Figure 2.11. Distribution of pyroclastic units and general geology in the Hoon Hay Park area.

Figure 2.12A. Outer medial deposits, bedded, and well sorted, consisting dominantly of lapilli with rare bombs up to 15 cm.

Figure 2.12C. Bedded outer medial deposits. Note the contrast between the weathered area (yellow, due to devitrification) and fresher area (orange).

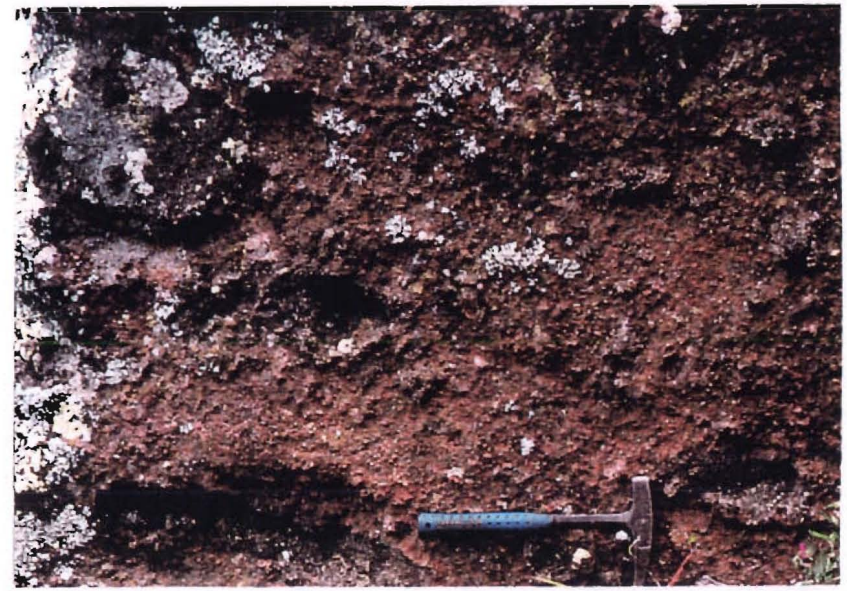

Figure 2.12B. Medial deposits, round bombs dominant (top left), with occasional flattened bombs (left of hammer).

Figure 2.12D. Cavernous weathering in the proximal facies.

activity as it strikes toward the inferred vent area. The eruption centre is difficult to locate, but would have probably been about 100 m to the south-east based on the dips in the area (Figure 2.11).

Hoon Hay Park 2

Pyroclastic deposits outcrop in a small area (0.11 km^2) approximately, 100 m north of Hoon Hay Park 1 (Figure 2.11). Bedded (24° NW) outer medial deposits outcrop at the northwestern edge of the area (Figure 2.12C) with average bomb size increasing down the exposure from 10 – 20 cm. Proximal deposits outcrop in a 'cavernous' area below the medial deposits, located just above the track (Figure 2.12D) and consist of flattened bombs and spatter that range in size up to 30 cm (Appendix 2E). The deposits thin towards the north and disappear near where the track splits. A small lava flow cuts through the medial deposits and is thought to be syn-eruptive. A large dike truncates the deposits and forms a steep cliff, but was emplaced after the pyroclastic activity. The eruption centre is difficult to locate but would have probably been about 100 m to the south, based on the two dips in the area. Due to the proximity of Hoon Hay Park 1 and 2 it seems likely that these cones represent a polygenetic cone that was built over possibly two separate eruptive phases (Figure 2.11).

2.4.6 Northern Gibraltar Rock

The area was mapped and described by Hibberd (1994) with pyroclastic deposits covering an area of approximately 0.5 km^2 (Figure 2.13). Medial deposits dominate the area, consisting of crudely bedded (defining a radial pattern), blocks and bombs (20 – 100 cm in thickness), with average size decreasing from the vent (60 – <10 cm) (Figure 2.14A&B) (Appendix 2F). Dark grey proximal material occurs in isolated outcrops and consists of welded and flattened clasts (Figure 2.14C). Proximal deposits grade into vent deposits with an increase in welding causing clasts to become totally fused and unrecognisable (Figure 2.14D). Hibberd (1994) noted that most of the eastern margin was capped by a spatter flow, however, geochemical analysis has revealed it is trachytic and hence unrelated to pyroclastic activity (see Section 4.2.1). There are several dikes in the area of which three strike toward the inferred vent region (Figure 2.13), and may be related to pyroclastic

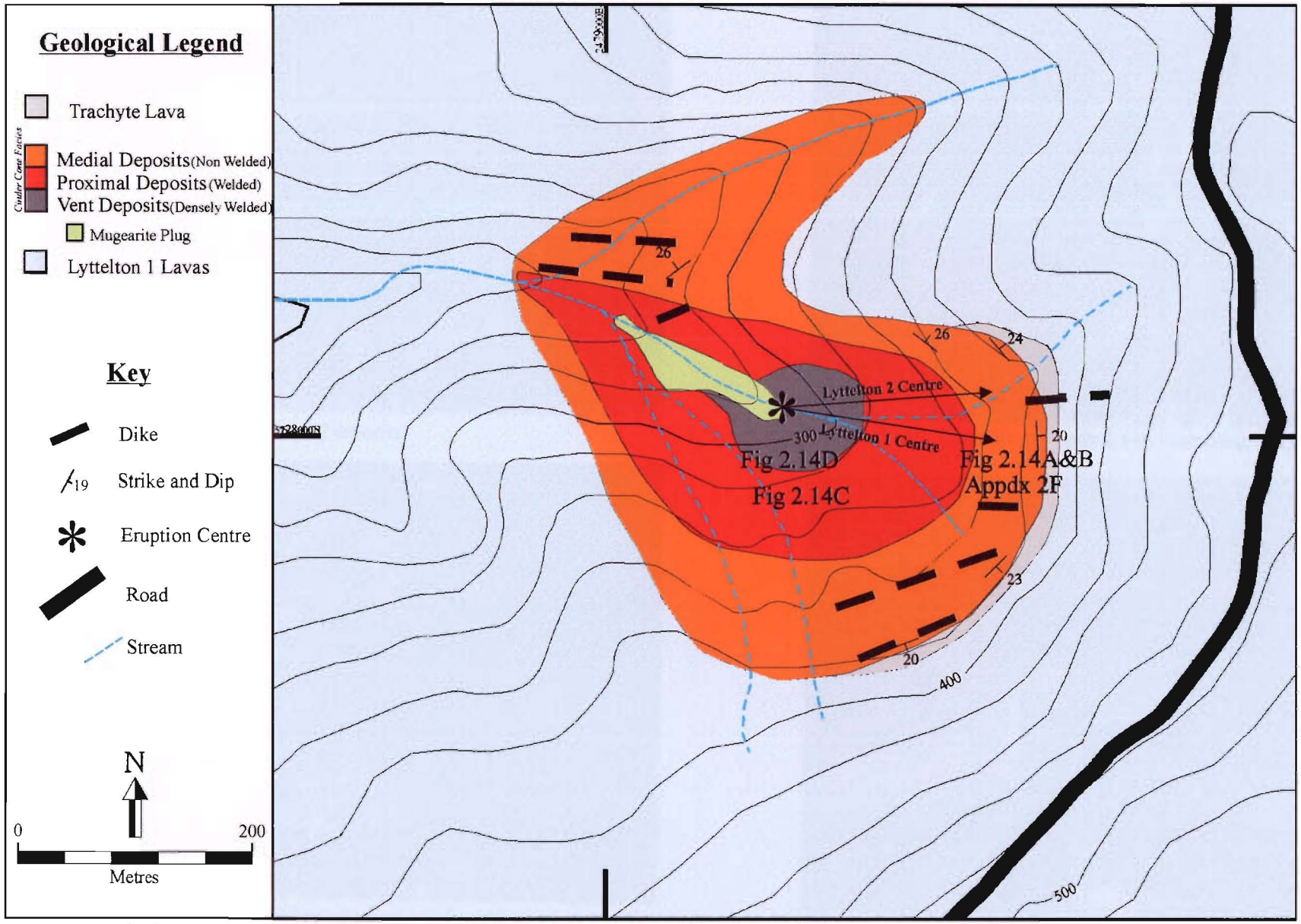

Figure 2.13. Distribution of pyroclastic units and general geology in the Northern Gibraltar Rock area.

Figure 2.14A. Bedded outer medial deposits.

Figure 2.14C. Near vent proximal deposits, clasts still recognisable but becoming densely welded.

Figure 2.14B. Close up of Figure 2.14A, consisting dominantly of small bombs and lapilli.

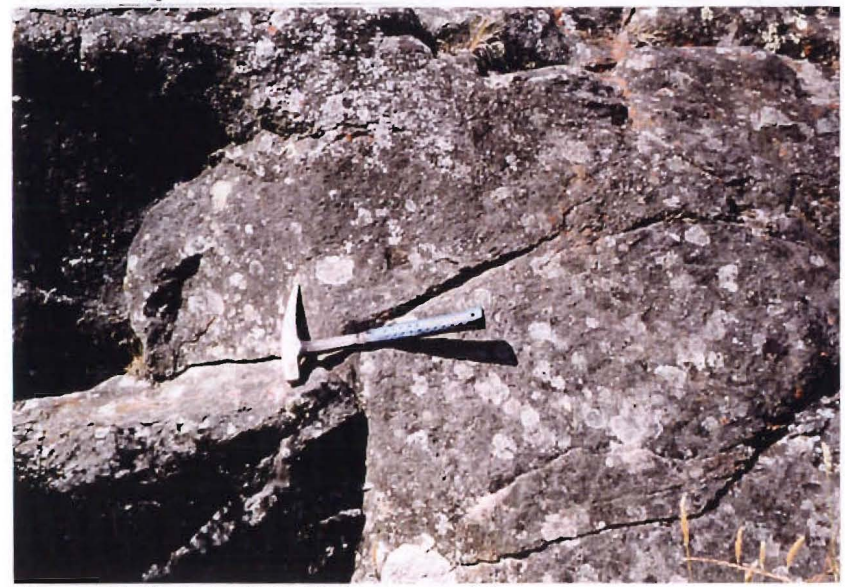

Figure 2.14D. Densely welded vent material.

activity. The eruption centre is located in the centre of the deposits based on outcrop patterns and dips in the area. A mugearite plug exposed in the centre of the vent area in a deeply eroded gully is interpreted to have fed deposits (Figure 2.13).

2.4.7 Southern Gibraltar Rock

The pyroclastic deposits of this area were mapped by Hibberd (1994), however due to poor exposure were not fully described as Northern Gibraltar Rock. Hibberd's (1994) interpretation was that pyroclastics outcropped in a circular area of 0.5 km^2 (Figure 2.15) with only distal and inner rim (due to inward dips) deposits present. Caution needs to be applied to this description as both dips appear to have been caused by secondary processes (eg. erosion). The exposure of the deposits was also found to be less extensive and isolated to one valley side (eg. 0.25 km^2) due to extensive dense vegetation. It would appear that Hibberd (1994) based his distribution on the assumption that the area was similar to the Northern Gibraltar Rock site, with the vent located very near the inward dipping dips. However medial deposits occur all along the southern side of the valley and at the southeastern edge consists of bedded (19° SE) lapilli and ash with occasional bombs up to 15 cm. At the top of a small cliff in the middle of the area, bombs (10 – 30 cm) are set in a finer lapilli and ash matrix (Figure 2.16A). Proximal deposits are poorly exposed but can be seen at the bottom of the cliff as flattened bombs and spatter (Figure 2.16B) (Appendix 2G). A spatter flow is also found amongst the proximal deposits that dips 30° to the east (Figure 2.16C). Outcrop of the vent facies is isolated but is seen to grade from the proximal facies, with a increase in densely welded massive black spatter (Figure 2.16D). Four dikes, ranging in width from 0.4-2 m, cut the area of which three may be related as they strike towards the inferred vent region. The inferred eruption centre is located near the northern edge of the vent deposits based on outcrop patterns and dips in the area (Figure 2.15).

2.4.8 Southern Mount Evans

The pyroclastic deposits were mapped and described by Mckenzie (1995) and cover an area of 1 km^2 (Figure 2.17). No vent or distal deposits outcrop in the area, which are dominated by medial deposits consisting of crudely bedded (~24° SE) bombs (fusiform & round) and block beds set in a finer matrix. Bombs up to 1m are found near the vent with < 10 cm found nearer the road. Proximal deposits are found at the northern edge and are

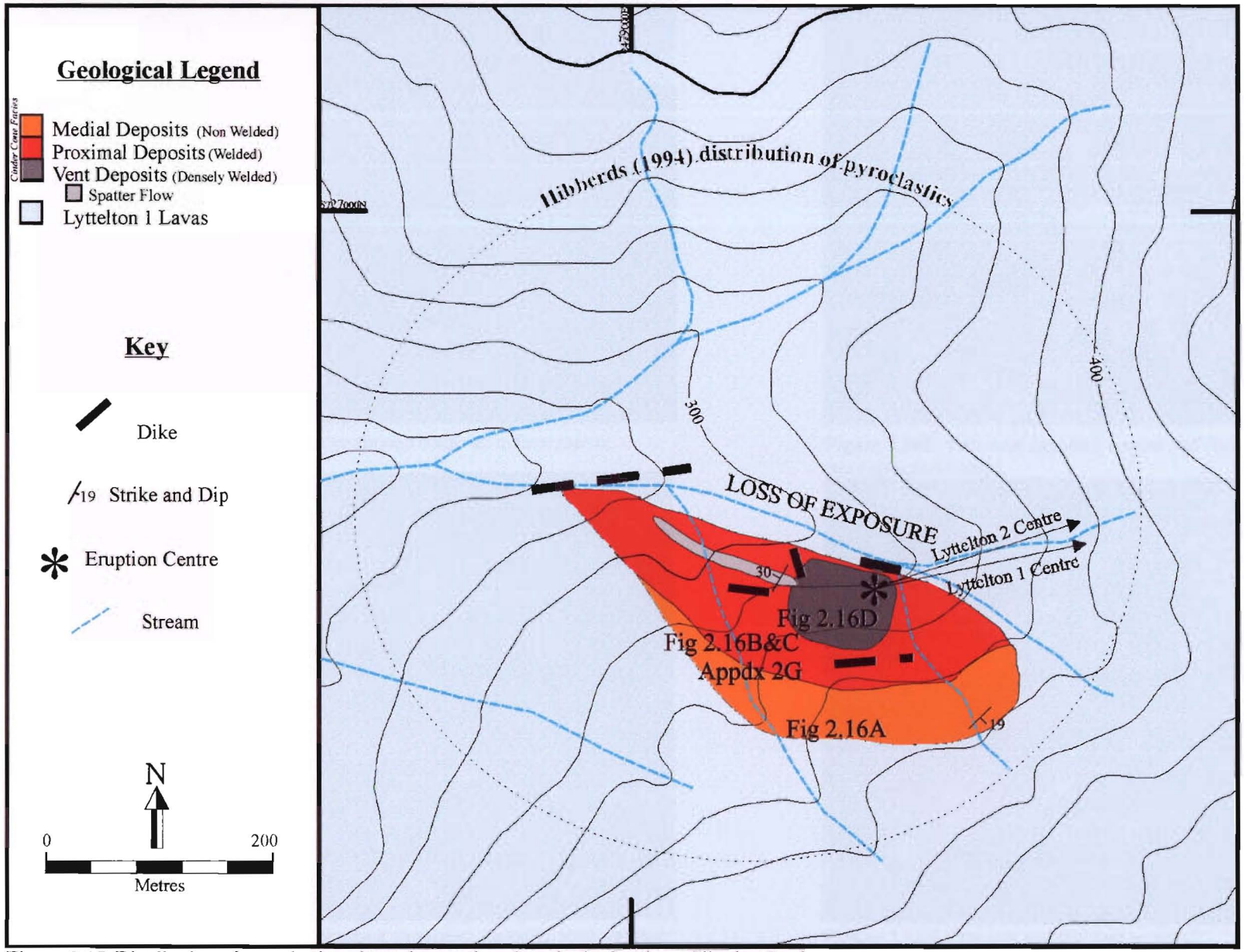

Figure 2.15. Distribution of pyroclastic units and general geology in the Southern Gibraltar Rock area.

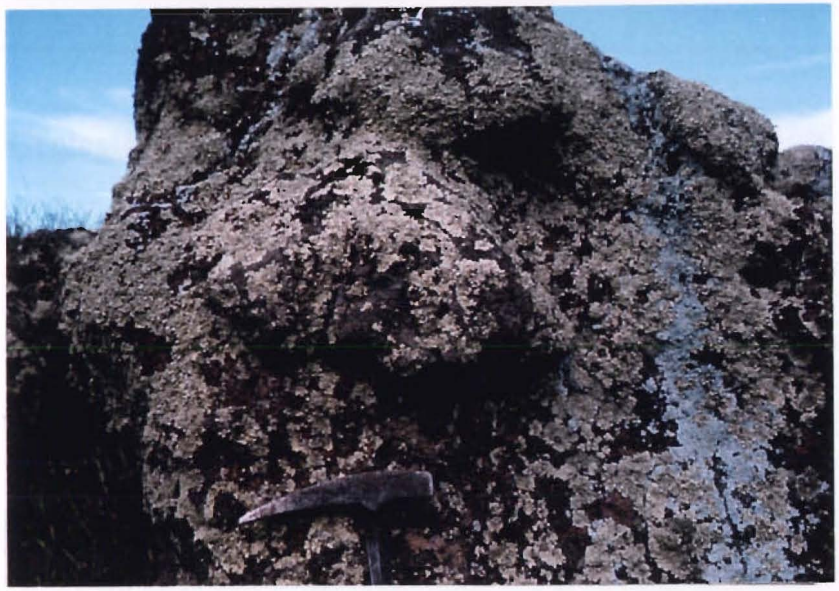

Figure 2.16A. Medial deposits, a large almond bomb set in finer matrix.

Figure 2.16C. Spatter flow set amongst proximal deposits, with crudely bedded medial deposits in the background.

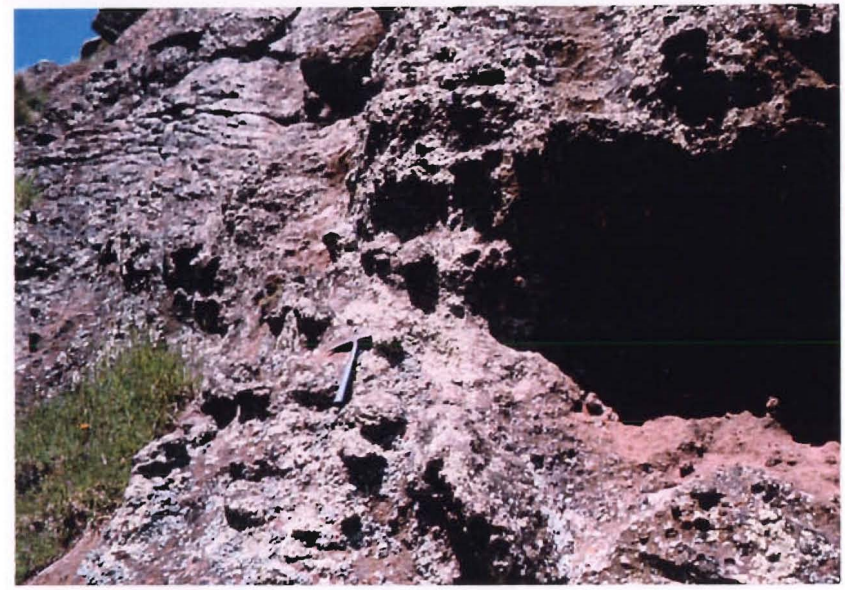

Figure 2.16B. Proximal deposits, spatter and flattened bombs dominate over more spherical bombs.

Figure 2.16D. Densely welded vent material.

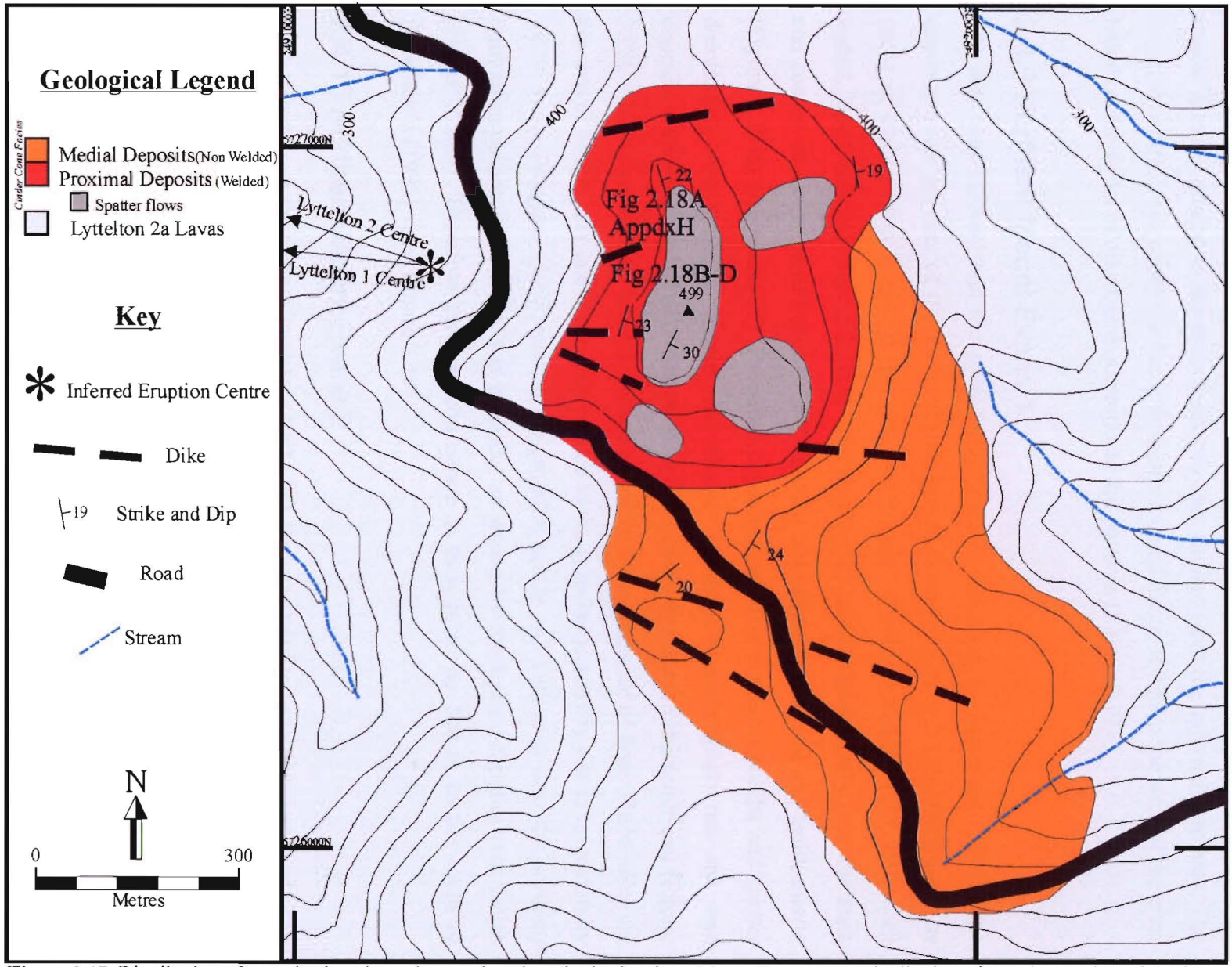

Figure 2.17. Distribution of pyroclastic units and general geology in the Southern Mount Evans area. Distribution of Lyttelton 2a lavas based on Mckenzie (1995).

well exposed in a long open cave (Appendix 2H). Deposits in the cave consist dominantly of flattened and non-flattened bombs set in a finer matrix (Figure 2.18A). Rare bombs range in shape from almond, fusiform, cylindrical and round, with one bomb reaching up to 4 m (Figure 2.18B). The deposits here differ from all the other areas due to the large exposure down the dip slope of the outer wall facies (proximal to outer medial) exposing several spatter flows (Figure 2.18C&D). Numerous dikes cut the area, of which many appear directly related to the pyroclastics as they radiate from the inferred vent area. The eruptive centre is not preserved but is probably located about 300 m to the west of the area, based on the strike of dikes, and outcrop and dip patterns (Figure 2.17).

2.4.9 Northern Mount Evans 1

The area was mapped and the pyroclastic deposits described by Slaughter (1995). The deposits cover an area of 0.8 km^2 with all facies exposed (Figure 2.19). Distal deposits occur at the southern extent of the area and consist of yellow, bedded (19° SW), well sorted, lapilli and ash (Figure 2.20A). Medial deposits outcrop extensively over the area, and consist of a mixture of bedded (24°S) bombs and blocks in a crystal and lapilli matrix (Figure 2.20B) (Appendix 2I). Proximal deposits consist of flattened bombs and spatter dominating over spherical bombs and blocks. Proximal deposits grade into the vent deposits which are capped by a spatter flow (5 m thick) that dips to the south-east (Figure 2.20C). Vent deposits are densely welded and have the appearance of lava. Three dikes cut the area of which only one is possibly related to the pyroclastic activity due to its proximity to the vent. Slaughter (1995) placed the eruption centre and vent area near the northern limit of exposure, however this is incorrect as shown by the inward dipping vent facies (Figure 2.20D). Therefore the eruption centre is thought to be 100 m to the south of Slaughter's (1995) vent (Figure 2.19).

2.4.10 Northern Mount Evans 2

This area was mapped by Slaughter (1995) but the pyroclastics were not described. The deposits cover an area of 0.7 km^2 and are located above a thick lava flow that creates a steep sided gully (Figure 2.21). Exposure is limited with most of the central region eroded out. Distal deposits are numerous in the southeast and consist of a yellowish, well-bedded (20 - 25° SE), well-sorted, lapilli, crystal, and ash unit that has rare bombs ranging in size

Figure 2.18A. Proximal deposits, spatter and flattened bombs dominating.

Figure 2.18C. Spatter flows capping the top of the proximal deposits.

Figure 2.18B. Very large bomb, approximately 2m long and 4m wide, found in proximal deposits.

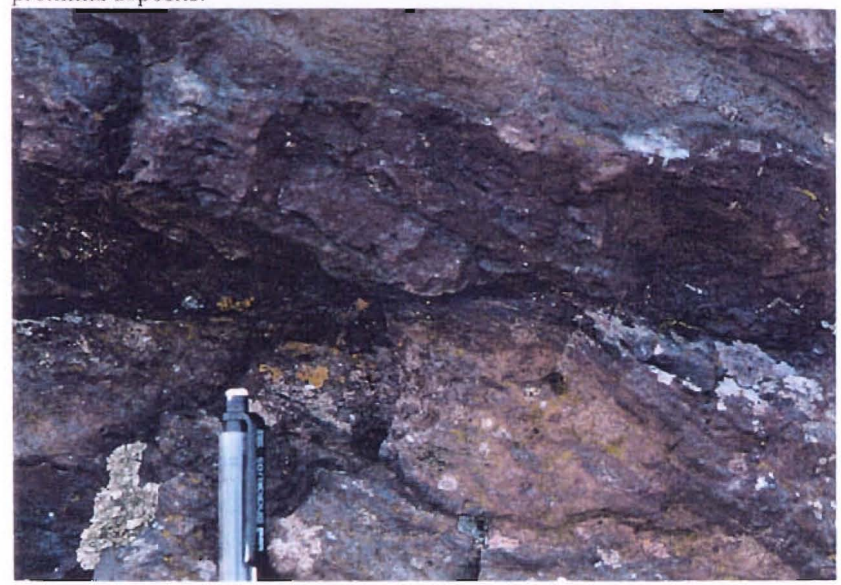

Figure 2.18D. Close up of the spatter flow in Figure 2.18C.

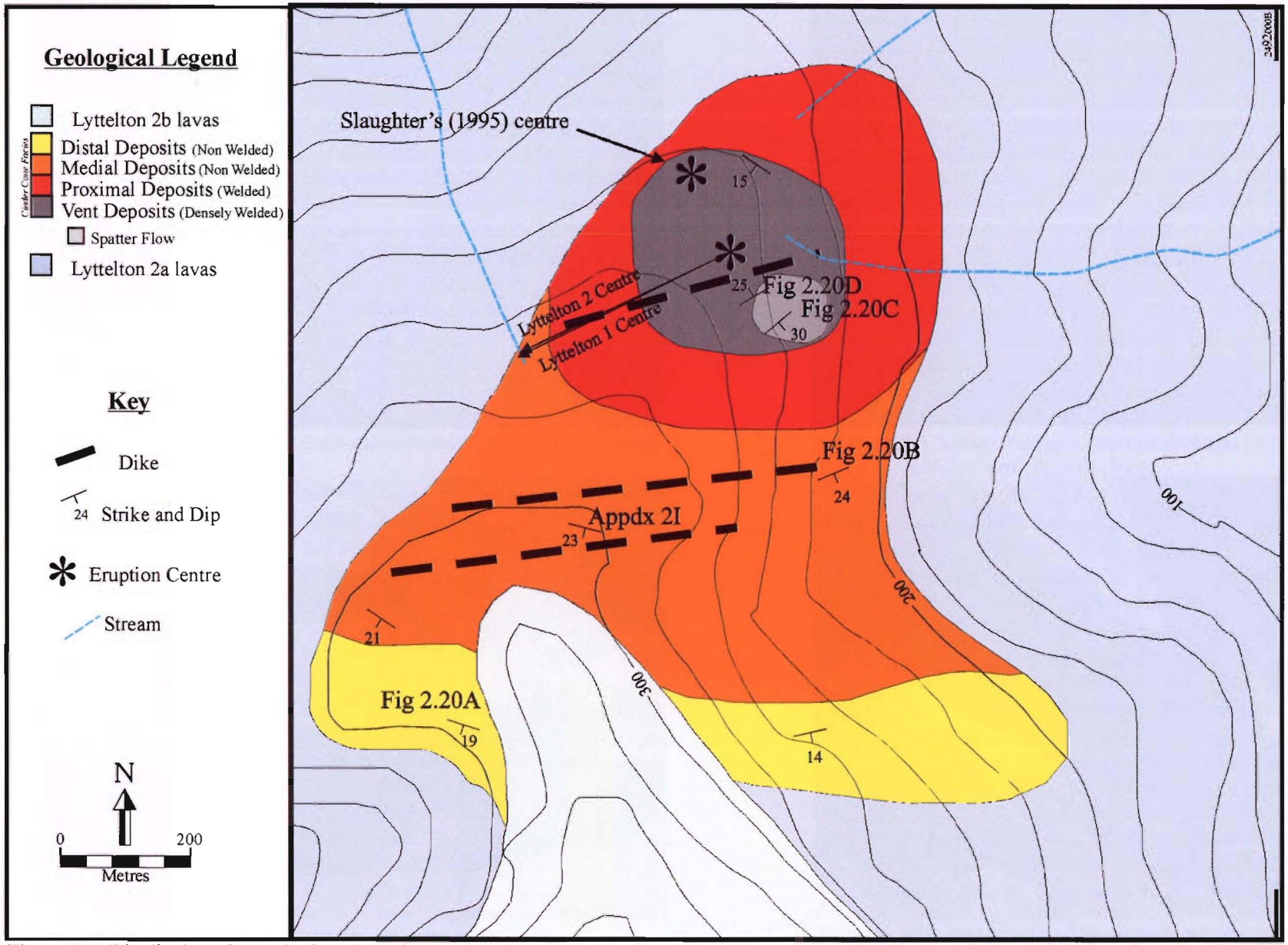

Figure 2.19 Distribution of pyroclastic units and general geology in the Northern Mount Evans 1 area. Distribution of L2a and L2b lavas based on Slaughter (1995).

Figure 2.20A. Distal deposits, bedded and well sorted, composed dominantly of ash and lapilli.

Figure 2.20C. Spatter flow capping proximal deposits.

Figure 2.20B. Medial deposits composed of bombs (< 10 cm) set in a matrix of lapilli and small crystals (1 cm).

Figure 2.20D. Vent deposits, dark grey, densely welded and dipping inward towards the inferred vent area.

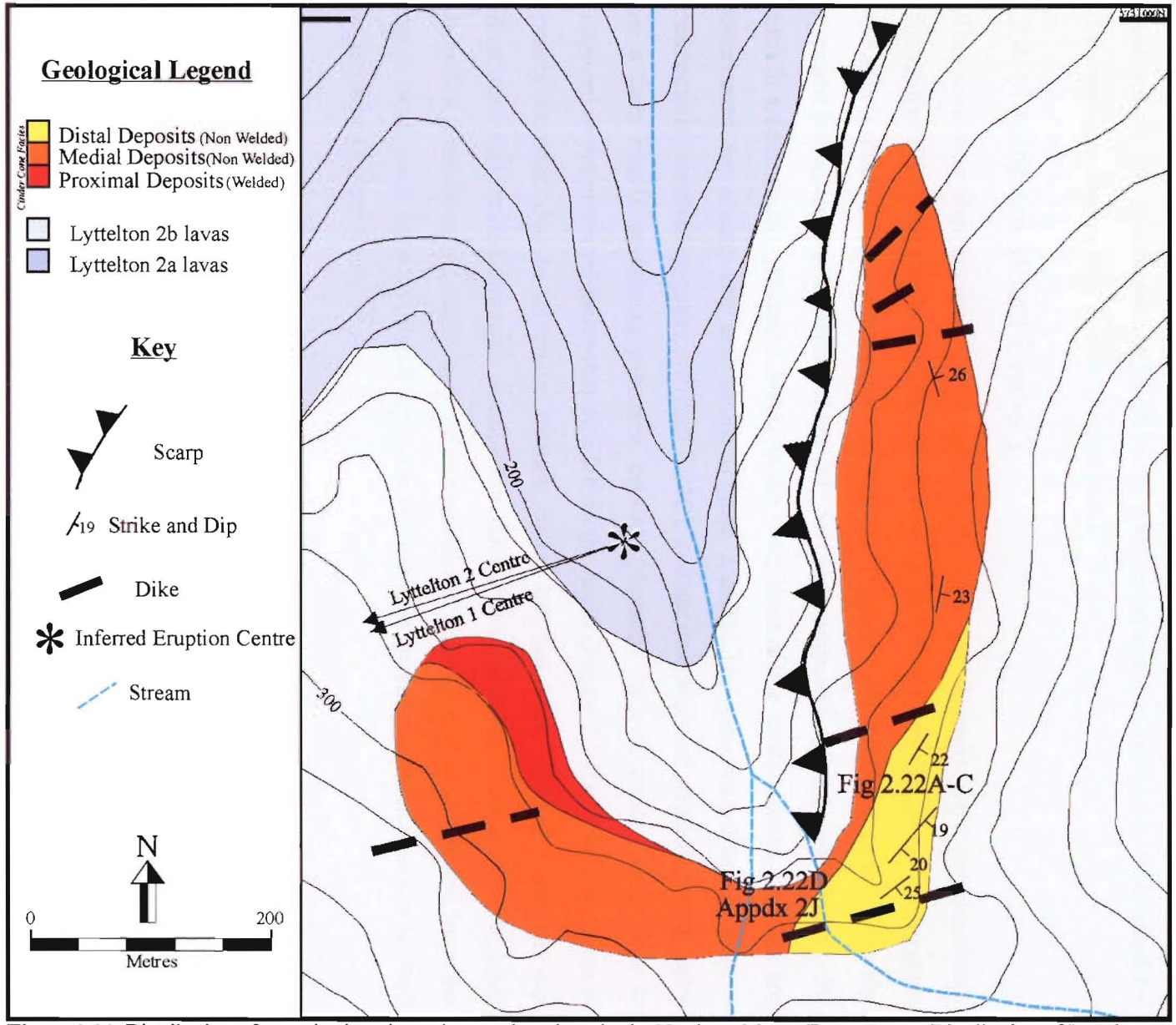

Figure 2.21. Distribution of pyroclastic units and general geology in the Northern Mount Evans 2 area. Distribution of Lyttelton 2a and 2b lavas based on Slaughter (1995).

up to 25 cm (Figures 2.22A-C). Medial deposits dominate the area and are best exposed in a small gully in the central southern region where they are seen to unconformably overlie an aphyric lava (Figure 2.22D) (Appendix 2J). The pyroclastics, that are in contact with the underlying lava are fine grained, but quickly grade upwards into a massive unit dominated by bombs (20 – 40 cm) in a fine matrix of crystals, lapilli and ash. Medial deposits in other parts are massive, consisting of bombs (< 50 cm) set in a finer matrix. On the western side, deposits consist of welded spatter that grades upwards into medial bomb and block deposits that are poorly exposed. The area is cut by five dikes, of which only the three in the north maybe related to the pyroclastic activity due to their strike toward the inferred vent region. No vent facies are found in the area but an eruption centre can be inferred by dip directions and outcrop pattern (Figure 2.21).

2.4.11 Northern Mount Evans 3

This area was also mapped by Slaughter (1995) but the deposits were not described. Slaughter (1995) had the deposits occurring over an area of 0.5 km^2 but this study suggests the area is much smaller and confined to 0.25 km^2 (Figure 2.23). Medial deposits are rarely exposed but when seen are well bedded (21° SE) and composed of bombs and blocks (~30 cm) in a finer matrix (Figure 2.24A). At the outer limit of the medial facies, deposits are dominated by coarse ash and lapilli (Figure 2.24B). The proximal deposits have a 'cavernous' weathering pattern (Figure 2.24C), and are composed of small-flattened clasts in a finer matrix containing pyroxene crystals (Apendix 2K). A small spatter flow is exposed in the proximal facies that dips 29° to the south (Figure 2.24D). The vent facies is poorly exposed due to extensive tussock cover, but has been inferred based on dip directions and limited outcrops. Small dikes throughout the deposits are inferred to have been fed from the cone, due to they strike towards the inferred vent area. Viewed from the north the deposits have an overall dip to the northeast, suggesting the vent area was located to the west (Figure 2.23).

Figure 2.22A. Distal deposits, consisting of lapilli, and small plagioclase crystals (1 cm).

Figure 2.22C. A rare large bomb in the distal facies.

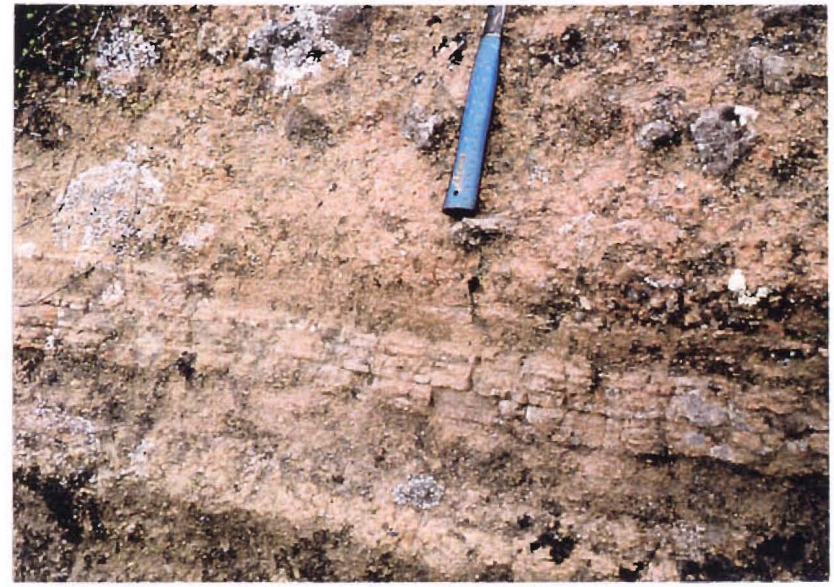

Figure 2.22B. A distinctly fine ash bed in the distal facies.

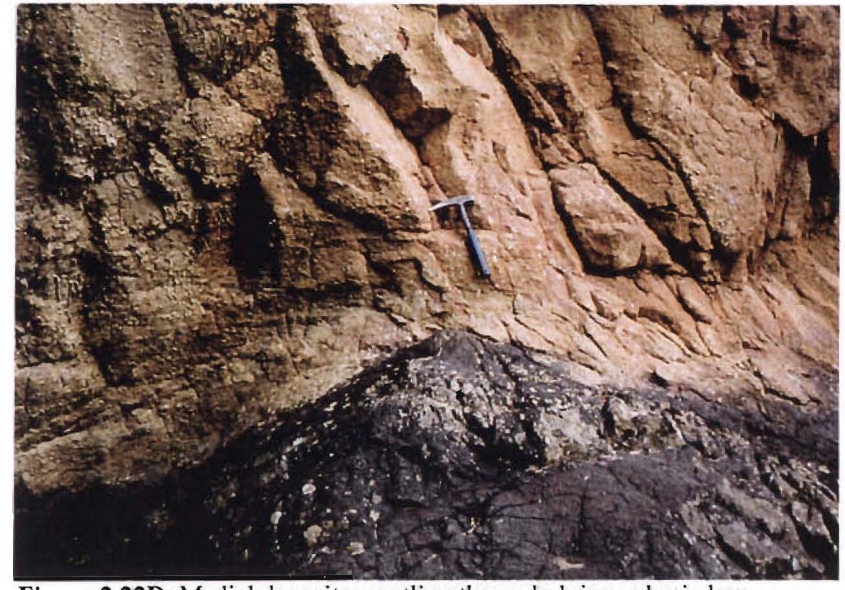

Figure 2.22D. Medial deposits mantling the underlying aphyric lava.

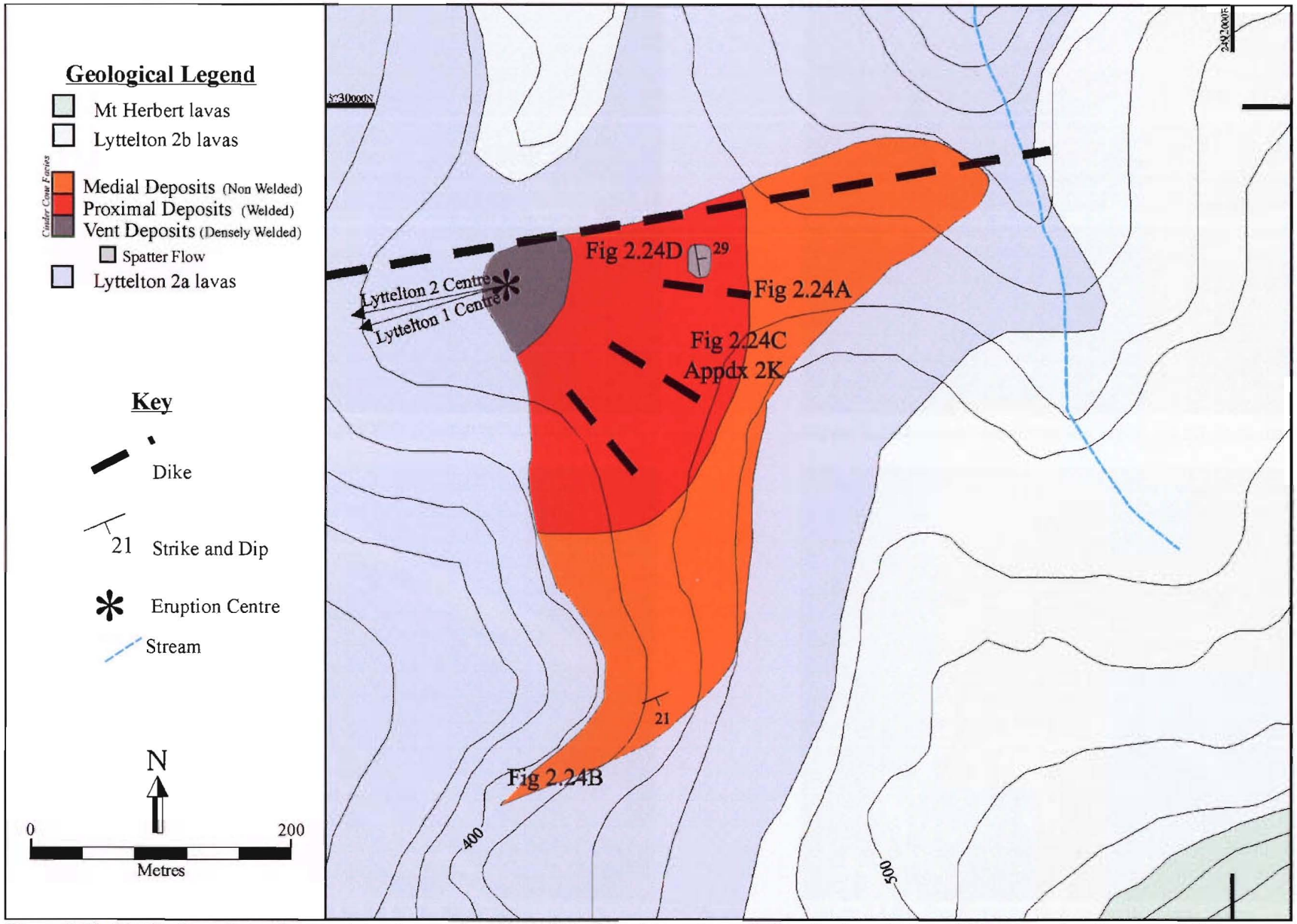

Figure 2.23. Distribution of pyroclastic units and general geology of Northern Mount Evans 3. Distribution of L2a and L2b lavas after Slaughter (1995).

Figure 2.24A. Medial deposits, elongate ribbon bomb set in a finer matrix.

Figure 2.24B. Outer medial deposits, lapilli and ash dominating over bombs.

Figure 2.24C. Cavernous weathering in the proximal facies.

Figure 2.24D. Small spatter flow in the proximal facies.

Chapter Three

PETROGRAPHY AND MINERALOGY

3.1 INTRODUCTION

Previous studies of the Lyttelton Volcano have generally ignored the petrographic features of cinder cones. Only 3 bombs and 3 tuff samples have been analysed petrographically by previous workers (Table 3.1) who mention cinder cones in their areas (eg. Coates 1976, Sewell 1985, Shearer 1986, Altaye 1989, Hibberd 1994, Slaughter 1995, and Mckenzie 1995). In this study seventy-seven thin sections were examined: 31 from bombs, 16 from proximal samples, 7 from vent areas, 8 from spatter flows, and 15 from distal and medial matrix material. Samples were collected from all the studied cones with sample type dependent on exposure (see Appendix 3 for sample list). Petrographic analysis was completed with a standard Zeiss polarising microscope using the terminology of Shelley (1985b, 1993). Full petrographic descriptions are given in Appendix 4A. Estimation of phenocryst and microphenocryst volume percentages was carried out visually, but an estimation of groundmass component was hampered by the extremely fine grained nature of crystals (cryptocrystalline), as well by staining and/or alteration. As a consequence, some estimates for groundmass phases simply indicate which mineral occurs in greater quantities than others.

All samples contain vesicles, of which percentage estimates were made visually. Nine slides were also re-cut and remounted with a blue epoxy resin. The blue stained slides were then scanned in at 300dpi and imported into and analysed by an 'Image Tool' (see Appendix 4B for full description of methods). This allowed the vesicle percentage to be determined more accurately, giving a comparison for visual estimates, and the results are shown in Appendix 4C. The blue stained slides were selected from the vent, proximal and medial facies. Distal facies could not be evaluated by this technique due to the high amount of secondary mineralisation filling the vesicles.

Table 3.1 List of samples and type of analysis carried out by previous workers on Lyttelton.

Author	No. of Cones	No. of Sample	Sample Type	Geochem	Petrography
Slaughter (1995)	3	2 samples	Bomb		46
			Dike cutting cone	26976A	19b
Mckenzie (1995)	1	2 samples	Dike cutting cone	27043A	CM43
			Dike cutting cone	27037A	CM32
			Spatter Flow	27039A	CM18
			Bomb		CM53
Hibberd (1994)	2	3 samples	Dike feeding cone	26319A	181
			Bomb	26321A	238
			Gabbro xenolith	26323A	252
Altaye (1989)	3	5 samples	Crystal lithic tuff		M36B3205
			Crystal lithic tuff		M36B5751
			Crystal lithic tuff		
			Crystal lithic tuff		
			Crystal lithic tuff		
Shearer (1986)	1	1 samples	Distal tuff		C
Sewell (1985)	3	0 samples			
Coates (1976)	5 Horizons	0 samples			

The anorthite content of plagioclase was determined using the Michel-Levy method described in Shelley (1985b). Olivine composition was estimated in low birefringent sections, using 2V angles. Note that 'iron oxides' refers to unidentified opaque minerals, probably Ti-magnetite.

3.2 PETROGRAPHY OF CINDER CONE FACIES

Except in the groundmass, there is little petrographic variation between the facies of cinder cones or between the different sites. The groundmass of distal and medial matrix material consists dominantly of devitrified glass while crystals dominate in the other facies. Groundmass texture variation is discussed next with phenocryst properties and textures discussed in the Mineralogy Section 3.3. Another variation between facies is in the amount and shape of vesicles in the different facies and this will be discussed in Section 3.4.

3.2.1 Distal Facies

Seven samples were collected from the distal facies at Southern Mount Cavendish, Northern Mount Cavendish, Witch Hill Scenic Reserve, and Northern Mount Evans 1 & 2. A yellow to orange hypocrystalline, vitrophyric groundmass dominates all samples. The groundmass is composed largely of devitrified glass with rare areas of unaltered glass surrounding small plagioclase microphenocrysts (hyalopilitic) (Figure 3.1A), Ti-magnetite, clinopyroxene and olivine. Olivine is usually completely altered to iddingsite.

The glass occurs in two forms 1) sideromelane, which is isotropic, transparent and usually yellow-orange in colour, and 2) tachylite that is opaque and partly crystalline (Figure 3.1B) (Fisher & Schmincke 1984, Heiken & Wohletz 1985). Tachylite forms angular lapilli fragments in samples SMC900, SMC901, SMC902, EN27 and EN11, which under high magnification near the edges can be seen to be made up of abundant Fe-Ti oxide crystals that cause its opacity. The plagioclase laths inside the lapilli are orientated in a sub-trachytic to trachytic texture, which also rarely contain olivine and clinopyroxene crystals. Due to the partly crystalline nature of tachylite, it is more resistant to weathering than sideromelane and forms coherent black 'islands' in an orange groundmass. Sideromelane alters to palagonite, a mixture of zeolites and smectite clays (Fisher & Schmincke 1984). The products of this alteration spread into the vesicles which are extensively filled with the

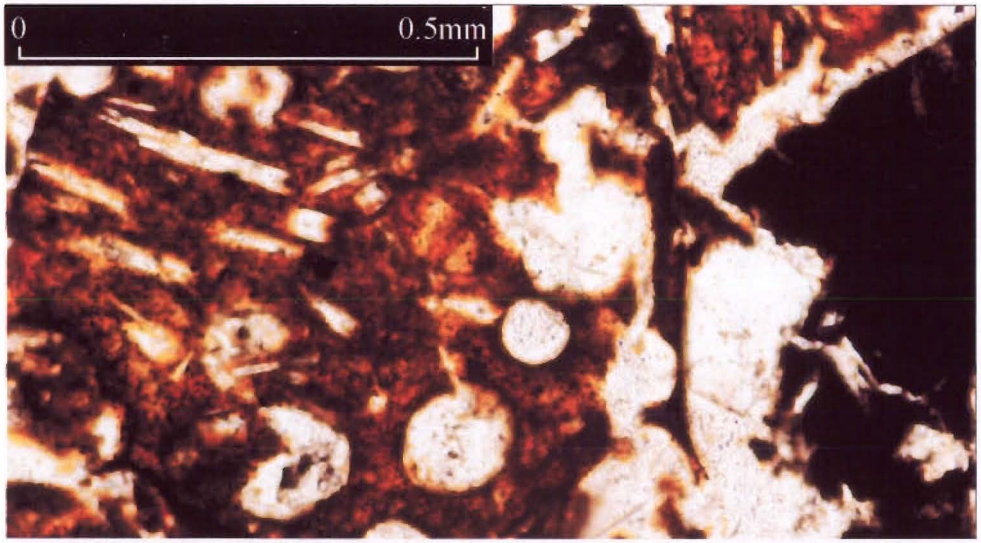

Figure 3.1A. Devitrified glass surrounded by tiny crystals of plagioclase, also note pseudo-cubic chabazite in vesicles (ppl) (Sample SMC9300).

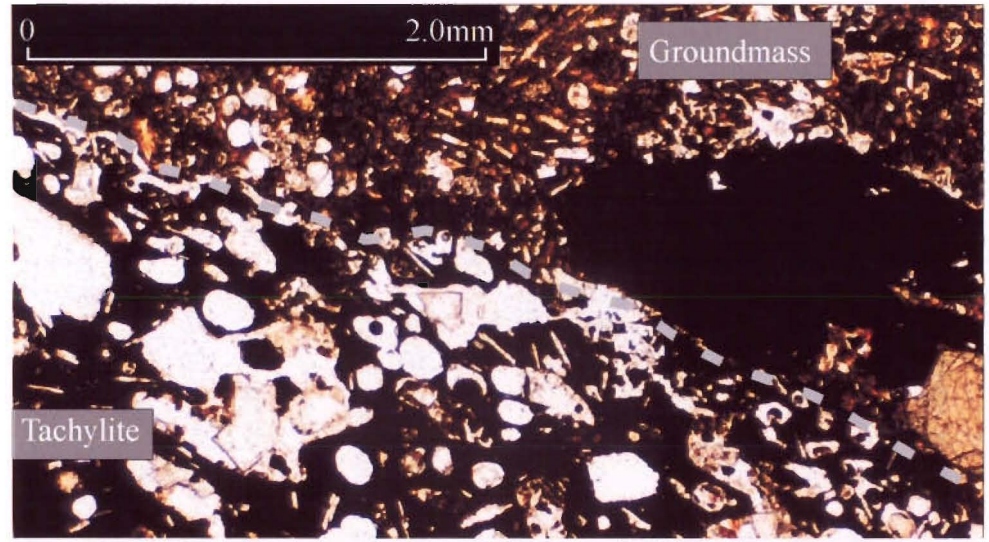

Figure 3.1B. Note the contrast between tachylite lapilli (dark vesicular area, bottom left) and devitrified groundmass. Chabazite in vesicles (ppl) (SMC9300).

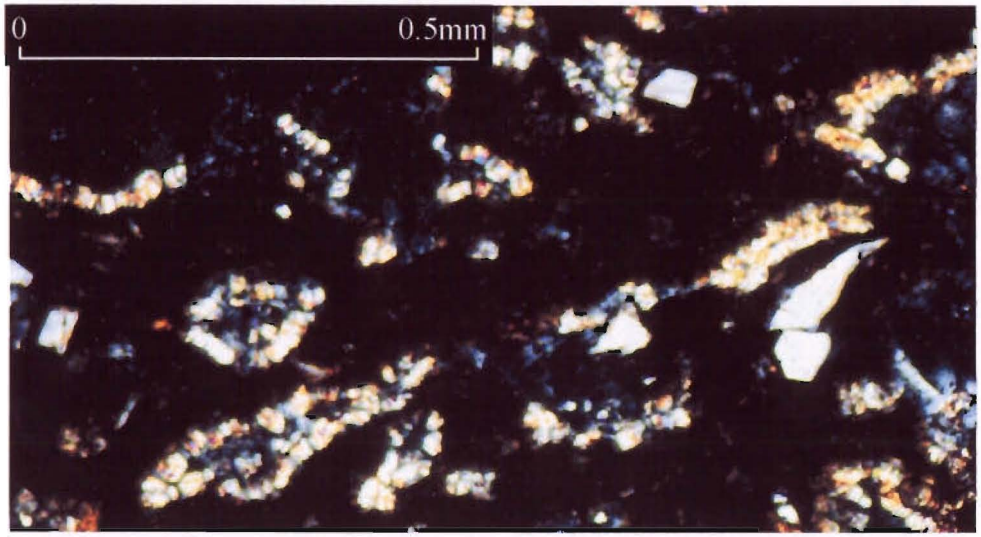

Figure 3.1C. Smectite clays lining vesicles in sample MC21 (xpl).

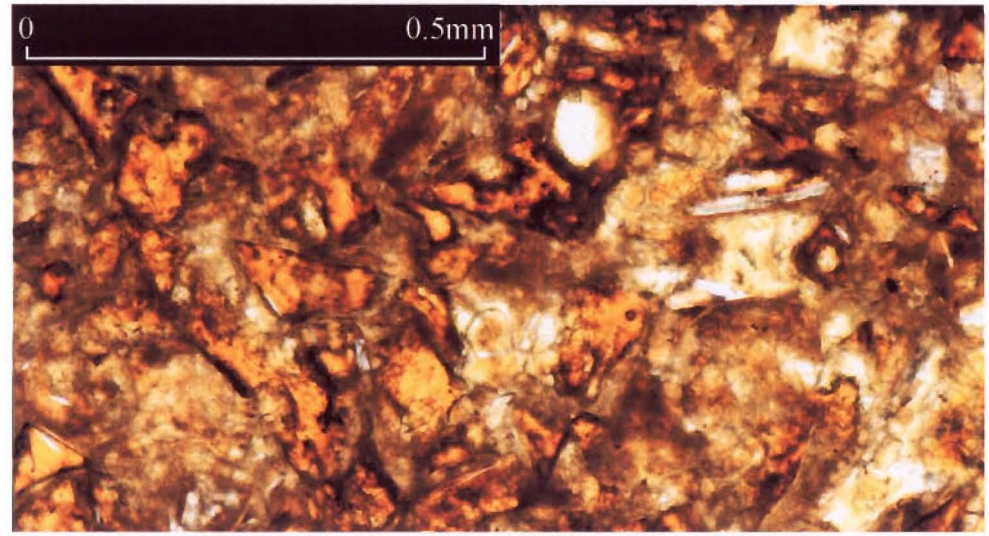

Figure 3.1D. Broken vesicles (shards) in sample WH3a (ppl).

zeolite chabazite, and occasionally smectite clays of the montmorillonite - beidellite series (Figure 3.1C). Vesicles are spherical in shape but in samples SMC9300, SMC9301, SMC9302 and WH3a remnant shards are seen that were formed during deposition or post-deposition compaction (Figure 3.1D).

3.2.2 Medial Facies

Petrography of the medial facies is discussed in two parts, matrix and bombs. Eight matrix samples were collected from Hoon Hay Park, Northern Gibraltar Rock, Southern Mount Evans, and Northern Mount Evans 1 and thirty-one bomb samples from all sites. The groundmass of the matrix of the medial facies is very similar to the distal facies except that there are fewer lapilli and more bombs. The matrix is hypocrystalline and vitrophyric and dominated by sideromelane glass, extensively devitrified. Set amongst the devitrified glass are microphenocrysts of plagioclase (hyalopilitic) with lesser amounts of Ti-magnetite, clinopyroxene and olivine (again altered to iddingsite). Vesicles are extensively filled with chabazite and smectite clays, and are spherical, although in some areas only remnant shards remain (Figure 3.2A). As in the distal facies, the shards would have formed either during deposition or during post depositional compaction.

Bombs are holocrystalline, porphyritic, pilotaxitic and intergranular. Fourteen bombs have a sub-trachytic to trachytic texture, and four bombs (GR13, GR20, ES5, EN20) are aphyric. Microphenocrysts of plagioclase are set in a cryptocrystalline groundmass which appears isotropic, but under closer examination is seen to be made dominantly of small Fe-Ti oxides and other crystals, with little or no glass (Figure 3.2B). These Fe-Ti oxides and other small crystals are arranged in many layers that give the groundmasss an isotropic appearance. Microphenocrysts of plagioclase feldspar dominate basalt and hawaiite bombs, but alkali feldspar is more common in mugearite and benmoreite samples. Ti-magnetite is also present along with clinopyroxene and iddingsitised olivine. Apatite is a common accessory phase. Swallow-tailed plagioclase microphenocrysts are common in all samples (Figure 3.2C). Evidence of magma mingling is found in samples SMC830a, SMC830b, HH2, HH9, GR13, GR16, GR20, ES2, ES5, EN20, EN2, between finely vesiculated mafic magmas and coarsely vesicular felsic magmas (Figure 3.2D). The vesicles in bombs are distributed so that small spherical ones are commonly isolated from larger deformed ones.

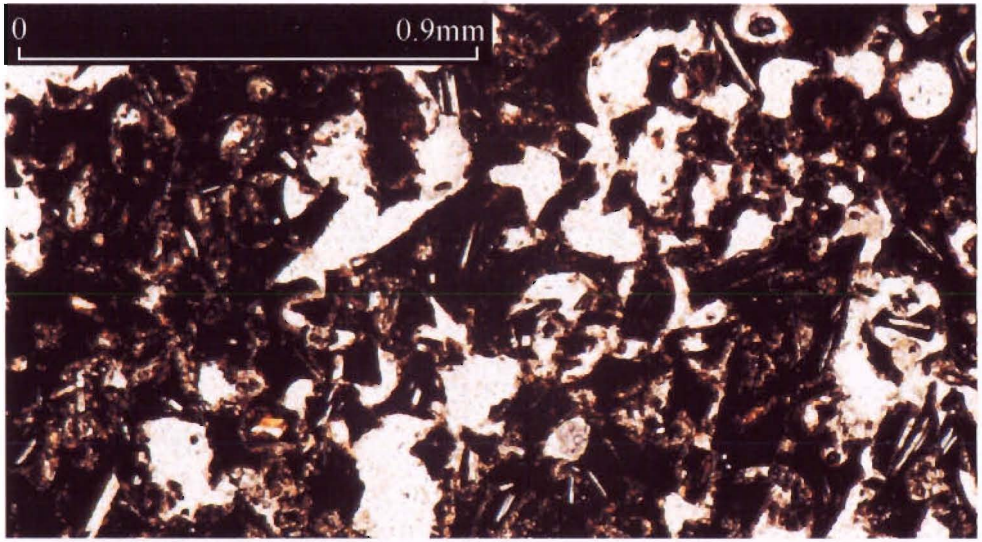

Figure 3.2A. Broken vesicles (shards) in sample EN16 (ppl).

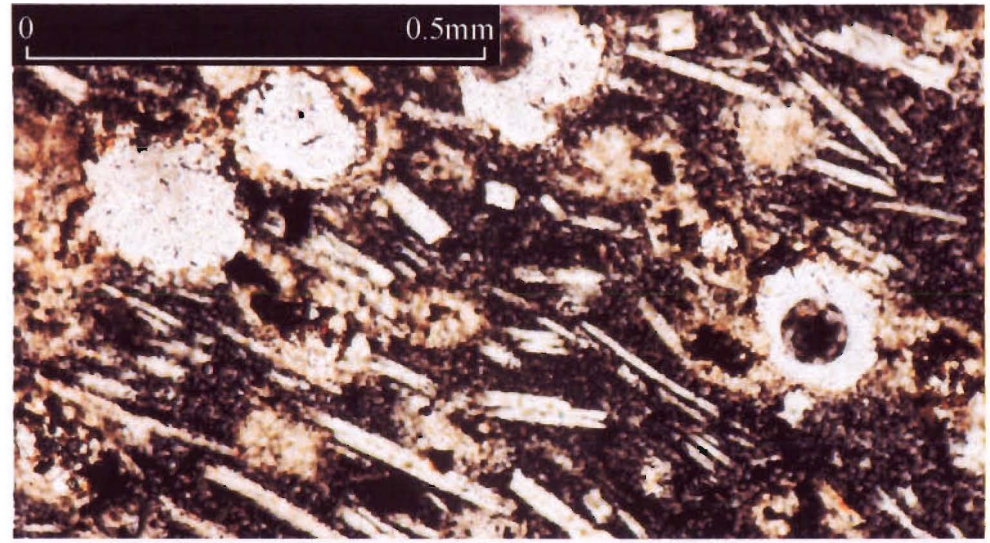

Figure 3.2B. Sample SMC830, that has been cut < 0.3 mm, showing the extremely fine grained nature of groundmass, and abundant Fe-oxides (ppl).

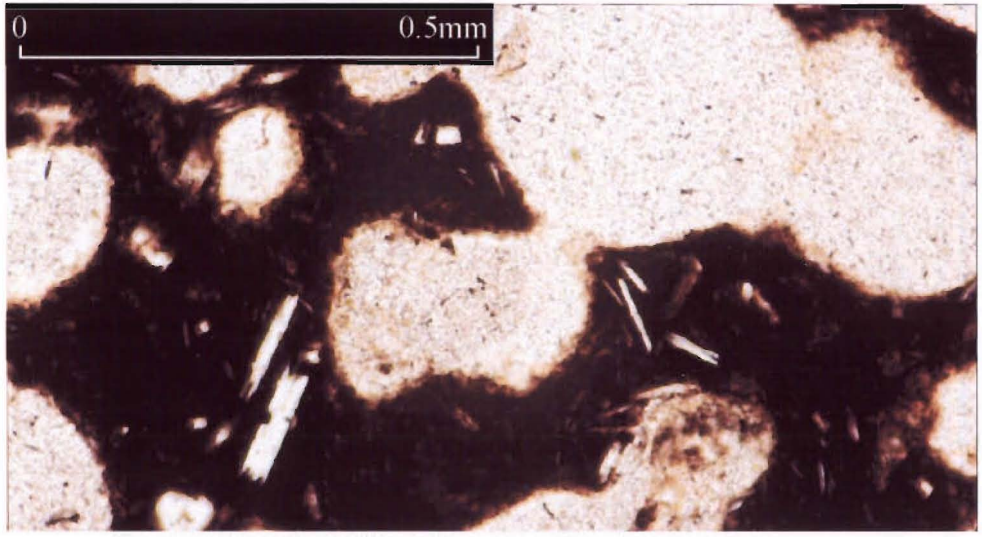

Figure 3.2C. Swallow-tailed plagioclase in sample (MC22) (ppl).

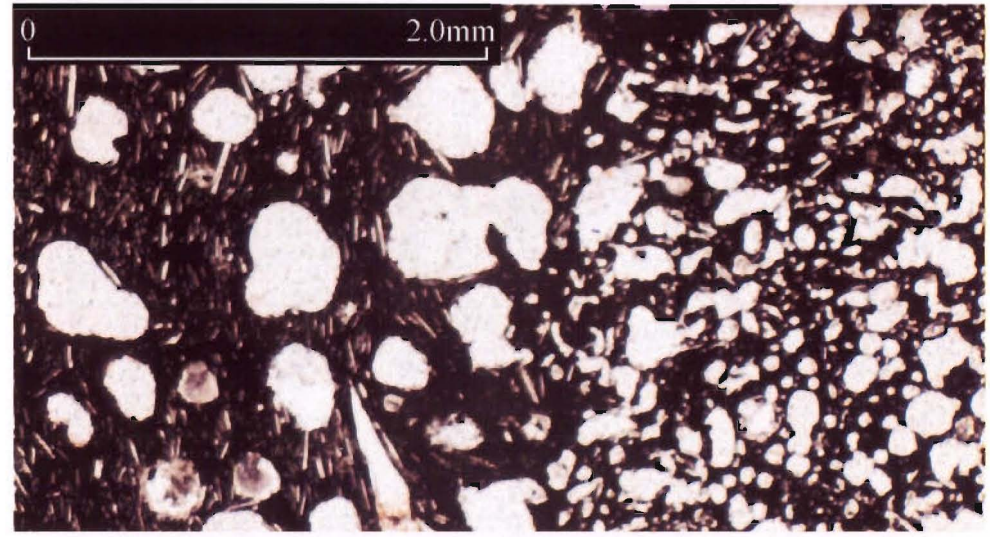

Figure 3.2D. Magma mixing in sample EN20, note the contrast between the felsic coarsely vesicular and mafic finely vesicular areas (ppl).

3.2.3 Proximal Facies and Spatter Flows

Sixteen proximal facies samples were taken from all sites except Witch Hill Scenic Reserve, Southern Gibraltar Rock, and Northern Mount Evans 3. Eight samples from spatter flows were taken from Northern Mount Cavendish, Castle Rock, Witch Hill Scenic Reserve, Southern Mount Evans, and Northern Mount Evans 1.

Proximal facies differ from the medial and distal facies as they consist entirely of fused bombs with no or little matrix supporting the clasts. Therefore, it is not surprising that the proximal deposits are very similar to the bombs in the medial facies. They are holocrystalline, porphyritic and intergranular. Proximal samples however show a complete gradation from pilotaxitic to sub-trachytic to trachytic (Figure 3.3A). The slightly more trachytic texture is due to most samples still being semi-fluid during deposition allowing flow to occur and alignment of the feldspar laths. The groundmass is also very similar to medial bombs with microphenocrysts of plagioclase set in a cryptocrystalline matrix. In some samples, however, the matrix is slightly more crystalline allowing volume percentages to be estimated. Plagioclase and magnetite dominate in the groundmass, although alkali feldspar is present in the mugearitic, benmoreitic samples. Swallow-tailed plagioclase is also common in the proximal facies, and mingling is present as it was in bomb samples, with finely vesicular mafic areas and coarsely vesicular felsic areas (Figure 3.3B)

Spatter flows are caused by high accumulation rates of bombs that mingle and flow down the sides of the cones. Therefore, it is not surprising to find evidence of magma mingling in spatter flows (Figure 3.3C). The vesicles in both proximal samples and spatter flows are irregular in shape due to the fact that most samples are semi-fluid to fluid during deposition causing vesicles to become deformed on emplacement, with only the smallest vesicles remaining spherical (Figure 3.3D).

3.2.4. Vent Facies

Seven vent facies samples were collected, from Southern Mount Cavendish, Northern Gibraltar Rock, Southern Gibraltar Rock and Northern Mount Evans 1. All samples are holocrystalline with little or no glass in the groundmass. Vent facies samples are porphyritic, intergranular with a pilotaxitic to sub-trachytic texture. Vent facies differ from

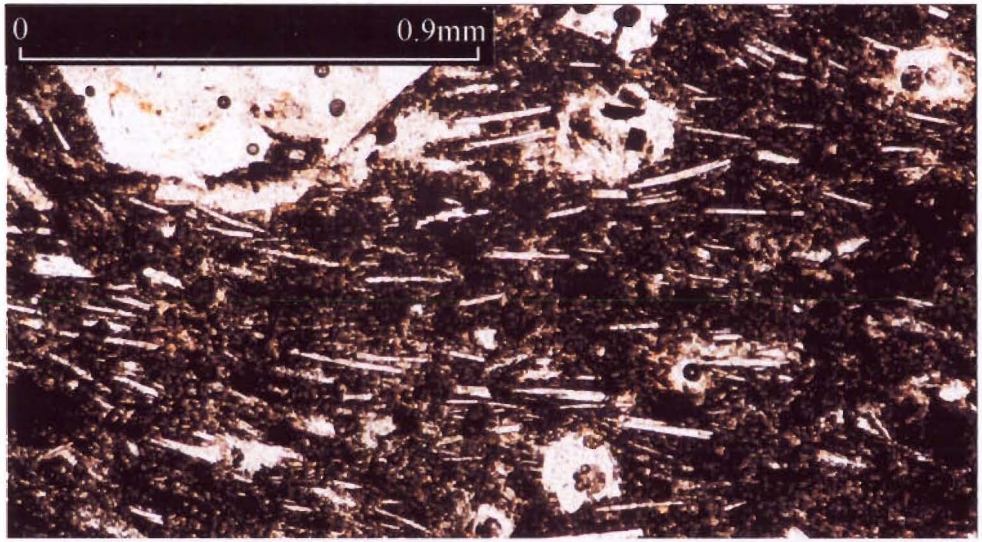

Figure 3.3A. Sample EN19 with a strongly developed trachytic texture (LPO/SPO) (ppl).

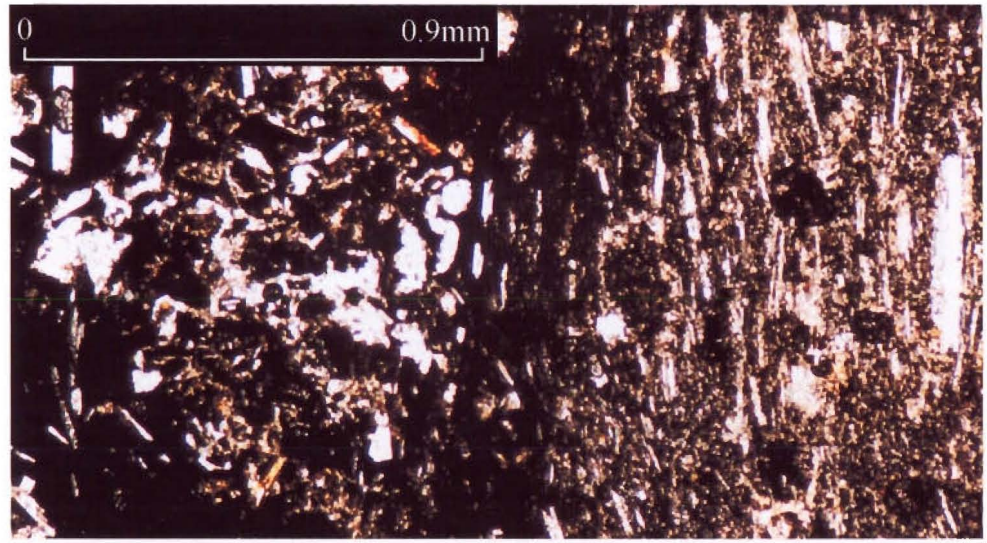

Figure 3.3B. Magma mixing in sample EN19 (ppl).

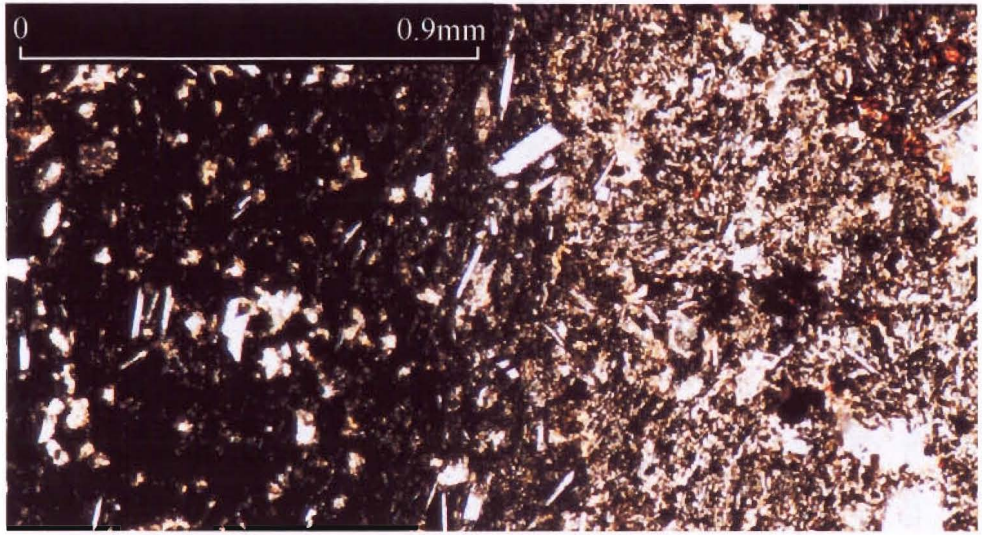

Figure 3.3C. Magma mixing in spatter flow DNS3 (ppl)..

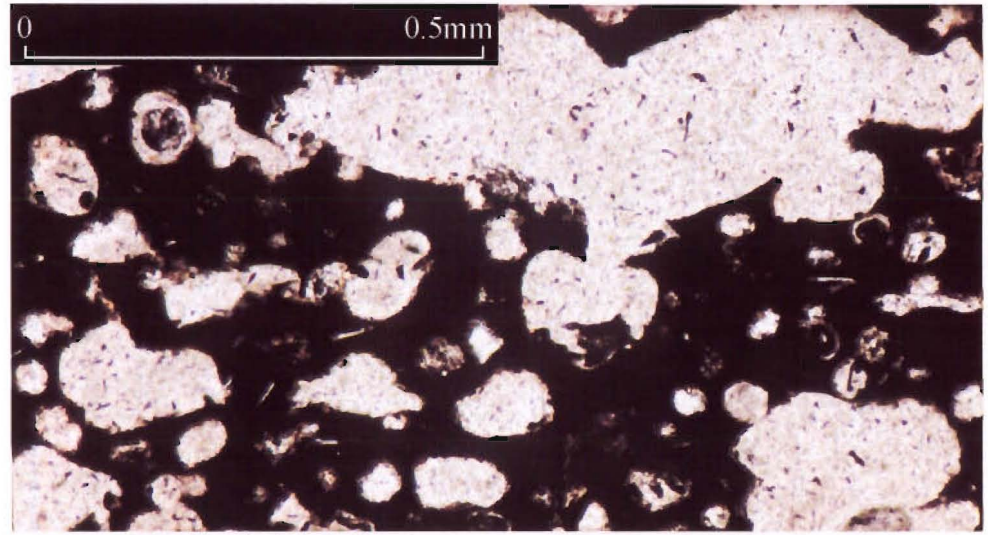

Figure 3.3D. Small isolated spherical vesicles surrounded by larger irregular (deformed) vesicles (ppl) (Sample FE1)..

the bomb samples and most proximal samples in that the groundmass is more crystalline allowing actual volume percentages to be calculated. The groundmass is again dominated by plagioclase with lesser amounts of magnetite, clinopyroxene and olivine. Olivine is heavily altered to iddingsite. Swallow-tailed plagioclase occurs less frequently than in the other facies. Vesicles are rare in the vent facies (Figure 3.4A), due its fluidal nature during deposition which allows secondary degassing. Samples SMC1226, EN26 and EN18 show signs of mingling, with felsic and mafic areas (Figure 3.4B).

3.3 MINERALOGY

3.3.1 Feldspar

Plagioclase feldspar is the dominant phenocryst in all sample types and also dominates microphenocryst and groundmass phases, except in mugearitic, benmoreitic, shoshonitic and latitic samples where alkali feldspar is more common. The anorthite content of plagioclase varies with whole rock silica content, but generally decreases with increased fractionation from basalt to benmoreite (Figure 3.5). Plagioclase crystals in the samples are commonly zoned, sieved and corroded. The variety of textures suggest that feldspar and other phenocrysts of any given sample are not simply the result of crystallisation from a single magma under a specific set of conditions, but must have grown under varying conditions of temperature and pressure and/or have been derived from magmas of different compositions. Therefore a discussion is useful in determining the possible mechanisms that were responsible.

Zoning

Zoning occurs in plagioclase because of the failure of diffusion inside the growing crystal to keep up with changing chemical and physical conditions outside the crystal (Smith & Brown 1988). However for zoning to be preserved, cooling must be sufficiently rapid to prevent further diffusion after growth (Muncill and Lasaga 1981). Zoning is most easily preserved in plagioclase, because of the resistance of plagioclase to solid-state re-equilibration due to the sluggish nature of CaAl – NaSi diffusive exchange at magmatic temperatures (Morse 1979). Zoning is common in all samples varying from normal to normal oscillatory and reverse, with unzoned crystals rare.

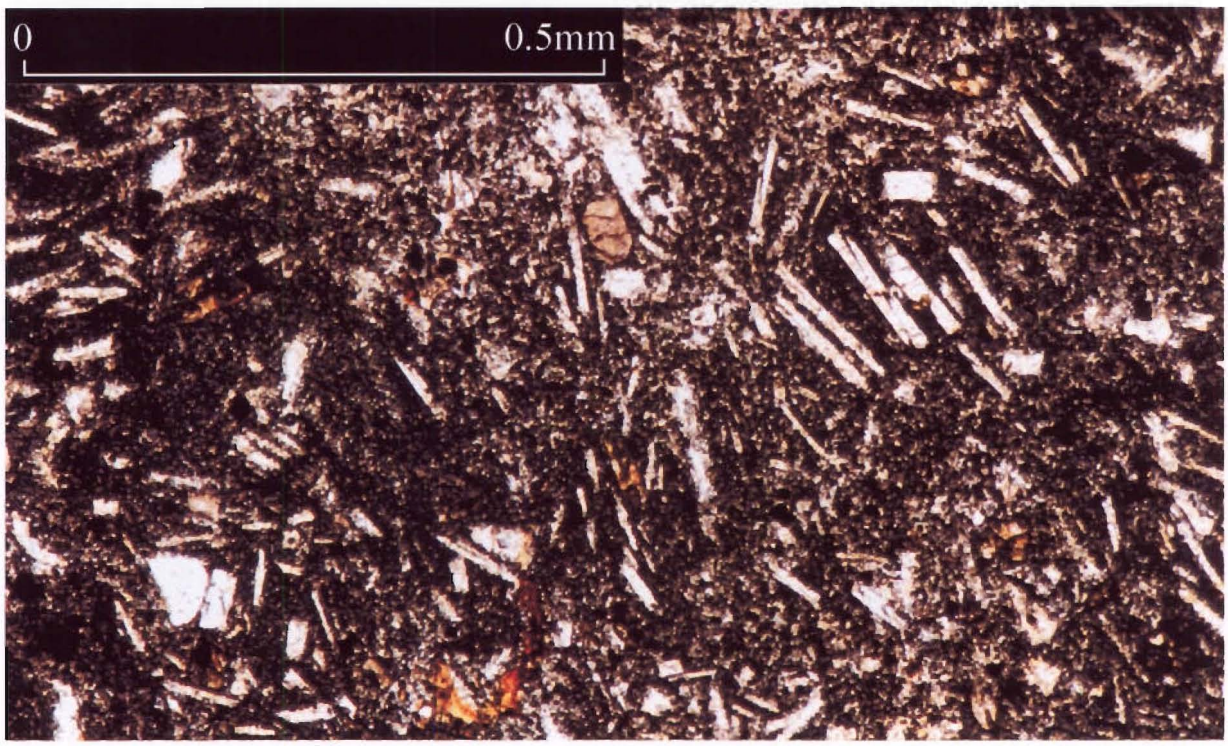

Figure 3.4A. Vent sample MC99, illustrating the extremely low vesicularity and typical groundmass textures (ppl).

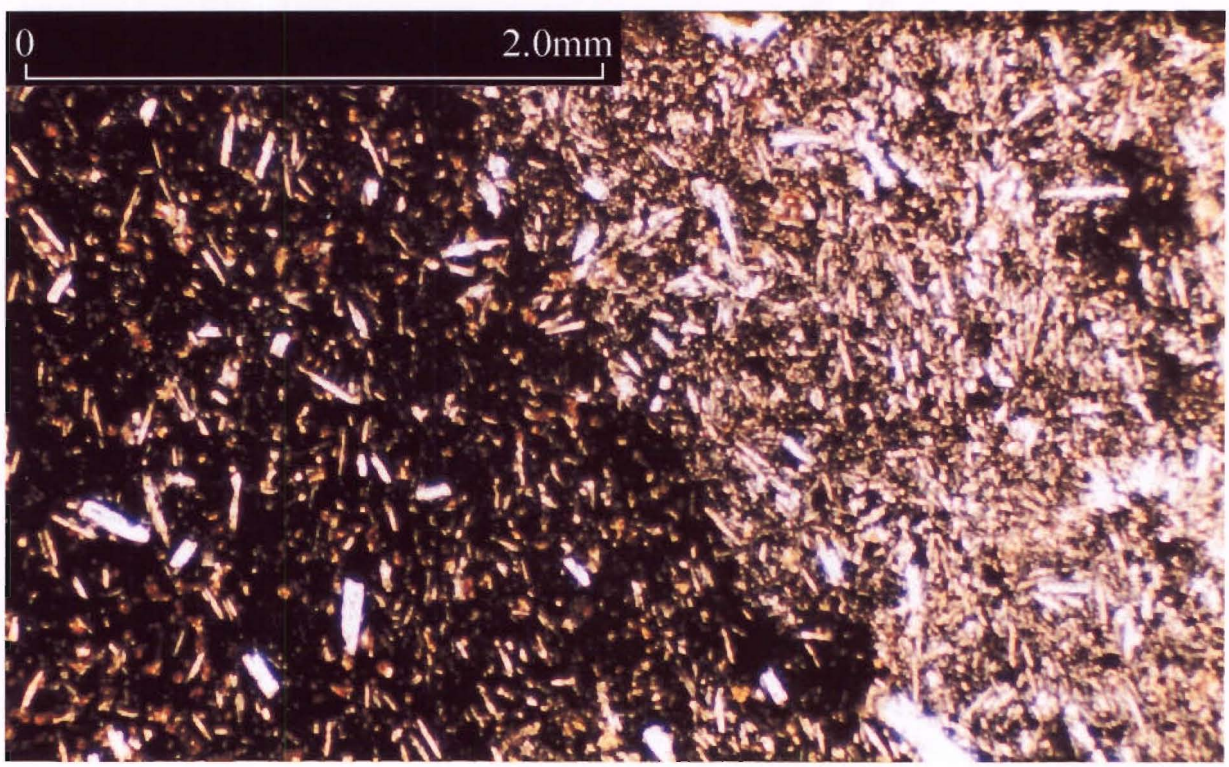

Figure 3.4B. Magma mingling in sample EN18, note the contrast between mafic and felsic areas (ppl).

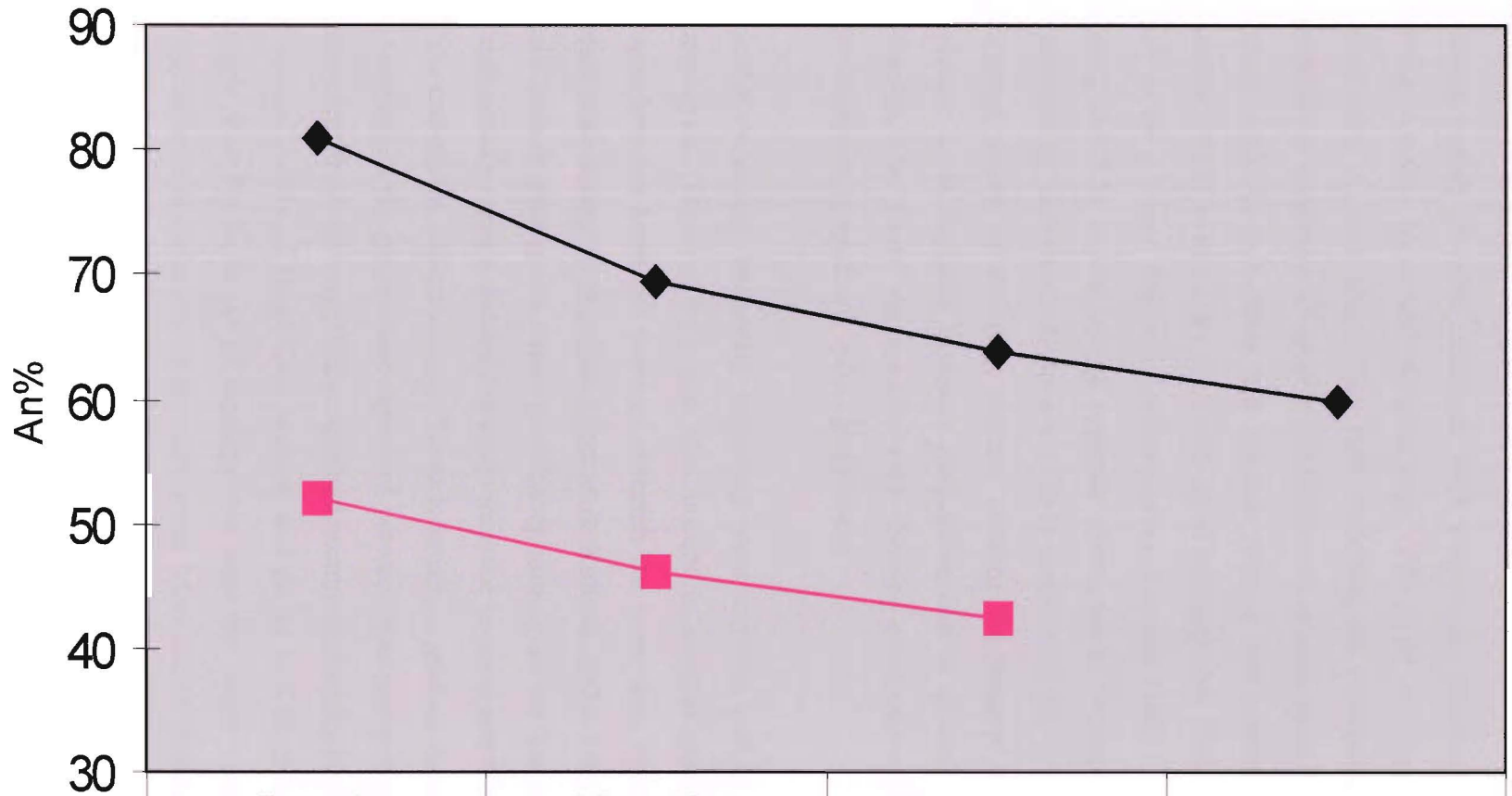

	Basalt	Hawaiite	Mugearite	Benmoreite
Phenocrysts	81	69	63	60
Groundmass	52	46	42	--

Figure 3.5. An% of plagioclase for phenocrysts and microphenocrysts in basalts to benmoreites.

Normal zoning is most common, with plagioclase phenocrysts and microphenocrysts having An-rich cores and Ab-rich rims. This type of zoning is caused by the melt crystallising An-rich plagioclase first, enriching the remaining melt with albite. As the temperature continues to drop crystallisation continues producing Ab-rich rims. Reverse zoning, with Ab-rich cores and An-rich rims is less common, and was suggested by Loomis (1982) to occur by the build up of incompatible elements adjacent to the crystal face or by a lesser degree of undercooling. Loomis (1982) also suggested that normal zoning could be caused by the opposite effect, where incompatible elements decrease or undercooling increases. Anderson (1984) suggested that zoning resulted from tidally triggered pulses of shearing motion, causing the magma to move and consequently replenish areas depleted in calcic plagioclase due to crystallisation and relatively slow diffusion. The "fresh" magma after each shearing event sets off a new cycle, starting with crystallisation of relatively calcic plagioclase.

Oscillatory zoning frequently occurs in most samples and is most distinctive in large phenocrysts (Figure 3.6A), but also occurs in smaller microphenocrysts. Oscillatory plagioclase has been the focus of research for more than 100 years but has so far still defied satisfactory explanation (Pearce & Kolisnk 1990, Smith and Brown 1988). The main feature that characterises oscillatory zoning is the occurrence of abrupt changes which usually mark a sudden outwards increase in An% and which may feature corrosion of the underlying crystal surface. There is usually a gradual change of An% (either reverse or normal) in the plagioclase deposited between successive sharp breaks (Shelley 1993). Early ideas from Bowen (1928) explained normal oscillatory zoning in plagioclase in terms of several cycles of plagioclase sinking and rising in a magma, but Loomis (1982) also thought that the build up of incompatible elements could cause oscillatory zoning if it occurred several times during crystallisation. More recent thinking has focused on magma mixing, with Lofgren (1974) demonstrating experimentally that compositional zoning in plagioclase could be caused by variations in pressure and temperature caused by the eruption or movement of magma. Nixon and Pearce (1987) continued with the magma mixing theory and showed that repeated injection of fresh, hot, basic magma into a chamber of already differentiated and cooled magma repeatedly, caused resorption of already crystallised plagioclase, allowing for new crystallisation on the resorbed surface.

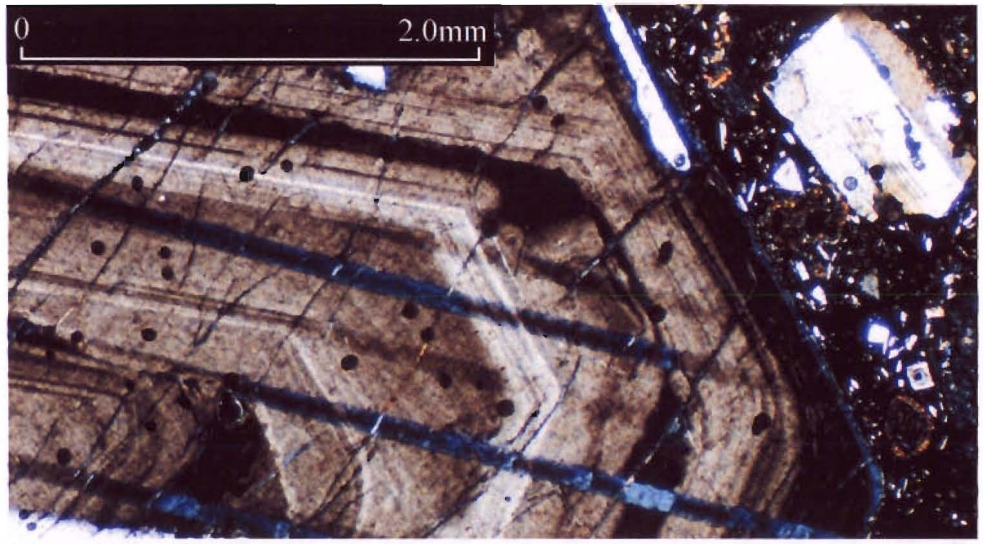

Figure 3.6A. Oscillatory zoning in large plagioclase crystal in sample GR1, a bomb sample from Southern Gibraltar Rock (xpl).

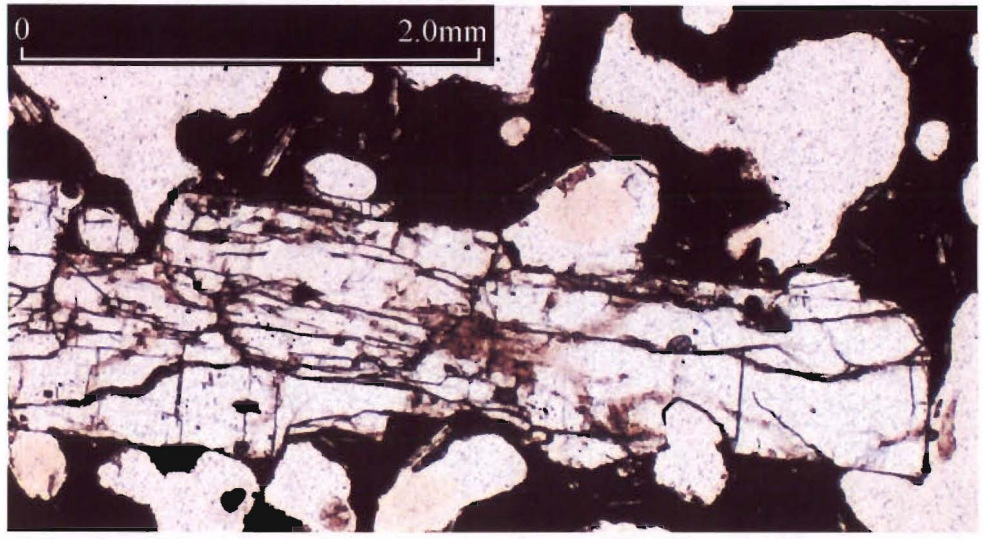

Figure 3.6C. Plagioclase phenocryst in sample SMC1126 (vent), that is extensively embayed and cracked (ppl).

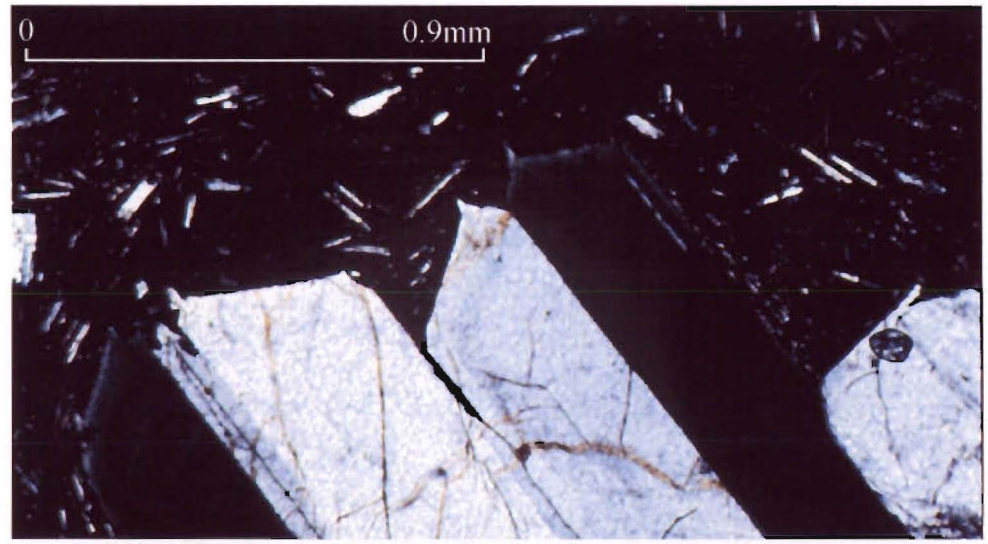

Figure 3.6B. A large phenocryst of plagioclase in sample EN17 (proximal), that has a skeletal end and that is also zoned (xpl).

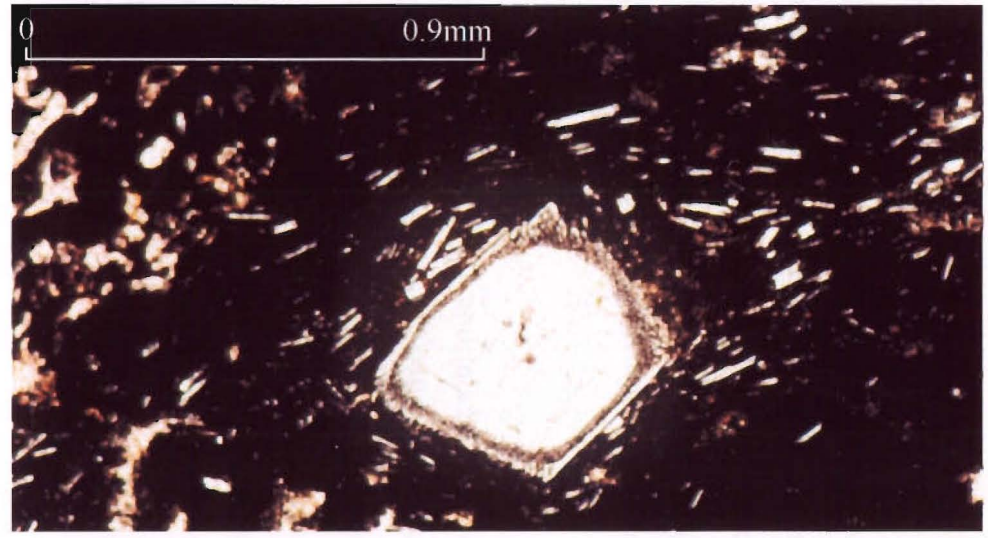

Figure 3.6D. An overgrown sieved plagioclase microphenocryst in sample WH1 (spatter flow) (ppl).

Magma mixing is common in the vent of cinder cones, with fresh magma mixing with stagnant magma and therefore seems a probable mechanism in smaller crystals. Larger crystals represent longer resident times in the magma, and hence have undergone a complex history allowing many oscillations to develop. Vance (1962) however, thought that due to the common fine scale, regularity and frequency of oscillatory zoning that it was unlikely magma mixing was the cause.

A few phenocrysts in some of the samples display no zoning at all, and this has also been noted for Lyttelton by Neumayr (1998) and elsewhere by Larsen et al. (1938). The problem with a lack of zoning is that you need time to allow total equilibration, thus Neumayr (1998) and Larsen et al. (1938) attributed the lack of zoning to crystals being accidentally caught up in a more slowly cooled magma. Another possible reason is that some crystals may represent zoned crystals that have been cut through their outer zone (during the thin section making process), creating the appearance of a unzoned crystal.

Resorption/ corrosion/ embayments

Plagioclase phenocrysts and microphenocrysts commonly show signs of resorption with rounded edges and corners. Resorption of the crystal faces occurs when the host magma is superheated above the plagioclase liquidus, or by the introduction of magma that is hotter and would crystallise more calcic plagioclase (Tsuchiyama 1985). Kuo & Kirkpatrick (1982) suggest a model involving the mixing of two chemically distinct magmas. Both magmas contain plagioclase phenocrysts to form a hybrid magma of intermediate composition and temperature compared to the initial liquids. The more albite-rich plagioclase phenocrysts from the more evolved melt will be superheated in the hybrid, whereas the more anorthite-rich plagioclase from the more primitive melt will be undercooled. The superheated crystals will show some resorption and become mantled by more anorthite rich material than the core. In contrast, the undercooled crystals will show more skeletal growth (Figure 3.6B) with a mantle more albite-rich than the core.

Neumayr (1998) suggested that both corrosion and changes in plagioclase composition could be caused by the simple movement of phenocrysts in convection currents, with corrosion occurring when the difference between the temperature of crystallisation and the ambient temperature of the surrounding magma becomes too great. Differences in

temperatures between the floor and roof of the Lyttelton main chamber would have been greater and so the chances of convection more likely.

Pearce et al. (1987) demonstrated that during the eruption of Mt St Helens, solution occurred as magma rose to the surface. In this case there was no evidence that corrosion was accompanied by a change in the composition of the magma. In feldspar, dissolution may take place in hydrous magma because the liquidus and solidus curves are depressed as pressure decreases and volatiles are released (Shelley 1993).

Plagioclase phenocrysts and other phenocrysts (eg olivine, clinopyroxene, and magnetite) commonly have small embayments (Figure 3.6C). Donaldson & Henderson (1988) also note embayments in quartz crystals caused by small bubbles near the crystal edges. Bubbles have the effect of setting up small-scale convection currents near crystals and effectively drill their way into the crystal face. Due to the large amount of vesicularity in most samples it seems likely that such a mechanism may be the result of some embayments.

Sieving

Sieve textures are common in most samples (Figure 3.6D & Figure 3.7E) with glass, clinopyroxene, or iron oxides as inclusions within the plagioclase. There are two explanations for sieving in the literature, magma mixing and decompression, and both probably occurred throughout the history of Lyttelton. Tsuchiyama (1985) showed experimentally that heating above the plagioclase liquidus causes solution of plagioclase phenocrysts and rounding. He also found that if phenocrysts had an An% lower than that of plagioclase in equilibrium within the melt, a fine sieve texture would develop on the corroded surfaces which is filled with magma that reacts, forming a more calcic rim. Stimac & Pearce (1992) also found that low An% plagioclase develops sieve textures during large changes in both liquid composition and temperature. Both Tsuchiyama (1985) and Stimac & Pearce (1992) found that when crystallisation resumes, subhedral to euhedral calcic crystals grow, and sieve textured relics often become coated by calcic overgrowths. Nelson & Montana (1992) however found experimentally that decreasing pressure causes An% to increase with disequilibrium and resorption. Rapid ascent of magmas would cause the pressure change, and this may also involve magma mingling.

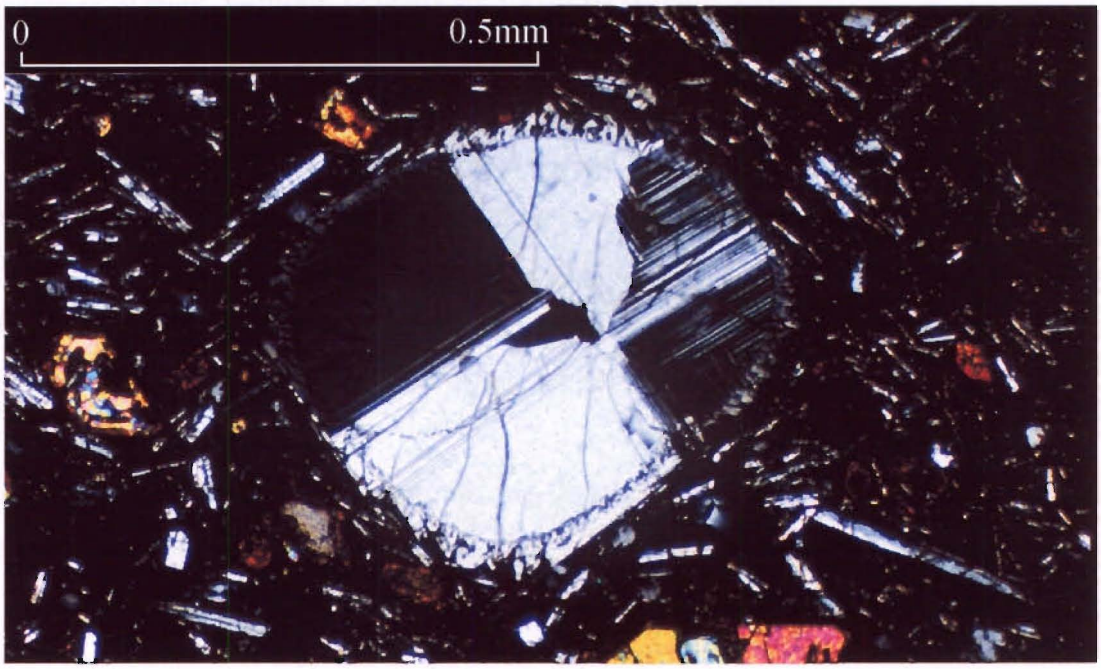

Figure 3.7E. A combination of Manebach or Pericline twins with Carlsbad or Albite twins, in bomb sample EN35, with a sieved rim (xpl).

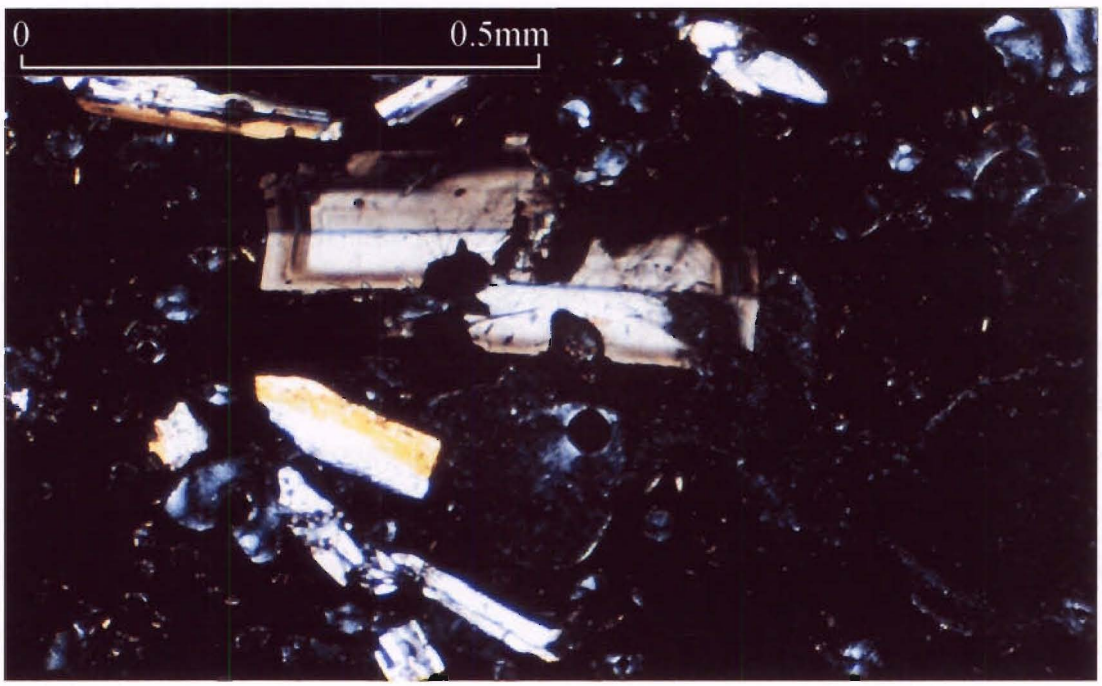

Figure 3.7F. An oscillatory zoned, Carlsbad twinned plagioclase that has been broken into two pieces, in bomb sample WH4 (ppl).

Alteration

Plagioclase phenocrysts and microphenocrysts are unaltered in all facies. However occasionally in some samples, crystals are fractured (Figure 3.7F).

3.3.2 Clinopyroxene

The clinopyroxene in the cinder cones is Mg-rich augite with lesser amounts of Fe-rich augite, with some crystals displaying simple and rarely polysynthetic twins (Figure 3.8A). Previous workers on Lyttelton (eg Altaye 1989, Slaughter 1995, Shearer 1986, Sewell 1985, Coates 1976) have also noted augite as common in the lavas. Iron-rich augites have been also noted, but as typical of more silicic lavas (Neumayr 1998).

Optically visible zoning is not common but does occur. In sample CR8a (Figure 3.8B) there is a distinct change in colour from a Mg-poor core (pale) to a Mg-rich rim (darker), and in sample SMC1126 an Fe-rich core is coated with a Mg-rich rim (Figure 3.8C). Zoning is a reflection of changes in the composition of the melt, where crystals displaying a Mg-poor rim can be explained by an increase in Si concentration in the surrounding magma during clinopyroxene crystallisation (Neumayr 1998). Therefore a Mg-rich rim implies that there must have been an influx of fresher basic magma. The crystal in sample SMC1126 is unusual as Fe-rich crystals are more typical of silica rich magmas, so this might suggest that the crystal has crystallised in a silica rich chamber that has been replenished by fresher basaltic magma. Another possibility is that the crystal may have crystallised in an isolated area of the magma chamber before being incorporated into fresher magma causing the Mg-rich rim.

Ophitic and sub-ophitic textures are observed in some samples (Figure 3.8B&D). McBirney and Noyes (1979) suggest that such textures are the result of simultaneous crystallisation of clinopyroxene and feldspar, with clinopyroxene nucleating and growing at a higher rate than feldspar. It is common to find magnetite poikilitically enclosed within clinopyroxene. Neumayr (1998) also found magnetite nucleating at the edges of clinopyroxene crystals. He thought this was the result of dissolution of clinopyroxene due to superheating as a result of mixing/mingling, which led to a supersaturation of magnetite.

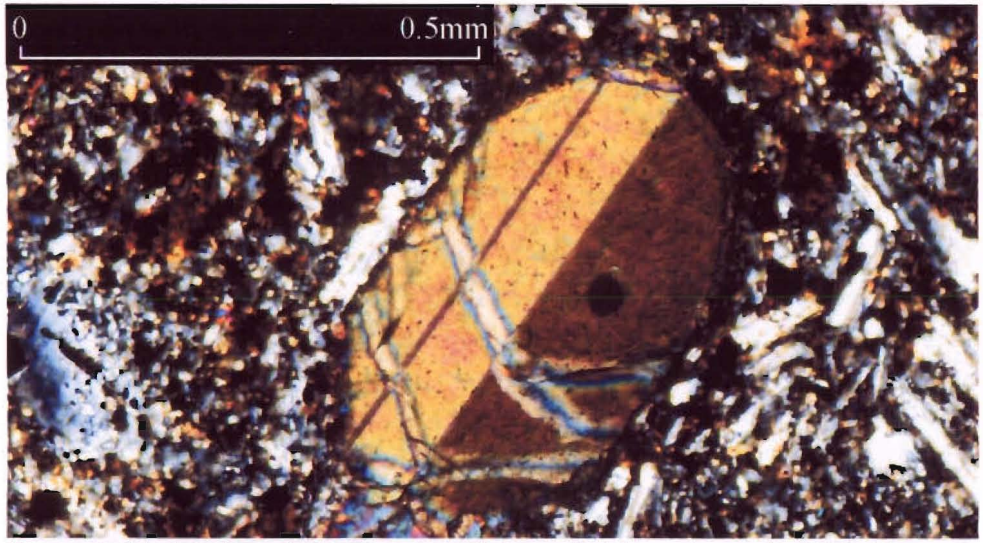

Figure 3.8A. A twinned clinopyroxene (Mg-augite) in vent sample GR3. Also note the rounded edges (xpl).

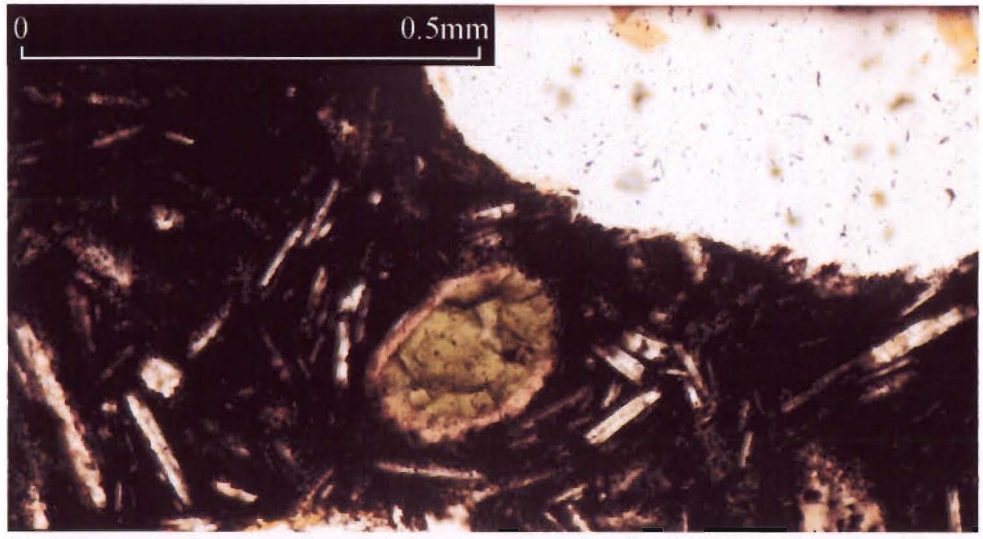

Figure 3.8C. A zoned clinopyroxene in vent sample SMC1126, with a Fe-rich core and a Mg-rich rim (fleshy colour) (ppl).

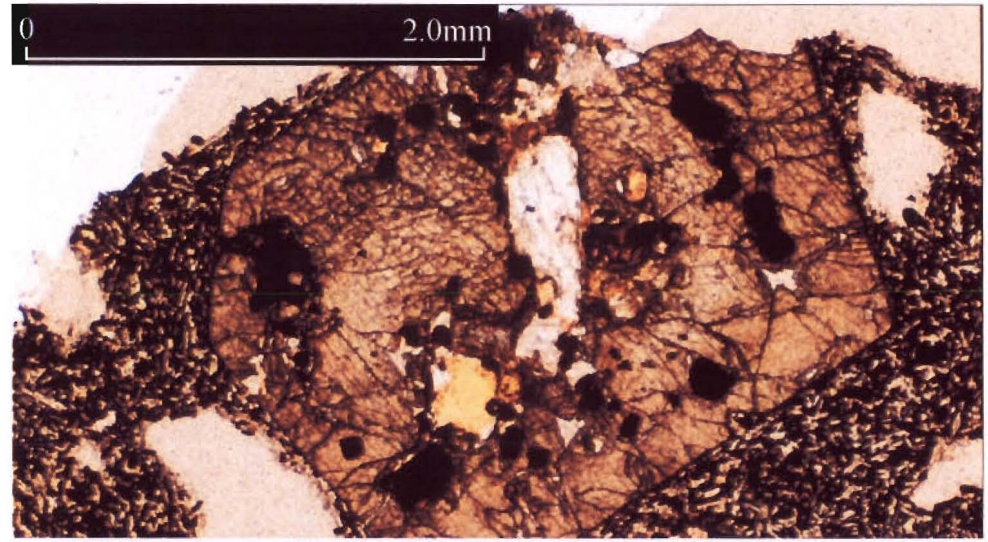

Figure 3.8B. A large zoned (pale core/dark rim) clinopyroxene (Mg-augite) in sample CR8a (proximal), with inclusions of plagioclase and magnetite (ppl).

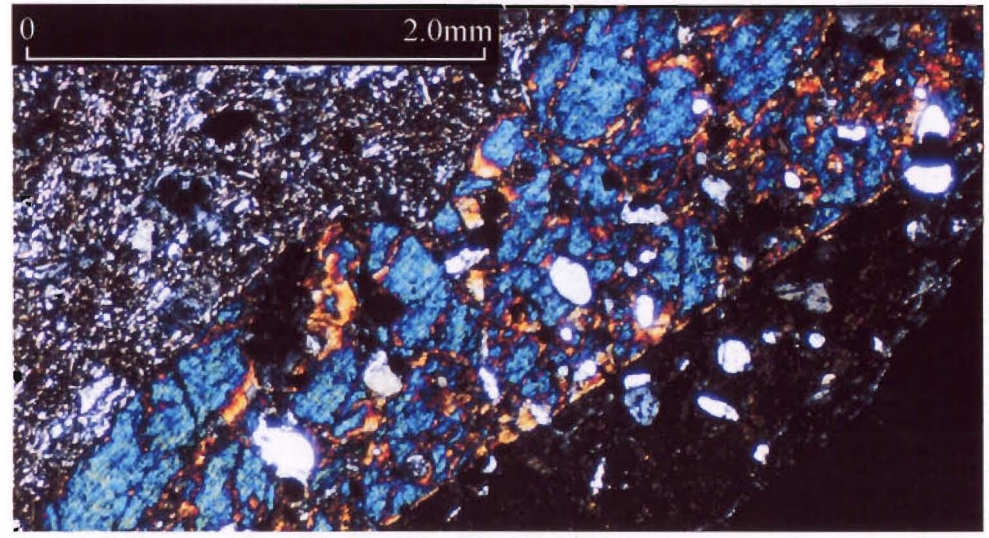

Figure 3.8D. A twinned clinopyroxene (Mg-augite) in sample DNS3 (spatter flow), with inclusions of plagioclase (ophitic), and magnetite (xpl).

growth components adjacent to the crystal, allowing magnetite to nucleate and grow. In sample CR8a this can be seen easily at the boundary between the overgrowth (Figure 3.8B), and is probably caused by the injection of fresher magma.

3.3.3 Olivine

Olivine is the third most common phenocryst and is commonly altered to iddingsite and/or bowlingite. Iddingsite consists of a mixture of smectite, chlorite, and goethite, and less commonly amorphous silica, calcite, talc and mica (Wilshire 1958). As noted by Delvigne et al. (1979) the formation of iddingsite is generally initiated at the margins of olivine crystals (Figure 3.9A), and appears to invade the crystals progressively, until in the most extensively altered samples, the original olivine is entirely transformed. There are also some samples that have an unaltered rim surrounded by iddingsite that is overgrown with less altered olivine and this may represent a period of hydration-oxidation succeeded by further crystallisation Neumayr (1998). Another explanation for this zoning pattern may be selective alteration of the core (D. Shelley, pers. comm. 1999) (Figure 3.9B).

Iddingsite forms deuterically at low temperatures under oxidising conditions (Haggerty & Baker 1967, Coleman 1982, Smith et al. 1987). Gay & Le Maitre (1961) suggest that olivine alters via "continuous transformation in the solid state", whereby Mg, Fe^{2+}, and Si are released from the olivine and replaced by Fe^{3+}, Al, and Ca. During this alteration, Fe is converted from its ferrous to ferric state and its proportion (relative to Mg) is increased. H_2O is added, Mg is subtracted, and Si remains unchanged (Neumayr 1998).

Bowlingite is regarded as an olivine alteration product formed under non-oxidising conditions (Wilshire 1958). When the environment becomes oxidising, bowlingite may itself be altered to a complex mixture of smectite, chlorite, antigorite, and/or chrysotile, with minor amounts of talc, mica, and quartz (Deer et al. 1982).

Alteration of olivine to iron oxides is not as common as alteration to iddingsite but still very common in proximal and bomb samples (Figure 3.9C&D). Haggerty & Baker (1967) found that during the high temperature oxidation of olivine, iron gradually exsolves from the lattice as an opaque oxide phase. The iron oxide phase which forms is either magnetite

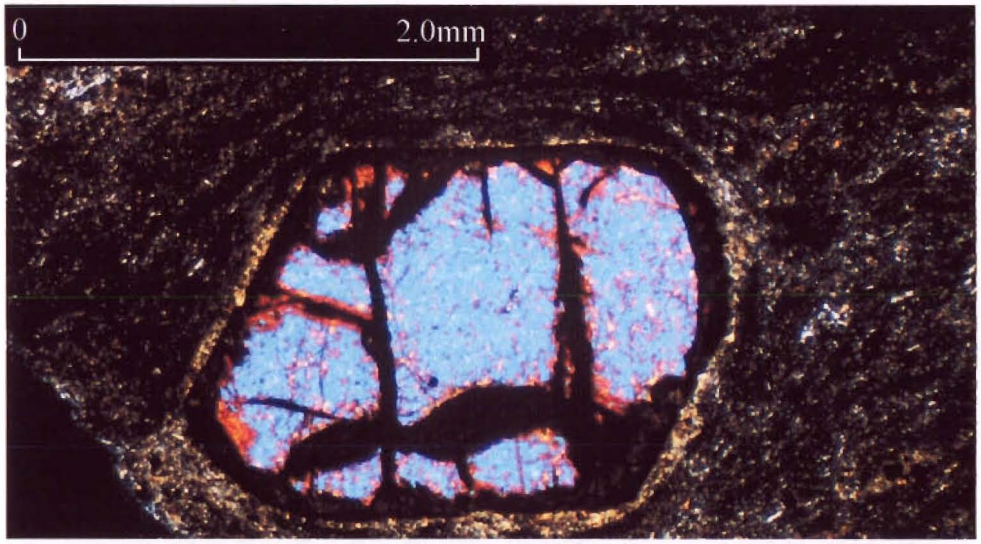

Figure 3.9A. Iddingsitised olivine in sample ES15a (spatter flow) (xpl).

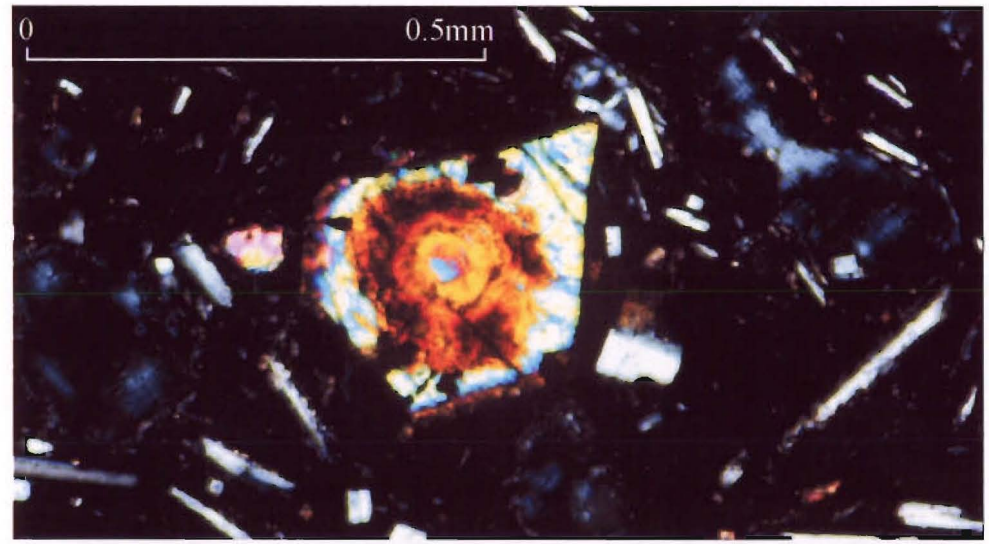

Figure 3.9B. Iddingsitised olivine, illustrating selective alteration of the core, in bomb sample SMC331a (xpl).

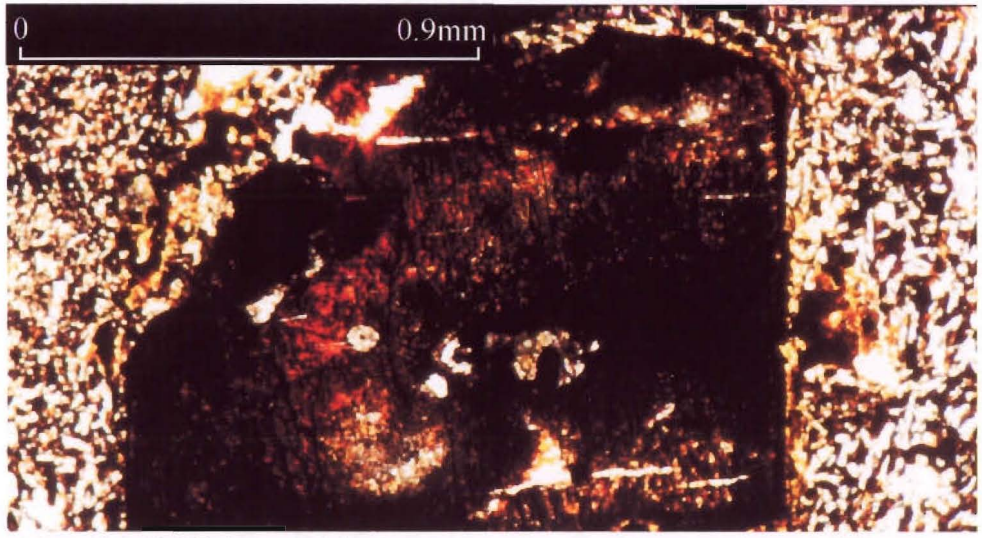

Figure 3.9C. Olivine crystal altered to a mixture of iron oxides and iddingsite in sample MC15 (proximal) (ppl).

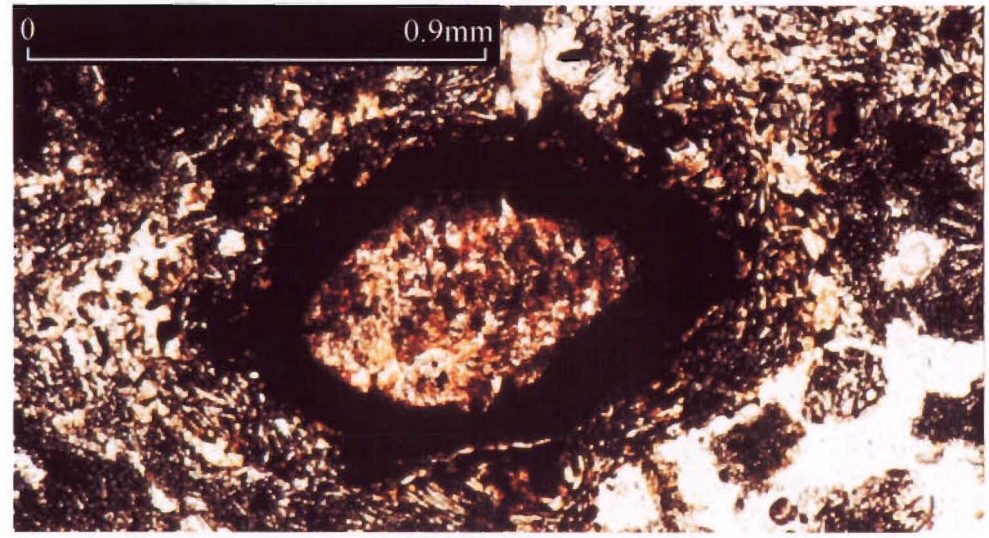

Figure 3.9D. An olivine crystal that has been altered to iddingsite and also developed an opaque rim of iron oxides in sample CR8a (proximal) (ppl).

or hematite, depending on the availability and the partial pressure of oxygen and on the temperature of formation. Haggerty & Baker (1967) found that olivines from samples which show positive reheating effects, such as scoriaceous clasts at the top of lava flows, tend to contain hematite rather than magnetite in their secondary assemblage. Searle (1962) also found hematised olivine at Three Kings Scoria Cone, Auckland.

Olivines in some of the samples display embayments, corrosion, and rounding of edges. Sharp edges probably reflect skeletal growth whereas corrosion and rounding are probably the result of the injection of fresher magma raising the melt temperature above the liquidus of olivine.

3.3.4 Iron Oxides

It is difficult to distinguish magnetite and ilmenite on the basis of shape, therefore two slides (DNS3, GR22) were recut and polished, and then examined under transmitted light. Both slides showed very small amounts of ilmenite present but with Ti-magnetite dominant. Previous workers on Lyttelton also noted the occurrence of Ti-magnetite as phenocrysts, microphenocrysts, as a groundmass phase, and as inclusions. Tanguy et al. (1997) also found ilmenite and Ti-magnetite common as a groundmass oxide phase in Etnaean lavas. Neumayr (1998) suggested that inclusions of magnetite are a reflection of its early crystallisation while skeletal magnetite (Figure 3.10A) is caused by a high degree of undercooling as a result of a rapid drop in temperature.

3.3.5 Minor Minerals

Apatite

Apatite occurs as tiny crystals and inclusions in most samples and previous workers have also noted it common in lavas as a groundmass phase. Neumayr (1998) found that in more siliceous lavas such as rhyolites and trachytes, apatite formed larger needles that were often included within plagioclase crystals. He related the crystallisation of apatite to a decrease in P_2O_5, with a distinct decrease at approximately 54% SiO_2, correlating with large needles seen in thinsection. Duncan (1978) also noted the crystallisation of apatite in mugearites and benmoreites in Etnean lavas. Apatite in the groundmass commonly forms small needles, most are colourless, although occasionally some are pale-brown. Round

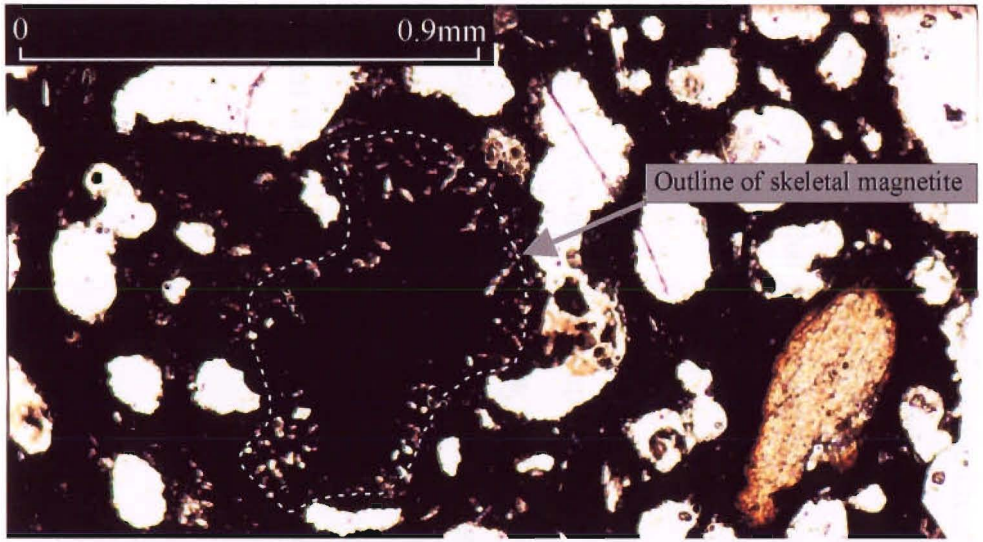

Figure 3.10A. A skeletal magnetite crystal in bomb sample MC19 (ppl).

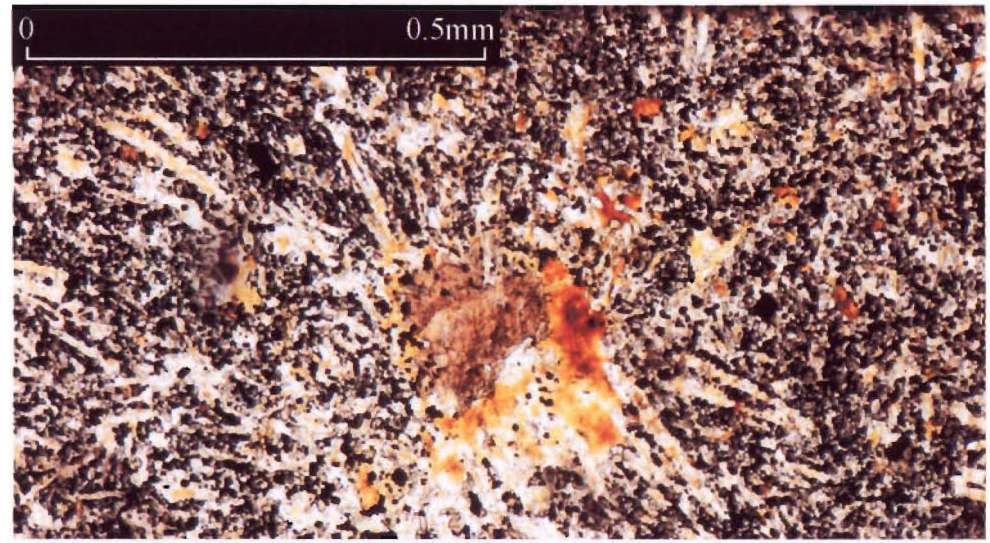

Figure 3.10B. A small amphibole crystal in sample EN26 (vent). Note small biotite crystals in some of the vesicles in the surrounding groundmass (ppl).

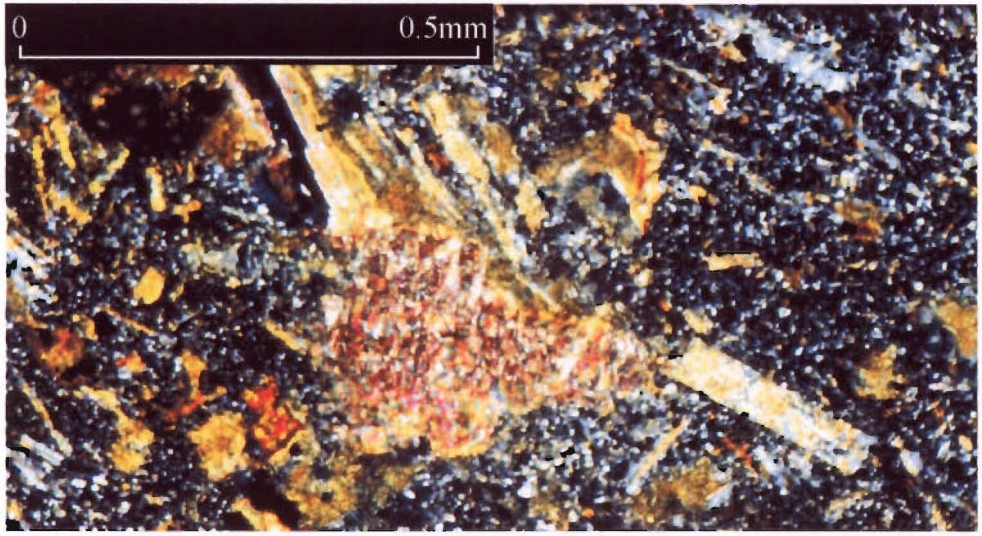

Figure 3.10C. A biotite crystal in sample EN26 (vent), showing its distinctive mottled extinction (xpl).

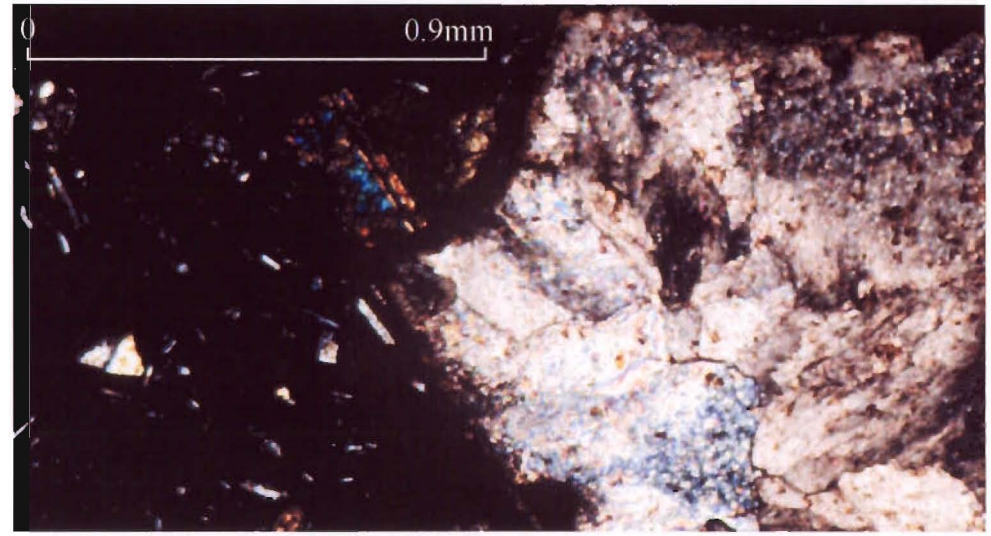

Figure 3.10D. Calcite infilling a vesicle in bomb sample GR1 (xpl).

microphenocrysts are found in some samples, mostly as inclusions in plagioclase phenocrysts and microphenocryts. As suggested by previous workers (eg Sewell 1985, Neumayr 1998), the occurrence of apatite represents the remains of relict high-pressure mineral phases.

Amphibole

Amphibole occurs in samples HH5 and EN26. It is anhedral and occurs as very small crystals (Figure 3.10B). Neumayr (1998) found kaersutite in one L1 lava, while Shearer (1986), Altaye (1989), and Coates (1976) found amphibole phenocrysts, either brown hornblende or kaersutite. Neumayr (1998) and Sewell (1985) suggested kaersutite is xenocrystic because it is absent in the groundmass, and requires hydrous conditions and high pressures to grow as a stable phase. Tanguy et al. (1997) found kaersutite in Etnaean lavas and also suggested a xenocrystic origin.

Orthopyroxene

Orthopyroxene occurs in samples MC15, DNS3, EN18, and EN2, and is subhedral to anhedral in shape. Altaye (1989), Slaughter (1995) and Neumayr (1998) all note the occurrence of orthopyroxene in the lavas they studied. Slaughter suggested orthopyroxene characterised L2a lavas but Neumayr (1998) suggested it also occurs in some L1 lavas and not all L2a lavas, so it should not be used "as a basis for L1-L2a separation". Neumayr (1998) suggests that its occurrence is related to the assimilation of basement sediments, which occurred periodically during the history of Lyttelton Volcano.

Biotite

Biotite is common in sample EN26, with its distinctive pleochroism and mottled extinction, but it also occurs rarely in other samples as small flakes. Its occurrence is restricted to vesicles which suggests that it is a late vapour phase or secondary mineral. Neumayr (1998) also found biotite in vesicles (Figure 3.10C) in L1 lavas and Chester et al. (1985) noted biotite in some mugearitic and benmoreitic Etnean lavas. Both these authors suggest that biotite has crystallised as a late stage magmatic or hydrothermal mineral.

3.3.6 Secondary Minerals

Zeolites

Zeolites are common in all facies but are most dominant in the distal tuffs and form from the weathering of microlites and volcanic glass (Philips & Griffen 1981, Fisher & Schmincke 1984). Chabazite is the dominant zeolite (Figure 3.1B) having a distinctive pseudo-cubic appearance and very low birefringence. Natrolite also occurs but is less common, and has a fibrous radiating form. Zeolites usually form well-developed crystals in the vesicles, and amygdales of basalts are generally considered to be the result of late stage fluids that permeated them after their extrusion (Deer et al. 1992).

Calcite

Calcite occurs only in sample GR1 (Figure 3.10D), but has been noted elsewhere in Lyttelton lavas (Neumayr 1998) and Akaroa pyroclastics (Johnston 1990). Its occurrence in vesicles and veins is due to its crystallisation in the later stages of hydrothermal deposition (Deer et al. 1992).

3.3.7 Xenoliths

One quartzite xenolith was found in slide ES5 (Figure 3.11). There is no reaction rim but the matrix does have a slight orange/brown discolouration, which may be devitrified glass. The xenolith is made up of granoblastic unstrained quartz crystals that are ca. 0.3mm across. Some of the quartz grains display euhedral shapes suggesting that during entrainment they underwent dissolution before recrystallising. The dissolution of the quartz could also explain the glassy matrix, which has since become devitrified.

Previous workers on Lyttelton have also found quartz xenoliths (eg Shearer 1986, Neumayr 1998) and these have been attributed to the entrainment of basement lithologies. Shearer (1986) attributed xenoliths in the Dyers Pass area to the Charteris Bay Sandstone and Neumayr (1998) also suggests that entrainment of Torlesse basement might be responsible. However the Torlesse material would have to be very clean to achieve the monomineralic xenoliths and he therefore suggests that "enclaves may represent Torlesse vein material which contains little else but quartz". The source for the xenolith in sample ES5 is difficult to determine but due to being composed of quartz grains, it is most likely from Cretaceous/Tertiary sandstone, which are found in the Charteris Bay area.

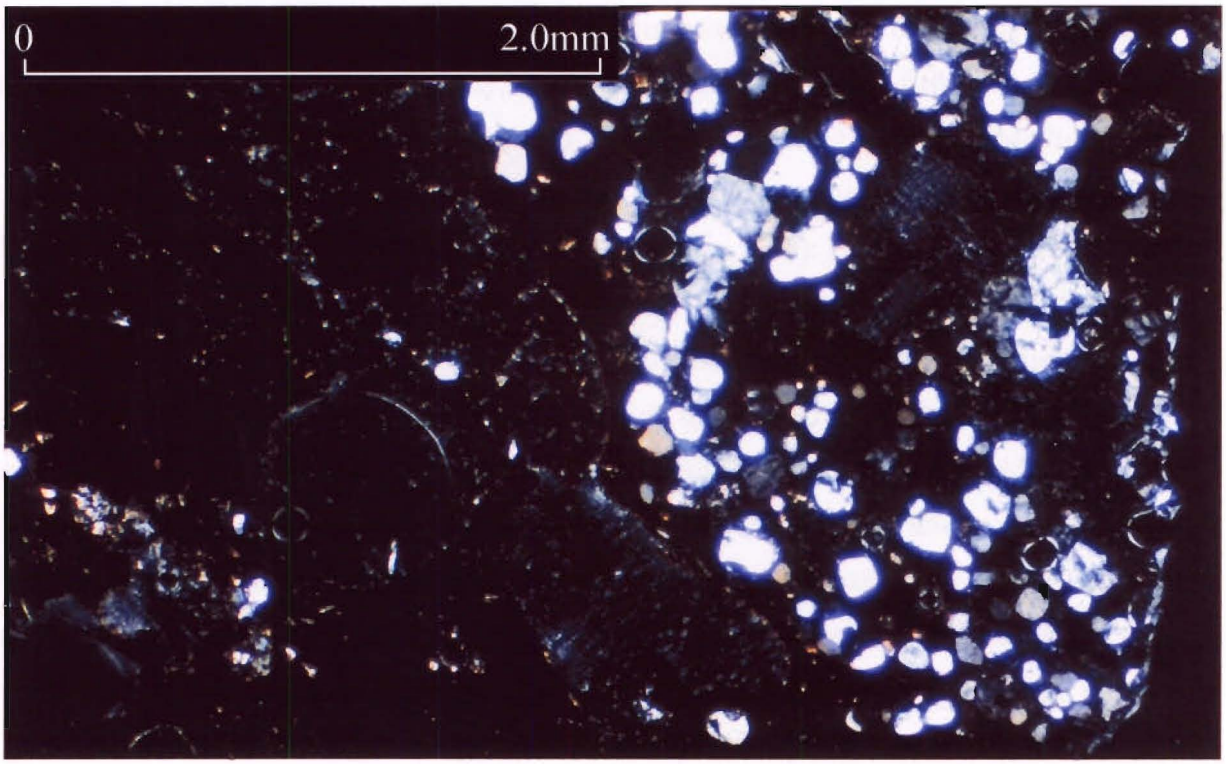

Figure 3.11. Quartzite xenolith in bomb sample ES5 (xpl).

3.4 VESICULARITY

Variations in vesicle size, shape and abundance in lavas and scoria reflect the interplay of original volatile content and viscosity, rates of decompression and diffusion, coalescence and interference of adjacent vesicles, and deformation during flowage (McPhie et al. 1993). Overall vesicularity in samples is seen to decrease from approximately 37% in bombs and tuff samples to 14% in vent samples (Figure 3.12). Johnston (1990) also found a similar trend in bomb samples, having an average vesicularity of about 33% with more welded samples having a lower vesicularity of about 23%. Houghton & Wilson (1989) found that low viscosity basaltic magmas with high discharge rates (ie high gas rise speed) and no magma:water interaction, have vesicularities of 70-80% for non-welded deposits. However as inferred discharge rate falls (ie low gas rise speed), this allows magma in the vent to degas and hence become more viscous, causing an increasing proportion of dense ejecta is generated (eg Houghton & Hackett 1984). Brown et al. (1990) also found wide variations in cone deposits at Punatekahi, and attributed it to varying eruption density. Therefore it seems that due to low vesiculation (30-50%) and wide variations that the deposits are dominantly the dominant products of Strombolian type eruptions, with variation in vesicles due to varying resident times in the vent.

Tuff samples have the second highest vesicularity and Fisher & Schmincke (1984) cite several sources of gas that can cause vesiculation in tuff deposits: (1) gas within the fluidising phase of the depositing system (derived from the eruptive centre, from air incorporated during transit, or from rain falling during movement of the system), (2) gas given off by hot pyroclasts, (3) air rising from the underlying ground, (4) water evaporating from snow or watersoaked soil beneath a layer of hot ash, or (5) rain that turns to steam as it percolates downwards into hot ash.

The shape of the vesicles is also seen to vary among the different types of facies. Welded samples (ie vent, proximal, and spatter) have vesicles that are dominantly irregular in shape and show signs of deformation. The deformation would have been caused by samples still being semi-fluid during deposition allowing compaction or flow. Bomb samples have a bimodal type of population with large vesicles having deformed shapes and smaller vesicles being more isolated and spherical in shape. Mangan & Cashman (1996)

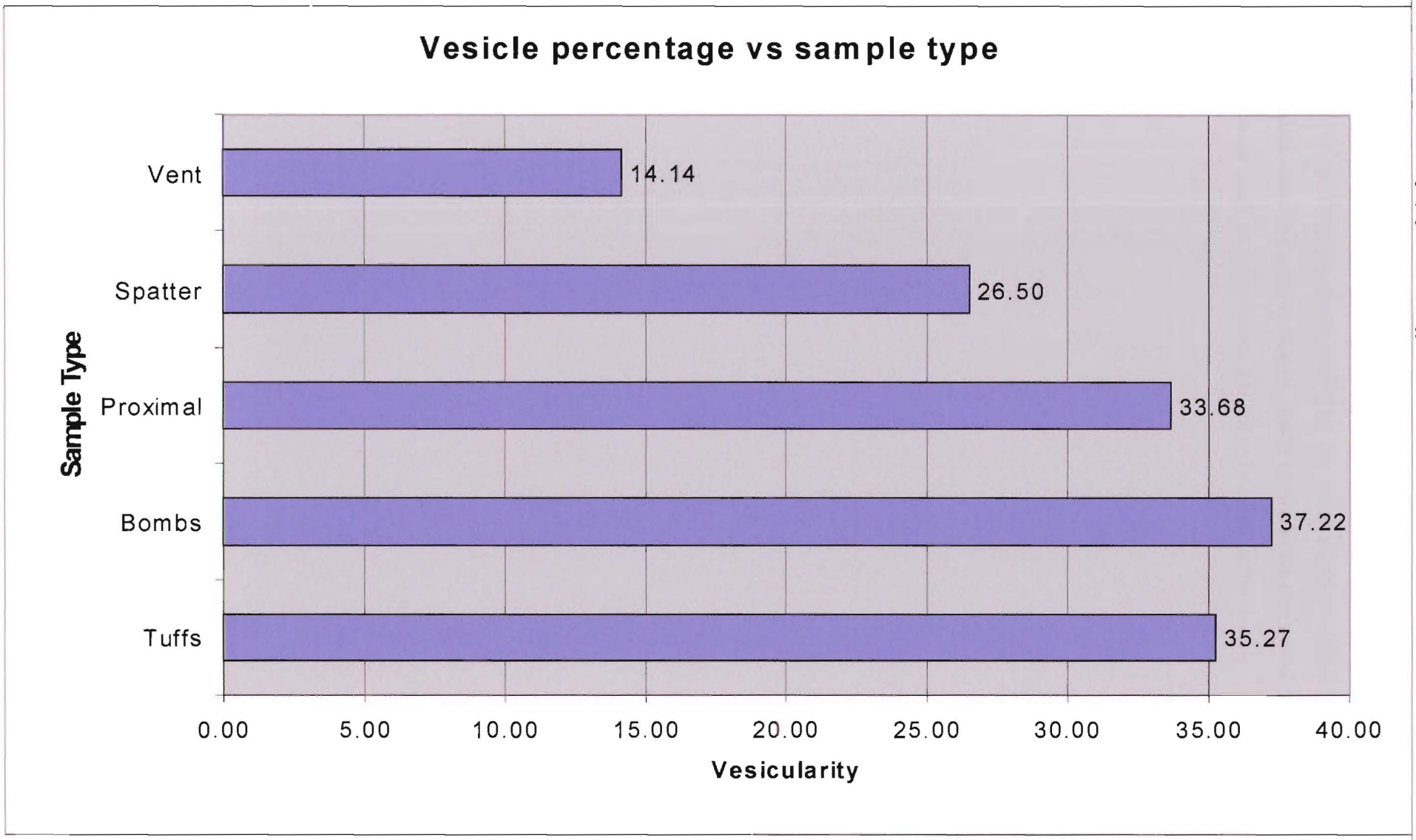

Figure 3.12. Variation of vesicularity within the different facies and including spatter flows.

explained this type of variation as a process of coalescence. Large vesicles are swept past smaller vesicles as they rise faster, and they are more likely to collide with larger vesicles causing coalescence (ie larger vesicles). Small vesicles rise more slowly and are less likely to coalesce with large vesicles causing them to become isolated.

Chapter Four

GEOCHEMISTRY

4.1 INTRODUCTION

The aim of this chapter is to classify and interpret the geochemistry of cinder cones of Lyttelton Volcano and their related products (eg spatter flows). 112 samples were collected from all study sites (see Appendix 3A), from all facies except the distal facies. One distal facies sample (31056) was analysed but due to extensive devitrification and the presence of zeolites, further study was not undertaken.

Geochemical analysis was carried out by XRF spectrometry using the methods listed in Appendix 5A, and the results are given in Appendix 5B. Analyses from Hibberd (1994), Slaughter (1995), and Mckenzie (1995) have also been included (see Table 3.1, and Appendix 5C).

4.2 CHEMICAL CLASSIFICATION

Classification of samples from each area is based on the total alkali vs silica (TAS) diagram of Le Maitre (1989), as recommended by IUGS for the classification of igneous rocks.

4.2.1 Total alkali vs. silica

Southern Mount Cavendish (Figure 4.1A)

Twenty-three samples were analysed: 10 bombs, 3 proximal samples, 1 vent sample, 1 distal tuff, 2 dike samples, and 6 lava samples. All but two of the cinder cone samples are hawaiites with one mugearite, and one basalt. The basalt composition is a distal tuff with a 'loss on ignition' (LOI) of 4.62, and is thus considered too hydrated to be reliable. The hawaiitic dike found in the medial facies strikes toward the centre of the cone and was probably emplaced during the final phases of activity.

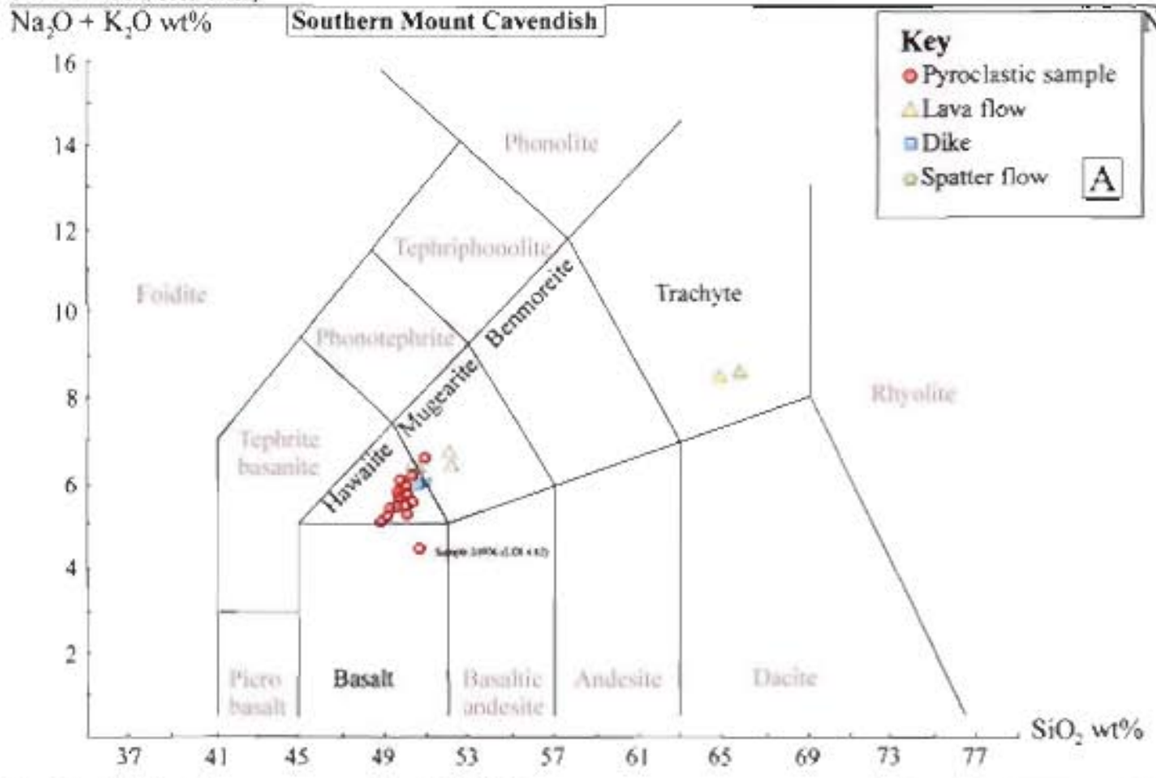

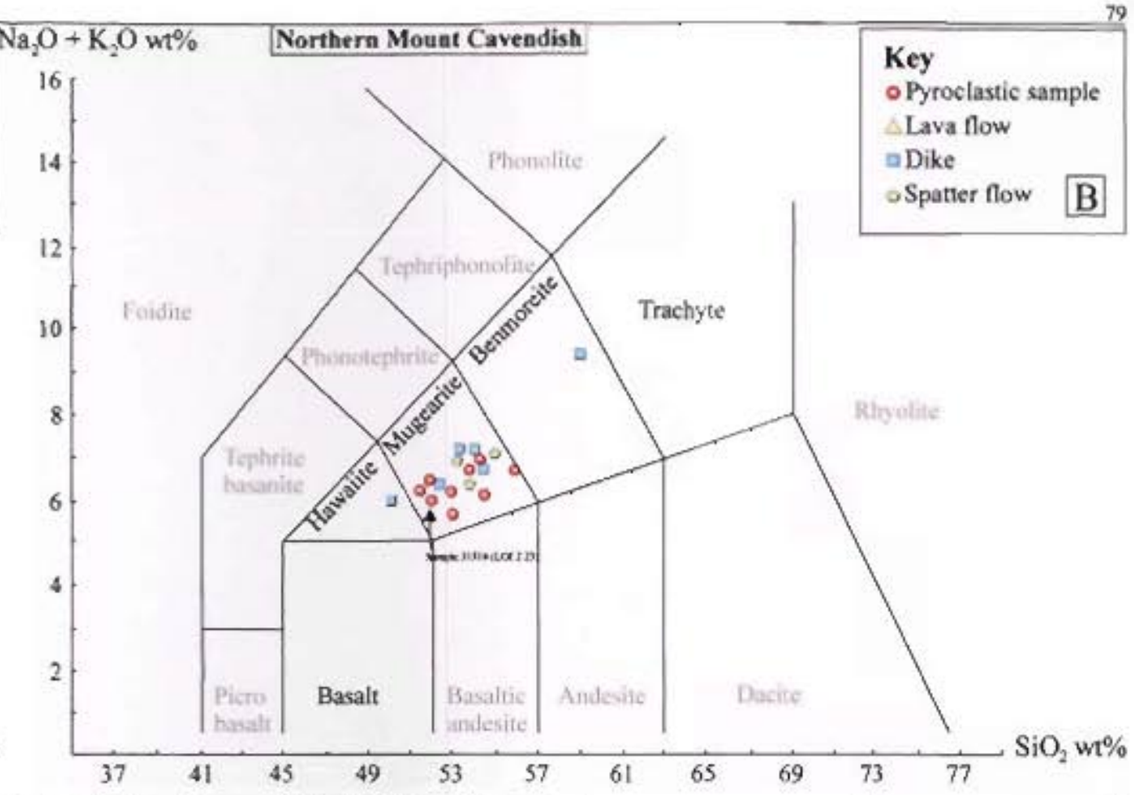

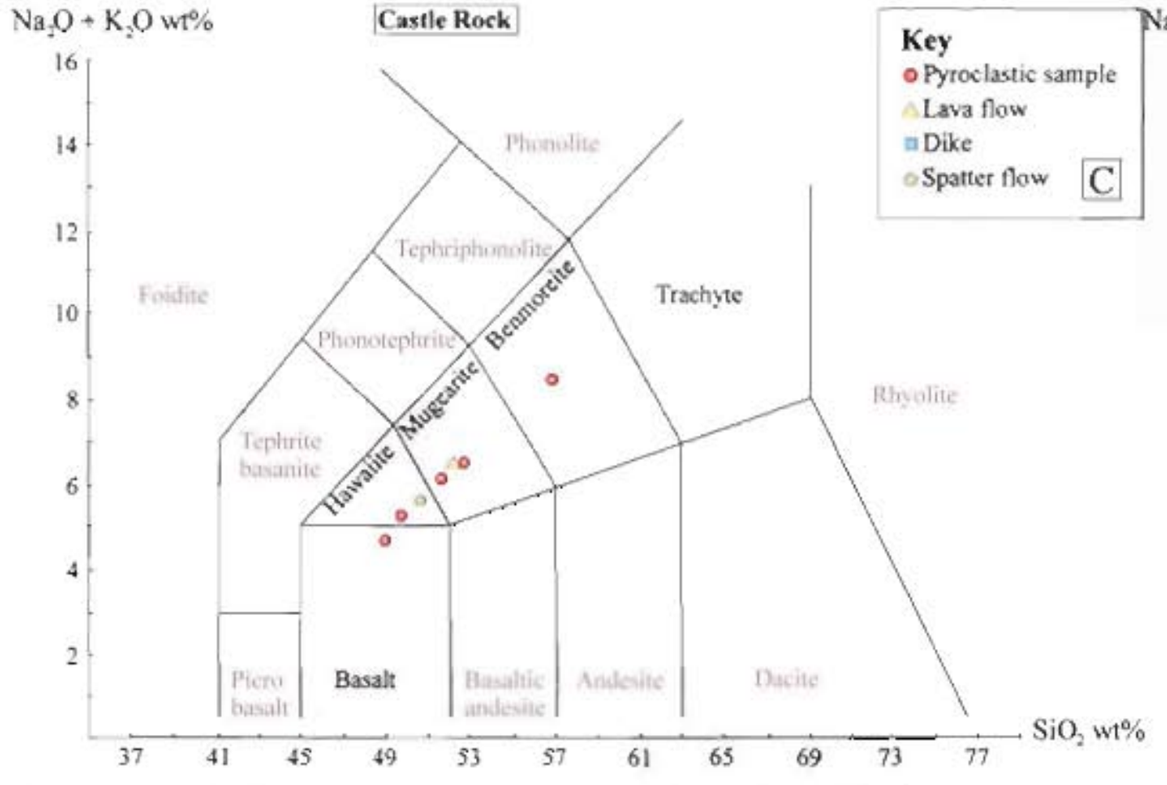

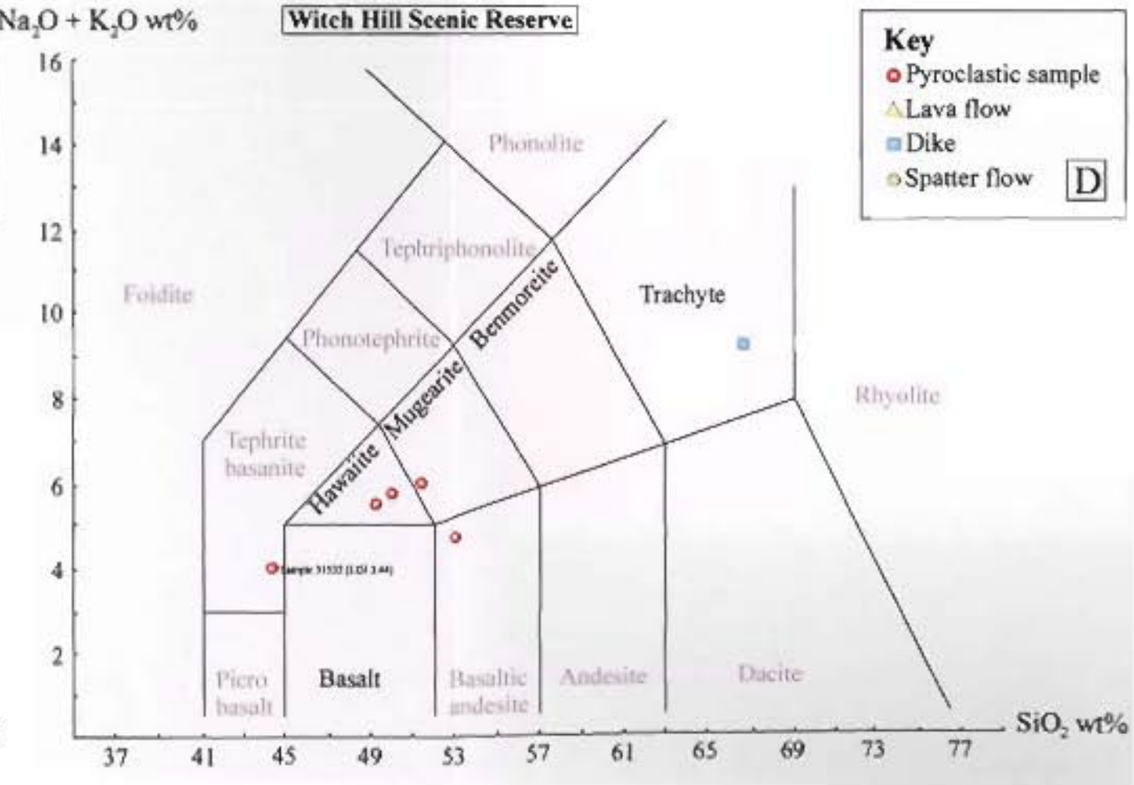

Figure 4.1A-D. Classification of Lyttelton pyroclastics, spatter flows, dikes and lavas for each site.

Three lavas were sampled and all have different compositions, trachyte, mugearite, and hawaiite. The hawaiitic lava is found directly below the cone and is about 3 - 4 m thick pinching out onto the trachyte lava. It is possible that since the chemistry of the hawaiite lava and the cinder cone deposits are so similar that this may represent an early eruptive product of the cone. The mugearitic lava is also probably related to the cinder cone, due to it outcropping on the flanks of the medial facies, and possibly represents a late stage breach from the cinder cone due to its evolved composition. The trachyte lava is about 4 - 5 m thick and can be traced around the base of the cone and below the hawaiite lava, and hence is not related.

Northern Mount Cavendish (Figure 4.1B)

Eighteen samples were analysed: 6 bombs, 2 proximal samples, 1 vent sample, 3 spatter flows, and 6 dikes. One of the dikes is hawaiitic and another benmoreitic with all other samples mugearitic. The hawaiitic and benmoreitic dikes are chemically different to the pyroclastic deposits, and therefore unrelated. The mugearitic dikes have a similar chemistry to the pyroclastic deposits, but due to them cross cutting the pyroclastic deposits they are not related.

Castle Rock (Figure 4.1C)

Seven samples were analysed: 1 bomb, 4 proximal samples, 1 spatter flow, and 1 basal lava. The samples do not plot in a simple group like the previous two areas but instead are spread out, ranging from basaltic to benmoreitic. The spatter flow sample is hawaiitic and the basal lava is a mugearite. All samples are from the same eruptive phase, except the proximal benmoreite and appear to have evolved chemically with time. The proximal benmoreite probably originates from the large benmoreite/ trachyte dome that overlies the pyroclastics and is not directly related to the pyroclastic activity.

Witch Hill Scenic Reserve (Figure 4.1D)

Six samples were analysed: 4 bombs: 1 vent sample, and 1 dike. Bomb samples vary from 1 basanite (LOI 3.44), 1 basaltic andesite and 2 hawaiites. The vent sample is mugearitic, whereas the dike is trachytic and is not related to the cinder cone.

Hoon Hay Park (Figure 4.1E)

Nine samples were analysed: 6 bombs, 1 spatter flow, and 2 dikes. The bombs plot in two areas, three in the basaltic field and three in the mugearitic/benmoreitic field. The basaltic bombs were collected from the southern locality and the mugearitic/benmoreitic bombs collected from the northern locality. The spatter flow from the northern locality is benmoreitic and a dike from southern locality basaltic, suggesting that both were related to the pyroclastic activity. The other dike is rhyolitic and is not related. As mentioned in Section 2.4.5, it was thought that these two areas may represent a polygenectic cone that erupted in two phases, and this theory is consistent with the geochemical data above.

Northern Gibraltar Rock (Figure 4.1F)

Eight samples were analysed: 2 bombs, 2 proximal samples, 2 vent samples, 1 dike, and 1 from a lava flow. Hibberd's (1994) bomb and dike samples have also been included. Two of the bombs are mugearitic, the other benmoreitic (LOI 2.43), with the two proximal also mugearitic. The lava flow was originally thought to be a spatter flow in the field but as it is trachytic it is now thought to be unrelated to the cone. Hibberd's (1994) mugearite dike was sampled in the middle of the vent facies and is interpreted to be the feeder dike, whereas the hawaiitic dike is unrelated, due to its less evolved chemistry.

Southern Gibraltar Rock (Figure 4.1G)

Five samples were analysed: 1 bomb, 2 vent and 2 dikes. The bomb and one of the vent samples are basaltic, the other vent sample is mugearitic. One of the dikes is basaltic and this probably would have been the feeder dike due to similarities in chemistry between it and the bomb samples. The other dike is mugearitic and this is also probably related, as it strikes towards the inferred vent area and has a similar chemistry to the other vent sample. The evolved chemistry of the mugearitic samples suggests that both have been emplaced during the final phases of pyroclastic activity.

Southern Mount Evans (Figure 4.1H)

Nine samples were analysed: 3 bombs, 4 dikes and 2 spatter flows. One bomb sample is basaltic the other two are mugearitic. Three of the dikes are hawaiites and are probably

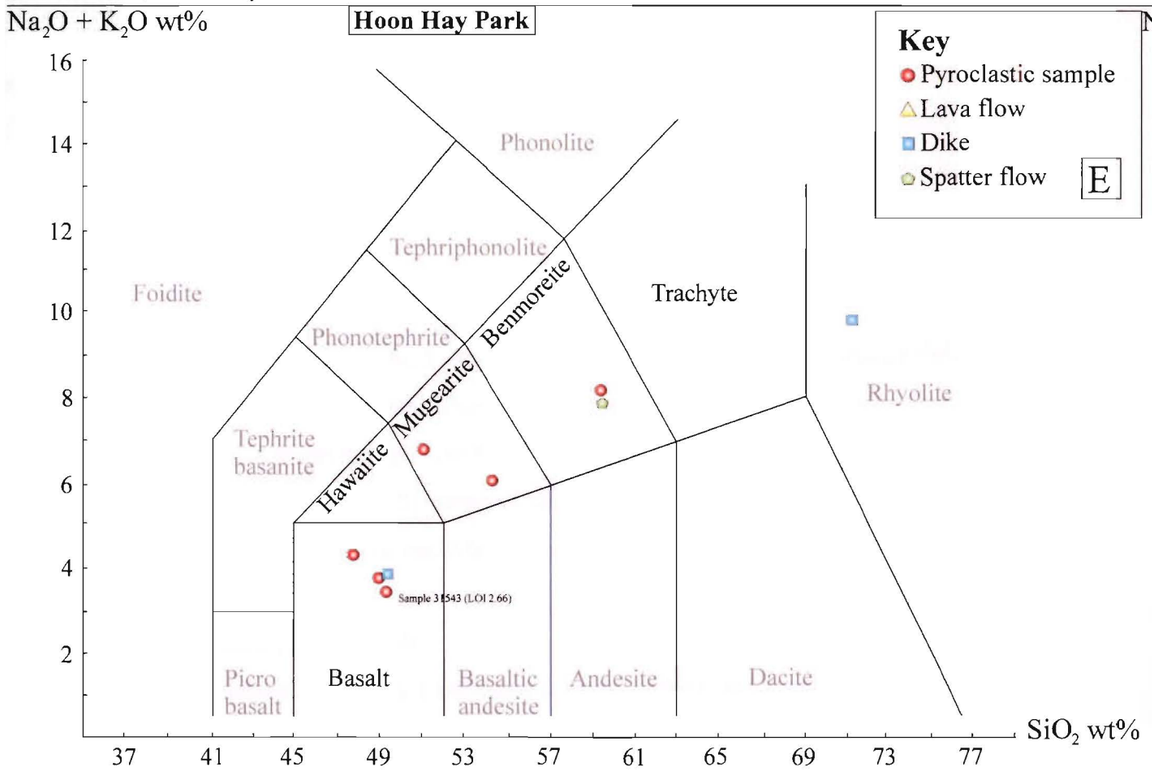

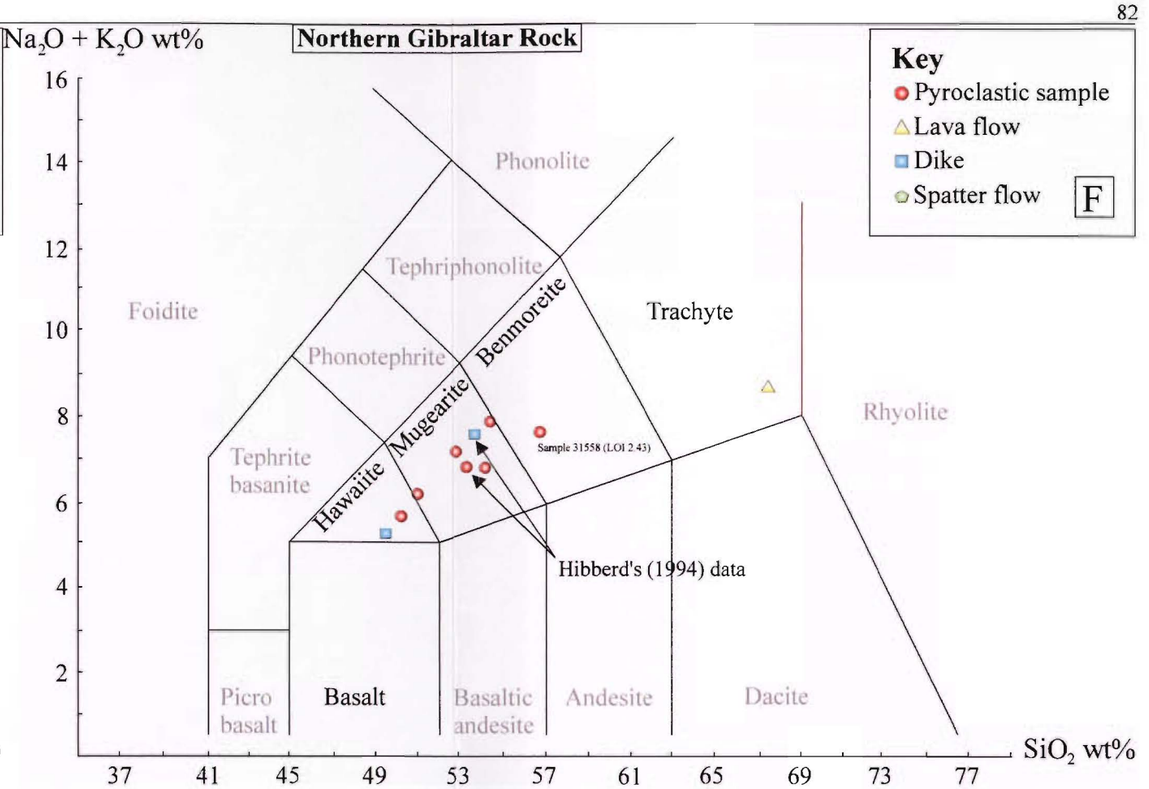

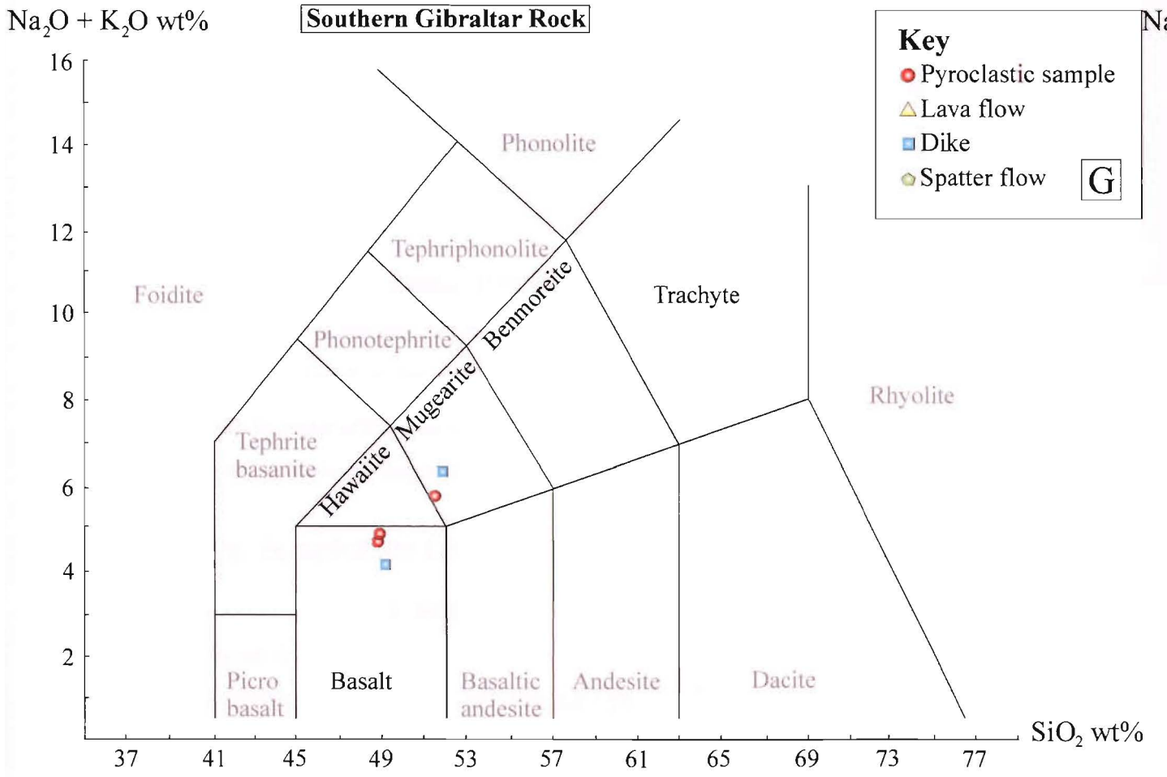

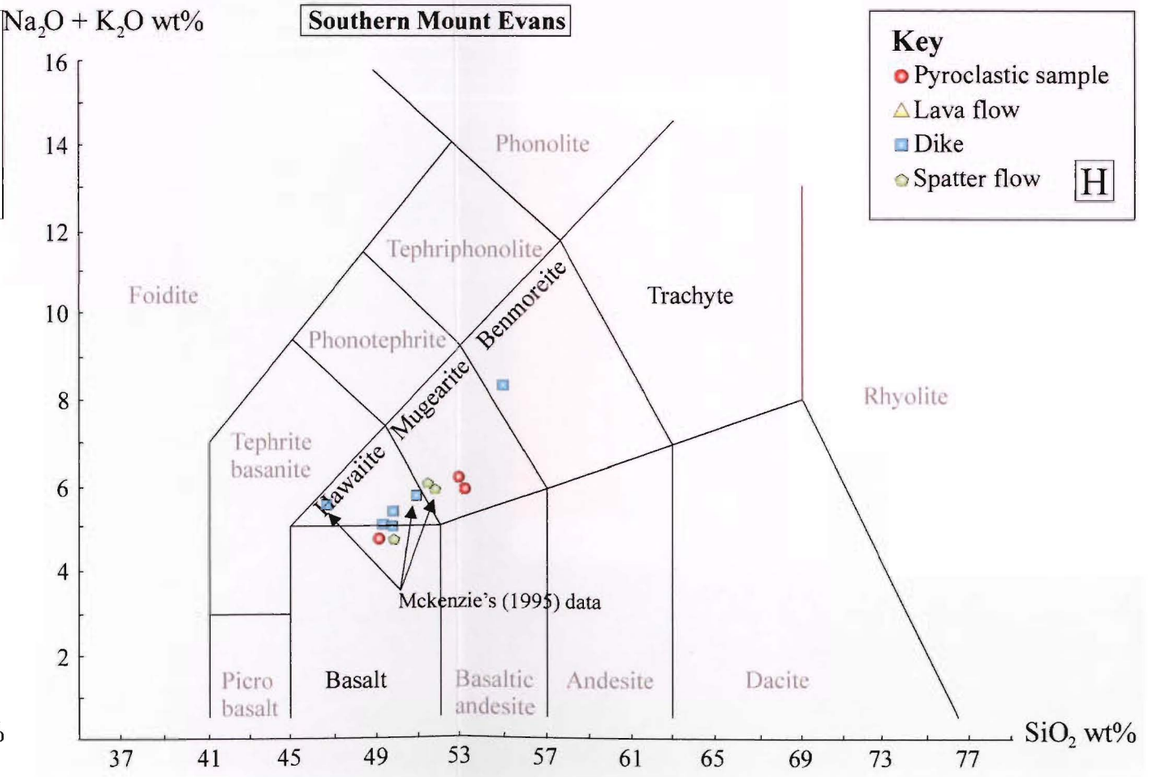

Figure 4.1E-H. Classification of Lyttelton pyroclastics, spatter flows, dikes and lavas for each site.

related to pyroclastic activity, due to striking toward the inferred vent area. The dike other is benmoreitic and not related. The spatter flow samples are basaltic and mugearitic. Mckenzie's (1995) samples include two hawaiite dikes and one spatter flow that is the same composition as the spatter flow analysed in this study.

Northern Mount Evans 1 (Figure 4.1I)

Nine samples were analysed: 2 bombs, 2 proximal samples, 2 vent samples, 2 spatter flow samples and 1 dike sample. All samples except for the dike plot within the hawaiite field. The dike sample plots is trachytic, and cuts the pyroclastic deposits, suggesting that it was a later stage event. Slaughter (1995) sampled another dike that also cut through the pyroclastic deposits and this is also a trachyte.

Northern Mount Evans 2 (Figure 4.1J)

Ten samples were analysed: 4 bombs, 1 proximal sample, 3 dikes, and 2 lavas. The bombs range widely from hawaiite to basaltic andesite, shoshonite, and latite. The proximal sample is also shoshonitic. Two of the dikes are hawaiitic and strike toward the inferred vent area, and are thought to have been fed by the cone. The other is benmoreitic, and cuts the pyroclastic deposits, and is thought not to be related. The lava flow samples from above and below the cone are hawaiites, and are probably not related.

Northern Mount Evans 3 (Figure 4.1K)

Eight samples were analysed: 3 bombs, 1 vent, and 4 dikes. Two of the bombs are hawaiites whereas the other is basaltic (LOI 2.39), with the vent sample mugearitic. Three of the dikes are probably related to the cone as they all strike toward the inferred vent area and range from basalt to mugearite. The other dike is also mugearitic but is not thought to be related as it cuts the pyroclastic deposits, suggesting that it is a late stage feature.

4.2.1 Alkaline vs. Subalkaline Classification

All samples are plotted on a TAS diagram with the discrimination line of Irvine and Baragar (1971) (Figure 4.2). All the samples plot above the line suggesting that they are alkaline. Neumayr (1998) found a similar trend in the Lyttelton lavas with only a few sub-

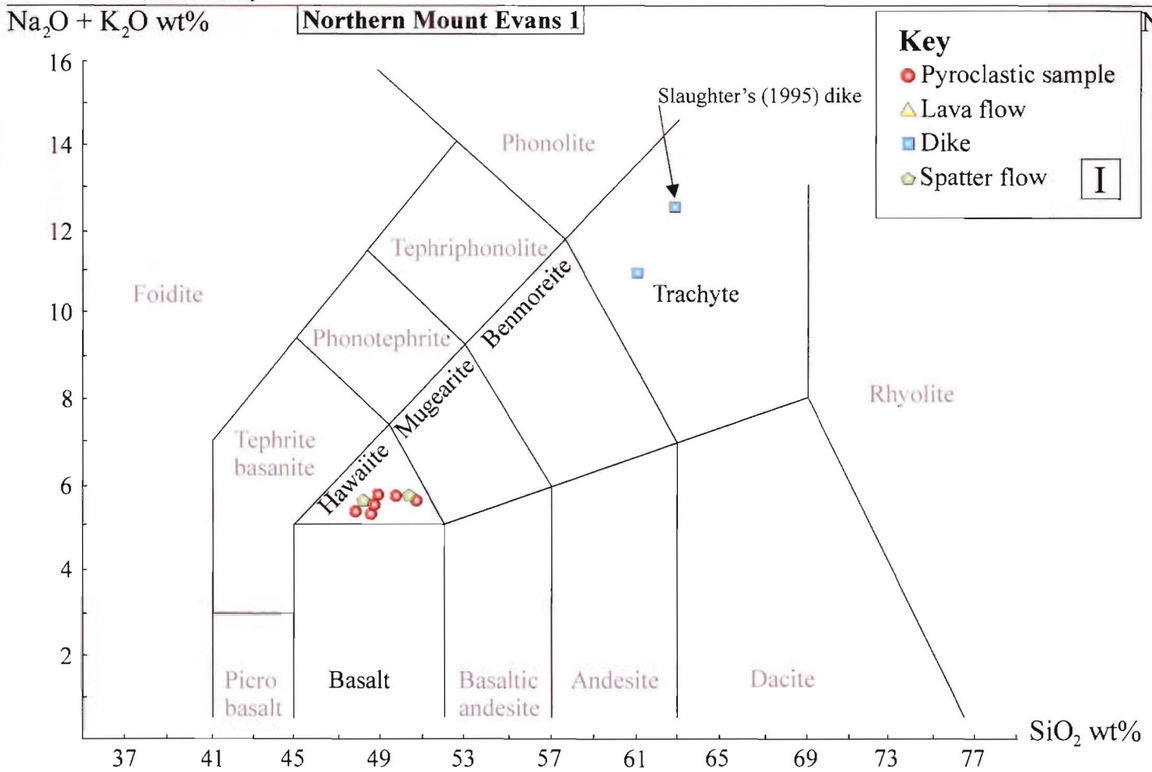

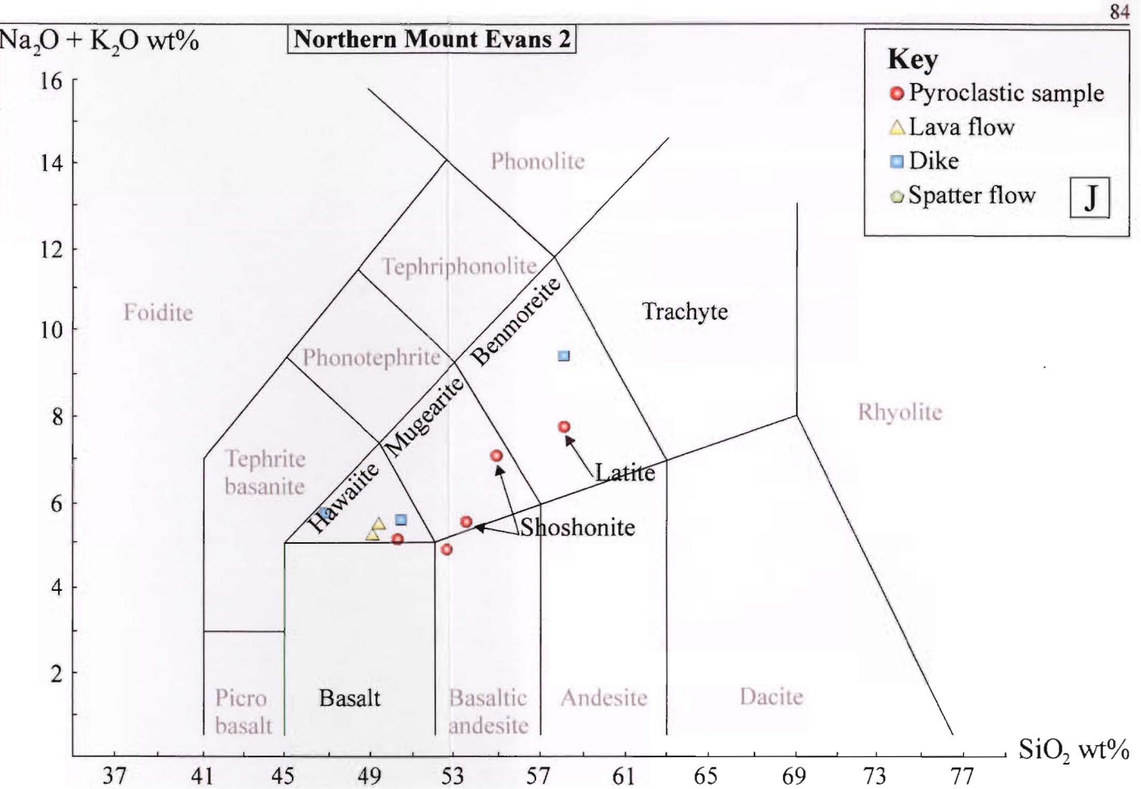

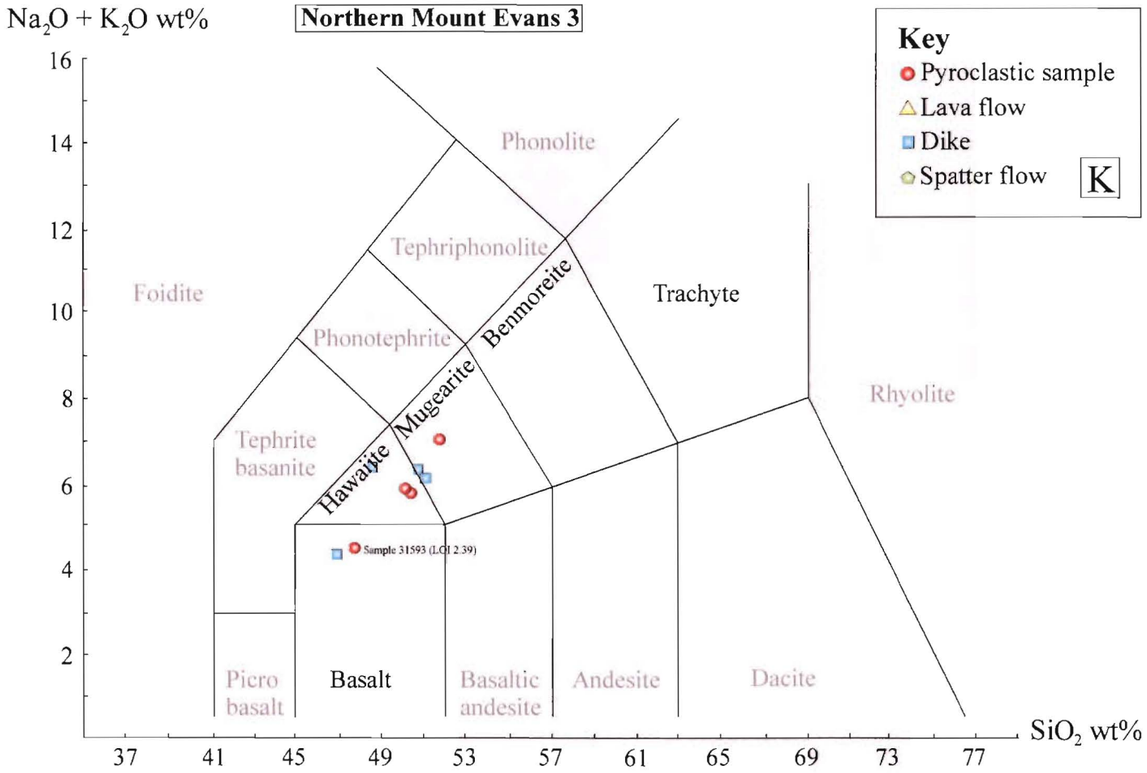

Figure 4.1I-K. Classification of Lyttelton pyroclastics, spatter flows, dikes and lavas for each site.

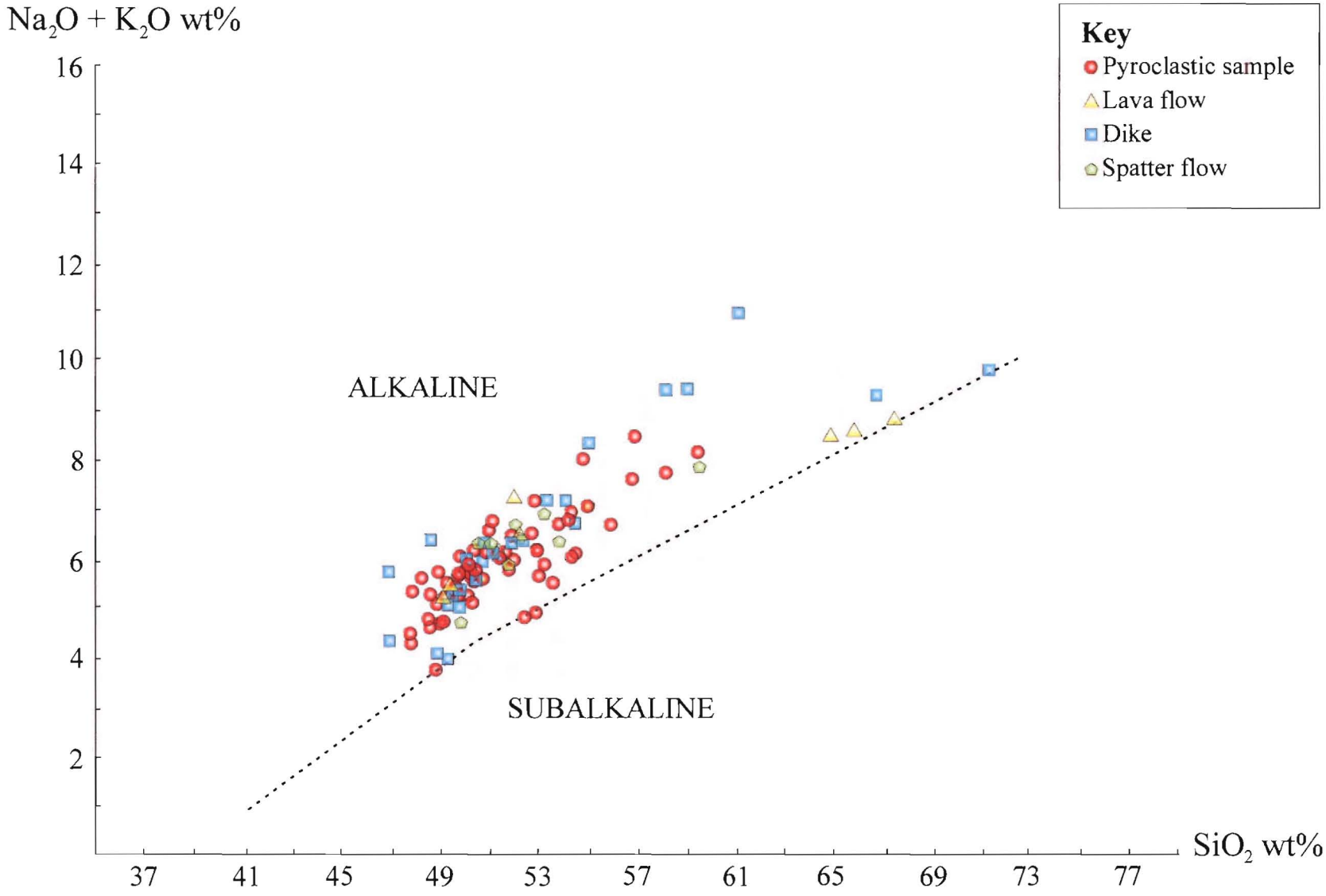

Figure 4.2. Alkaline and subalkaline division for all samples analysed.

alkaline samples that he suggested were due to basement sediments being assimilated during some stage before ascent.

4.2.2 AFM Diagram

The division between the tholeiite (significant iron enrichment) and calc-alkaline lavas is after Irvine and Barager (1971). All samples are plotted (except those with LOI >2) and define a trend with a small degree of iron enrichment (Figure 4.3). Iron enrichment trends are due to the inability of iron-rich phases (eg Ti-magnetite) to be fractionated during early crystallisation. Hall (1987) found that a small degree of iron enrichment is typical of alkali rocks as have previous workers on Lyttelton lavas (Neumayr 1998, Hibberd 1994, and Shearer 1986).

4.2.3 Discrimination Diagrams

Rollinson (1993) states that discrimination diagrams seldom provide unequivocal confirmation of former tectonic settings and therefore should only be used to suggest an affiliation. High field strength elements such as Ti, Zr, Y and Nb are commonly used to determine the paleo-tectonic-magmatic environment as they are immobile in aqueous fluids. The three diagrams used in this study are from Pearce & Cann (1973), Mullen (1983) and Meschede (1986) with all samples plotted. The Lyttelton Volcanic Group has been classified as 'within-plate' alkali basalts by previous workers (Neumayr 1998, Altaye 1989), and the results from this study are consistent with this finding (see below).

Pearce & Cann (1973) (Fig 4.4A)

The samples in Pearce & Cann's (1973) diagram plot in the 'within-plate basalt' and 'calc-alkali basalt' fields. The large spread of the data is due to samples containing cumulus Ti-bearing phases such as titanomagnetite and clinopyroxene which skew the results (Rollinson 1993). Samples that plot outside the fields are the chemically evolved trachytes that do not fit the parameters of the diagram (eg 20%>CaO+MgO>12%). Neumayr's (1998) basalt data have also been plotted and it overlaps the data from this study.

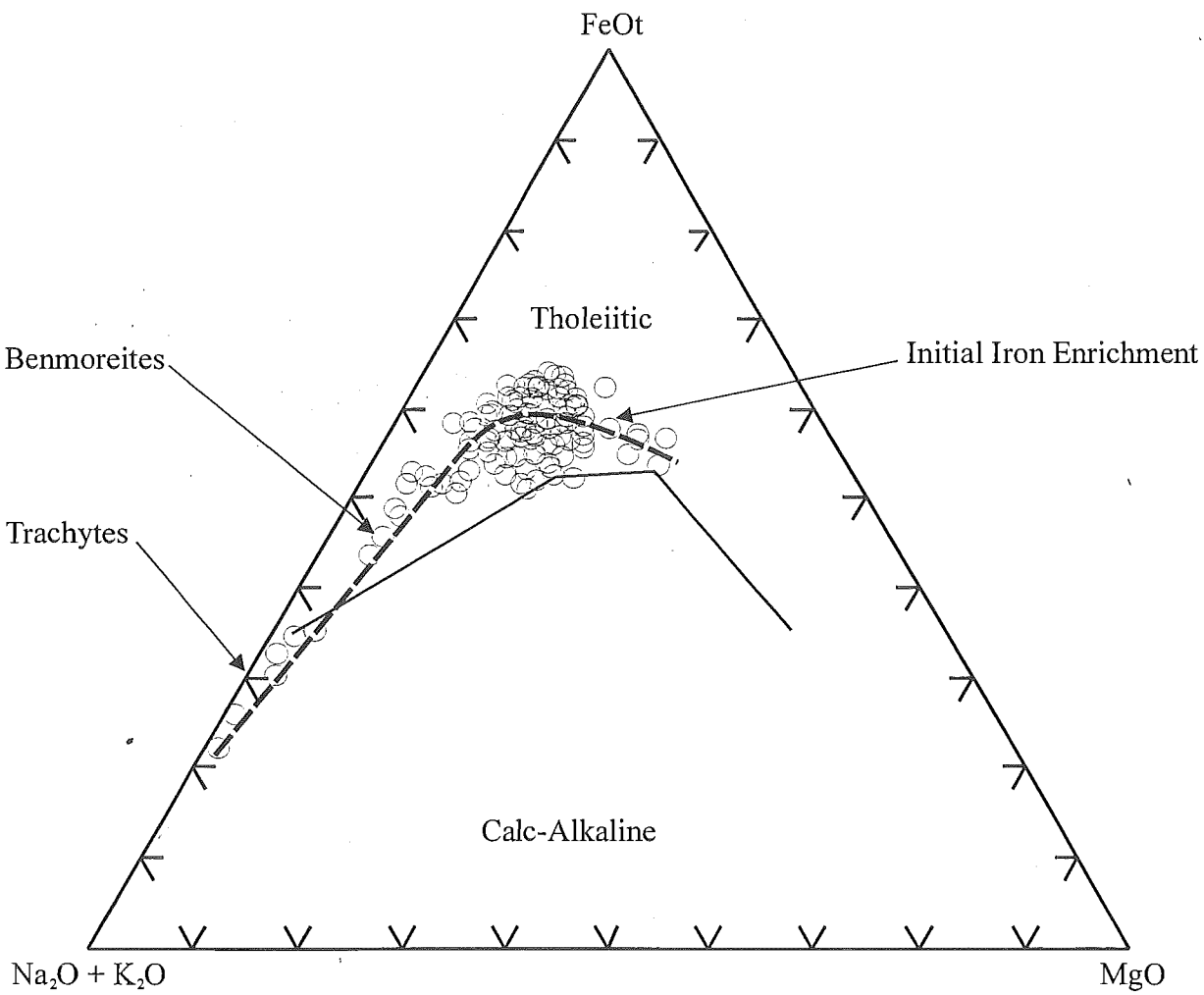

Figure 4.3. AFM diagram after Irvine and Barager (1971). All data are plotted with a LOI<2.

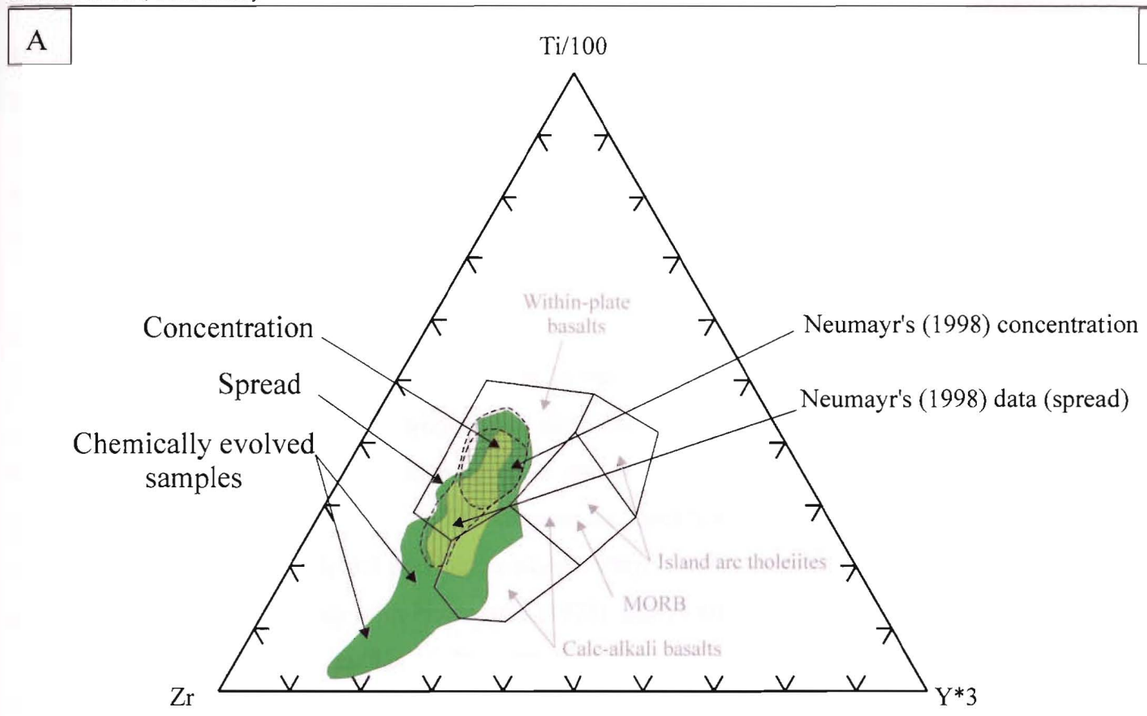

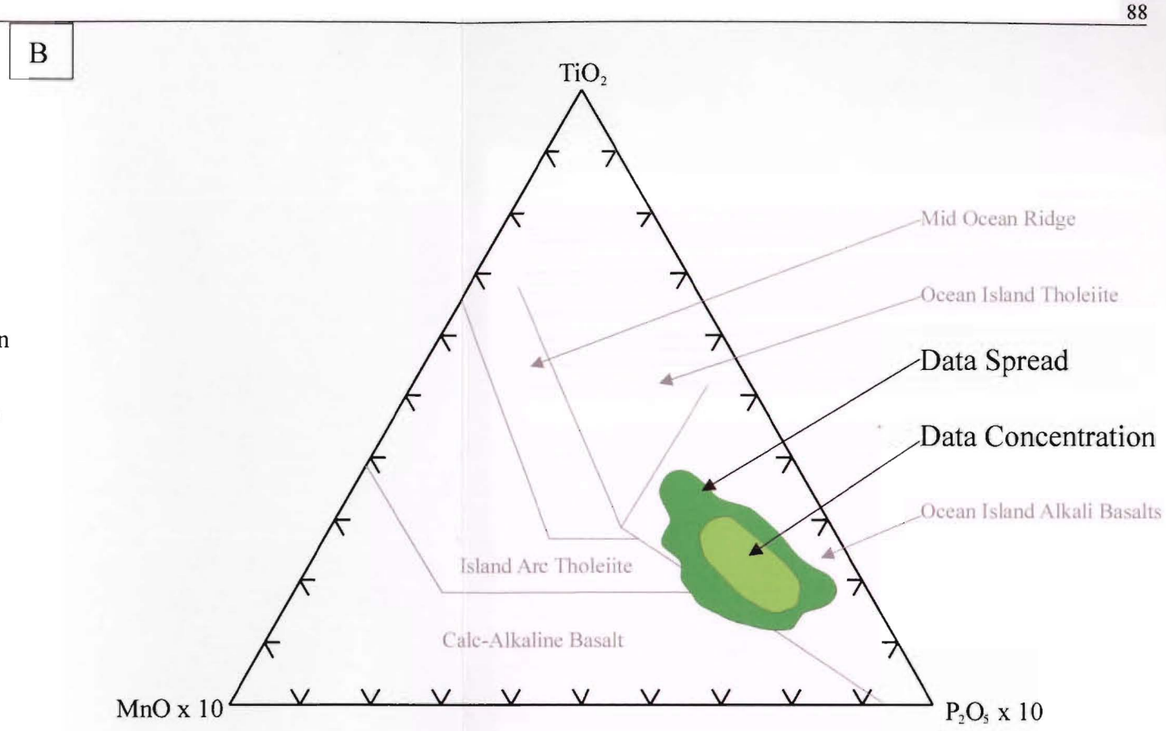

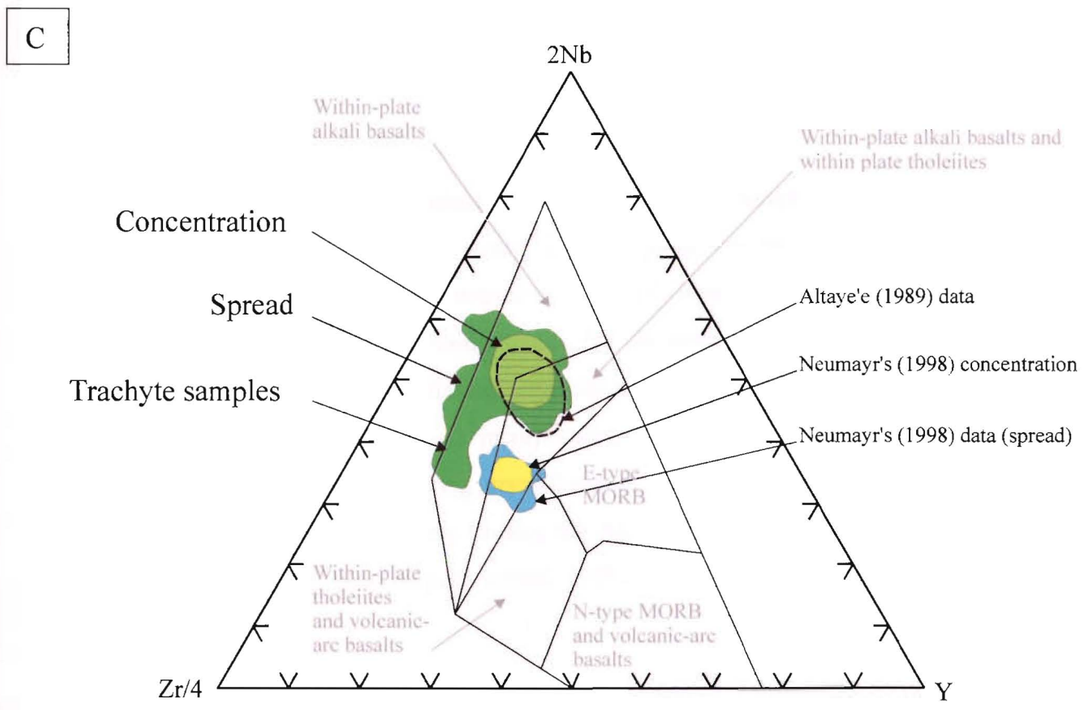

Figure 4.4. Discrimination diagrams based on trace element concentrations. **A)** is based on Pearce & Cann (1973). **B)** is based on Mullen (1983). **C)** is based on Meschede (1986). (Note that N-type MORB is from a normal mid ocean ridge environment and the E-type MORB is from plume influenced region).

Mullen (1983) (Figure 4.4B)

The samples in Mullen's (1983) diagram plot in the 'ocean island alkali basalt' field. The data has a smaller spread in the diagram (than in Figure 4.4A) due to fitting the parameters better (eg 45-54wt% SiO_2, 0.16-0.24wt% MnO, 0.14-0.74wt% P_2O_5 and 0.81-3.07wt% TiO_2).

Meschede (1986) (Figure 4.4C)

The samples in Meschede's (1986) diagram plot in the 'within-plate alkali basalt' field with a lesser amount plotting in the 'within-plate alkali basalts and within plate tholeiites'. The spread of values outside the boxes is again due to these samples not fitting the parameters (eg 20%>CaO+MgO>12%). This diagram has been used however to show the similarities between this work and previous workers. Altaye's (1989) data for Lyttelton 2 lavas plots on top of this study with Neumayr's (1998) data plotting just below. Most of Altaye's (1989) samples, as in this study, were hawaiites and mugearites, which may account for the similarity between the two plots.

4.3 CHEMICAL VARIATION

All pyroclastic samples (eg bombs, proximal samples, vent samples) have been plotted together on the same graphs, and their trends are discussed below.

4.3.1 Major Element Variation

Major element data were plotted against SiO_2 for pyroclastic samples (Figure 4.5), excluding those with a LOI > 2. The scatter in most plots can be attributed to the porphyritic nature of most samples and magma mingling (S. Weaver, pers. comm. 1999). Na_2O, K_2O, and P_2O_5 all have increasing trends for all areas, reflecting the relative incompatibility of these elements during crystallisation. P_2O_5 does become more compatible above 52% SiO_2 due to its incorporation into apatite. Al_2O_3 is the only component that shows no change during crystallisation, due to plagioclase crystallises together with clinopyroxene and olivine, causing the Al_2O_3 content to be buffered by the crystallising assemblage (S. Weaver, pers. comm. 1999). The five remaining components

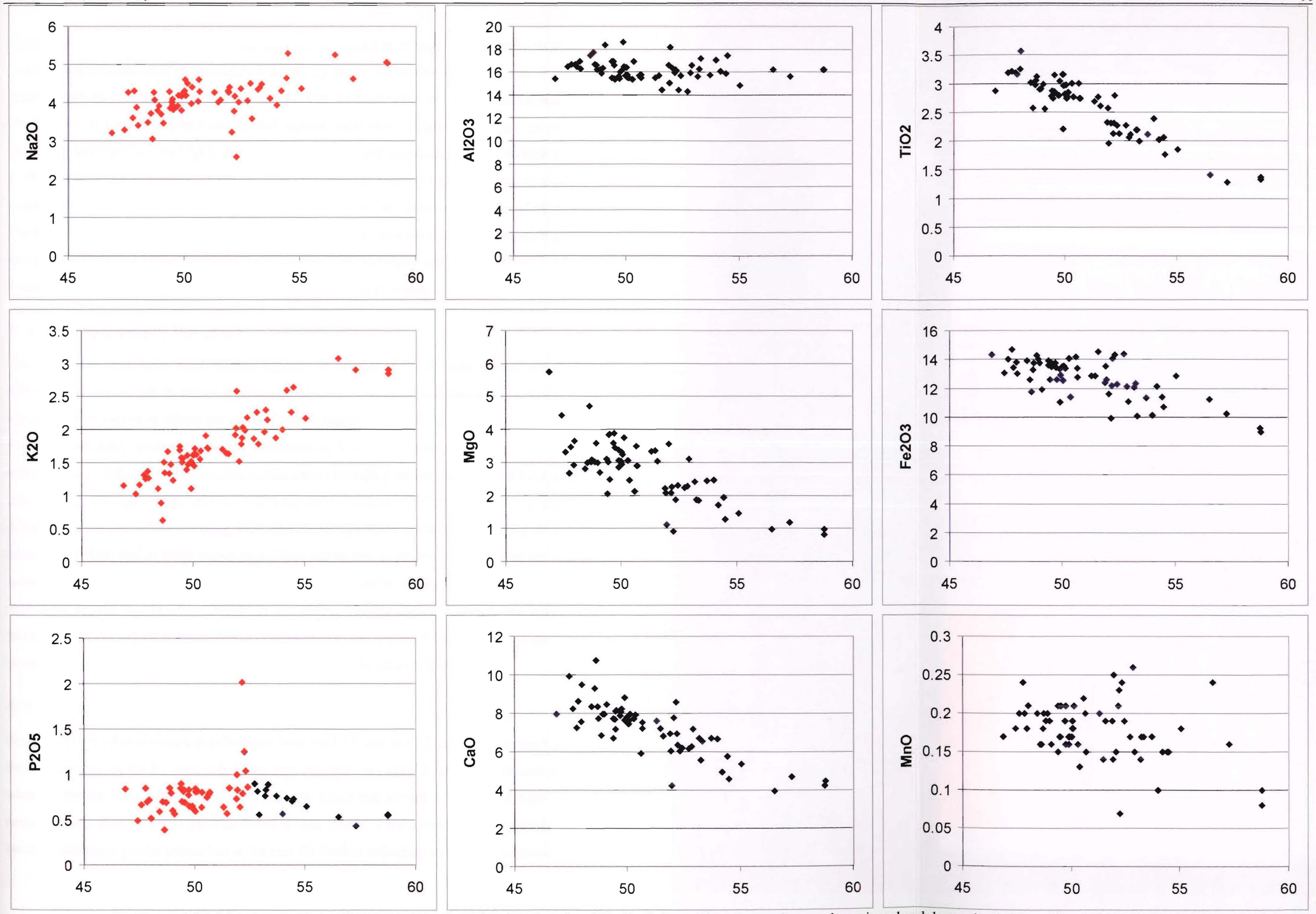

Figure 4.5. Major element Harker diagrams, with all graphs plotted against SiO_2. Fe_2O_3 is total iron. Increasing trends are in red and decreasing in blue with no change in black.

(MgO, CaO, TiO_2, Fe_2O_3, and MnO) all decrease, a reflection of their compatibility with increasing fractionation. MgO is removed mostly by the crystallisation of olivine, and to a lesser extent by clinopyroxene. CaO is removed by crystallisation of clinopyroxene and plagioclase. If CaO and MgO are plotted against each other (Figure 4.6) there is an increasing trend up to ~5% MgO, after which there is a rapid decrease. Peterson & Moore (1987) correlated the increase to the removal of CaO and MgO from the magma in the coprecipitation of plagioclase and clinopyroxene, with the decrease due to olivine fractionation. TiO_2 decreases due to the crystallisation of Ti-magnetite. The decreasing trend in Fe_2O_3 is due to the fractionation of olivine, clinopyroxene and Ti-magnetite. The scattered decrease in MnO is due to the fractionation of clinopyroxene and olivine.

4.3.2 Trace Element Variation

Trace element data have been plotted against Zr (Figure 4.7). Zr was chosen as a differentiation index due to large variations in the concentration in samples and due to its insensitivity to alteration (Neumayr 1998). Four elements (V, Cr, Ni, Sr) decrease because of the compatibility of elements during fractionation. V is fractionated into clinopyroxene and magnetite while Cr shows rapid depletion due to its high partition coefficient for early minerals, eg clinopyroxene, olivine and magnetite (Neumayr 1998). Ni also rapidly decreases in samples with increasing SiO2, due its high partition coefficient, allowing easy access to olivine, and at early stages into Ti-magnetite and pyroxene. Depletion of Sr is achieved by the fractionation of feldspar and exceptionally strong depletion implies prolonged crystal fractionation (Noble et al. 1969). The remaining elements all have increasing trends, which reflects their incompatible nature, although Ba starts to become more compatible at higher SiO_2wt%, due its incorporation in alkali feldspar.

4.3.3 L1 or L2 Magmas

Neumayr (1998) found chemical differences between L1 lavas and L2 lavas. The trends he found were due to the L1 lava pile being less evolved than the L2 lava pile. Therefore when he plotted CaO, MgO and TiO_2 vs SiO_2 he found that overall L1 lavas had higher concentrations than L2 lavas. He also found similar trends in trace element plots with L1 lavas containing a greater proportion of Ni and Th, further reflecting its less differentiated

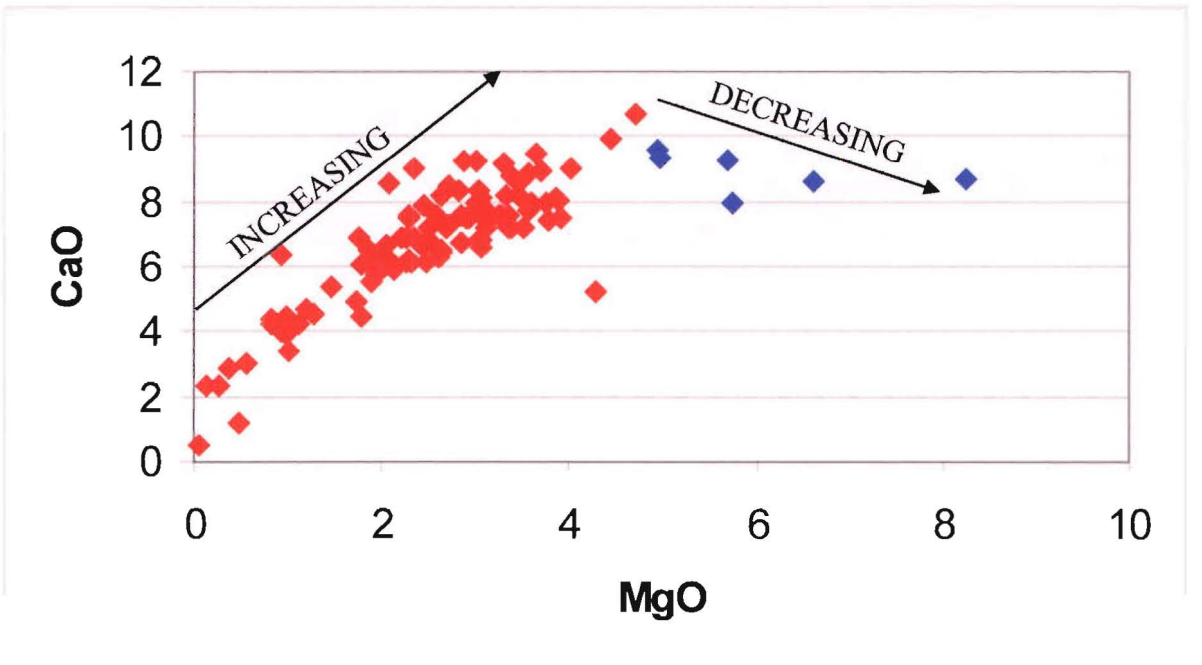

Figure 4.6. Bivariate plot of CaO vs MgO. The change in slope at about 5 wt% MgO suggests a change in the fractionating phases at this point (based on a similar diagram after Peterson & Moore 1987).

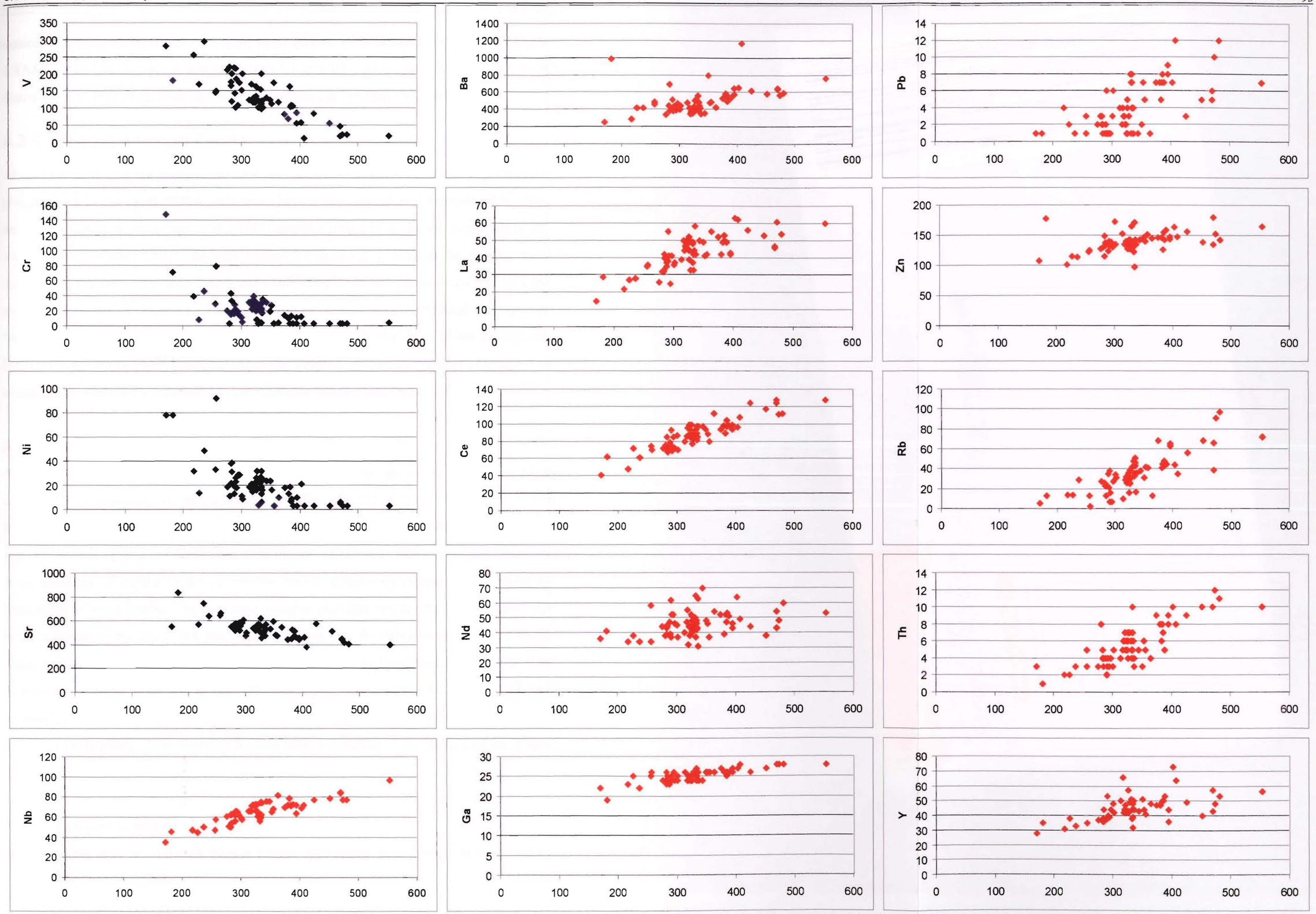

Figure 4.7. Trace elements vs Zr (abscissa), note increasing trends are in red while decreasing trends are in blue (all values in ppm)

nature. A comparison of L1 and L2 lavas to L1 and L2 pyroclastics is illustrated in Figure 4.8A&B. Due to the evolved nature of both L1 and L2 cinder cone samples, there is no distinct variation in plots, with most samples plotting in Neumayr's (1998) L2 area.

4.3.4 Variation Amongst Facies

At all sites there is some variation in chemistry between samples. From the TAS diagrams (Figure 4.1A-I) it is apparent that some areas have a large variation in samples while others have little variation. Houghton et al. (1999) found a progressive change in chemistry in a cinder cone at Crater Hill, Auckland, caused by chemical zoning in the magma rising through the conduit. They also found that some samples in late phase eruptions were less evolved than earlier samples. The less evolved nature was interpreted to represent 'stagnant' magma that was stored in blind portions of the feeder dike, before mixing with fresh-arriving magma and being subsequently erupted. Therefore transects through four cones in this study were conducted to see if similar trends could be identified.

Southern Mount Cavendish (Figure 4.9A)

A vertical transect taken through one side of the cone showed consistent variation, with an increase in Zr concentration up the section. Bombs collected at the bottom of the section had the lowest Zr concentration and a degassed block in the outer medial facies had the highest. A vent sample collected from near the top of the vent facies plots just below the main grouping of medial facies (ie bombs) points, suggesting emplacement around the deposition of most bombs. The two dike samples plot just beside two vent samples that were collected at the top of the vent area, implying that the dikes were emplaced as late stage events. The most evolved samples are the late stage flow samples and hence are interpreted to have been fed by the cone as a late stage event. No changes in clast morphology (ie degassing, size etc) could be directly related to changes in chemistry and therefore are probably controlled by physical processes acting at the surface of the magma in the vent.

Northern Mount Cavendish (Figure 4.9B)

Although this area was erupted from a fissure type rather than a cone, it has excellent

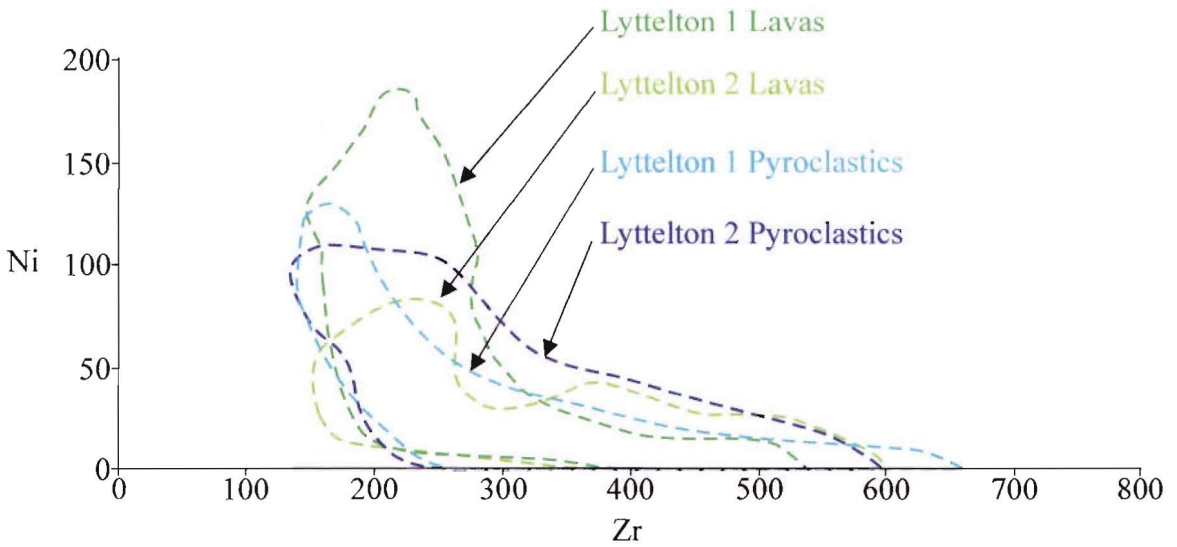

Figure 4.8A. Comparison of Neumayr's (1998) data for L1 and L2 lavas with L1 pyroclastics and L2 pyroclastics from this study. Ni (ppm) is plotted against Zr (ppm).

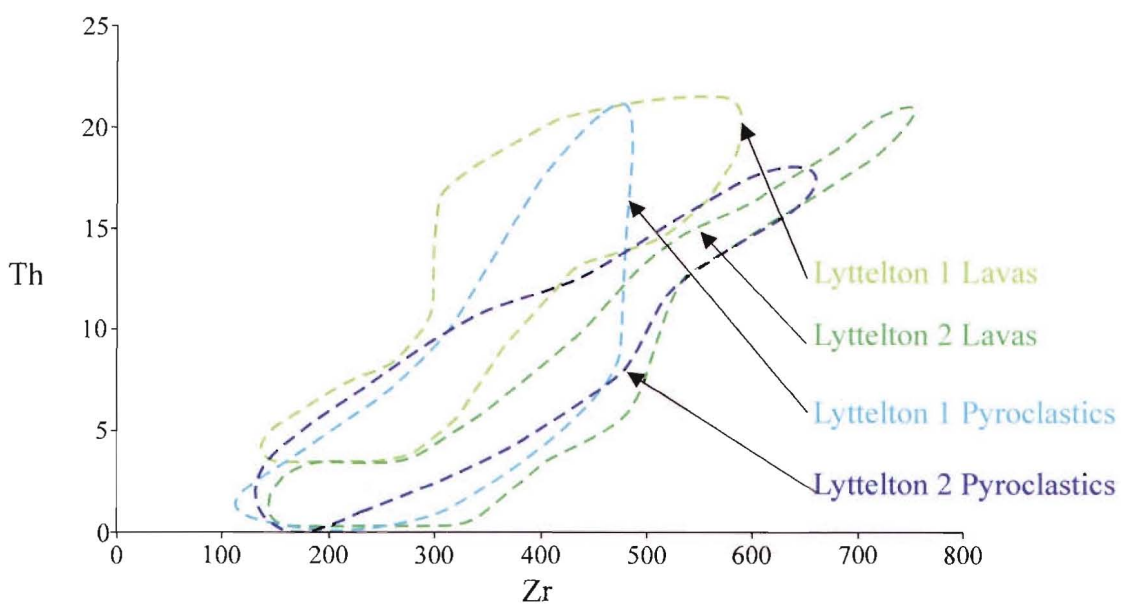

Figure 4.8B. Comparison of Neumayr's (1998) data for L1 and L2 lavas with L1 pyroclastics and L2 pyroclastics from this study. Th (ppm) is plotted against Zr (ppm).

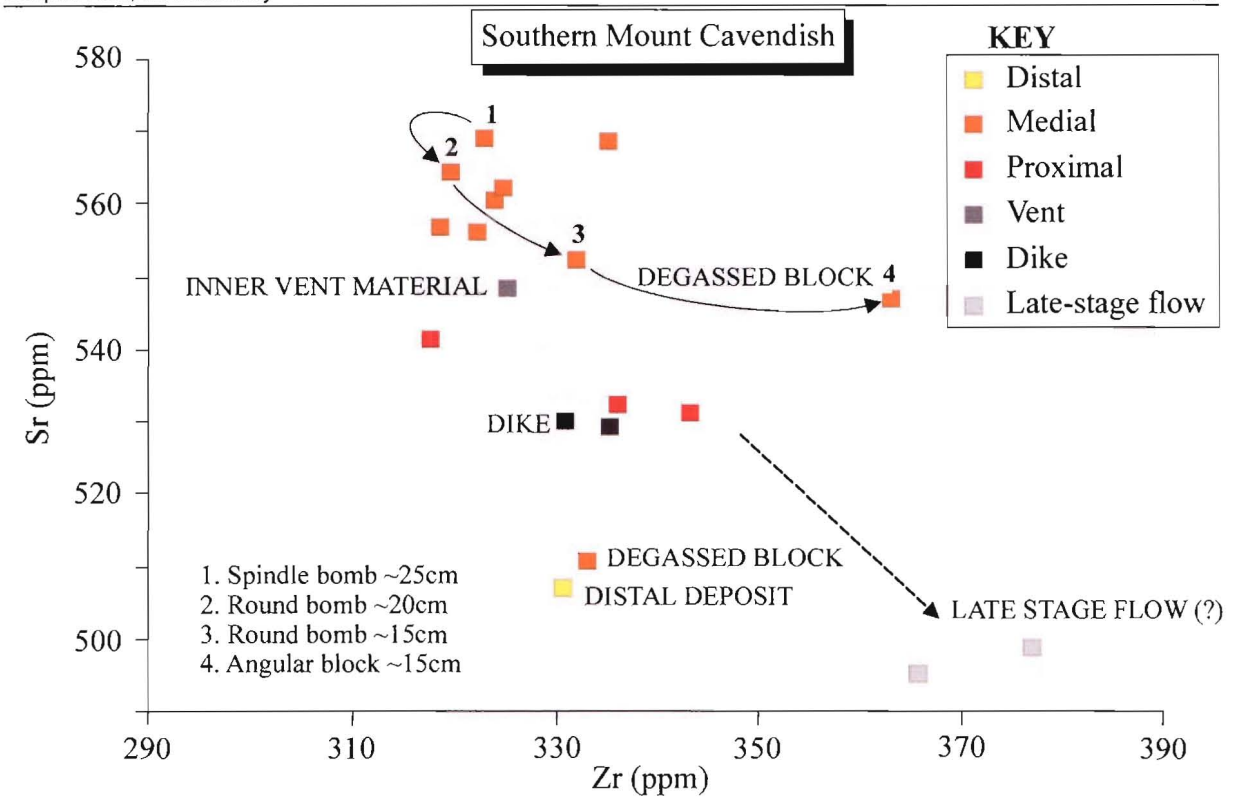

Figure 4.9A. Graph illustrating the variation in geochemistry in the Southern Mount Cavendish cinder cone. Numbers 1 - 4 are samples taken up a 20 m section.

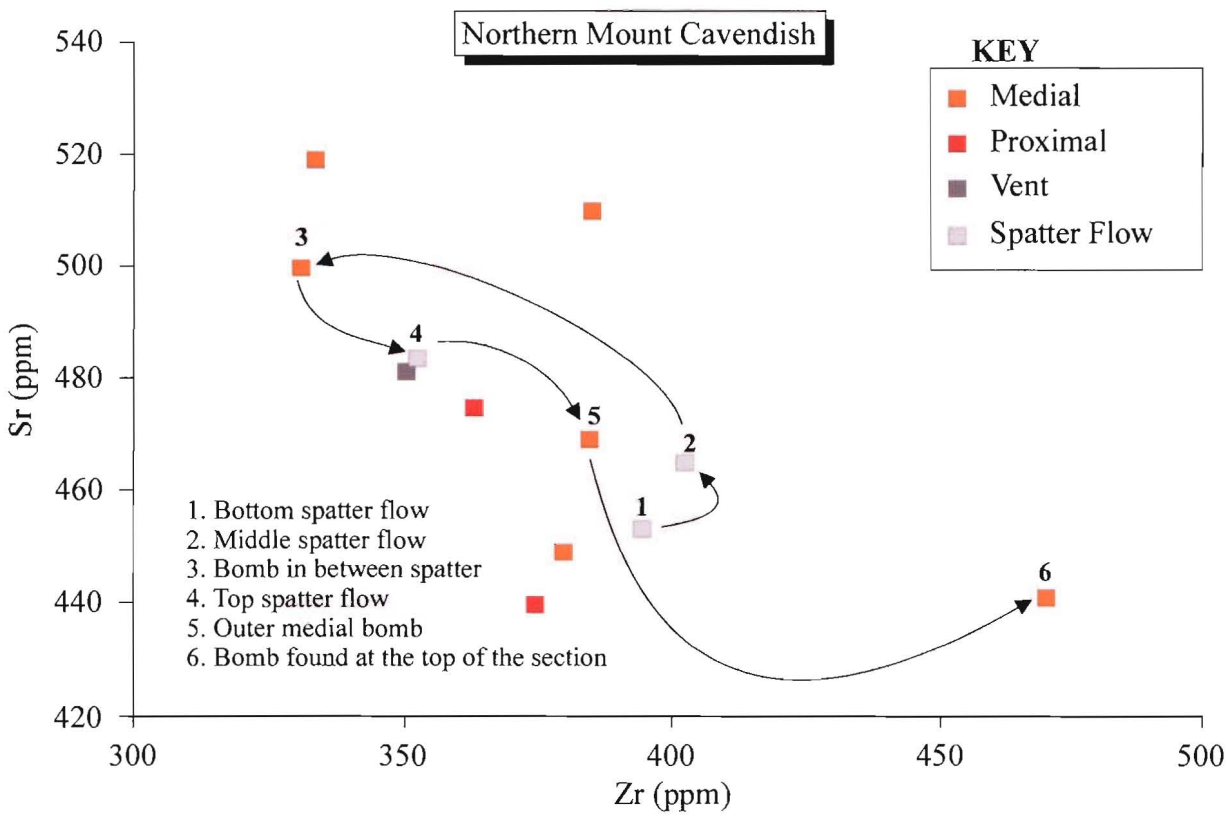

Figure 4.9B. Graph illustrating the variation in geochemistry in the Northern Mount Cavendish cinder cone. Numbers 1 - 6 are samples taken up a 30 m section.

vertical exposure allowing samples to be taken up a vertical transect. Figure 4.9A shows that the two lowest spatter flows in the section have higher concentrations of Zr than the samples above it with a bomb sample taken from the outer medial deposits having the highest. Therefore after the deposition of the first two spatter flows, it appears that there was recharging in the vent and the introduction of a fresher basic magma. The introduction of fresh hot magma would have been a likely trigger for the explosive eruptions and may explain the overlying spatter flows. Petrographic evidence for the recharge is seen in the top spatter flow with sample DNS3 showing signs of magma mixing, corrosion, oscillatory zoning and sieving in plagioclase phenocrysts.

Northern Gibraltar Rock (Figure 4.10A)

Samples could not be taken through a vertical transect due to the topography. However a horizontal cross-section through the cone was possible, with samples taken from the vent, proximal and medial facies. The samples revealed two distinct groupings, the first suggests an early explosive event, with spatter material dominant, with the second less explosive, dominated by bombs and blocks.

Northern Mount Evans 1 (Figure 4.10B)

Samples again could not be taken in a vertical transect but a horizontal cross-section was possible. The exposure differs to that of Northern Gibraltar Rock in that the cinder cone is not as deeply eroded, hence later stage deposits were dominantly sampled causing a small deviation in between samples, and no strong trends. Late stage proximal deposits however are slightly more evolved than earlier deposits.

4.4 PETROGENESIS

Evaluation of the petrogenesis of Lyttelton magmas is beyond the scope of this study, however a discussion on the data presented in this study compared to previous work is important in providing evidence for eruptive mechanisms.

The initiation of volcanism on Banks Peninsula was suggested by Sewell (1985) to be

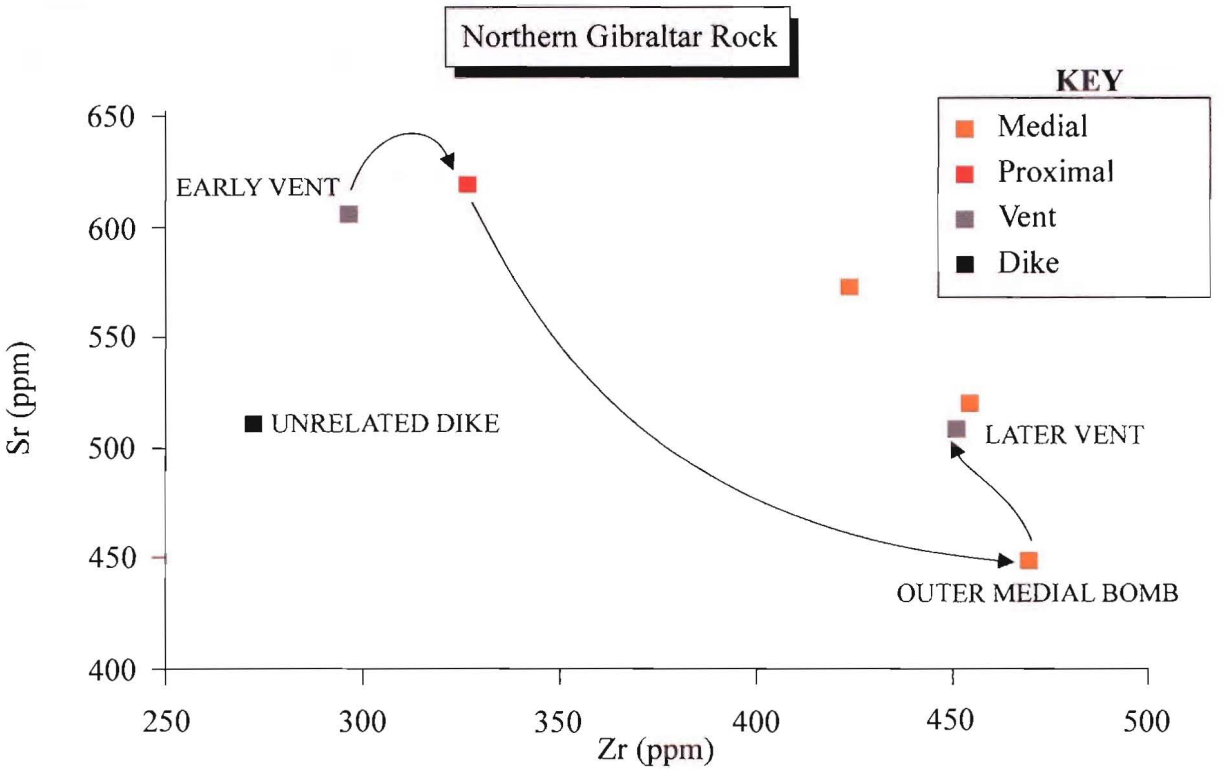

Figure 4.10A. Graph illustrating the variation in geochemistry in the Northern Gibraltar Rock area, suggesting a chemical evolution with time in the samples.

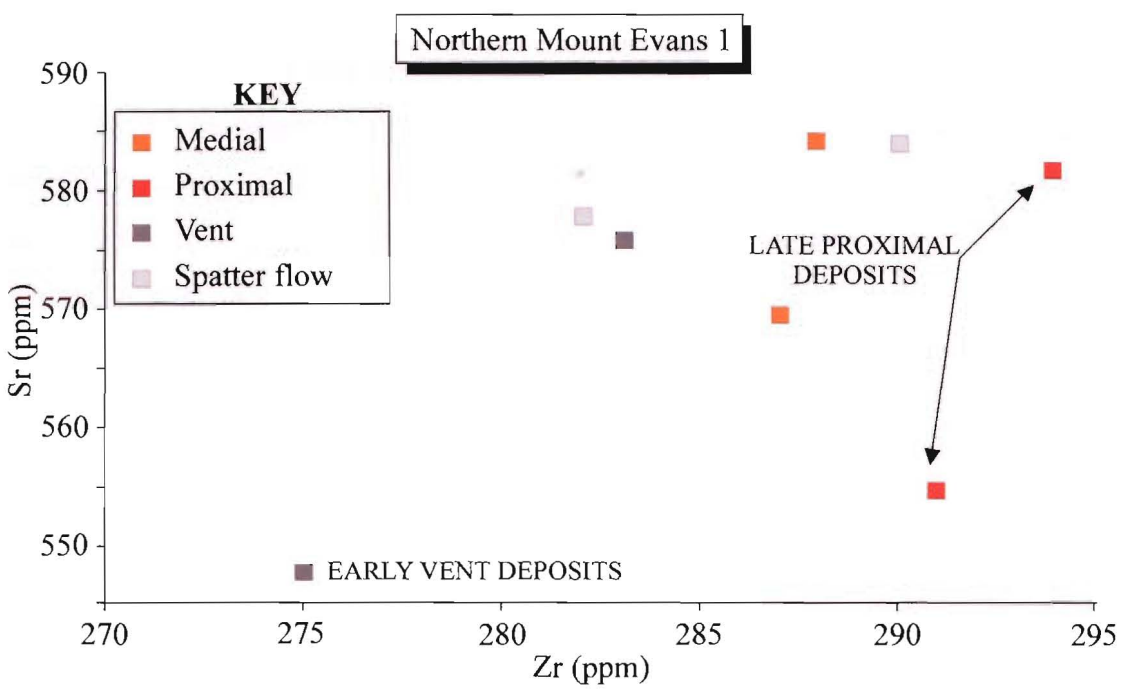

Figure 4.10B. Graph illustrating the variation in geochemistry at Northern Mount Evans 1. Samples again appear to chemically evolve with time with early proximal samples being less evolved than later vent and spatter flow samples (note the small variation in Sr and Zr values compared to the Figures 4.9A&B, and 4.10A).

caused by "a major within-plate stress field, corresponding to the intersection of E - W trending faults of the Chatham Rise and NW – SE trending faults of the Kaikoura Orogen, probably triggered mobilisation and rise of mantle fluids and the local updoming of peridotite in the lithosphere beneath the present position of Banks Peninsula during the middle Miocene". The development of alkali olivine basalts by partial melting of mantle peridotite at depths of < 70 km has been suggested by experimental work (Ringwood 1975) with the ultimate source being the low velocity zone between 80-150 km. Lyttelton alkaline rocks have a moderate to strong light rare earth element (REE) enrichment trend (Weaver & Smith 1989) indicating a garnet-bearing source. Garnet contains heavy REEs and the resulting melt is enriched in light REEs, therefore suggesting that Lyttelton magmas were generated by the partial melting of a garnet peridotite source < 70 km. These early magmas rose to the Moho where they underwent re-equilibration, crystal fractionation, and crustal contamination (Neumayr 1998). The onset of Lyttelton volcanism occurred at approximately 11 Ma with initial lavas showing strong enhanced crustal contamination (Weaver 1991, Figure 4.11). Later Lyttelton lavas have a transitional alkaline basalt to trachyte trend of sodic composition, with little contamination. The samples collected from this study dominantly plot above the early trend or on the later trend, and this is a result of most of the sites being located in or on the later Lyttelton lavas.

Neumayr (1998) suggested that the main Lyttelton magma chamber probably occurred at approximately 15 km depth with a high level chamber(s) at a depth of about 3-4 km. Gerard (1953) also suggests a high level chamber existed, due to low aeromagnetic anomalies in Lyttelton Harbour. A similar scenario has been suggested at Mt Etna with a deep storage area for magma at ~20 km (Sharp et al 1980) with higher level chambers at approximately 6 km (Hirn et al 1991). Condomines et al. (1995) suggest that beneath Mt Etna primitive magmas generated in the mantle rise up and collect in the deep seated lower crustal reservoir (~20 km). Fractionation of the magma involving predominantly mafic phases leads to the development of less dense melts that then ascend to the surface, with each eruption suggested to represent a distinct magma pulses (Armienti et al. 1994).

Neumayr (1998) suggests that the whole magma system for Lyttelton underwent chemical

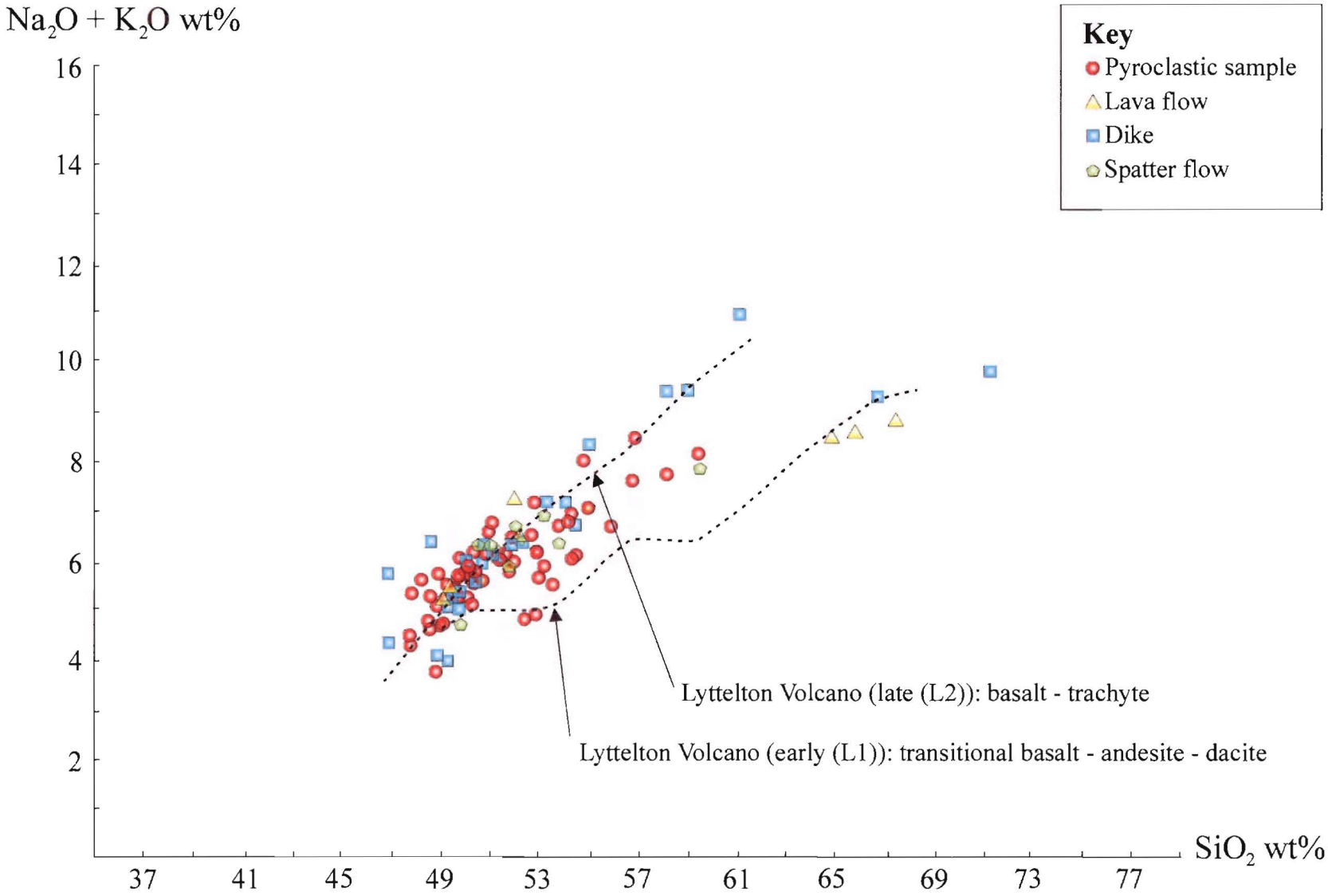

Figure 4.11. Compositional trends taken from Weaver (1991) for Lyttelton lavas. Pyroclastic samples dominantly plot above the early trend or on the late trend.

evolution with time and became progressively more fractionated. Constant replenishment caused limited differentiation in the main chamber with initial activity dominantly basaltic. The increase in dikes throughout Lyttleton's history allowed for increasing differentiation at higher levels and hence lavas became more evolved (eg mugearites, benmoreites, and trachytes). The main chamber also probably became zoned during quiescent times as found by Fitzgerald (1991) during the evolution of the Castle Rock.

The development of cinder cones on Lyttelton also changed throughout its history. Early cinder cones are basaltic (eg Hoon Hay Park 1, Southern Gibraltar Rock) like the early lavas. Later formed cinder cones vary, with some hawaiitic (eg Northern Mount Evans 1, Southern Mount Cavendish) and others mugearitic (eg Northern Mount Evans, Northern Gilbraltar Rock). The variation is due to the increasing development of dikes, allowing volatile rich magma to reach the surface with limited differentiation, hence basalt and hawaiitic cinder cones. Whilst the mugearitic cones represent magma that has resided for longer in the edifice, allowing increased differentiation. The fact that cinder cones are most common in later activity suggests that as activity shifted from L1 to L2, dikes became more common allowing the development of more explosive flank eruptions.

The differentiation in all samples is attributed to crystal fractionation as suggested by previous workers on the lavas of Lyttelton (eg Coates 1976, Sewell 1985, Shearer 1986, Weaver & Sewell 1986, Altaye 1989, Slaughter 1995, and Neumayr 1998). Olivine, clinopyroxene, plagioclase and Ti-magnetite are the main crystallising phases. Crystallisation of apatite and alkali feldspar also caused changes in more evolved samples with a depletion in P_2O_5 and Al_2O_3 respectively.

Chapter Five

DISCUSSION AND INTERPRETATION

5.1 INTRODUCTION

The aim of this chapter is to discuss the mechanisms responsible for the deposits discussed in Chapter Two. The deposits are the remnants of explosive flank eruptions that occurred throughout the development of Lyttelton. Due to the eroded nature of the deposits a review of the literature is needed to infer possible mechanisms. Ascent of magma on Lyttelton is discussed, along with components involved in generating explosive basaltic eruptions, cinder cone eruption dynamics, and the resulting deposits.

5.2 MAGMA ASCENT

Cinder cones are the surface expression of the movement of magma below the surface and hence a discussion on the development of dikes is important since they are commonly responsible for the transport of magma from depth to the surface.

5.2.1 Dike development and magma storage

The propagation of dikes has been geophysically measured on Mt Etna (Murray 1990, Rymer et al. 1993), Reunion Island (Lenat et al. 1989) and Hawaii (Wilson & Head 1988). The general consensus is that magma is injected laterally either from a shallow magma reservoir (eg Reunion Island, Hawaii) or from the central conduit (Mt Etna) (Figures 5.1&5.2). The shallow reservoirs are short lived with erupted flank lavas showing extensive plagioclase crystallisation and being only mildly explosive. At Mt Etna, magma enters the volcanic pile permissively with a high level of magma in an open conduit giving steady persistent activity (Guest et al. 1974, Wadge 1977, Guest & Duncan 1981, Sanderson et al. 1983, Chester et al. 1985, Murray 1990, Hughes et al. 1990). Dike-like intrusions leading to flank eruptions radiate out at various depths from the central conduit

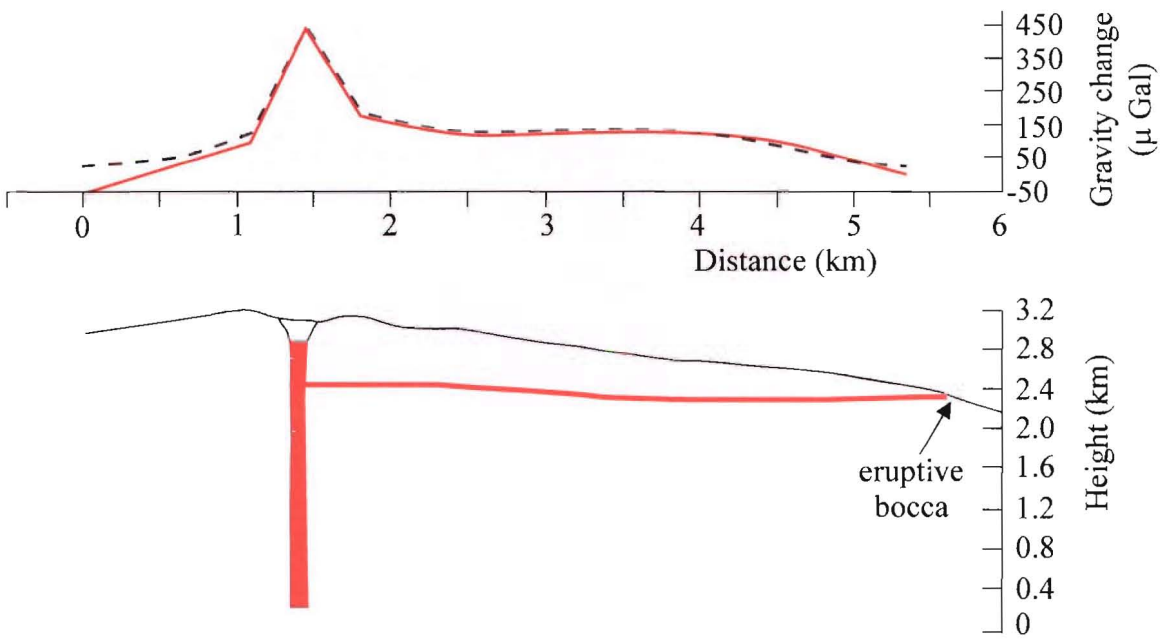

Figure 5.1 Computed gravitational effect from a 2.5D model of the 1990-1991 changes in magma level within the summit feeder and the proposed fissure region beneath the upper southern flank at Mount Etna. The density of the intrusions is assumed to be 2,800 kg m, the same as the surrounding material. Note that the total strike width of the feeder pipe is 50 m and the width of the dike is 4 m. The model does **not suggest** that these are the limits of the bodies, simply that these are the sort of changes between June 1990 and June 1991 which would fit the observed gravity data. Indeed the feeder pipe is almost certainly extends down to a large magma reservoir well below sea level. Seismic data indicate sources at 2 km depth, which roughly coincides with the modelled base here. The approximate location of the main eruptive vent for the 1991-1992 activity is also shown, although in fact it is slightly to the east of this profile (into the page) (fromRymer et al. 1993).

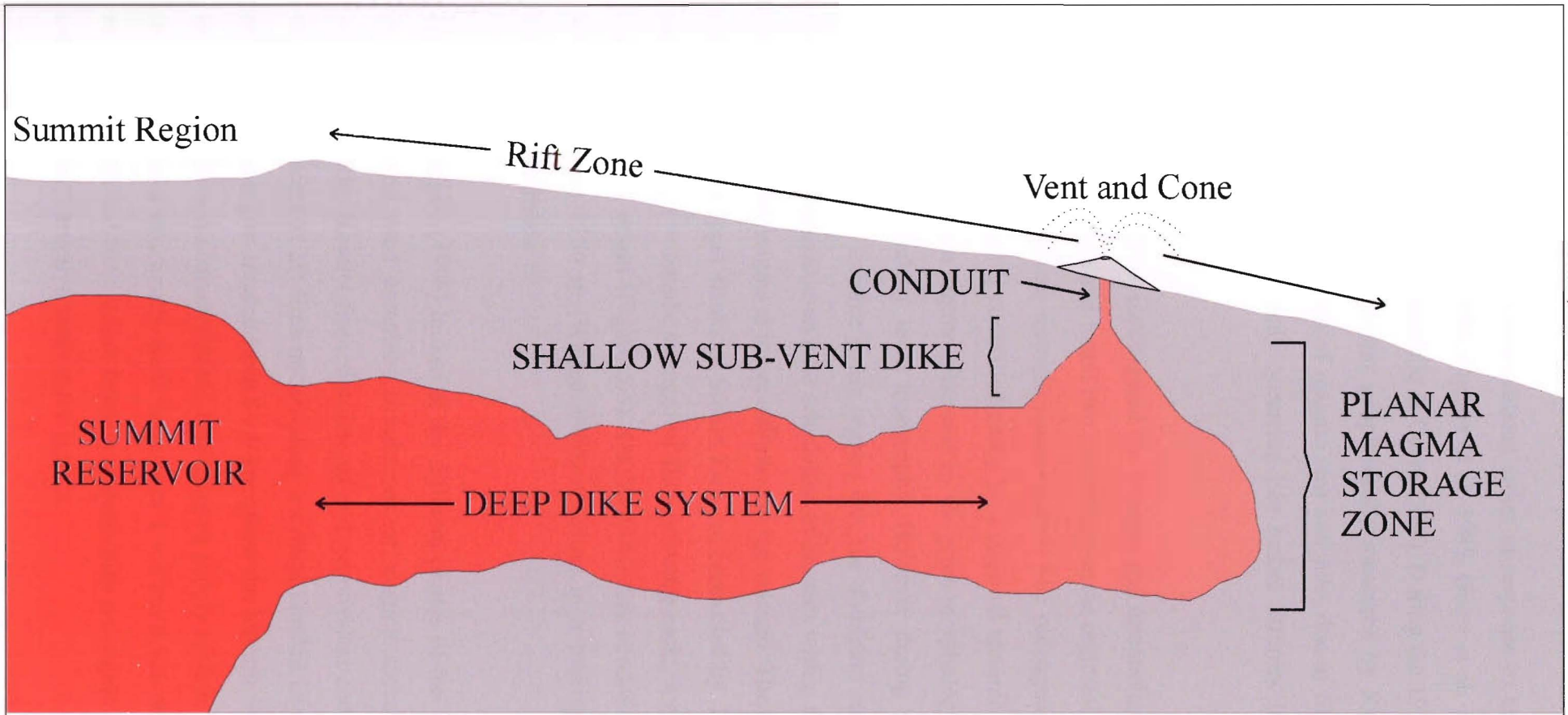

Figure 5.2. Proposed nomenclature for the common elements of a basaltic dike system along a rift, and for the subvent region. "Planar magma storage area" and "shallow subvent dike" are considered to be more realistic descriptions of the subvent magma geometry than "chamber" or "reservoir", which imply a relatively large equant body, as distinct from the feeder dike (after Wilson & Head 1988).

and may be emplaced in fissures dilated either in response to tectonism or gravitational forces (Murray & Pullen 1984, Chester et al. 1985, Guest et al. 1987, McGuire & Pullen 1989, Rymer et al. 1993, Bonafede & Cenni 1998). During the 1991-1993 eruptions on Mt Etna the intrusion of a dike was geophysically measured by Rymer et al (1993). They found that the 1991 intrusion of magma was aseismic, due to filling a previous fracture, with low microseismicity only occurring just before Strombolian flank activity due to vigorous vesiculation.

McGuire & Pullen (1989) investigated the location and orientation of eruptive fissures and feeder dikes on Mt Etna and found two controlling stress regimes: (1) a gravitational stress regime, and (2) a regional tectonic stress regime. The propagation of dikes on Mt Etna during the present time is controlled partly by a regional tectonic stress regime and partly by a gravitational stress regime generated by the gross morphology of the volcanic edifice, and which is modified by local topography. However during the early history of the volcano the regional tectonic stress regime was the dominant control of feeder-dike and eruptive fissure disposition and the orientation of stresses within this regime is reflected in the pattern of older fissures at lower altitudes on the volcano. The broad radial distributions of fissures on the upper flanks of Mount Etna are controlled by: $P_m > \tau + \theta_3$. Where: P_m = magma pressure; τ = tensile strength of the enclosing rock; θ_3 = minimum compressive stress of external origin (Figure 5.3). On Mt Etna, this condition is best satisfied at an altitude of about 1750 m (Wadge 1976) resulting in a maximum frequency of radial fissures at this altitude.

Dobran & Coniglio (1996) looked at the different phases of the 1974 and 1989 eruptions on Mt Etna and used computer simulations of magma ascent to assess the internal plumbing system. Results from simulations and geophysical and geological data suggest that magma ascent at Mt Etna occurs along a central conduit or inclined conduits from a magma storage region located from 8 – 9 km below the summit, depending on the regional tectonic stresses and characteristics of the magma supply system. The results also suggest the existence of a structurally weak zone from 1 – 4 km below the summit where magma may accumulate and from which fracture systems may propagate leading to magma ascent and gas loess with eruptive vents at the surface.

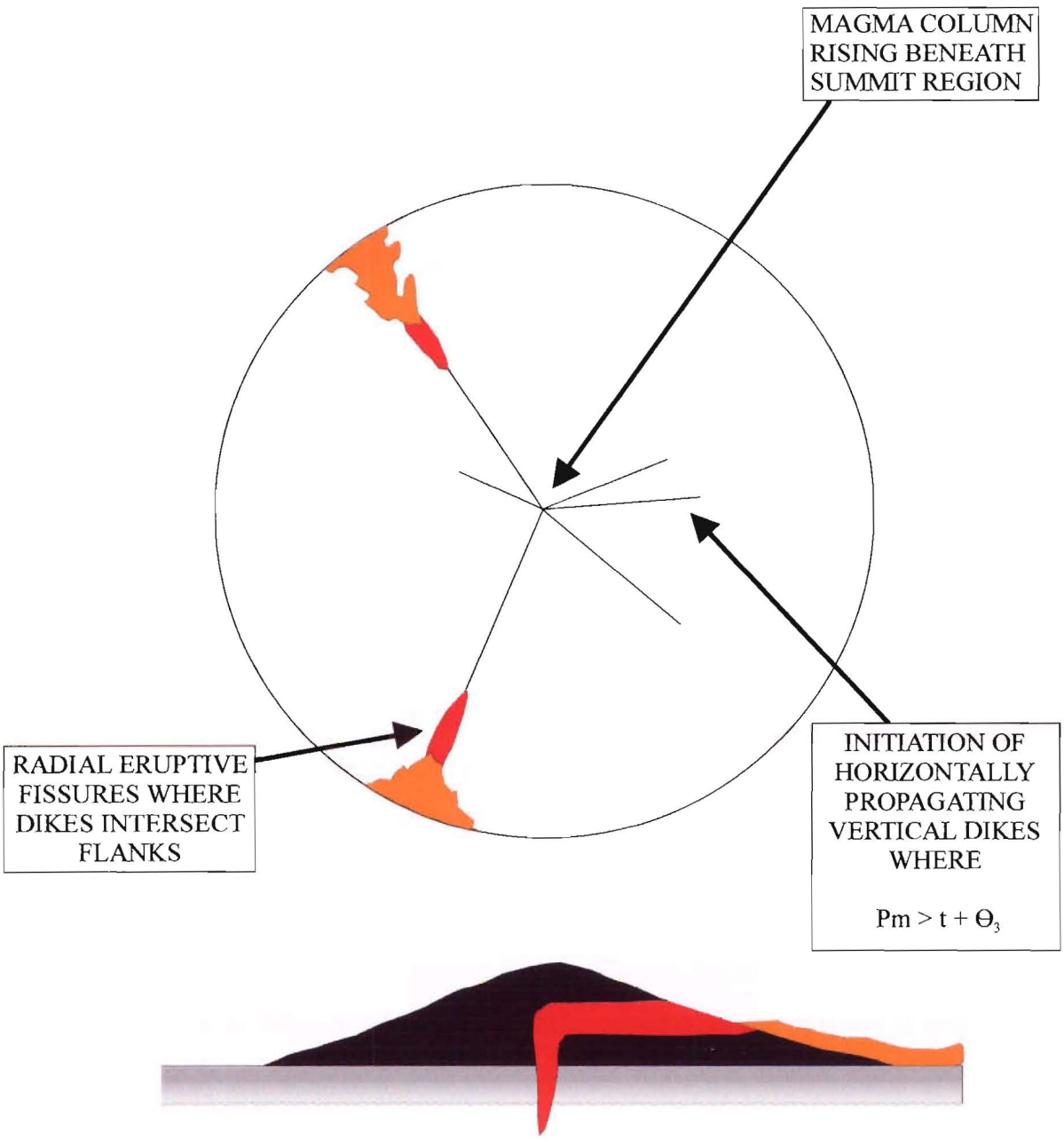

Figure 5.3 The broad, radial distribution of fissures on the upper flanks of Mt Etna can be explained most successfully within the framework of gravitational stress regime, in vertical dikes propagating horizontally from a rising magma column intersect the flanks froming radially disposed eruptive fissures. Magma is rising beneath the topographic centre of the regular volcanic cone which is externally stressed due to gravity alone, fracturing of the walls of the conduit results in the formation of a vertical, horizontally propagating dike. Given sufficient magma pressure this will intersect the cone flank to produce an eruptive fissure which bears a radial relationship to the topographic centre of the cone. Repetition of such an event results in the formation of numerous radial fissures that, due to regular cone morphology, are normal to the contours at all points (from McGuire & Pullen 1989).

Volcanic activity on Mt Etna is critically dependent upon the working of the deep reservoir with its gradual filling of magma leading to increasing pressure and distension in the overlying crust causing failures in a radial direction in the volcanic edifice (Tanguy et al. 1997). The deep magma reservoir at Mt Etna has been constantly replenished during its history by the influx of basaltic magma from the mantle, undergoing limited differentiation through crystal fractionation, causing dominantly hawaiitic lavas (Condomines et al. 1995). Exceptionally high activity in the last 25 years has been characterised by unusually frequent flank eruptions and strongly explosive summit eruptions caused by the influx of a new batch of magma within the deep reservoir (Tanguy et al. 1997). This increase in activity is characterised by the generation of a shallow plumbing system, allowing increased assimilation and increasing differentiation (Armienti et al. 1994).

5.2.2 Evolution of Lyttelton dikes

The evolution of dikes played an important part in the development of Lyttelton Volcano, not only by feeding flank lavas and domes, but by also feeding cinder cones (Shelley 1988). Dike emplacement occurred throughout its history and hence it has a well developed radial dike swarm. Shelley (1987) used the dike swarm to define the two main eruptive centres for the volcano. Shelley (1988) found the shapes of the radial dikes to be blade-like and dikes show a wide range of flow directions, evenly balanced between upward and downward flow with the majority in an outwards horizontal direction. He thought that this was likely to be due to dikes propagating outwards, downwards and upwards (Figure 5.4) and found this to be in agreement with other authors who have studied radial dikes (eg Parsons 1939, Fiske & Jackson 1972, Smith 1978, Sanderson 1982, Wilson & Head 1988).

Shelley (1987) found that dikes around the crater wall vary considerably in chemical composition, with dikes on the southwestern flanks near Gebbies Pass being basaltic whereas dikes further round by Mount Cavendish were mugearitic to benmoreitic. He attributed the change in composition to the evolution of the volcano caused by changes in the composition of the magma chamber. Neumayr (1998) found similarly that L1 lavas are dominated by basalts and L2 lavas by more evolved mugearites and benmoreites. Thus it appears that as activity on Lyttelton changed from centre L1 to L2 the magma underwent

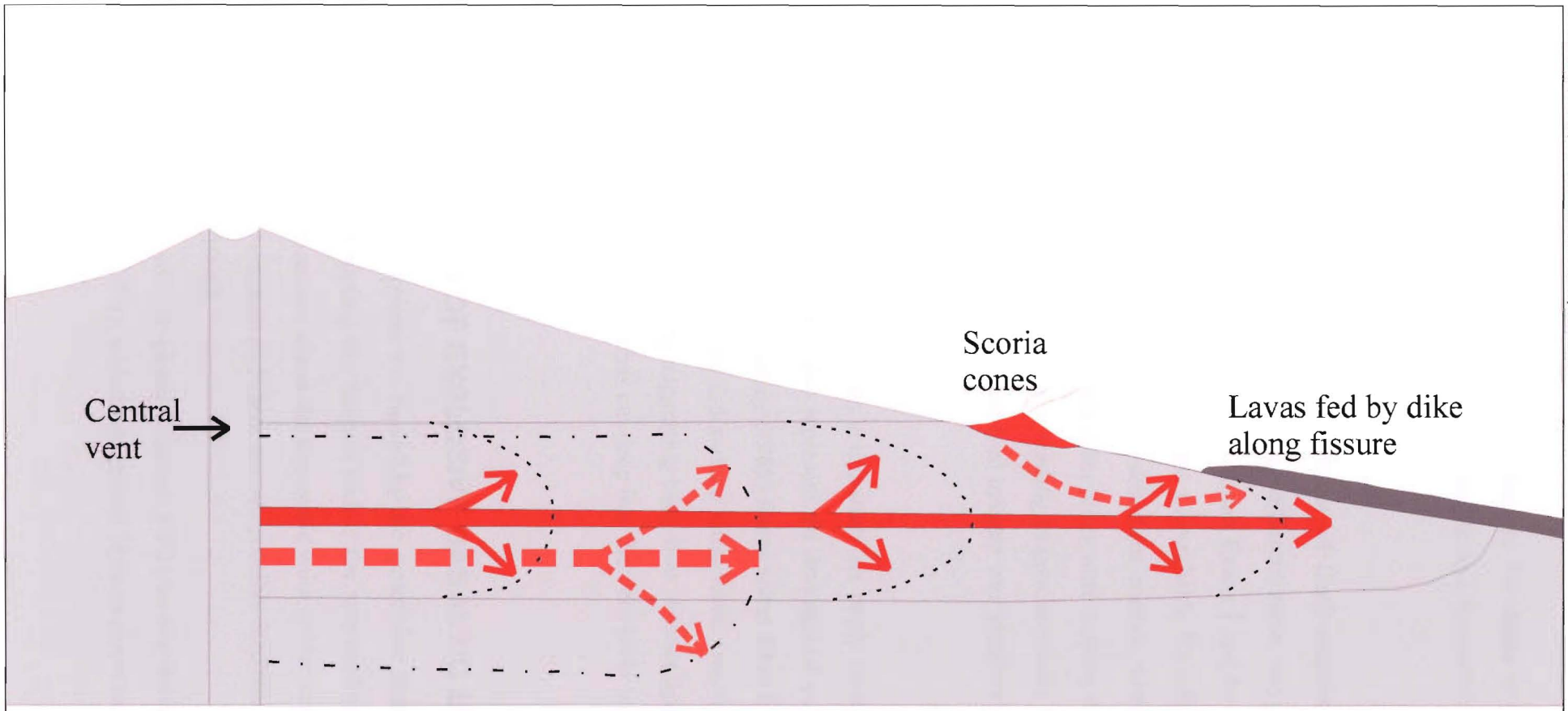

Figure 5.4. Schematic vertical cross section through a volcano showing the profile of a radial dike. Fine dashed lines show progressive positions of a dike. Thick arrowed lines are primary flow directions found in the marginal facies of the dike. Dot-dash line shows a possible later stage enlargement of the dike. The thick dashed arrowed lines indicate on the left, secondary flow directions for parts of the dike intruded during that later stage, and on the right, secondary drainage patterns related to extrusion of lava from the dike further down the flanks of the volcano (after Shelley 1988).

chemical evolution and increasing differentiation. The dikes in this study are dominantly mugearites and benmoreites with a few basalts and hawaiites; this is due to sampling mostly Lyttelton 2 dikes.

As mentioned, Shelley (1988) suggested that all flank eruptions on Lyttelton were fed directly from the central conduit, but with different areas varying geochemically so that some are dominantly hawaiitic (eg North Mount Evans 1 and Southern Mount Cavendish), and others mugearitic (eg Northern Mount Cavendish). Therefore it seems probable that some dikes were tapping magmas that reached the surface relatively quickly and erupted explosively (ie hawaiitic areas), while other dikes were tapping magma fed by chambers in which differentiation had taken place, leading to geochemically more evolved magmas. It is possible the ascent of the more evolved magma was triggered by injections of hot fresh magma from lower levels.

The feeder dikes for the cinder cones in this study are rarely seen, and although this may be due to lack of outcrops it may also represent the drainage of magma back into the fissure after eruption. On Lyttelton, Shelley (1988) found some dikes have vertical upwards flow orientations suggesting that they fed surface lavas while Guard (1999) found dominantly downwards flow in a vent plug suggesting back-flow. Feeder dikes of cinder cones that are seen occur only where erosion has cut deep into the vent areas (eg Southern Gibraltar Rock & Northern Gibraltar Rock).

5.3 GENERATION OF EXPLOSIVE BASALTIC ERUPTIONS

Pyroclastic basaltic eruptions are caused by the generation and rapid expansion of a gas phase capable of disrupting the magma and/or the surrounding wall rock (Houghton & Wilson 1989). Overpressure above the lithostatic value in the magma reservoir is necessary to start an explosive eruption and there are two possible mechanisms (Blake 1981, Parfitt et al. 1993, Scandone 1996):

1. Exsolution of a volatile phase (Section 5.3.2) or the intrusion of new magma in a reservoir (Section 5.3.4), with development of an overpressure above the strength of the

rocks surrounding the magma chamber, which causes the opening of fractures (Rubin 1993, Tait et al. 1993).

2. Positive density contrast of liquids lighter than surrounding rocks (Ryan 1987) deriving, for example from the differentiation in a magma reservoir with the accumulation of a light differentiate at the top of the chamber and the development of stress above the strength of the rocks (Section 5.3.4).

5.3.1 Volatile Content

The volatile content of any magma is the dominant controlling factor in the degree of explosivity. Fisher & Schmincke (1984) state that in most basaltic (and andesitic) magmas, H_2O, CO_2 and SO_2 are the three principal volatiles with lesser amounts of H_2, CO, S_2, O_2, HCl, N_2, HF, and HB. The water content of basaltic magmas varies according to the tectonic environment, with MORB's having lesser amounts compared with alkali basalts and island arc basalts (Sparks et al. 1994).

5.3.2 Exsolution

The solubility of volatiles is heavily dependent on confining pressure (Cashman & Mangan 1994). At a certain depth the solubility in the melt of H_2O, SO_2, and CO_2 will decrease so that they begin to exsolve from the magma to become separate fluid phases. Cas & Wright (1987), state that the depth at which this occurs depends on the magma type, the actual volatile content and the vapour pressure of the dissolved H_2O, CO_2, and SO_2 relative to the confining pressure. Sparks (1978) suggests that exsolution will begin when any volatile species is supersaturated by a small amount (~ 0.1 MPa) and that initial bubble sizes are a few microns. Exsolution commences when the vapour pressure equals the confining pressure. Therefore the higher the magmatic volatile content, the higher the vapour pressure exerted, and the greater the depth at which exsolution will begin.

There are two types of exsolution (Cas & Wright 1987). *First Boiling* or decompressional exsolution vesiculation is when an exsolved phase has a vapour pressure that can disrupt the magma if it continues to increase. Vapour pressure is however dependent on the initial volatile content of the magma and on its temperature. *Second Boiling* or crystallisation – induced exsolution –vesiculation is caused by crystallisation, which has the effect of

concentrating the dissolved volatile components in the remaining liquid magma, causing higher vapour pressures. Cooling of magma reservoirs leads to the formation of anhydrous crystals with the result that the remaining melt becomes enriched in volatiles. When the solubility limit is met, gas exsolution occurs and the magma chamber increases both in volume and pressure as vesiculation proceeds. Ultimately, the internal pressure needs to exceed the strength of the surrounding rocks to trigger an eruption (Vergniolle & Mangan 1999).

The pre-eruptive volatile content of basalts is relatively low, normally ~ 1 wt% of combined water, carbon dioxide, and sulphur, with measurements at Kilauea, Etna, Stromboli, and Pacaya indicating that basaltic eruptions generally release ~ 10^5 metric tons/day of H_2O, CO_2 and SO_2 to the atmosphere during peak activity (Vergniolle & Mangan 1999). Degassing of basaltic systems occurs as a two-stage process (Chester et al. 1985, Gerlach 1986). CO_2 reaches supersaturation at depths ~ 30 km and begins to exsolve and continues to do so until the magma is within a few kilometres of the surface (Figure 5.5). On Kilauea, for example, the magma resides at the summit reservoir located at ~ 8 to 2 km depth having exsolved ~ 90% of its original CO_2 as a separate fluid phase. The second stage of degassing involves the exsolution of H_2O, and to a lesser extent, S and this occurs in the conduit at a very shallow level, within a few hundred metres of the vent (Figure 5.5).

5.3.3 Growth of bubbles

Bubble growth after initial exsolution in an erupting magma is a consequence of decompression. Sparks et al. (1994) suggest that bubbles can grow in two ways: (1), by the continued exsolution of gas out of a supersaturated melt; and (2), due to expansion of existing gas in the bubble as pressure is reduced. Sparks (1978) found that diffusion of gas is controlled by the composition, solubility, and concentration of dissolved volatiles and on the degree of supersaturation of these volatiles. The expansion of bubbles Sparks (1978) found to be controlled by the rise velocity of the magma, the rate at which tephra is disrupted and renewed at the free surface, and by the rise of the bubble itself. Diffusional growth is more dominant for small bubbles and decompressional growth is dominant for

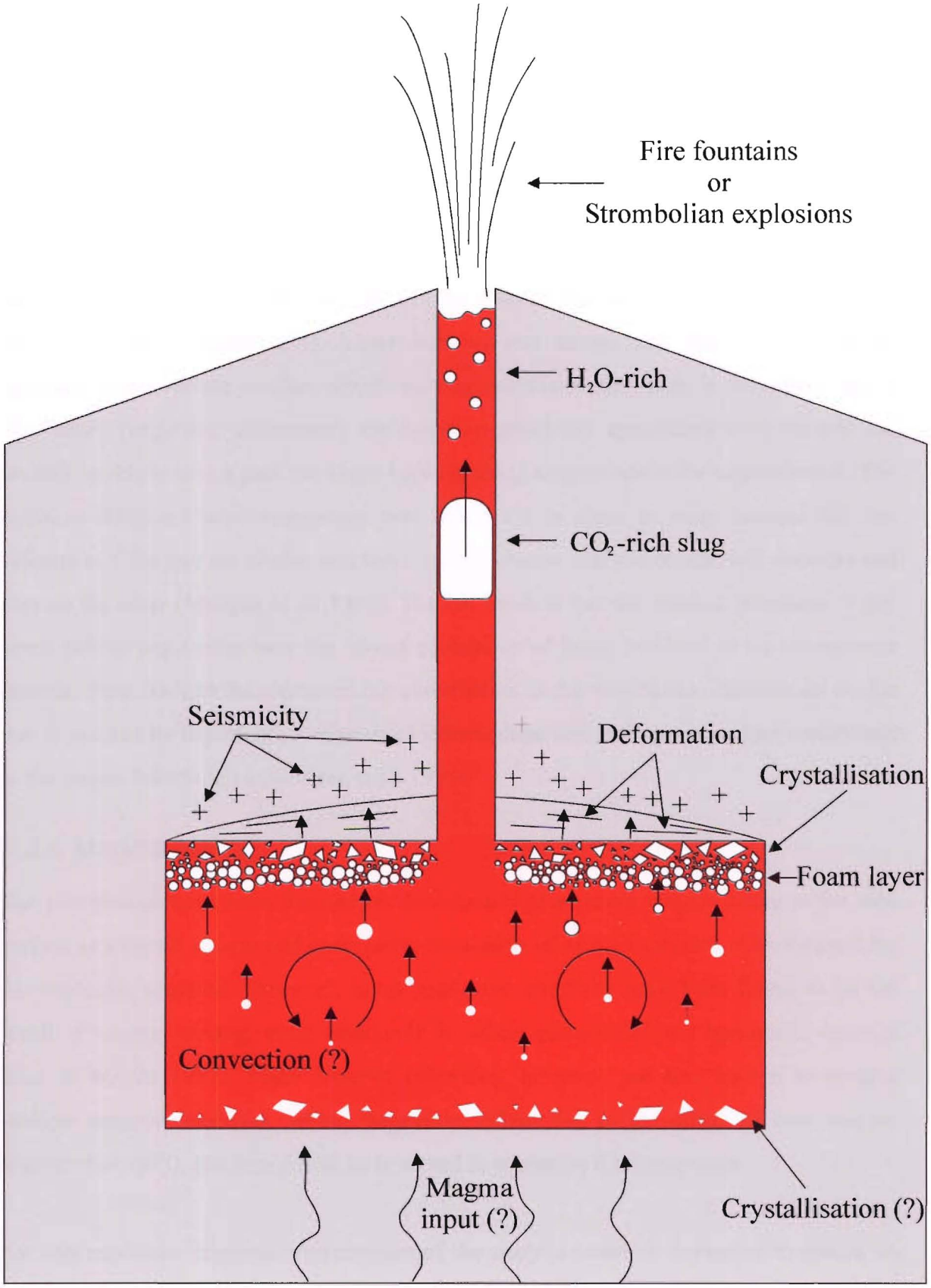

Figure 5.5. Diagrammatic sketch of two stage degassing in a volcano (after Vergniolle & Mangan 1999).

large bubbles; and all bubbles at low pressures. Wilson & Head (1981) suggested that as an existing bubble grows and moves through the magmatic liquid, new (10 micron-sized) bubbles would also be created as a result of increasing supersaturation.

Growth by coalescence between two bubbles is controlled by the linear collision efficiency (Sahagian 1985, Sahagian et al. 1989), a dimensionless quantity that is a function of (1) the radius of the collecting bubble (r) and (2) the ratio of the captured bubble radius to the collecting bubble radius (r`/r). Large bubbles rise fastest and thus have a greater opportunity to overtake smaller, slower-moving bubbles in their path. If the radius ratio is very small (large size difference), the collision efficiency approaches zero because the smaller bubble is swept past the larger bubbles along streamlines in the adjacent melt. The collision efficiency also approaches zero when r`/r is close to unity because the rise velocities of the pair are similar and there is little chance that one bubble will overtake and capture the other (Mangan et al. 1993). The net result is that the smallest members of any given bubble population have the lowest probability of being involved in the coalescence process. This leads to the characteristic perturbation in the vesicle size distribution profile that is marked by depletion of bubbles of intermediate size and corresponding enrichment in the largest bubble sizes (Mangan et al. 1993).

5.3.4 Magma Mixing

The previous sections have focused on the scenario of a simple magma rising to the sub-surface as a closed system and undergoing exsolution of its own volatiles, which then drive the explosive eruption. However, many explosive eruptions have been found to be the result of magma mixing, most commonly in silicic pumice fall and ignimbrite deposits (Cas & Wright 1987). Many basaltic volcanoes, however, are also known to possess shallow magma reservoirs, which frequently inflate due to the influx of new magma (Parfitt et al 1993), and hence may be involved in explosive flank eruptions.

For any explosive eruption, overpressure of the magma reservoir is needed to induce an eruption. This overpressure may be generated by exsolution of a volatile phase from the magma during ascent and/or through crystallisation. Alternatively, Vergniolle & Mangan (1999) state that replenishment from a deep magma source may be the triggering

mechanism. The input of an additional volume of bubbly magma (basalts are saturated in CO_2 at depths > 15 km) combined with the volume increase due to the decompressional expansion of tiny bubbles that enter and rise toward the roof of the chamber, may sufficiently pressurise the system to trigger an eruption. If the new magma also came into contact with a colder magma this would cause rapid crystallisation and exsolution of volatiles and would also cause overpressure (Cas & Wright 1987).

5.4 CINDER CONE ERUPTION DYNAMICS

Strombolian and Hawaiian eruptions producing scoria cones are caused by near-surface expansion and explosive disruption of gas bubbles within a low to moderate viscosity magma (Vergniolle & Mangan 1999). The following section reviews observed eruptions and theoretical modelling.

5.4.1 Observed Eruptions

Accounts of observed cinder cone forming eruptions are numerous in the literature (eg Thorarinsson et al. 1973, Self et al. 1974 (Heimaey, Iceland), Guest et al. 1974, McGetchin et al. 1974, Chester et al. 1985 (Mt Etna, Sicily), Lenat et al. 1988 (Piton de la Fournaise), Head & Wilson 1989 (Hawaii)). Initial eruptions start with the venting of gas, with each eruption being preceded by a seismic crisis (Wood 1980). Initial explosions can be continuous with 30-50 occurring per minute (Chester et al. 1985, Wood 1980), increasing in some cases to nearly continuous Hawaiian fire fountaining. Initial activity can start along fissures but is usually quickly localised to a number of points (Head & Wilson 1989), as seen by Thorarinsson et al. (1973) at Heimaey. During the main cone building phase eruptions consist of discrete, often rhythmic bursts that disrupt the magma and eject showers of incandescent lava fragments or pyroclasts (Vergniolle & Mangan 1999). The maximum height of cones is commonly reached within a few days, after which explosion frequency and intensity decreases (Wood 1980).

Ejection angles during initial Hawaiian eruptions are near vertical but become progressively less during Strombolian eruptions (75°-45°) (Vergniolle & Mangan 1999). Lava levels in the craters are the dominant cause of variation in angles between the two

eruptive styles on Mt Etna and at Heimaey (Chester et al. 1985, Self 1974). Low lava levels generate near vertical eruption angles while higher levels cause a wider variation. It was also witnessed at Heimaey that material would accumulate back inside the vent and block the crater during large voluminous eruptions. After such blockages, dense black clouds of ash would be ejected until the vent became unblocked (Self et al. 1974).

During Hawaiian eruptions, the structure of the fountain is essentially that of a sustained gas jet carrying a dispersed load of centimetre to metre sized molten clasts. Eruption temperatures are highest in the core of the fountain (1150-1200°C), creating an incandescent yellow-white axis that extends almost to the top of the fountain. The thermal core of the fountain passes outward into a fiery orange red region of slightly cooler temperature and lower clot density, and then to a sparse, black halo of chilled pyroclasts (Vergniolle & Mangan 1999). Magma viscosity is usually higher in Strombolian eruptions, either because of cooling with eruption temperatures as low as 1080°C, or because of the involvement of more evolved magmas, commonly alkaline basalt or basaltic andesite. Gas release is episodic rather than continuous, which leads to larger overpressures, more intense eruptions, and higher degrees of magma fragmentation compared to Hawaiian-style activity. Chester et al (1985), from the edge of a crater in July 1979 on Mt Etna, observed that 30 seconds before a large explosion, the whole surface of the lava lake swelled into a giant blister causing gaping cracks to appear in the congealed crust and reveal incandescent lava below. The blister would then burst with a resounding bang and eject material 150m or more above the lava surface. Smaller explosions were seen to occur around the edge of the lake and each explosion was accompanied by a loud hissing, ejecting material only a few metres in the air.

The effusion of lava from cones has been seen to occur at all stages of cone forming eruptions. Lavas produced at the beginning of explosive eruptions usually occur at the end of eruptive fissures. During explosive eruptions, lava can be produced in three ways: (1), by the fast accumulation of hot fluid spatter remobilising and flowing (ie spatter flows); (2), by magma overflowing the crater rim; and (3), by eruptions through small boccas on the sides of cones (Guest et al. 1974). Late stage flows, however, are most common, due to degassed lava breaching unstable cone walls.

Head & Wilson (1989), during Hawaiian eruptions, observed that two variables, magma gas content and magma volume flux, are the main controls on basaltic pyroclastic eruptions. These two variables determine the dynamic structure of a fire fountain and the size of clasts within it (Figures 5.6A&B). In turn, the local temperature and the accumulation rate become important in determining the structure and morphology of pyroclastic deposits (Figure 5.6C). For example, in the outer parts of fire fountains, clasts undergo faster cooling, and on accumulation on the surface, contribute to the building of a pyroclastic cone (if accumulation rate is low). However, if accumulation rates are high, rootless (spatter) flows will form (Figure 5.6D).

5.4.2 Theoretical Modelling

Wilson & Head (1981) first suggested that basaltic eruptions could be simulated in a homogenous flow model, with no differential motion between the liquid and gas phases. They proposed that factors such as bubble coalescence and a slow rise speed and/or small viscosity would produce Strombolian style eruptions. However, Vergniolle & Jaupart (1986) discounted the homogenous model and suggested that such a model would only be valid for viscous magmas. For basaltic magmas Vergniolle & Jaupart (1986) suggested that a two-phase (eg separate) flow framework would be more appropriate and that gas and liquid phases should be treated independently. Evidence to support such an approach was found by Chouet et al. (1974) who observed basalt magmas to have a volume ratio of gas to melt of between 2×10^4 and 10^5. Vergniolle & Jaupart (1986) found such a ratio impossible to achieve in a homogeneous flow with exsolution, thus providing evidence for separate flow.

The two-phase flow regimes are illustrated in Figure 5.7, and each is described below based on descriptions in the literature (eg Wallis 1969, Butterworth & Hewitt 1977, Whalley 1996, Vergniolle & Mangan 1999). Bubbly flow is characterised by a suspension of bubbles (~ 30%) of approximately uniform size in a continuous liquid; the corresponding eruptive regime is effusive. At a gas content of ~70%, bubbles can coalesce, either in the magma reservoir or in the transport system, causing large bullet-shaped bubbles to form. This regime is called slug flow and is typical of more Strombolian type eruptions. Slug flow makes a transition to annular flow at gas volume fractions above 70%.

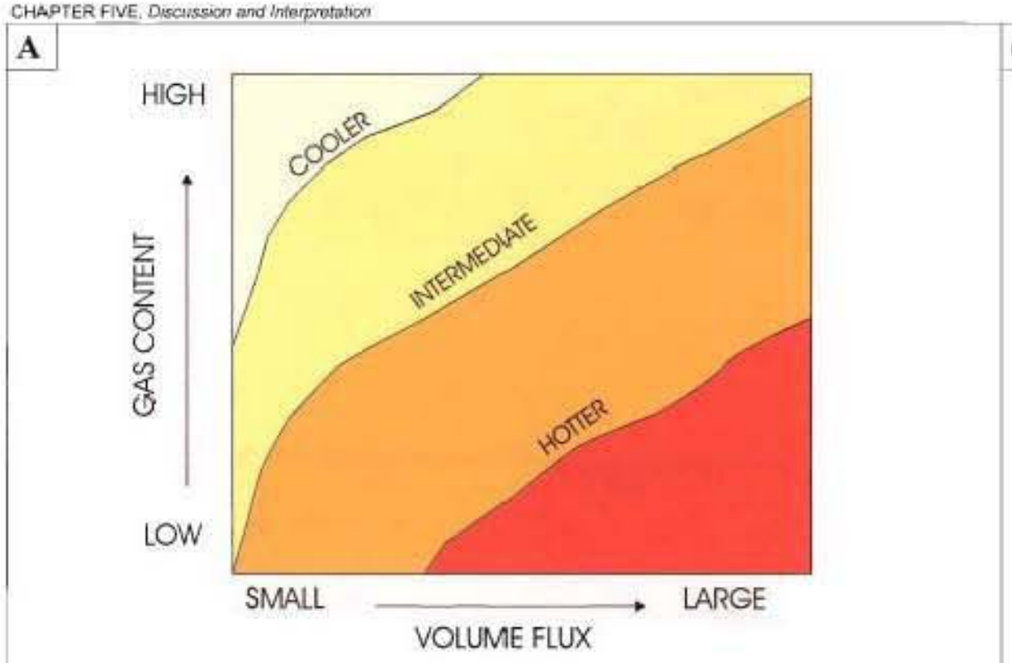

Figure 5.6. A) The dependence of local temperature on gas content and volume flux. Contours of temperature are qualitive and are based on calculations by Wilson & Head (1989). **B)** The dependence of local accumulation rate on gas content and volume flux. **C)** Pyroclast/deposit diagram illustrating the relationship between mean pyroclast temperature and pyroclast accumulation rate. **D)** Sketch of the relationship of pyroclastic fountain dynamic structure and resulting post-eruption facies, deposits and morphology. These relationships apply over a wide range of scales observed in basaltic eruptions (all diagrams after Wilson & Head 1989).

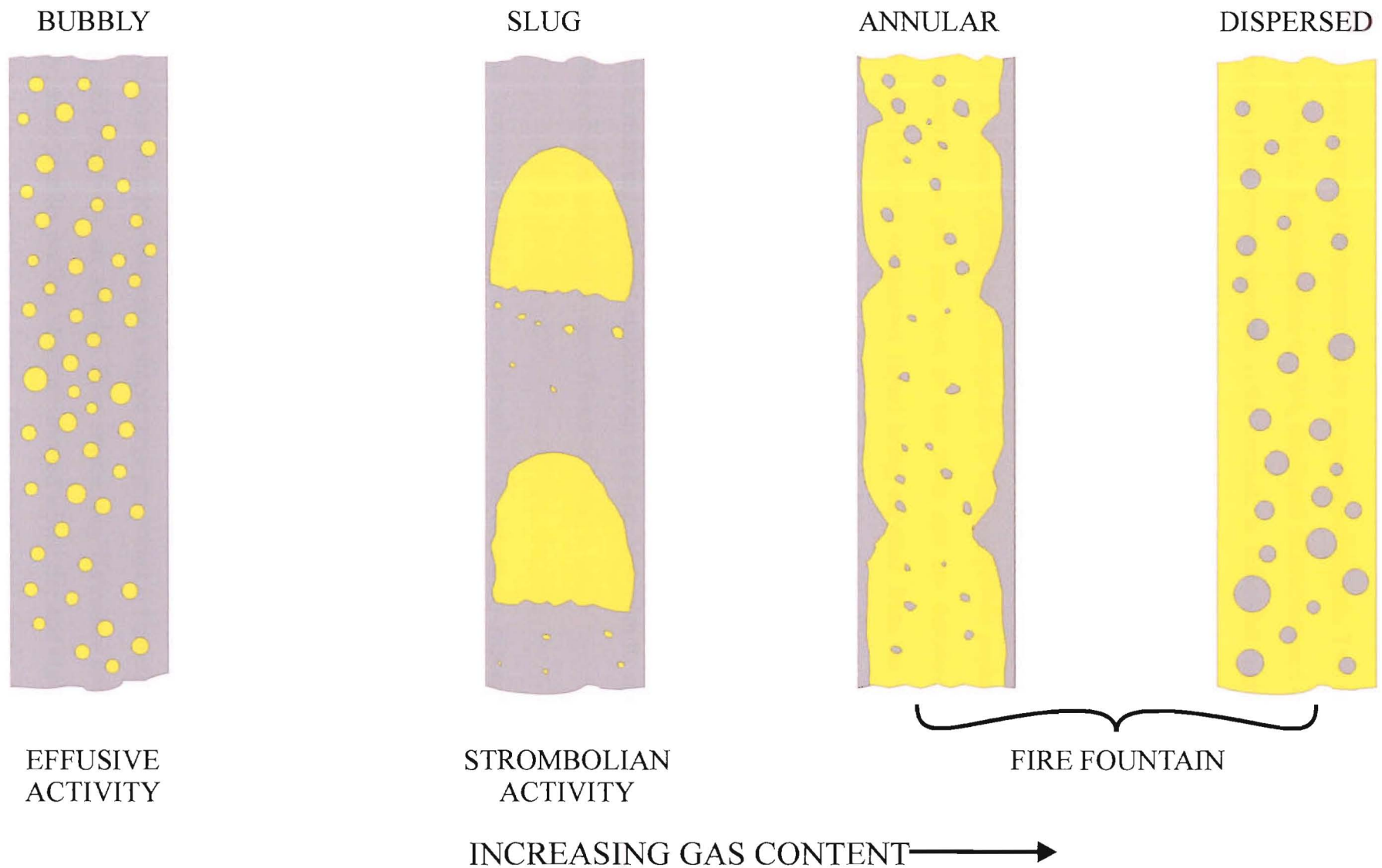

Figure 5.7. Classification of two-phase flow and their volcanic counterpart. Note that the gas fraction increases from the left to the right (after Whalley 1996, and Vergniolle & Mangan 1999).

The gas forms a central jet surrounded by an annulus of magma. Two types of annular flow exist: at gas volume fractions close to 70%, the liquid falls downward under its own weight while the gas phase moves upwards in the conduit; at somewhat higher gas fractions, the liquid is driven upwards by the gas jet. If the gas volume fraction is substantially larger than 70%, the magma around the central gas core is shed into magma droplets which are carried upwards by the gas jet. When the continuous layer of liquid has entirely disappeared, the regime is called a dispersed flow.

Vergniolle & Jaupart (1986) and Vergniolle & Mangan (1996) explain that Hawaiian fire fountains entrain gas and trap lava on the walls and are therefore in the annular and dispersed regimes with continuous liquid being expelled from the conduit. Strombolian eruptions would be in the slug regime because bubbles have dimensions comparable with those of the vent. Therefore the differences between the different eruption styles is linked to the amount of gas. Vergniolle & Jaupart (1986) suggest that this scheme can be visualised in the evolution of a batch of magma erupting initially in a Hawaiian fountain. As the amount of gas reduces, the eruption changes from annular to slug then bubbly, with the fountain reducing in height and eruption type (eg. Hawaiian to violent Strombolian to quieter Strombolian eruptions to the effusion of lava).

Jaupart & Vergniolle (1988) presented results from laboratory experiments simulating the degassing process in Hawaiian and Strombolian eruptions. Gas bubbles were generated at the bottom of a tank filled with a viscous liquid and topped by a small open conduit. The long thin conduit constricts the flow, simulating a dike or the top of a large magma chamber. The viscosity of the liquid and the amount of gas release flux are varied during the experiments. The basic situation found was that bubbles rise and accumulate on the roof of the tank in a foam layer. At a critical thickness the bubbles coalesce and the foam collapses, generating a gas pocket whose size varied depending on the liquid viscosity and surface tension. At a low viscosity a single large gas pocket is formed, which flows into the conduit, and erupts in an annular flow regime (eg Hawaiian eruption). At a higher viscosity, many smaller pockets of air are formed which rise and burst intermittently from the conduit (eg Strombolian activity). These experiments imply that the presence of constrictions in the chamber and conduit play a major role in eruption behaviour.

Parfitt & Wilson (1995) investigated the transition between Hawaiian style lava fountaining and Strombolian explosive activity. Parfitt & Wilson (1995) looked at how the velocity of magma from depth, volatile content and magma viscosity control eruption style. Their model was based on the degree of coalescence between gas bubbles in the magma, which allowed the transition between the two extreme styles of activity to be simulated. The results showed that the speed at which magma rose controlled eruption type with the magma speed controlled by gas content and viscosity. Strombolian activity occurred at lower rise speeds and Hawaiian activity at higher rise speeds (Figure 5.8), with activity between the two extremes transitional. The transition from Hawaiian to Strombolian activity occurred at lower rise speeds for higher viscosities, and lower gas contents and was explained by higher viscosities and lower gas contents which reduce the amount of bubble coalescence and cause Strombolian activity to be suppressed even at low rise speeds.

The most interesting result of Parfitt & Wilson (1995) was the observation that a change from Hawaiian to Strombolian activity was not dependent on a reduction in gas content as previously suggested (Jaupart & Vergniolle 1988, Vergniolle & Jaupart 1986, 1990). Instead a reduction in gas content at a constant rise speed reduces the amount of bubble coalescence that occurs and moves the eruption toward the Hawaiian end of the spectrum (Figure 5.8). Parfitt & Wilson (1995) also show that if an eruption is initially Hawaiian, a reduction in the gas content eventually leads to passive effusion of lava rather than Strombolian activity. Therefore without an accompanying decline in rise speed, a decline in gas content would not cause a change from Hawaiian to Strombolian activity.

5.4.3 Location of fragmentation

Vergniolle & Jaupart (1986, 1990), as mentioned in Section 5.4.2, propose that magmatic foams form by the accumulation of bubbles in a static layer at the reservoir roof. Fragmentation occurs when this foam layer catastrophically collapses due to pervasive failure of bubble films. Sparks (1978), Wilson & Head (1981), Parfitt & Wilson (1994, 1995), Dobran & Conigilio (1996) however suggest that foams are formed in the conduit at very shallow depths as the magma nearing the surface decompresses. Fragmentation occurs

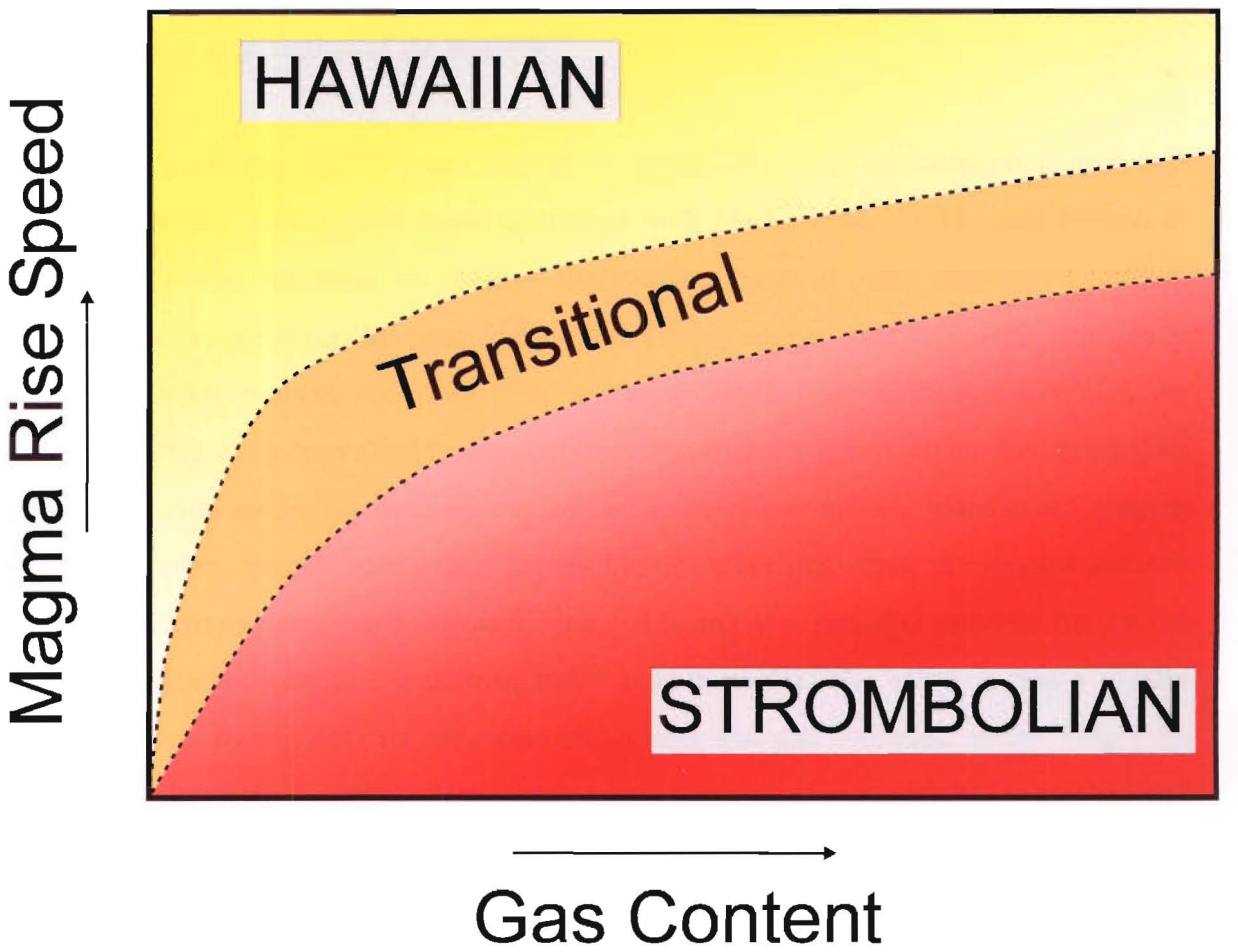

Figure 5.8. The variation in style of explosive basaltic eruptions shown as a function of magma rise speed and gas content (after Parfitt & Wilson 1995).

when the proportion of bubbles exceeds that of the maximum packing. Mader et al. (1994) also suggest that formation may be the result of high strain rates imparted by rapid expansion and acceleration of the magma.

Mangan & Cashman (1996) found that their results of a high vesiculation density and extreme nucleation rates were more consistent with Mader et al. (1994), and Dobran & Conigilio (1996), implying an intense vesiculation burst at high degrees of volatile supersaturation. However, Mangan & Cashman (1996) suggest that "runaway" nucleation is the dominant process occurring over a narrow depth interval during ascent in the conduit. Parfitt & Wilson (1995) demonstrated that high magma ascent rates rather than elevated volatile contents control the explosivity of basaltic eruptions. Mangan & Cashman (1996) therefore suggest that strong supersaturation develops when the magma ascends through a characteristic depth of nucleation (~120 m) at a rate that exceeds the rate at which volatiles can exsolve and form stable bubble nuclei. The effect is that a rapidly rising magma "overshoots" its saturation curve such that gas evolution cannot keep pace with decompression. Therefore, at a certain point, the limit of metastability is reached and the magma vesiculates explosively.

Mangan & Cashman (1996) suggest that the rapid expansion and acceleration of the magma driven by disequilibrium gas release may (as suggested by experiments conducted by Mader et al. 1994) provide the impetus for fragmentation. Mangan et al. (1993) and Cashman et al. (1994) found vesicularities in effusive lavas greater than 75%, that would imply that vesicularity does not itself lead to disruption. Therefore Mangan & Cashman suggest that fragmentation is a process of ductile deformation and breakup similar to that in observed liquid jets (eg. Richards et al. 1994, Stone 1994). Thus, while the acceleration leading to fragmentation is the result of an intense, disequilibrium vesiculation burst, the breakup itself is caused by the hydrodynamics of the two-phase flow. In their model, magma vesicularity is homogeneous with respect to dissolved volatiles at depth, with minor lava drainback during fountaining causing the clast vesicularity and structure to be dependent largely on the timing of quenching.

5.5 CINDER CONE DEPOSITS

Cinder cones are relatively small but common volcanoes that form by the eruption of low viscosity, generally basaltic magma in Strombolian or Hawaiian eruptions (Vespermann & Schmincke 1999). Cinder cones are made up of welded spatter, occasional lava flows, but mostly layers of blocks, bombs, lapilli and ash. The following section concentrates on the internal structure of cinder cones, common products, and a interpretation of Lyttelton cinder cones.

5.5.1 Internal structure and morphology of cinder cones

The morphology of cinder cones depends on numerous factors including 1) total volume of erupted material, 2) range of median ejecta velocity, 3) ejection angles, 4) wind speed and direction, 5) nature and size of particles, 6) occurrence of lava overflows, 7) phreatomagmatic intercalculations and 8) vent geometry (Vespermann & Schmincke 1999).

The low eruption column and coarseness of pyroclasts ejected during cinder cone eruptions causes limited dispersal with more than half the material falling within ~500 m of the vent allowing cones to grow to hundreds of metres at rates of ~ 0.1 to 5 $m.hr^{-1}$ (Vespermann & Schmincke 1999). The outer slope angles of cinder cones range from 20°-30° and this angle is related to the equilibrium angle of repose for tephra rolling and sliding down the sides (McGetchin et al. 1974). Steepening beyond 30-35° causes ejecta at the top of the cone to slough-off and roll down the sides of the cone, forming a ring of talus that extends beyond the original ballistic limit of ejecta. The overall plan of cones is mostly circular but some are asymmetrical. The possible mechanisms for asymmetrical cones are: 1) inclined explosive jets piling pyroclastic material on one side of the vent, 2) influence of the wind, 3) the removal of a portion of the cone by lava that has burrowed out underneath it, 4) cone growth with simultaneous lava extrusion (the pyroclastic debris being unable to accumulate where lava is flowing), and 5) an elongate eruptive vent (Chester et al. 1985).

Cinder cones range in height from 45-450 m and in diameter from 250-2500 m with the majority between 50-100 m high and 400-600 m wide (Macdonald 1945, Scott & Trask

1971, Porter 1972, Bloomfield 1975, Gutmann 1979, Hammill 1979, Settle 1979, Wood 1980). The dimensions of fresh cones follow two general relationships: $H_{CO} = 0.18W_{CO}$, $W_{CR} = 0.40W_{CO}$, where H_{CO} = cone height, W_{CR} = crater diameter and W_{CO} = basal cone diameter (Figure 5.9). The difference in size is related to variations in magnitude and duration of eruptions with 50% of eruptions lasting less than 30 days and 95% being over in one year or less (Wood 1980). Volumes of cones plus lava flows range between 10^5 and $10^9 m^3$ (Vespermann & Schmincke 1999).

5.5.2 Products of cinder cone eruptions

In explosive basaltic eruptions, magma fragments into bubbly, molten clots. Gas bubbles within the melt undergo decompressional expansion in the conduit and the eruption column causing the clot to inflate as it rises. The magnitude and rate of pressure drop, the viscosity of the melt, and the timing of solidification, or quenching, control how far the inflation proceeds, and thus determines the vesicularity, or percent void space, of the clast (Vergniolle & Mangan 1999).

Initial eruptions of cinder cones in volcanic fields are usually phreatomagmatic due to the rising magma mixing with groundwater (Figure 5.10). However, cinder cones on the slopes of volcanoes are usually isolated from water with initial eruptions dominantly Hawaiian. Ejection angles for initial eruptions are near vertical and continuous causing limited cooling of clasts, and hence rapid near vent accumulation of spatter. Gas loss in initial eruptions is high with fountaining usually short lived, causing the magma to increase slightly in viscosity. The increase in viscosity causes a decrease in gas rise speed allowing coalescence and hence more discrete Strombolian eruptions. Due to the discrete eruptions, clots have more interaction with the air, develop fluidal morphologies, and fall to the ground as discrete clasts. Near vent bombs undergo less cooling and thus are usually still fluid so that they flatten on landing and anneal, or weld, to an existing surface if hot enough (Vergniolle & Mangan 1999). Due to continued degassing and mixing with fresher magma, there is usually a mixture of well-shaped bombs (fresh magma) and blocks (degassed magma). Blocks are more viscous than bombs due to increased cooling in the vent before ejection and are thus more angular. The discrete nature of the Strombolian

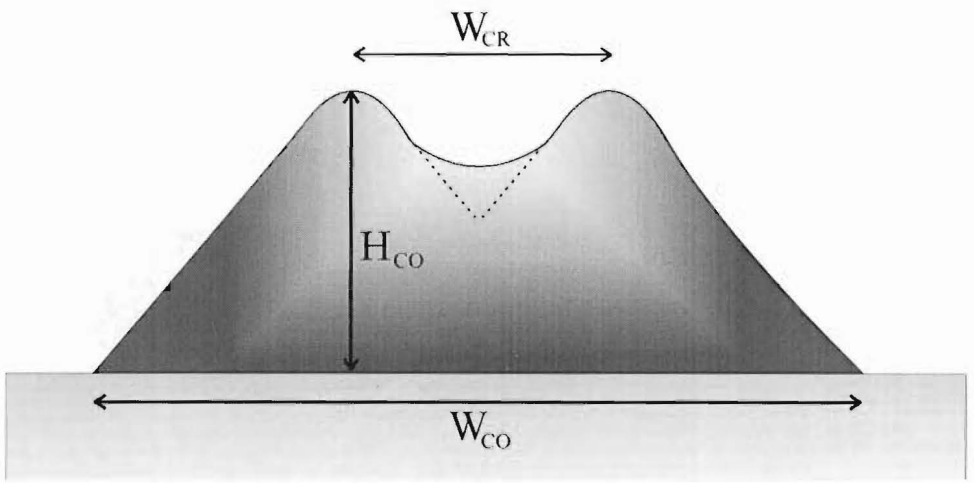

Wood (1980) parameters

W_{CR} = Basal Cone Diameter
H_{CO}= Cone Height
W_{CR} = Crater Diameter

Where H_{CO}= 0.18W_{CO}
And W_{CR} = 0.40W_{CO}

Figure 5.9. Schematic diagram illustrating the dimensions of cinder cones (after Wood 1980).

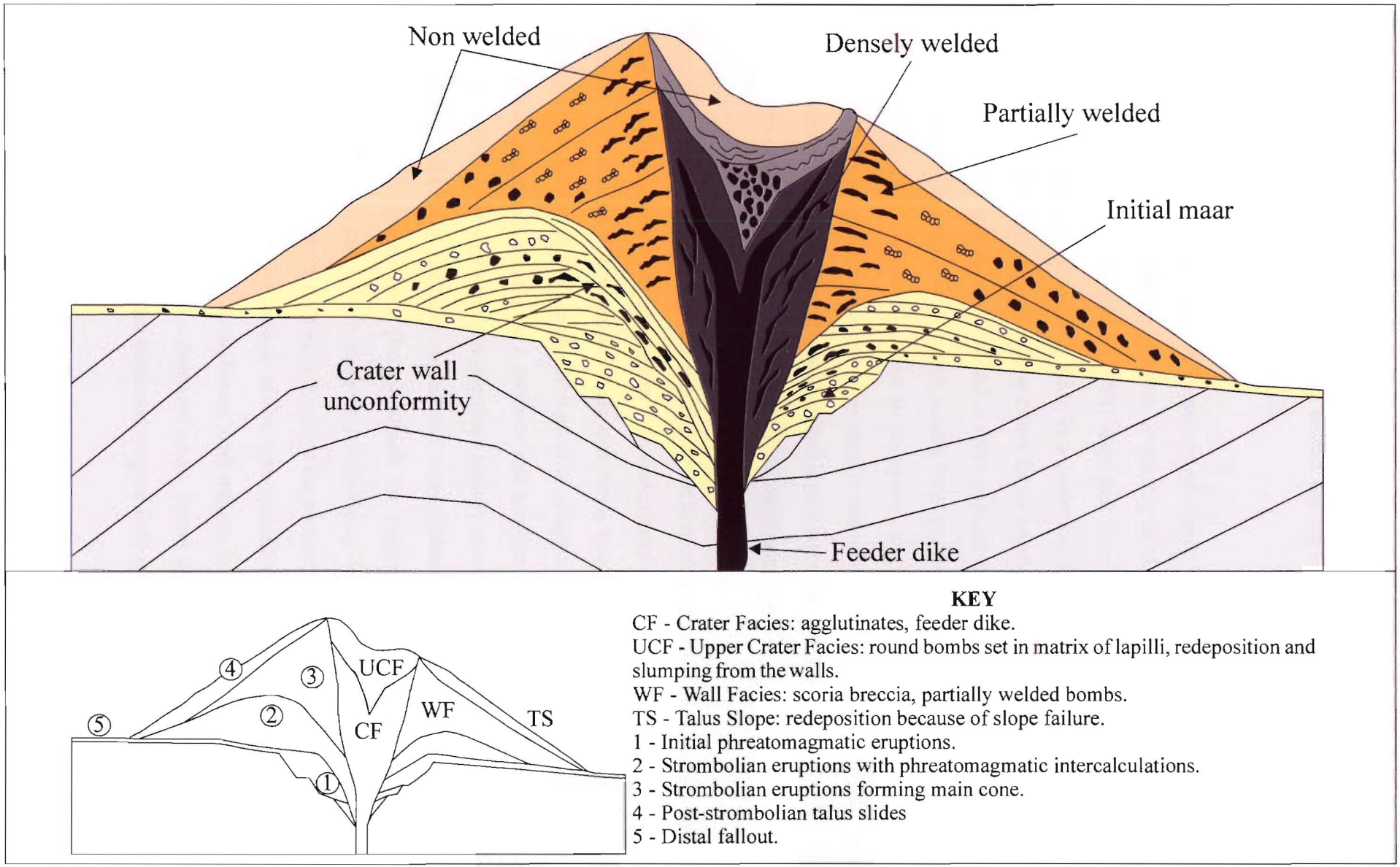

Figure 5.10. Morphology and internal structure of a volcanic field cinder cone (after Vespermann & Schmincke 1999).

eruptions causes clasts to be deposited in beds, with each reflecting a single eruptive period. Beds are a mixture of bombs and blocks and are usually framework supported by a matrix of smaller material (ash and lapilli).

Variable sorting is common due to eruptions of clasts with different vesicularities and densities, or particle aggradation of ashes, or mixing of clasts transported by fall and flow. Hence Vespermann & Schmincke (1999) state that there are commonly two main facies that can be distinguished from each other in a cinder cone: a) an inner crater facies and b) an outer wall facies. The deposits of the crater facies consists of erupted lava spatter, which was hot on landing and became welded to form agglutinate. In a transitional area, passing outward towards the crater wall facies, scoria fragments may be welded together but can still be recognised as individual clasts. In the crater interior, lava lakes or lava flows can develop. The upper crater facies characteristically consists of round bombs set in a poorly sorted matrix of lapilli, overlain by well-sorted lapilli layers up to several metres thick. The lapilli layers can extend much further than the actual cinder cone (Figure 5.10).

Clast vesicularity varies widely and this is a reflection of processes acting in the vent and during deposition. Near vent spatter has low vesicularity (<20%) due to post depositional degassing and compaction whereas bomb and block vesicularity varies widely (40-85%). Houghton & Wilson (1989) suggest that if a magma is fragmented at the peak of vesiculation, the result should be a more-or-less uniform assemblage of clasts. However this will only be met when the magma rises rapidly to shallow depths and is discharged sufficiently quickly to preclude significant non-explosive degassing. Therefore lower ascent rates and eruption rates (below which the magma will not fragment) will have broader vesicularities due to new magma incorporating degassed vent magma (Houghton & Hackett 1984). Brown et al. (1994) illustrate the variation in vesicularity by the presence or absence of a crust on the surface of the vent magma (Figure 5.11). During periods of intense eruptions no crust can form, hence fresh magma is erupted with a high vesicularity. During less intense eruptions, a degassed crust forms that is disrupted during episodic eruptions, causing both fresh and degassed magma with a wide range of vesicularity to be erupted.

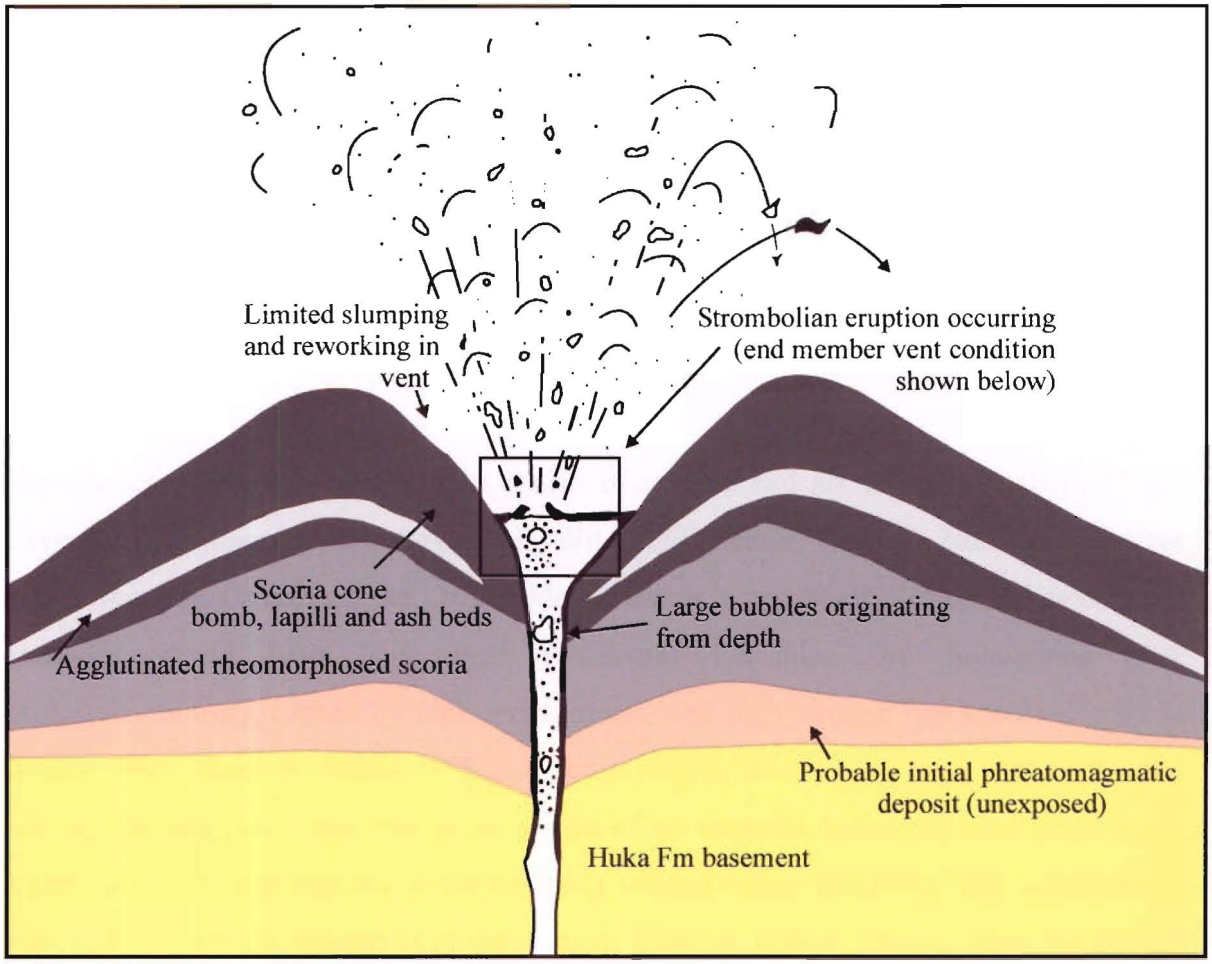

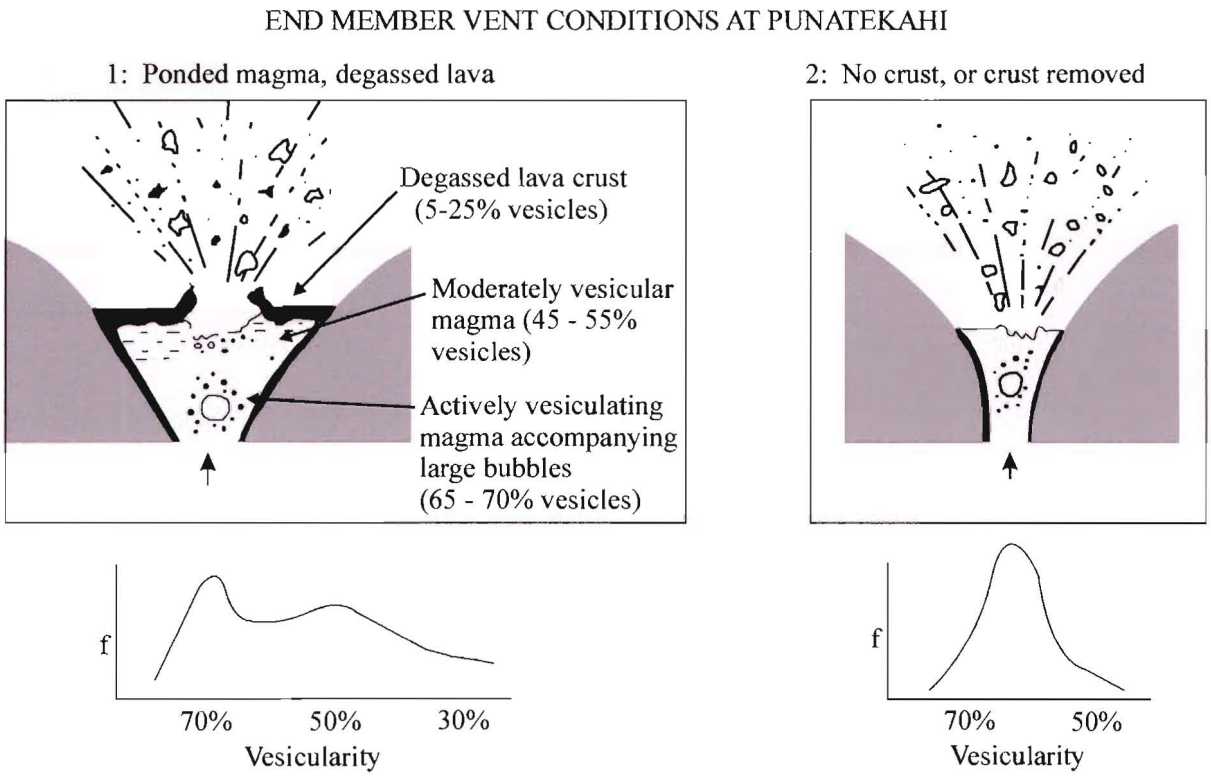

Figure 5.11. Diagrammatic section through Punatekahi vent indicating features associated with Strombolian activity, together with end member vent conditions and resultant vesicularity of clasts (f = frequency of samples with % vesicularity) (after Brown et al. 1994).

5.5.3 Interpretation of Lyttelton cinder cones

Cinder cones are commonly divided into inner crater facies and outer wall facies. In this study, however, the outer wall facies is divided into three separate facies (ie proximal, medial, and distal) with each facies distinguishable on welding, dip direction, block size, colour and the presence or absence of some clasts.

Vent Facies

Vent facies deposits dominate early phases of activity and are seen at Southern Mount Cavendish, Northern Mount Cavendish, Witch Hill Scenic Reserve, Northern Gibraltar Rock, Southern Gibraltar Rock, North Mount Evans 1 and North Mount Evans 3. Early eruptions would have been near continuous Hawaiian fire fountaining (50+ explosions/minute), caused by high gas contents, and high magma rise speeds (Parfitt & Wilson 1995, Head & Wilson 1989). Ejection angles would have been high with little cooling, causing rapid near vent accumulation of hot material. Individual clast shape is not preserved in vent deposits due to their densely welded nature caused by high accumulation rates and extreme fragmentation of the magma. Welding is most obvious when the deposit is struck by a hammer, due to its extremely hard and almost 'flinty' nature. Welded deposits resemble lava and may dip inwards towards the eruptive centre. The lack (<20%) of vesicles in the vent facies is interpreted as due to degassing and compaction during emplacement. Lack of vesicles may also be due to degassing during rheomorphism, as high accumulation rates in the vent facies may feed spatter flows that are commonly found in the proximal facies (~25%).

Proximal Facies

Proximal facies deposits grade out from the vent facies with a decrease in densely welded spatter to more welded deposits with a greater preservation of clasts, due to their moderate accumulation rates and longer flight times. Clasts are characteristically flattened (~80%) representing their semi-fluid nature during deposition. Welding decreases slightly, due to the decrease in accumulation rate and increase in cooling and flight times. The development of an ash and lapilli matrix is more common due to more Strombolian style eruptions. The degree of flattening is related to clast size, temperature and accumulation

rate, with rare spherical bombs indicative of longer flight times and higher cooling. Clasts are vesicular, with vesicles ranging in size from 0.5-0.8 m, and volume percentage from 10 to 60%. The wide variation in vesicularity is due to variations in accumulation rate and flight times. Spatter flows are frequent in the facies and this is related to high accumulation rates in the vent facies, allowing clasts to 'tack' together and flow by rheomorphism. Spatter flow thickness varies from site to site and this is a result of varying accumulation rates at each site.

Medial Facies

Medial facies deposits are dominated by bomb, block and lapilli beds and grade slowly from proximal deposits. A variety of bombs are found, varying from large scoriaceous fragments to less vesiculated blocks with a variety of shapes (Figure 5.12). The typical shapes are shown in Table 2.2 and Figure 2.2, and are common in the facies due to increased flight times and slower accumulation rates, allowing increased cooling and solidification. Some bombs have multiple-chilled margins, suggesting that they have rolled back into the vent and been re-ejected. Eruption type is dominantly Strombolian, causing deposits to be bedded, due to more discrete eruptions, the result of a decrease in gas content and increased coalescence and slug flow (Parfitt & Wilson 1995). The deposits are unwelded because the clasts solidified during flight, due to increased cooling. Degassed blocks are common and this is due to the development of crust in the vent between eruptions, a crust that is subsequently erupted by the next event. With increasing distance from the vent, deposits contain increasing quantities of ash and lapilli matrix, and the average bomb size decreases. As the largest bombs commonly occur at the top of the facies clast, size also appears to increase up section. The latter is probably also due to the decrease in gas content, causing the magma to increase in viscosity, thus causing larger bombs. Average vesicularity is ~40% but this again varies widely (10-60%), and is due to Strombolian eruptions commonly erupting a mixture of fresh and degassed magma.

Distal Facies

Distal facies deposits are dominated by lapilli, ash and crystals. Deposits are usually well sorted and bedded, reflecting their air-fall deposition, with rare bombs up to 0.3 m. Rare

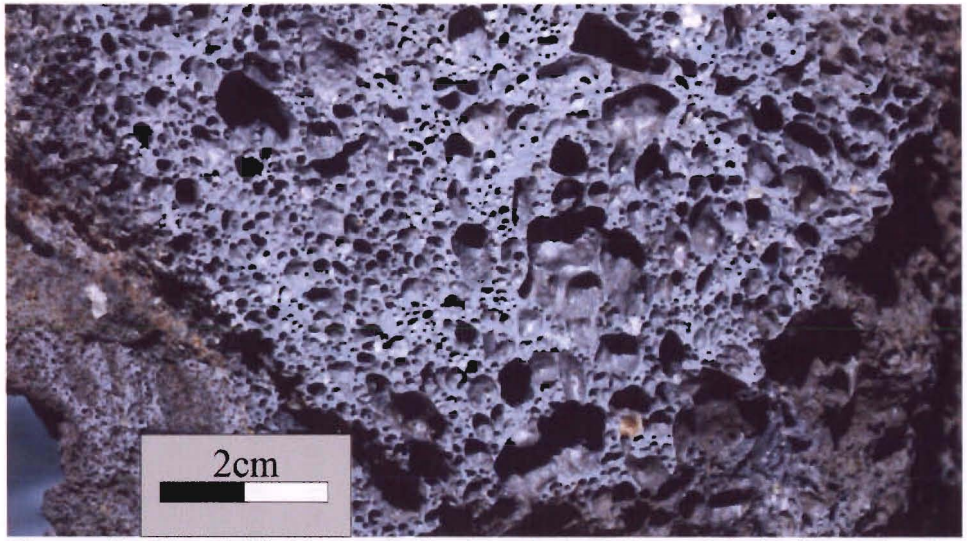

Figure 5.12A. A highly vesicular bomb (~70% vesicles), found in the proximal facies, interpreted to represent actively vesiculating magma.

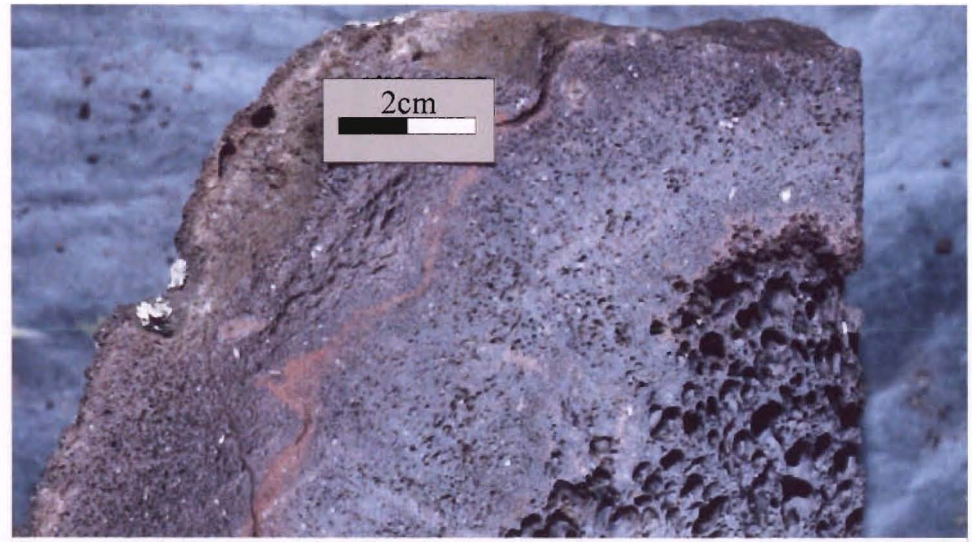

Figure 5.12B. A reworked bomb, that is interpreted to represent actively vesiculating magma that has been ejected, rolled back into the vent, mixing with less vesicular magma before being re-ejected.

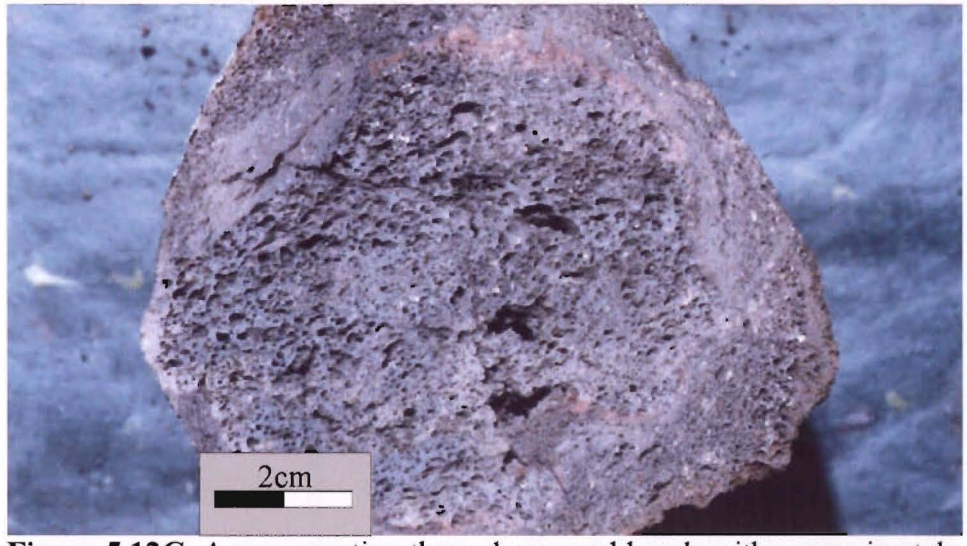

Figure 5.12C. A cross-section through a round bomb with approximately 40% vesicles.

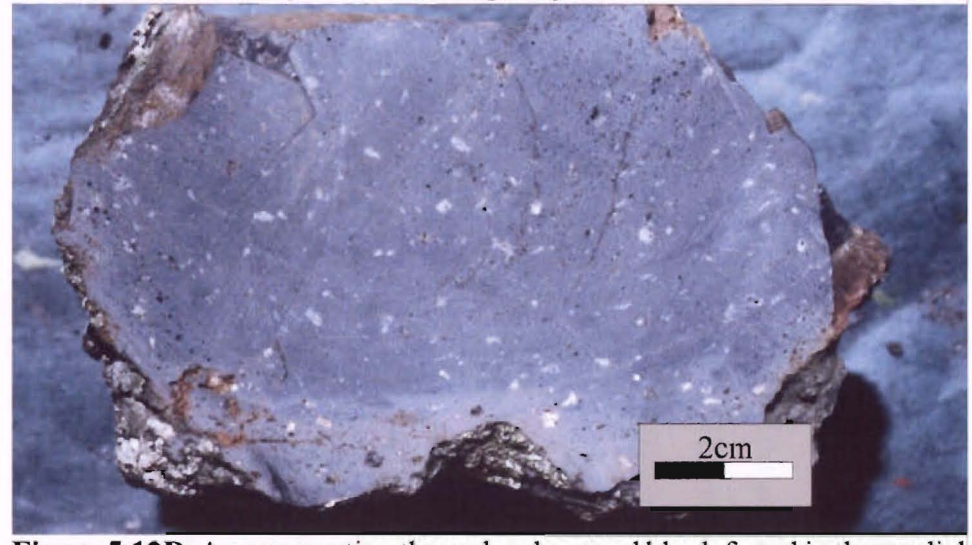

Figure 5.12D. A cross-section through a degassed block found in the medial facies with <20% vesicles.

bombs represent discrete explosions where clasts have been ejected at very low angles, probably caused by a high magma level in the vent. Some may represent clasts that rolled down the outer slope of the cone. Some beds in the distal facies are extremely fine grained, and this is a result of clearing eruptions that release large plumes of fine ash. The eruption type is dominantly Strombolian although some distal deposits may represent material from earlier Hawaiian eruptions. Lapilli fragments are glassy and this represents fast cooling due to their small size, and hence large air interference.

Size of cinder cones on Lyttelton

From the parameters of Wood (1980) it is possible to get an indication of sizes of cones during their peak of activity. A major problem is that cinder cones weather very easily because they are composed of loose beds of tephra. However, from field observations, the amount of weathering can be estimated and the original cone height constructed through dips and facies variations. Some dikes fed from cinder cones were noted in the field, but not in every cone. The cinder cone dikes are thought to be present only at deep levels in the cones, so their presence indicates deep erosion of the outer walls of the cinder cone. Where cone dikes are lacking, it is likely that the cone has not been deeply eroded, which suggests the aerial extent of such cones is close to the original. The aerial extent of the more eroded cones were also measured, but they have probably been more superficially reduced in size. Heights are given in Table 5.1 but it must be emphasised that all heights are very approximate. The largest cones were those at North Mount Evans 1 and Southern Mount Evans with estimated basal diameters of ~1600 m and heights of ~280 m. The smallest cone studied is at Hoon Hay Park, with an estimated basal diameter of ~400m and a height of ~70 m. Average cone height is 140 m and average basal diameter 775 m, very similar to the averages determined by Wood (1980) for 910 cinder cones.

5.5.4 Model for Lyttelton Cinder Cone Eruptions.

Based on the previous discussion it is possible to illustrate the key features and mechanisms responsible for cinder cones on Lyttelton Volcano.

Table 5.1. Estimated cone heights of Lyttelton cinder cones.

Area	Estimated basal diameter	Estimated height
Southern Mount Cavendish	~500m	~100m
Northern Mount Cavendish	~700m	~130m
Castle Rock	INSUFFICENT EXPOSURE	
Witch Hill Scenic Reserve	~750m	~135m
Hoon Hay Park 1	~400m	~70m
Hoon Hay Park 2	~500m	~100m
Northern Gibraltar Rock	~600m	~110m
Southern Gibraltar Rock	~440m	~80m
Southern Mount Evans	~1600m	~280m
North Mount Evans 1	~1580m	~280m
North Mount Evans 2	~670m	~120m
North Mount Evans 3	~780m	~140m
Average	~775m	~140m

Hawaiian Eruptions (Figure 5.13A)

Initial activity was dominantly Hawaiian with continuous eruptions of a low viscosity magma. Eruption rate is similar to the ascent rate of the magma and hence the magma level in the vent is low. Clast size is small due to extreme fragmentation and high vesiculation. High vesicularities and high ascent rates prevent coalescence. Hence, initial deposits are dominated by vent and proximal facies type deposits due to the large amount of erupted spatter undergoing limited cooling.

Strombolian Eruptions (Figure 5.13B)

Late stage activity was dominated by Strombolian eruptions. Due to more discrete eruptions and the loss of gas, magma viscosity would have increased causing slower magma ascent rates. The eruption rate, however, would have been slower than rise rate of the magma causing an overall increase in the level of the magma in the vent. The slower rise speeds also cause discrete eruptions due to the coalescence of slow rising bubbles. The slow eruption rates also cause a degassed crust to form at the top of the magma column in the vent; this is subsequently disrupted during each eruption. Hence late stage deposits are characterised by a mix of clasts but dominated by blocky clasts, and with vesicularity ranging from 25-70%.

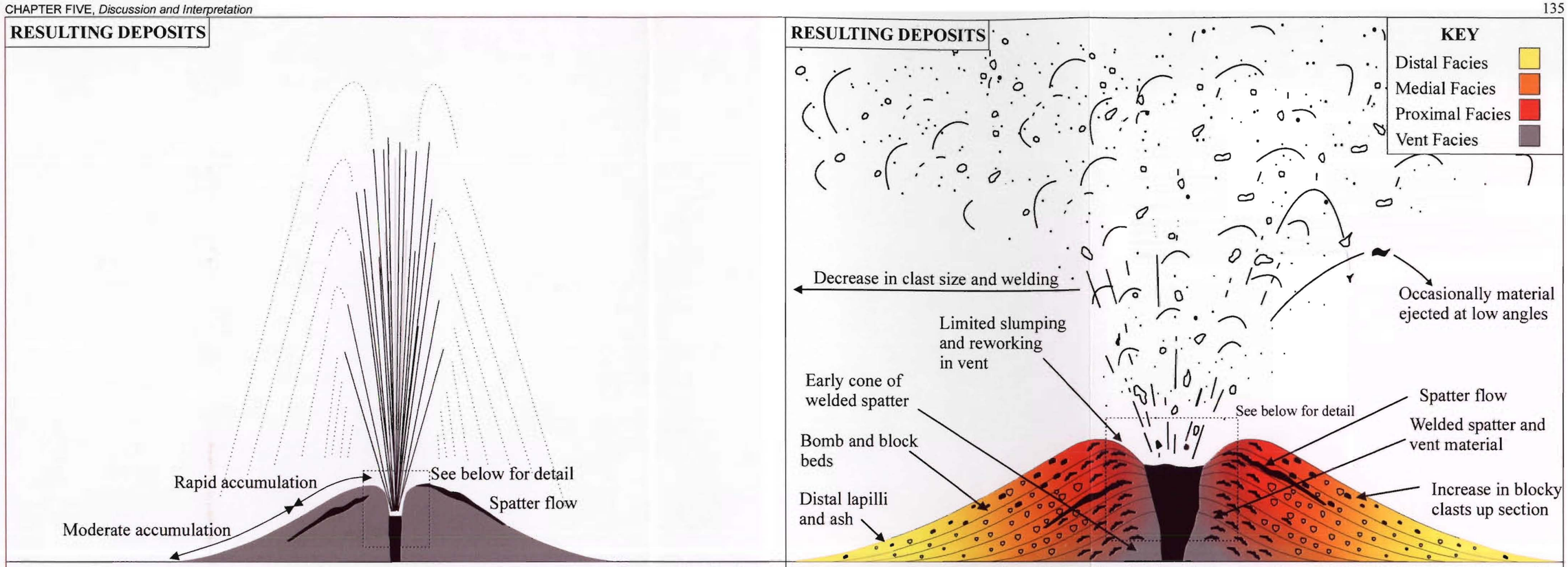

A) Initial activity consisting of continuous to near continuous Hawaiian lava fountaining. Spatter dominates with mostly proximal and vent facies . Spatter flows common due to fast accumulation rates near the vent.

B) Late stage activity consisting of more discrete Strombolian eruptions. Blocks and bombs dominate with bedded medial and distal facies.

Figure 5.13. Diagrammatic model for Lyttelton cinder cones illustrating vent processes and resulting deposits. A) Initial Hawaiian eruptions. B) Late stage Strombolian eruptions.

Chapter Six

CONCLUSIONS

6.1 HISTORY OF LYTTELTON VOLCANO

The development of cinder cones has played an important part in the development of Lyttelton Volcano and the following is a summary of conclusions outlined in previous chapters.

The first phase of Miocene volcanism began with the development of subalkaline rhyolites and andesites (Figure 6.1A). These early volcanic rocks represent early Lyttelton-type melts that interacted significantly with Torlesse basement. Early eruptive products "paved the way" for the development of Lyttelton by establishing "clean" routes to the surface, allowing limited interaction of basement and more basaltic volcanism.

Early Lyttelton volcanism (L1) was centred on "Head of the Bay" and was dominated by effusive activity causing the volcano to develop a conical shape (Figure 6.1B). Activity was fed by a 15-20 km-deep reservoir that was consistently being replenished from a deeper source, causing limited differentiation and dominantly basaltic products. Due to the small size of the edifice at this early stage, gravitational stresses were low, causing limited emplacement of radial dikes. The lack of dikes would have also caused limited flank eruptions, resulting in activity being concentrated at the summit, causing it to steepen sharply relative to the flanks. The continued growth of the edifice would have led to an increase in gravitational stresses, and hence to an increase in the propagation of radial fractures. Distension within these fractures, caused by increasing magma pressure, allowed radial dikes to form, of which some fed flank eruptions (ie cinder cones) (Figure 6.1C). An increase in radial dikes would have caused an increase in the volume of the central conduit, hence some larger dikes may have become more differentiated, causing the development of occasionally more fractionated lavas.

A) UPDOMED BASEMENT. Subalkaline rhyolites and andesites erupting (domes and flows). Heavy crustal assimilation of initial Lyttelton melts.

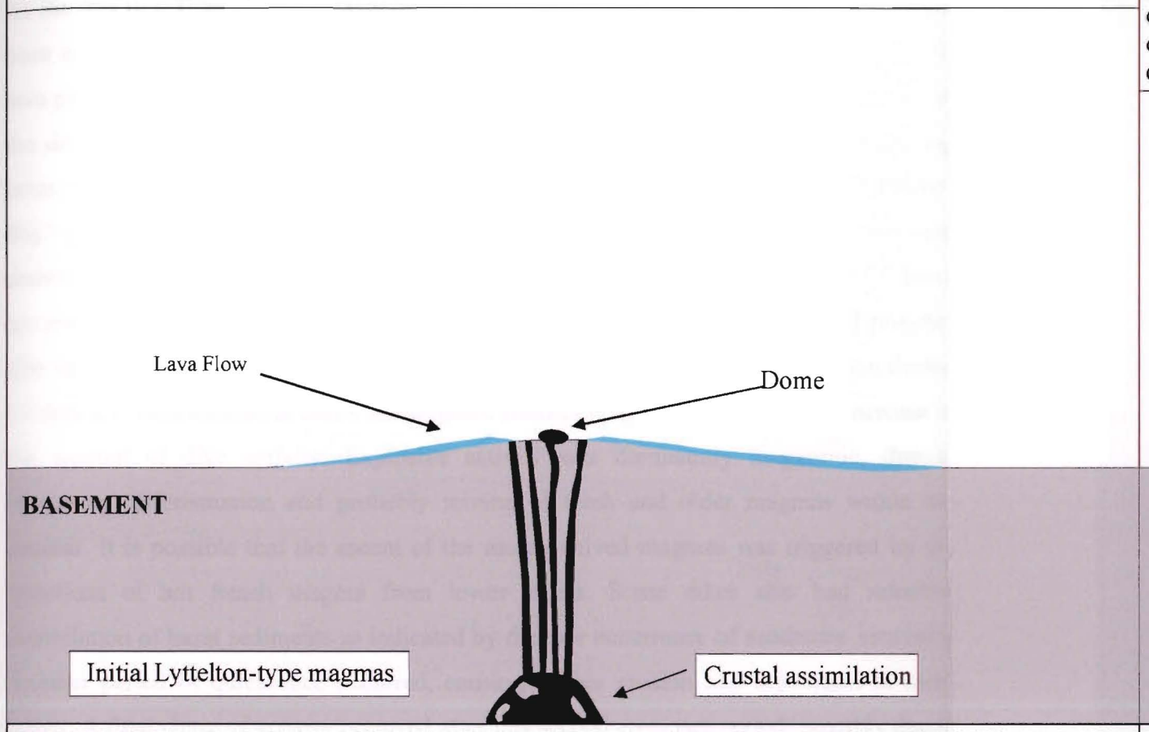

B) INITIAL L1 DEVELOPMENT. Lavas are dominantly basaltic with most being fed from the central conduit. Some lavas are slightly contaminated probably due to continued crustal assimilation during the development of the main chamber. Due to the small size of the edifice, gravitational stresses are low, as is radial dike emplacement and hence there is limited cinder cone activity. The lack of dikes causes activity to be concentrated at the summit, causing it to steepen relative to the flanks.

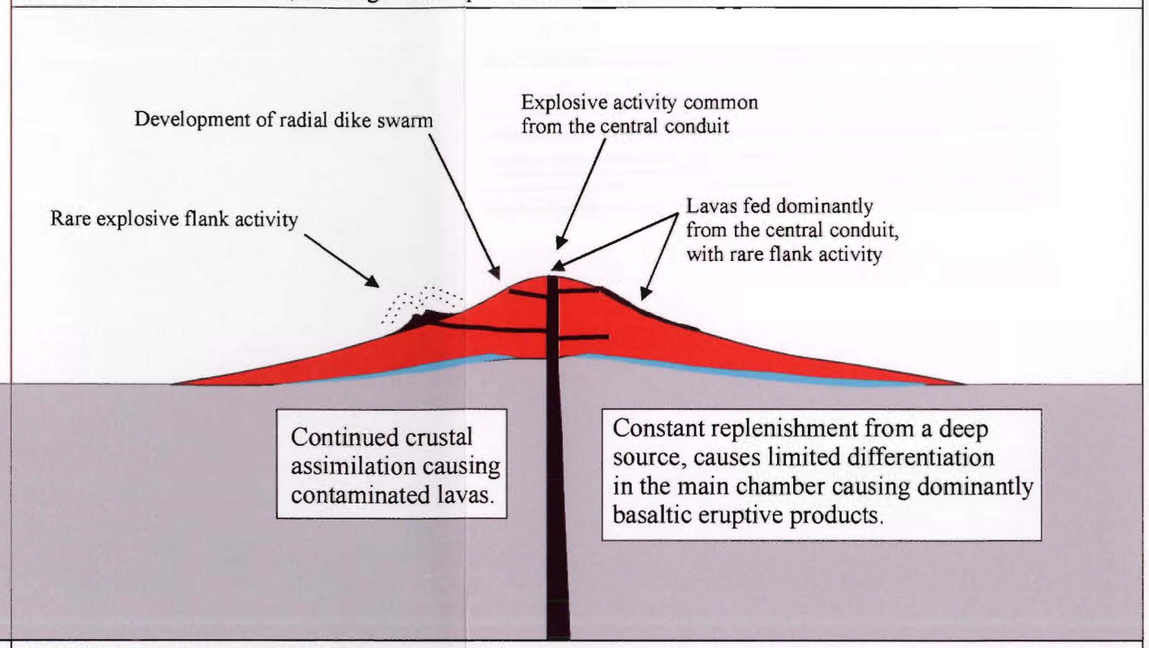

C) CONTINUED L1 DEVELOPMENT. The increasing size of the edifice, and the gravitational stress acting on it, cause an increase in the propagation of radial fractures and hence dikes. The increasing emplacement of dikes leads to common flank activity, with eruptions less common from the central vent.

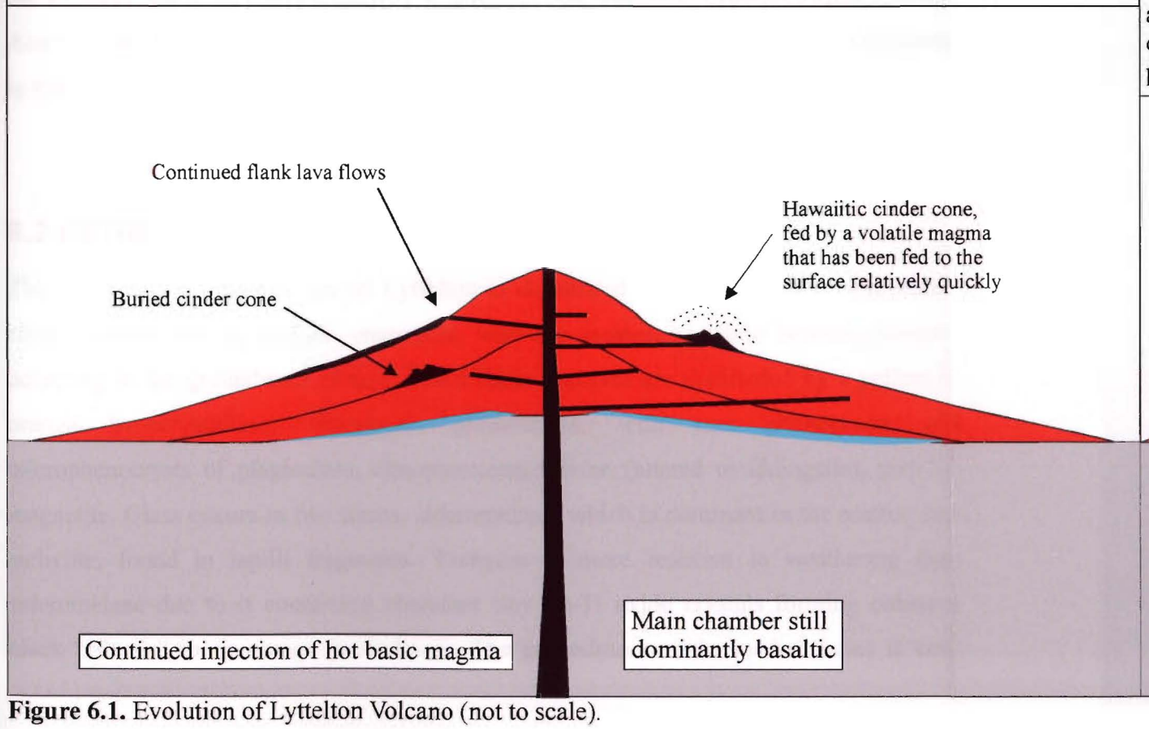

D) DEVELOPMENT OF L2. At the end of L1 there was sector collapse of the eastern flank and erosion of the L1 edifice. L2 lavas quickly overtopped the eroded L1 cone and were dominantly erupted on the western, northern and eastern flanks. Radial dikes are now very common due to the large size of the edifice with flank activity dominating over summit activity. Lavas and cones are commonly more differentiated due to increased differentiation in the main chamber, caused by diminishing replenishment. Possible development of a shallow plumbing system deep down in the edifice feeding some differentiated cones and lavas.

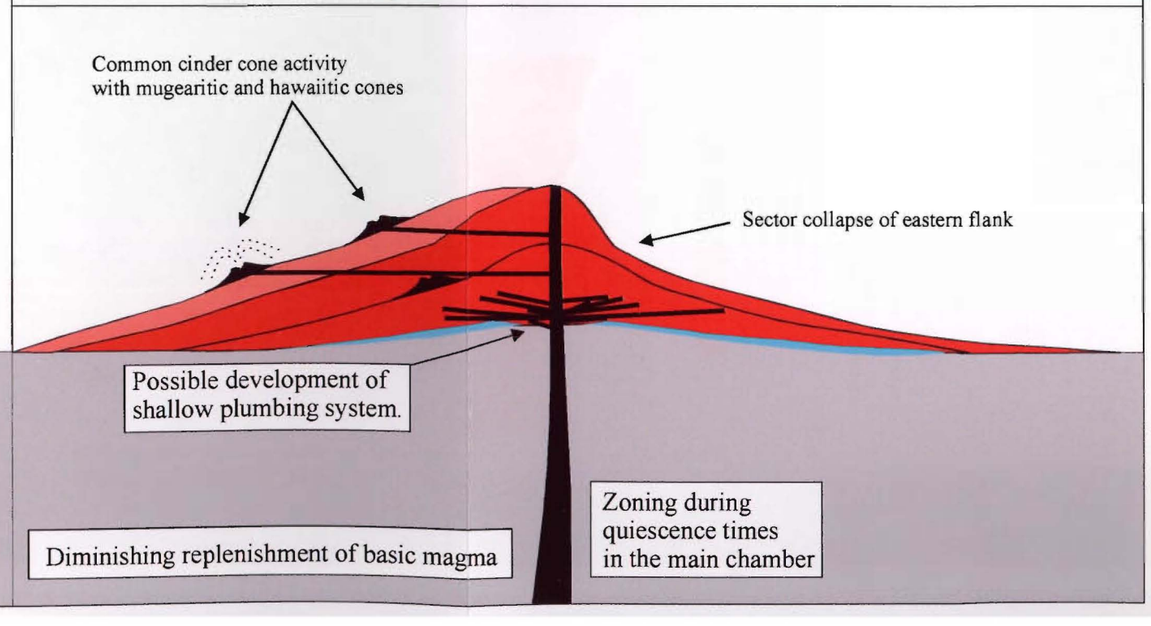

Figure 6.1. Evolution of Lyttelton Volcano (not to scale).

At the end of L1, there was a large-scale collapse of the eastern flank, which may have been associated with the violent eruption of rhyolitic lavas that are found at the top of the lava pile (Neumayr 1998). Following the collapse there was a period of erosion that led to the development of lahars, slope wash deposits and deep weathering of the underlying lavas. Activity migrated during this erosional period, moving to a centre near "Charteris Bay" (Shelley 1987). Initial L2 lavas quickly overtopped the eroded L1 cone, and were dominantly erupted on the western, northern and eastern flanks (Neumayr 1998). L2 lavas are more evolved than L1 lavas due to differentiation in the main chamber and possibly also deep down in the central conduit. Explosive flank activity was more common during L2 than L1, with numerous cones and eruptive fissures (Figure 6.1D) due to an increase in the amount of dike activity. Explosive activity was dominantly mugearitic, due to increasing differentiation and probably mixing of fresh and older magmas within the conduit. It is possible that the ascent of the more evolved magmas was triggered by the injections of hot freash magma from lower levels. Some dikes also had selective assimilation of basal sediments as indicated by the rare occurrence of sandstone xenoliths. Another period of quiescence occurred, causing further erosion and deposition of more lahars. A final phase of activity occurred after this second erosional period, possibly due to one final injection of fresh magma into the main reservoir, depositing lavas dominantly on the northern and north-eastern flanks (Neumayr 1998), with little explosive flank activity. Activity then shifted to the Mount Herbert region and then onto Akaroa, before returning to the vicinity of the eroded crater of Lyttelton Harbour.

6.2 PETROLOGY OF CINDER CONES

The petrology of cinder cones on Lyttelton is dominated by four minerals; plagioclase, clinopyroxene, olivine and Ti –magnetite, with the greatest variation between samples occurring in the groundmass phases. Distal facies samples are dominated by a yellow to orange hypocrystalline, vitrophyric groundmass, with rare phenocrysts and microphenocrysts of plagioclase, clinopyroxene, olivine (altered to iddingsite), and Ti-magnetite. Glass occurs in two forms, sideromelane, which is dominant in the matrix, and tachylite, found in lapilli fragments. Tachylite is more resistant to weathering than sideromelane due to it containing abundant tiny Fe-Ti oxide crystals forming coherent black "islands" in an orange groundmass. The groundmass of the medial facies is very

similar to the distal facies, being dominated by sideromelane, with less lapilli and more bombs. The groundmass of the vent, proximal and medial bomb samples is holocrystalline, porphyritic, and intergranular. Bomb samples and some proximal samples have sub-trachytic to trachytic texture with vent samples more pilotaxitic. Swallow-tailed plagioclase microphenocrysts are common in proximal and bomb samples, and evidence for magma mixing is common amongst all samples.

The four main phenocryst phases show a wide range of mineral textures suggesting that for any given sample they are not the result of crystallisation from a single magma under a simple set of conditions. Each phenocryst has grown under varying conditions of temperature and pressure and/or been derived from magmas of different compositions. The alteration of olivine to iddingsite is common in all samples, with alteration to iron oxides only occurring in proximal and medial facies as a result there of reheating. Ti-magnetite is the dominant iron oxide with lesser amounts of ilmenite. Apatite is common in the groundmass of most samples, phenocrysts occur in some mugearitic samples. Xenocrystic amphibole occurs rarely, as does orthopyroxene, the appearance of which is related to the assimilation of basement sediments.

Late stage magmatic and/or secondary minerals include biotite (late stage or hydrothermal), chabazite and natrolite (hydrothermal alteration of glass), and calcite (late stage hydrothermal). One xenolith, found in a sample from Southern Mount Evans, indicates the potential for at least intermittent assimilation of the basement. The xenolith is made up of clastic quartz grains and is most likely from Cretaceous/Tertiary sandstones, found directly below the volcano and exposed in the Charteris Bay area.

6.3 GEOCHEMISTRY OF CINDER CONES

Cinder cones are mostly hawaiitic and mugearitic, and all belong to the alkaline basalt-hawaiite-mugearite-benmoreite-trachyte association.

Major and trace elements show smooth trends with incompatible elements increasing with increasing SiO_2 and compatible elements decreasing. These enrichment and depletion trends are a result of crystal fractionation of plagioclase, clinopyroxene, olivine, Ti-magnetite and apatite.

Late formed cinder cone samples are more evolved than earlier samples, with early bomb samples having lower Zr concentrations than later vent samples. However, some degassed blocks were found to have lower Zr concentrations than bombs lower in the stratigraphic succession in outer wall facies. This is interpreted as indicating a mixture of fresh and older stagnant (degassed) magma in the late stage eruptive products. Further evidence for magma mingling is provided petrographically, with most samples showing evidence of mixing between mafic and felsic magmas.

6.4 PHYSICAL FEATURES OF CINDER CONES

Cinder cones on the Lyttelton Volcano were formed by explosive basaltic eruptions caused by the generation and rapid expansion of gas. To erupt explosively, the pressure in the magma chamber needs to exceed the lithostatic pressure, and this may occur as a result of the exsolution of volatiles or the intrusion of new magma. Crystallisation in the magma chamber may also cause an increase in pressure by concentrating volatiles in the residual magma.

Eruption type (ie Hawaiian or Strombolian) was controlled by the ascent rate of the magma. During initial eruptions of the cones, ascent rate would have been high due to high vesicularities, allowing little time for coalescence of bubbles and causing the magma to erupt in a continuous dispersed regime (eg Hawaiian). As ascent rates decreased there was time for increased coalescence allowing the development of large bubbles and eruption of magma in a slug regime (eg Strombolian). Late stage lavas developed when the gas content got too low to sustain an explosive eruption.

The morphology of cinder cones depends on many factors including 1) total volume of erupted material, 2) range of median ejecta velocity, 3) ejection angles, 4) wind speed and direction, 5) nature and size of particles, 6) occurrence of lava overflows, 7) phreatomagmatic intercalculations and 8) vent geometry (Vespermann & Schmincke 1999). These factors all contribute to the development of cinder cone but each acts in different degrees on different clasts, and allows cinder cones to be divided into facies (ie outer wall, and inner crater). In this study, four facies were recognised, based on welding, dip direction, block and bomb size, colour and the presence or absence of some clasts.

6.4.1 Vent Facies

Vent facies deposits represent early eruptive material and crater material. Deposits are grey/black in colour and densely welded due to rapid near vent accumulation of hot material. Vesicularity is low (< 20%), due to secondary degassing and compaction during emplacement; as a consequence, clast shape is rarely preserved in the facies. Deposits resemble lava in most areas, with the rare occurrence of dips inward toward the eruptive centre a distinctive feature.

6.4.2 Proximal Facies

Proximal facies deposits grade from the vent deposits with a decrease in densely welded material to welded material and a greater preservation of clasts. Increased preservation of clasts is due the deposits travelling further from the vent and hence undergoing more interaction with the air and thus cooling. However, clasts were still semi-fluid during deposition and this feature is characteristic of the facies with 80% of clasts having flattened shapes. Welding decreases slightly due to the decrease in accumulation rate and increase in cooling and flight times. The occasional development of an ash and lapilli matrix is due to the development of more Strombolian type eruptions. Clast vescularity ranges from 10 to 60% and this is due to a mix a fresh and stagnant magma being erupted. Deposits nearest the vent are grey in colour, but with an increasing distance from the vent deposits take on a strong red colouration. Clast size is visibly seen to decrease with increasing distance from the vent from ~0.8 m to ~0.3 m. In places the deposits may be weakly bedded. Spatter flows are common in the facies and these are interpreted to have been fed from the vent facies by the rapid accumulation of hot fluidal material.

6.4.3 Medial Facies

Medial deposits are dominated by bomb, block and lapilli beds and grade slowly from proximal deposits with a decrease of spatter to bedded bombs and blocks and an increase in a distinctive ash/lapilli matrix. Clast preservation is high due to increased distance from the vent: this is because clasts had longer cooling periods before deposition. Flattened clasts only occur rarely and due to their general absence, the deposits are non-welded. Clast size ranges from 0.15 m-0.35 m with rare larger clasts up to 4 m, found mainly in the highest part of the facies. Overall, however, clast size decreases from the vent with outer medial material commonly ranging in size from ~0.07 m-0.15 m. Due to the dominantly Strombolian nature of eruptions they are usually crudely bedded, with dips ranging from 20-30°. Clasts are mainly blocks and bombs, but there is also a matrix of a fine grained ash and lapilli.

6.4.4 Distal Facies

Distal facies deposits are found furthest from the vent location and are usually yellow in colour due to the alteration of the dominant ash material. Deposits are dominated by ash but there is also a mixture of lapilli fragments and crystals. Rare bombs do occur (~0.3 m) and these represent clasts that have been ejected at low angles from the vent. Fine ash layers can also occur, and these represent occasions where the vent became blocked and then cleared by a eruption causing a dense ash cloud. Lapilli fragments are glassy and represent fast cooling due to their small size.

6.5 RECOMMENDATIONS FOR FUTURE WORK

This study has found several areas of interest that need further research.

- A similar study to this one could focus on the cinder cones of Akaroa Volcano which seem more common than on Lyttelton. It would be of interest to see if the deposits are similar to those found on Lyttelton, and whether or not they show the same chemical evolution trends.

- The lahars mapped by Neumayr (1998) and in this study in the Mount Cavendish area need further investigation. During this study it was found that they can be easily traced over large areas and contain a variety of clasts.

- The small ridge to the south of the Southern Mount Cavendish area, above the Major Hornbrook Track is interesting. It was mapped by Neumayr (1998) as a lahar. However, on closer examination it appears to be a lava flow that flowed down a very steep grade or over a cliff and became fragmented and blocky !.

- More work in the Purau Bay/ Mount Evans area is needed to define the boundary of the L1/L2 lavas. A transect up the side of Mount Evans would be useful and may provide some insights.

- More dating of the pyroclastic deposits and L1 and L2 lavas and dikes is essential if we are to fully understand the relationship between the various events that have been proposed in recent studies of the evolution of Lyttelton Volcano.

ACKNOWLEDGEMENTS

As always, a project of this sort requires the help of many people. Firstly thanks to my supervisor Professor Jim Cole, for tirelessly proof reading all my drafts (requiring endless pencils), his enthusiasm and comments, "*I would use paler colours or supply sunglasses to examiners!!*". Associate Professors Steve Weaver and David Shelley for their constructive comments regarding the Geochemistry, Petrology, Discussion and Conclusions. Dr Bruce Houghton for taking time out to discuss the deposition and fragmentation models and for providing some recent papers. Dr Jens Richnow, for his time in showing me how to use "Image Tool", and Dave *"scumbag"* Milner, Matt *"the sifter"* Avery, and Graham Leonard for also proof reading final drafts.

Thanks to all of the technicians at the Geological Sciences Department. Firstly John *"thankyou for your attention"* Southward for all his help and patience on all things computing (ie even coming in on weekends to fix our problems!!!). Dr Kerry Swanson for all his help with the photomicrograph machine and supplying me with a camera, and always a good laugh when least expected. Rob Spiers for allowing me to play on the rocksaw and for cutting, staining and polishing all my thin sections. Stephen Brown for showing me how to play with all his expensive toys in the geochemistry lab, so that my rocks could be turned into numbers. And letting me continue playing even when I poured a molten (~1030°C) sample down the inside of the bead casting machine (whoops). Julie-Ann Hale for help with Mason Trust application forms and all forms of advice and conversation. Joan Mawson for putting up with my inability to return theses at the correct time and for keeping my diary full with lunchtime seminars. Cathy Knight for supplying sample bags, a mapboard, compass and all the other things I didn't have. Jane Guise for finding me a microscope, fixing it, and for always supplying a friendly chat. Arthur Nicholas for turning all my slides into images and always supplying lots of superlatives in any conversation. Thanks also to Michele Wright for all things financial.

The elephantine financial expense of the project was somewhat abetted by several sources. A University of Canterbury Master's Scholarship was a great help as was The Mason Trust Fund and of course Mum.

To all the farmers and The Department of Conservation for allowing me unrestricted access to their land. Especially the paranoid farmer at North Gibraltar Rock .

Brian and Josie at Big Fresh (my part-time job) who have been so understanding over the past six and half years in letting me take leave when work at varsity was increasing. Especially over the last six months it has been really appreciated.

Thanks to my room mates, Cam for supplying conversation on all topics completely unrelated to geology (eg playstation/rugby/cricket etc), and Fee on all other topics (and for answering the phone). To other 4th Floor inhabitants (eg Lou, Debs, Kylie, Kirstine, Matt, Rich, Danny) for entertaining conversation and advice at some time or another. Extra thanks also to Fee, Neisha, and Graham for helping me crush some of my samples and to Stu for suggesting that I apply for a scholarship!!!!!!!!

Finally to my friends and family overseas thanks for sending me endless e-mails to keep my interest up, when things were looking bleak. To Mum, Pat and George for some great home cooked meals during last 12 months. Neisha for her friendship, encouragement, and imperturbability for putting up with all my complaining, moaning, whining, stubbornness and stress over the past four years. And Mum and David, well with out your support and guidance over the past 24 and a bit years there would have been no way that I would have ever made it this far.

Andrew Livermore
June 28th 1999

REFERENCES

Adams, C.J. 1981: Migration of Late Cenozoic volcanism in the South Island of New Zealand and the Campbell Plateau. *Nature* 294: 153-155.

Altaye, E. 1989: The geology and geochemistry of the north-east sector of Lyttelton Volcano, Banks Peninsula. Unpublished MSc thesis, University of Canterbury.

Anderson, A.T. Jun. 1984: Probable relations between plagioclase zoning and magma dynamics, Fuego Volcano, Guatemala. *The American Mineralogist* 69: 660-676.

Anon 1990: The Banks Peninsula Landscape. Queen Elizabeth Trust, Information Booklet.

Armienti, P.: Pareschi, M.T.; Innocenti, F.; Pompilio, M. 1994: Effects of magma storage and ascent on the kinetics of crystal growth. *Contributions to Mineralogy and Petrology* 104: 594-608.

Bal, A.A. 1997: Sea caves, relict shore and rock platforms: evidence for the tectonic stability of Banks Peninsula, New Zealand. *New Zealand Journal of Geology and Geophysics* 40: 299-305.

Bell, D.H. 1978: The engineering geology of Banks Peninsula Loess Deposits. Paper presented at a seminar on "Slope Stability and Urban Development", Department of Extension Studies, University of Canterbury, 24-25 Feb. 1978, 1-35.

Blake, S. 1981: Volcanism and the dynamics of open magma chamber. *Nature* 289: 783-785.

Blake, S. 1984: Volatile oversaturation during the evolution of silicic magma chambers as an eruption trigger. *Journal of Geophysical Research* 89: 8237-8244.

Bloomfield, K. 1975: A late-Quaternary monogenetic volcano field in central Mexico. *Geologishes Rundschau* 64: 476-497.

Bonafede, M.; Cenni, N. 1998: A porous flow model of magma migration within Mt. Etna: The influence of extended sources and permeability anisoptropy. *Journal of Volcanology and Geothermal Research 81: 51-68.*

Bowen, N.L. 1928: Evolution of the Igneous Rocks. Princeton, University Press Reprinted Dover Publications, Inc. 344p.

Bradshaw, J.D.; Adams, C.J.; Andrews, P.B. 1981: Carboniferous to Cretaceous on the Pacific margin of Gondwana: The Rangitata Phase of New Zealand. *In*

Cresswell, M.M. & Vella, P (*eds*) Gondwana Five. Balkema, Rotterdam. 217-221.

Brady, L.F.; Webb, R.W. 1943: Cored bombs from Arizona and California volcanic cones. *The Journal of Geology* 51: 398-410.

Brown, L.J.; Weeber, J.H. 1992: Geology of the Christchurch urban area. Published by the Institute of Geological & Nuclear Sciences Ltd, Lower Hutt, New Zealand. 104p.

Brown, S.J.A. 1990: Strombolian deposits of the K-Trig basalts Taupo. Unpublished BSc (Hons) thesis, University of Canterbury

Brown, S.J.A.; Smith, R.T.; Cole, J.W.; Houghton, B.F. 1994: Compositional and textural characteristics of the strombolian and surtseyan K-Trig basalts, Taupo Volcanic Centre, New Zealand: implications for eruption dynamics. *New Zealand Journal of Geology and Geophysics* 37: 113-126.

Butterworth, D.; Hewitt, G.F. 1979: Two-phase flow and heat transfer. Oxford University Press, London, 514p.

Cas, R.A.F.; Wright, J.V. 1987: Volcanic successions modern and ancient. Chapmen and Hall, Melbourne, 528p.

Cashman, K.V.; Mangan, M.T. 1994: Physical aspects of magmatic degassing II. *In* Carroll, M.R. & Holloway, J.R. (*eds*). Volatiles in Magmas, *Reviews in Mineralogy* 30:447-478.

Cashman, K.V.; Mangan, M.T.; Newman, S. 1994: Surface degassing and modifications to vesicle size distributions in Kilauea basalt. *Journal of Vocanology and Geothermal Research* 61: 45-68.

Chester, D.K.; Duncan, A.M.; Guest, J.E.; Kilburn, C.R.J. 1985: Mount Etna, the anatomy of a volcano. University Press Cambridge.

Coates, G.F. 1976: A statigraphic study of the Lyttelton Volcano. Unpublished BSc (Hons) thesis, University of Canterbury.

Colman, S.M. 1982: Chemical weathering of basalts and andesites; evidence from weathering rinds. *U.S. Geological Survey Professional Paper* 1246: 51p.

Condomines, M.; Tanguy, J.C.; Michand, V. 1995: Magma dynamics at Mt Etna: Constraints from U-Th-Ra-Pb disequilibria and Sr – isotopes in historical lavas. *Earth Planet and Science Letters* 132: 25-41.

Cox, G.J. 1994: Mountains of fire; the volcanic past of Banks Peninsula. Christchurch, Canterbury University Press, 32p.

Deer, W.A.; Howie, R.A.; Zussman, J. 1982: Rock-forming minerals: Volume 1A: Orthosilicates. 2nd edition. Longman Group Limited.

Delvigne, J.; Bisdom, E.B.A.; Sleeman, J.; Stoops, G. 1979: Olivines, their pseudomorphs and secondary products. *Pedologie* 29: 247-309.

Dobran, F.; Congilio, S. 1996: Magma ascent simulations of Etna. *Journal of Geophysical Research* 101: 713-731.

Donaldson, C.H.; Henderson, C.M.B. 1988: A new interpretation of round embayments in quartz crystals. *Mineralogical Magazine* 52: 27-33.

Dorsey, C.J. 1981: The Stratigraphy, petrography and geochemistry of the Diamond Harbour Group, Banks Peninsula. Unpublished BSc (Hons) thesis, University of Canterbury.

Dorsey, C.J. 1989: The geology and geochemistry of Akaroa Volcano, Banks Peninsula, New Zealand. Unpublished PhD thesis, University of Canterbury.

Duncan, A.M. 1978: The volcanics of the Adrano area, Mount Etna, Sicily. *Geology Magazine* 115: 273-285.

Falloon, T.J. 1982: The geology of the Onawe-French Farm-Wainui area, Akaroa Volcano, banks Peninsula. Unpublished BSc (Hons) thesis, University of Canterbury.

Fiske, R.S.; Jackson, E.D. 1972: Orientation and growth of Hawaiian rifts: the effects of regional structure and gravitational stresses. *Proceedings of the Royal Society of London A* 329: 299-326.

Fisher, R.V. 1961: Proposed classification of volcanoclastic sediments and rocks. *Geological Society of America Bulletin* 72: 1409-1414.

Fisher, R.V. 1966: Rocks composed of volcanic fragments and their classification. *Earth Science Reviews* 1: 287-298.

Fisher, R.V.; Schmincke, H.U. 1984: Pyroclastic Rocks. Springer-Verlag, Berlin, 472p.

Francis, P.W. 1973: Cannonball bombs, a new kind of volcanic bomb from Paeaya Volcano Guatemala. *Geological Society of America Bulletin* 84: 2791-2794.

Gay, P.; Le Maitre, R.W. 1961: Some observations on iddingsite. *American Mineralogist* 46: 92-111.

Gerard, V.B. 1953: Aeromagnetic observations over the Banks Peninsula area and the Mernoo Bank. *New Zealand Journal of Science and Technology* 35: 152-160.

Gerlach, T.M. 1986: Exsolution of H_2O, CO_2, and S during eruptive episodes at Kilauea Volcano, Hawaii. *Journal of Geophysical Research* 91: 12177-12185.

Guard, F. 1999: Volcanology and geochemistry of the Diamond Harbour Group, Banks Peninsula, New Zealand. Unpublished MSc thesis, University of Canterbury.

Guest, J.E. 1982: Styles of eruption and flow morphology on Mt Etna. *Memoirs for the Society of Geology* 23: 49-73.

Guest, J.E; Duncan, A.M. 1981: Internal plumbing of Mount Etna. *Nature* 290: 584-586.

Guest, J.E.; Kilburn, C.R.J.; Pinkerton, H.; Duncan, A.M. 1987: The evolution of lava flow fields: observations of the 1981 and 1983 eruptions of Mt. Etna, Sicily. *Bulletin of Volcanology* 47: 635-648.

Guest, J.E.; Huntingdon, A.T.; Wadge, G.; Brander, J.L.; Booth, B. Carter, S.; Duncan, A. 1974: Recent eruption of Mount Etna. *Nature* 250: 385-387.

Gutmann, J.T. 1979: Structure and eruptive cycle of cinder cones in the Pinacate volcanic field and the controls of Strombolian activity. *Journal of Geology* 87: 448-454.

Haggerty, S.E.; Baker, I. 1967: The alteration of olivine in basalt and associated lavas. *Contributions to Mineralogy and Petrology* 16: 233-273.

Hall, A. 1987: Igneous Petrology. Longman Scientific and Technical, London, 573p.

Hammill, M. 1979: Contrasting cinder cones on the flanks of Mount Etna, Sicily. *Geological Magazine* 116: 135-138.

Haast, H.F. 1948: The life and times of Sir Julius von Haast. Avery Press Limited, Wellington, New Zealand, 1142p.

Haast, J. Von 1860: Report of a geological survey of Mount Pleasant. Prov. Council Canterbury Session XVII, December 19.

Haast, J. Von 1879: Geology of the provinces of Canterbury and Westland. Lyttelton Times. 486p.

Harrison, J. 1999: Stabilisation of Port Hills Loess. Unpublished MSc thesis, University of Canterbury.

Hayward, B.W. 1987: Granite and marble: A guide to building stones in New Zealand. Geological Society of New Zealand guidebook 8. 56p.

Head, J.W.; Wilson, L. 1989: Basaltic pyroclastic eruptions: influence of gas-release patterns and volume fluxes on fountain structure, and the formation of cinder cones, spatter cones, rootless flows, lava ponds and lava flows. *Journal of Volcanology and Geothermal Research* 37: 261-271.

Heiken, G.; Wolhetz, K. 1985: Volcanic Ash. University of California Press, Los Angeles, 256p.

Hibberd, T.J. 1994: The geology of the Cooper Knob area, Lyttelton Volcano, Banks Peninsula. Unpublished BSc (Hons) thesis, University of Canterbury.

Hirn, A.; Nercessian, A.; Sapin, M.; Ferrucci, F.; Wittlinger, G. 1991: Seismic heterogeneity of Mt Etna: structure and activity. *Journal of Geophysical Research* 105: 139-153.

Hobden, B.J. 1990: The volcanic geology and geochemistry of the Le Bons Bay area, Lyttelton Volcano, Banks Peninsula. Unpublished BSc (Hons) thesis, University of Canterbury.

Houghton, B.F.; Hackett, W.R. 1984: Strombolian and phreatomagmatic deposits of Ohakune Craters Ruapehu, New Zealand: a complex interaction between external water and rising basaltic magma. *Journal of Volcanology and Geothermal Research* 21: 207-231.

Houghton, B.F.; Schmincke, H.U. 1989: Rothenberg scoria cone, East Eifel: a complex Strombolian and Phreatomagmatic volcano. *Bulletin of Volcanology* 52:28-48.

Houghton, B.F.; Wilson, C.J.N. 1989: A vesicularity index for pyroclastic deposits. *Bulletin of Volcanology* 51: 451-462.

Houghton, B.F.; Wilson, C.J.N.; Smith, I.E.M. (1999): Shallow-seated controls on styles of explosive basaltic volcanism: a case study from New Zealand. *Journal of Volcanology and Geothermal Research (In Press).*

Hughes, J.W.; Guest, J.E.; Duncan, A.M. 1990: Changing styles of effusive eruption on Mount Etna since AD 1600. . *In* Ryan, M.P. (*ed*) Magma Transport and Storage, John Wiley and Sons, Brisbane, 385-406.

Hutton, F.W. 1885: Sketch of the geology of New Zealand. Quarterly Journal Of the Geological Society 41:215-217.

Irvine, T.N.; Barager, W.R.A. 1971: A guide to the chemical classification of common volcanic rocks. *Canadian Journal of Earth Sciences* 8: 523-545.

Johnston, D.M. 1990: Cinder cones in the Pigeon Bay – Port Levy Area, Banks Peninsula. Unpublished MSc thesis, University of Canterbury.

Johnston, D.M.; Cole, J.W.; Houghton, B.F. 1997: Physical volcanology of Miocene basaltic pyroclastic deposits at Pigeon Bay: remnants of scoria cones of Akaroa Volcano, Banks Peninsula, New Zealand. *New Journal of Geology and Geophysics* 40: 109-115.

Jones, A. 1997: The mapping of erosional features using geophysical techniques, Heathcote Quarry Reserve, Port Hills, Christchurch. Unpublished BSc (Hons) thesis, University of Canterbury.

Juapart,C.; Vergniolle, S. 1988: Laboratory models of Hawaiian and Strombolian eruptions. *Nature* 331: 58-60.

Kuo, L.C.; Kirkpatrick, R.J. 1982: Pre-eruption history of phyric basalts from DSDP Legs 45 and 46: Evidence from morphology and zoning patterns in plagioclase. *Contributions to Mineralogy and Petrology* 79: 13-27.

Le Maitre, R.W. 1989: A classification of igneous rocks and glossary of terms. Oxford, Blackwell, 193p.

Larsen, E.S.Jr.; Irving, J.; Gonyer, F.A.; Larsen, E.S.3rd. 1938: Petrologic results of a study of the minerals from the Tertiary volcanic rocks of the San Juan region, Colorado. *The American Mineralogist* 23: 227-257.

Lenat, J.; Bachelery, P.; Bonneville, A.; Tarits, P.; Cheminee, J. Delorme, H. 1988: The December 4, 1983 to February 18, 1984 eruption of Piton de la Fournaise (La Reunion, Indian Ocean): description and discussion. *Journal of Volcanology and Geothermal Research* 36: 87-112.

Liggett, K.A.; Gregg, D.R. 1965: Geology of Banks Peninsula. *Department of Scientific and Industrial Research Information Series* 51: 9-25.

Lofgren, G. 1974: Temperature-induced zoning in synthetic plagioclase feldspar. *In* Mackenzie, W.S.; Zussman, J. (*eds*), The Feldspars, Manchester University Press, 362-375.

Loomis, T.P. 1982: Numerical simulations of crystallisation processes of plagioclase in complex melts: the origin of major and oscillatory zoning in plagioclase. *Contributions to Mineralogy and Petrology* 81: 219-229.

Mader, H.M.; Zhang, Y.; Phillips, J.C.; Sparks, R.S.J.; Sturtevant, B.; Stopler, E. 1994: Experimental simulations of explosive degassing of magma. *Nature* 372: 85-88.

Mangan, M.T.; Cashman, K.V.; Newman, S. 1993: Vesiculation of basaltic magma during eruption. *Geology* 21: 157-160.

Mangan, M.T.; Cashman, K.V. 1996: The structure of basaltic scoria and reticulite and inferences for vesiculation, foam formation, and fragmentation in lava fountains. *Journal of Volcanology and Geothermal Research* 73: 1-18.

Marshall, P. 1893: On a tridymite trachyte of Lyttelton. *Transaction and Proceedings of the New Zealand Institute* 26: 368-387.

Macdonald, G.A. 1945: Ring structure at Mauna Kea. *American Journal of Science* 243: 210-217.

Macdonald, G. A. 1967: Forms and structures of extrusive basaltic rocks. *In* Hess, H.H.; Poldervaart, A. (*eds*) Basalts: The Poldervaart treatise on rocks of basaltic composition, Wiley-Interscience Publishers, New York, 1-61.

Macdonald, G.A. 1972: Volcanoes. Prentice and Hall, Englewood Cliffs, New Jersey. 510p.

McBirney, A.R.: Noyes, R.M. 1979: Crystallisation and layering of the Skaergaard Intrusion. *Journal of Petrology* 20: 487-554.

McGetchin, T.R.; Settle, M.; Chout, B.A. 1974: Cinder cone growth modelled after Northeast crater, Mount Etna, Sicily. *Journal of Geophysical Research* 79: 3257-3272.

McGuire, W.J.; Pullen, A.D. 1989: Location and orientation of eruptive fissures and feeder-dykes at Mount Etna; influence of gravational and regional tectonic stress regimes. *Journal of Volcanology and Geothermal Research* 38: 325-344.

Mckenzie, C.J. 1995: The volcanic geology of the Southern Mt Evans-Upper Purau Valley Area, Lyttelton Volcano, Banks Peninsula. Unpublished BSc (Hons) thesis, University of Canterbury.

McPhie, J.; Doyle, M.; Allen, R. 1993: Volcanic textures. Tasmanian Government Printing Office, Tasmania. 197p.

Meschede, M. 1986: A method of discriminating between different types of mid-ocean ridge basalts and continental tholeiites with the Nb-Zr-Y diagram. *Chemical Geology* 56: 207-218.

Morse, S.A. 1979: Influence of augite on plagioclase fractionation. *Journal of Geology* 87: 202-208.

Mullen, E.D. 1983: $MnO/TiO_2/P_2O_5$: a minor element discriminant for basaltic rocks of oceanic environments and its implications for petrogenesis. *Earth Planet and Science Letters* 62: 53-62.

Muncill, G.E.; Lasaga, A.C. 1981: Modelling variations in plagioclase oscillatory zoning that result from solid-state diffusion. *Geological Society of America, Abstracts with Programs* 13: 156.

Murray, J.B.; Pullen, A.D. 1984: Three dimensional model of the feeder conduit of the 1983 eruption of Mt. Etna Volcano, from ground deformation measurements. *Bulletin of Volcanology* 47: 1145-1163.

Murray, J.B. 1990: High-level magma transport at Mount Etna volcano, as deduced from ground deformation measurements. *In* Ryan, M.P. (*ed*) Magma Transport and Storage, John Wiley and Sons, Brisbane, 357-384.

Nelson, S.T.; Montana, A. 1992: Sieve-textured plagioclase in volcanic rocks produced by rapid decompression. *American Mineralogist* 77: 127-137.

Neumayr, R.E. 1998: The geology of the Lyttelton 1 Volcano. Unpublished MSc thesis, University of Canterbury.

Nixon, G.T.: Pearce, T.H. 1987: Laser-inferferometry study of oscillatory zoning in plagioclase: the record of magma mixing and phenocryst recycling in calc-alkaline magma chambers, Iztaccihuatl volcano, Mexico. *The American Mineralogist* 72: 1144-1162.

Noble, D.C.; Haffty, J. Hedge C.E. 1969: Strontium and magnesium contents of some natural peralkaline silicic glasses and their petrographic significance. *American Journal of Science* 267: 598-608.

Oborn, L.E.; Suggate, R.P. 1959: Sheet 21, Christchurch. Geological map of New Zealand, 1:250 000 DSIR, Wellington, New Zealand.

Parfitt, É.A.; Wilson, L. 1994: The 1983-86 Pu'u 'O'o eruption of Kilauea volcano, Hawaii; a study of dike geometry and eruption mechanisms for a long lived eruption. *Journal of Volcanology and Geothermal Research* 59: 179-205.

Parfitt, E.A.; Wilson, L. 1995: Explosive volcanic eruptions – IX. The transition between Hawaiian-style lava fountaining and Strombolian explosive activity. *Geophysical Journal International* 121: 26-232.

Parfitt, E.A.; Wilson, L.; Head, J.W. 1993: Basaltic magma reservoirs: factors controlling their rupture characteristics and evolution. *Journal of Volcanology and Geothermal Research* 55: 1-14.

Parsons, W.H. 1939: Volcanic centres of the Sunlight Area, Park County, Wyoming. *Journal of Geology* 47: 1-26.

Pearce, J.A.; Cann, J.R. 1973: Tectonic setting of basic igneous rocks determined using trace element analysis. *Earth and Planetary Science Letters* 19: 290-300.

Pearce, T.H., Kolisnik, A.M. 1990: Observations of plagioclase zoning using interference imaging. *Earth Science Reviews* 19-26.

Pearce, T.H.; Russell, J.K.; Wolfson, I. 1987: Laser-interference and Normarski interference imaging of zoning profiles in plagioclase phenocrysts from the May 18, 1980 eruption of Mount St. Helens, Washington. *American Mineralogist* 72: 1131-1143.

Peterson, D.W.; Moore, R.B. 1987: Geologic history and evolution of geologic concepts, Island of Hawaii. *In:* Decker, R.W.; Wright, T.L.; Struffer, P.H. (*eds*). *Volcanism in Hawaii,* U.S.G.S. Professional Paper 1350, Vol. 1, 149-189p.

Philips, W,.R.; Griffen, D.T. 1981: Optical Mineralogy, the Non-Opaque minerals. W.H. Freeman, San Francisco, California, 667p.

Porter, S.C. 1972: Distribution, morphology, and size frequency of cinder cones on Mauna Kea, Volcano, Hawaii. *Geological Society of America Bulletin* 83: 3607-3612.

Richards, J.R.; Lenhoff, A.M.; Beris, A.N. 1994: Dynamic break up of liquid-liquid jets. *Physics of Fluids* 6:2640-2655.

Ringwood, A.E. 1975: Composition and petrology of the Earth's mantle. McCraw-Hill.

Rollinson, H. 1993: Using geochemical data. Longman Scientific and Technical, Singapore, 352p.

Rubin, A.M. 1993: Tensile fracture of rock at high confining pressure; implication foe dyke propagation. *Journal of geophysical Research* 98: 15919-15935.

Ryan, M.P. 1987: Neutral buoyancy and the mechanical evolution of magma systems. *In.* Mysen, B.O. (*ed*). Magmatic processes: Physico-chemical Principles. Geochemical Society Special Publication 1: 259-287.

Rymer, H.; Murray, J.B.; Brown, G.C.; Ferrucci, F.; McGuire, W.J. 1993: Mechanisms of magma eruption and emplacement at Mt Etna between 1989 and 1992. *Nature* 361: 439-441.

Sahagian, D. 1985: Bubble migration and coalescence during the solidification of basaltic bubble flows. *Journal of Geology* 93: 205-211.

Sahagian, D.; Anderson, A.; Ward, B. 1989: Bubble coalescence in basalt flows: Comparison of a numerical model with natural examples. *Bulletin of Volcanology* 52: 49-56.

Sanderson, T.J.O. 1982: Direct gravitational detection of magma movements at Mount Etna. *Nature* 297: 487-490.

Sanderson, T.J.O.; Berrino, G.; Corrado, G.; Grimaldi, M. 1983: Ground deformation and gravity changes accompanying the March 1981 eruption of Mount Etna. *Journal of Volcanology and Geothermal Research* 16: 266-315.

Self, S.; Sparks, R.S.J.; Booth, B. Walker, G.P.L. 1974: The 1973 Heimaey Strombolian scoria deposit, Iceland. *Geological Magazine* 111: 539-548.

Scandone, R. 1996: Factors controlling the temporal evolution of explosive eruptions. *Journal of Volcanology and Geothermal Research* 72: 71-83.

Scott, D.H.; Trask, N.J. 1971: Geology of the lunar crater volcanic field, Nye Country, Nevada. *U.S. Geological Professional Paper* 599: 1-22.

Searle, E.J. 1962: Quartzose xenoliths and pyroxene aggregates in the Auckland basalts. *New Zealand Journal of Geology and Geophysics* 5: 130-140.

Settle, M. 1979: The structure and emplacement of cinder cone fields. *American Journal of Science* 279: 1089-1107.

Sewell. R.J. 1985: The volcanic geology and geochemistry of central Banks Peninsula and relationships to Lyttelton and Akaroa volcanoes. Unpublished PhD thesis 2 Volumes, University of Canterbury.

Sewell, R.J. 1988: Late Miocene volcanic stratigraphy of central Banks Peninsula, Canterbury, New Zealand. *New Zealand Journal of Geology and Geophysics* 31: 41-64.

Sewell, R.J.; Gibson, I.J. 1988: Petrology and geochemistry of Tertiary volcanic rocks from inland Central and South Canterbury, South Island, New Zealand. *New Zealand Journal of Geology and Geophysics* 31: 477-492.

Sewell, R.J.; Weaver, S.D. 1990: Sheet N36 AC Akaroa West. Geological map of New Zealand. 1:50 000, Wellington, New Zealand.

Sewell, R.J.; Weaver, S.D.; Theile, R.J, 1988: Sheet M36 BD Lyttelton. Geological map of New Zealand. 1:50 000, Wellington, New Zealand.

Sewell, R.J.; Weaver, S.D.; Reay, M.B. 1992: Geology of Banks Peninsula. Scale 1:100 000. Institute of Geological and Nuclear Sciences map 3. Institute of Geological and Nuclear Sciences Ltd, Lower Hutt, New Zealand.

Sharp, A.D.L.; Davis, P.M.; Grey, F. 1980: A low velocity zone beneath Mount Etna and magma storage. *Nature* 287: 587-591.

Shearer, J.C. 1986: The geology of Governors Bay-Dyers Pass Road Area, Lyttelton Volcano, Banks Peninsula. Unpublished BSc (Hons) thesis, University of Canterbury.

Shelley, D. 1985a: Determining Paleo-flow directions from groundmass fabrics in the Lyttelton radial dikes, New Zealand. *Journal of Volcanology and Geothermal Research* 25: 67-79.

Shelley, D. 1985b: Optical Mineralogy. Elsevier, New York. 322p.

Shelley, D. 1987: Lyttelton 1 and Lyttelton 2, the two centres of the Lyttelton Volcano. *New Zealand Journal of Geology and Geophysics* 30: 159-168.

Shelley, D. 1988: Radial dikes of Lyttelton Volcano – their structure, form, and petrography. *New Zealand Journal of Geology and Geophysics* 31: 65-75.

Shelley, D. 1992: Port Hills; radial dikes, spatter cones and shapes of the two Lyttelton Volcanoes. *In* Campbell, J.K. (*ed*) Geological Society of New Zealand Field Trip Guides, Christchurch Conference, 95-102.

Shelley, D. 1993: Igneous and metamorphic rocks under the microscope. Chapmen & Hall, London, 445p.

Slaughter, G.N. 1995: The geology of the Mt Evans Area: Implications for the Stratigraphy of the Lyttelton Volcano. Unpublished BSc (Hons) thesis, University of Canterbury.

Smith, R.P. 1978: Geologic maps of part of the Spanish Peaks dike system, south-central Colorado. *Geological Society of America maps and chart series Mc-22.*

Smith, J.V.; Brown, W.L. 1988: Feldspar minerals. Springer-Verlag, New York, 828p.

Smith, K.L.; Milnes, A.R.; Eggleton, R.A. 1987: Weathering of basalt: formation of iddingsite. *Clays and Clay Minerals* 35: 418-428.

Sparks, R. 1978: The dynamics of bubble formation and growth in magmas: A review and analysis. *Journal of Volcanology and Geothermal Research* 3: 1-37.

Sparks, R.S.J.; Barclay, J.; Jaupart, C.; Mader, H.M.; Phillips, J.C. 1994: Physical aspects of magma degassing I. *In* Carroll, M.R. & Holloway, J.R. (*eds*). Volatiles in Magmas, *Reviews in Mineralogy* 30:413-445

Speight, R. 1908: Soda amphibole trachyte from Cass Peak. *Transactions and Proceedings of the New Zealand Institute* 40: 176-184.

Speight, R. 1917: The geology of Banks Peninsula. *Transactions and Proceedings of the New Zealand Institute.* 49:365-392.

Speight, R. 1924: The basic rocks of Banks Peninsula. *Records of the Canterbury Museum* 2: 239-267.

Speight, R. 1940: The basal beds of Akaroa volcano. *Transactions of the Royal Society of New Zealand* 70: 60-76.

Speight, R. 1944: The geology of Banks Peninsula – a revision Part 2. The Akaroa volcano. *Transactions of the Royal Society of New Zealand* 74: 232-254.

Stipp, J.J.; McDougall, I. 1968: Geochronology of the Banks Peninsula volcanoes, New Zealand. *New Zealand Journal of Geology and Geophysics* 11: 1239-1260.

Stimac, J.A.; Pearce, T.H. 1992: Textural evidence of mafic felsic magma interactions in dacite lavas, Clear Lake California. *American Mineralogist* 77: 795-809.

Stone, H.A. 1994: Dynamics of drop deformation and breakup in viscous fluids. *Annual Review of Fluid Mechanics* 26: 65-102.

Tait, S.; Jaupart, C.; Vergniolle, S. 1993: Pressure, gas content and eruption periodicity of a shallow crystallising magma chamber. *Earth and Planetary Science Letters* 92: 107-123.

Tanguy, J.; Condomines, M.; Kieffer, G. 1997: Evolution of the Mount Etna magma: Constraints on the present feeding system and eruptive mechanism. *Journal of Volcanology and Geothermal Research* 75: 221-250.

Theile, R.J. 1983: Basement geology of the Lyttelton volcano, Banks Peninsula. Unpublished MSc thesis, University of Canterbury.

Thorarinsson, S.; Steinthorsson, S.; Einarsson, T.; Kristmannsdottir, H.; Oskarsson, N. 1973: The eruption of Heimaey, Iceland. *Nature* 241: 372-375.

Tsuya, H. 1941: On the form and structure of volcanic bombs from volcano Miyake-sima. *Bulletin of the Earthquake Research Institute, Tokyo Imperial University* 19: 597-611.

Tsuchiyama, A. 1985: Dissolution kinetics of plagioclase in melt of system diopside-albite-anorthite, and origin of dusty plagioclase in andesite. *Contributions to Mineralogy and Petrology* 89: 1-16.

Vance, J.A. 1962: Zoning in igneous plagioclase: normal and oscillatory. *American Journal of Science* 260: 746-760.

Vergniolle, S.; Jaupart, C. 1986: Separated two-phase flow and basaltic eruptions. *Journal of Geophysical Research* 91: 12842-12860.

Vergniolle, S.; Juapart, C. 1990: Dynamics of degassing at Kilauea volcano, Hawaii. *Journal of Geophysical Research* 95: 2793-2809

Vergniolle, S.; Mangan, M. 1999; Dynamics of Hawaiian and Strombolian eruptions. *In Press.*

Vespermann, D.; Schmincke, H-U. Scoria Cones and Tuff Rings. *In Press.*

Wadge, G. 1976: Deformation of Mount Etna, 1971-1974. *Journal of Volcanology and Geothermal Research* 1: 237-263.

Wadge, G. 1977: The storage and release of magma on Mount Etna. *Journal of Volcanology and Geothermal Research* 2: 361-384.

Walker, G.P.L. 1973: Explosive volcanic eruptions – a new classification scheme. *Geologishes Rundschau* 62: 431-446.

Walker, G.P.L.; Croasdale, R. 1972: Characteristics of some basaltic pyroclastics. *Bulletin of Volcanology* 35: 303-317.

Wallis, G.B. 1969: One dimensional two-phase flow. McGraw-Hill, New York, 408p.

Weaver, S.D. 1980: An introduction to the geology of Lyttelton Volcano (excursion notes). *In* Field Trip Guides. Geological Society of New Zealand , Christchurch Conference, November 24-27, 1980.

Weaver, S.D. 1991: Cenozoic Volcanic Geology of Banks Peninsula. *In.* Coombs, D.S. (*ed*), Geol. Sic. Am. Kiwi Geotrip Guidebook. Misc Publication, University of Otago, 215-231.

Weaver, S.D.; Sewell, R.J. 1986: C2:Cenozoic volcanic geology of Banks Peninsula. *In*: Houghton, B.F. and Weaver, S.D. (*eds*). South Island Igneous Rocks. Tour Guides A3, C2 and C7. *New Zealand Geological Survey Record* 13: 39-64.

Weaver, S.D.; Smith, I.E.M. 1989: New Zealand Intraplate Volcanism. *In*: Johnston, R.W. Knutson, J. and Taylor, S.R. (*eds*). Intraplate volcanism in Eastern Australia and New Zealand. Cambridge University Press. 157-188.

Weaver, S.D.; Sewell, R.: Dorsey, C. 1985: Extinct Volcanoes. A guide to the geology of Banks Peninsula. *Geological Society of New Zealand Guidebook No. 7.*

Whalley, P.B. 1996: Two-phase flow and heat transfer. Oxford Science Publications, New York, 92p.

Wilshire, H.G. 1958: Alteration of olivine and orthopyroxenes in basic lavas and shallow intrusions. *American Mineralogist* 43: 120-147.

Wilson, L. 1980: Relationships between pressure, volatile content and ejecta velocity in three types of volcanic explosion. *Journal of Volcanology and Geothermal Research* 8: 297-313.

Wilson, L.; Head, J.W. 1981: Ascent and eruption of basaltic magma on the Earth and Moon. *Journal of Geophysical Research* 86: 2971-3001.

Wilson, L. Head, J.W. 1988: Nature of local magma storage zones and geometry of conduit systems below basaltic eruption sites, Pu'u 'O'o, Kilauea East Rift, Hawaii, example. *Journal of Geophysical Research* 93: 14785-14792.

Wilson, M. 1993: Igneous Petrogenesis. Chapmen and Hall, London, 466p.

Williams, H.; McBirney, A.R. 1979: Volcanology. Freeman, Cooper & Co., San Francisco, 397p.

Wood, C.A. 1980: Morphological evolution of cinder cones. *Journal of Geology and Geothermal Research* 7: 387-413.

Wright, J.V.; Smith, A.L.; Self, S. 1980: A working terminology for pyroclastic deposits. *Journal of Geology and Geothermal Research* 8: 315-336.

Yetton, M.D. 1986: Investigation and remedial methods for subsurface erosion control in Banks Peninsula loess. Unpublished MSc (Eng. Geol.) thesis, University of Canterbury.

APPENDIX 1: AIR PHOTOS

All areas were mapped on the following air photos, which were enlarged to A3 size for the selected outcrop area by a laser photocopier. All areas were mapped on overlay paper which were then transferred to enlarged topographic maps (NZMS 260 Sheet M36 Lincoln, N36 Akaroa) with the final maps drafted on "Corel Draw 8.0".

Mount Cavendish and Castle Rock areas

Run SN2634: N38, N39, N40, M42, M43, M44, M45.

Witch Hill Scenic Reserve

Run SN2634: L43, L44.

Hoon Hay Park

Run SN2634: J48, J49, J50.

Gibraltar Rock area

Run SN2634: I51, I52, I53, I54.

Mount Evans area

Run SN2634: P8, P9. P10, P11, P13, P15, P16, Q7, Q8, Q9, Q10, Q11, Q13, Q14, Q15, Q16.

APPENDIX 2A: SOUTHERN MOUNT CAVENDISH (see Figure 2.3 for location)

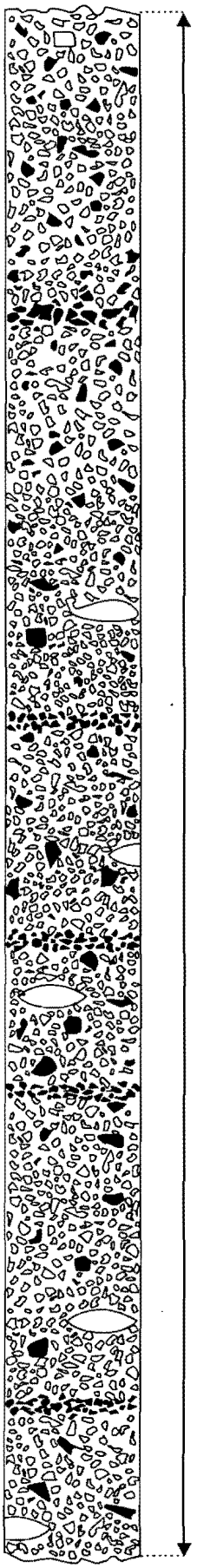

Outer medial facies. Deposits show little variation and are dominated by angular lapilli and ash. Angular, low vesicularity blocks are common, ranging from ~100mm - 300mm. Large bombs are rare with almond uni-polar fusiform, and ribbon shapes, ranging in length from 250mm - 300mm. Distinct coarser bands (~300mm thick) of lapilli (20-50mm) define bedding. One distinct blocky band found near the top of the section consists of clasts ranging from 200-250mm. Blocky clasts increase in frequency near the top of the section.

APPENDIX 2B: NORTHERN MOUNT CAVENDISH (see Figure 2.5 for location)

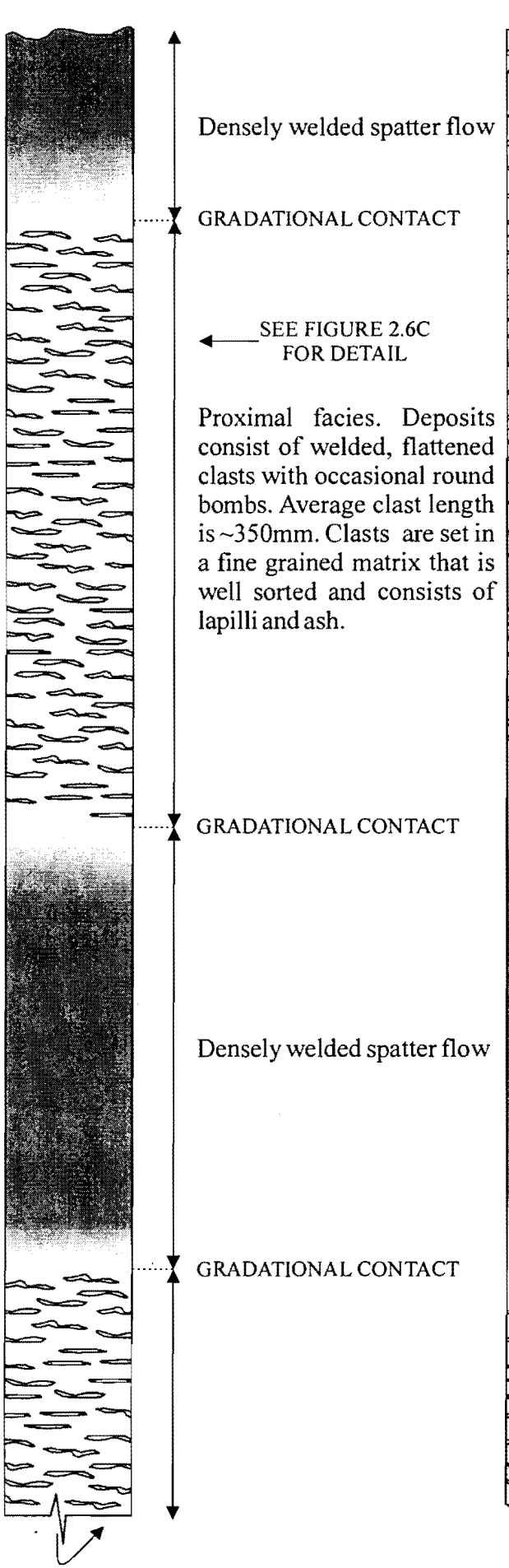

Densely welded spatter flow

GRADATIONAL CONTACT

SEE FIGURE 2.6C FOR DETAIL

Proximal facies. Deposits consist of welded, flattened clasts with occasional round bombs. Average clast length is ~350mm. Clasts are set in a fine grained matrix that is well sorted and consists of lapilli and ash.

GRADATIONAL CONTACT

Densely welded spatter flow

GRADATIONAL CONTACT

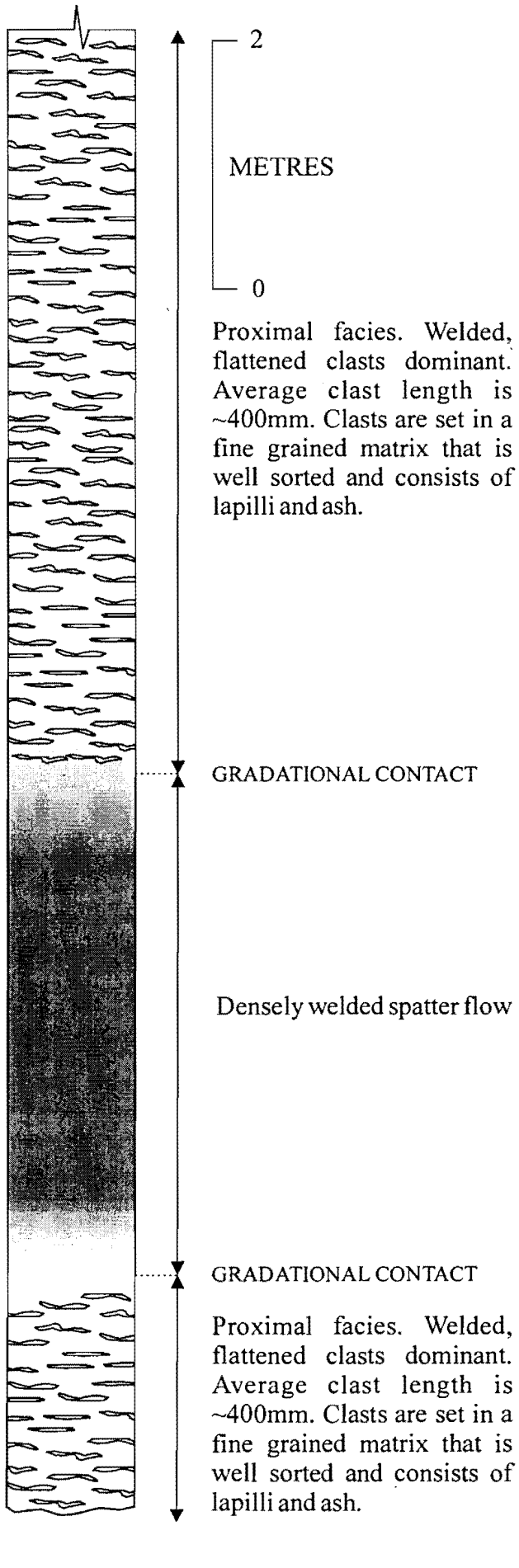

2

METRES

0

Proximal facies. Welded, flattened clasts dominant. Average clast length is ~400mm. Clasts are set in a fine grained matrix that is well sorted and consists of lapilli and ash.

GRADATIONAL CONTACT

Densely welded spatter flow

GRADATIONAL CONTACT

Proximal facies. Welded, flattened clasts dominant. Average clast length is ~400mm. Clasts are set in a fine grained matrix that is well sorted and consists of lapilli and ash.

APPENDIX 2C: CASTLE ROCK (see Figure 2.7 for location)

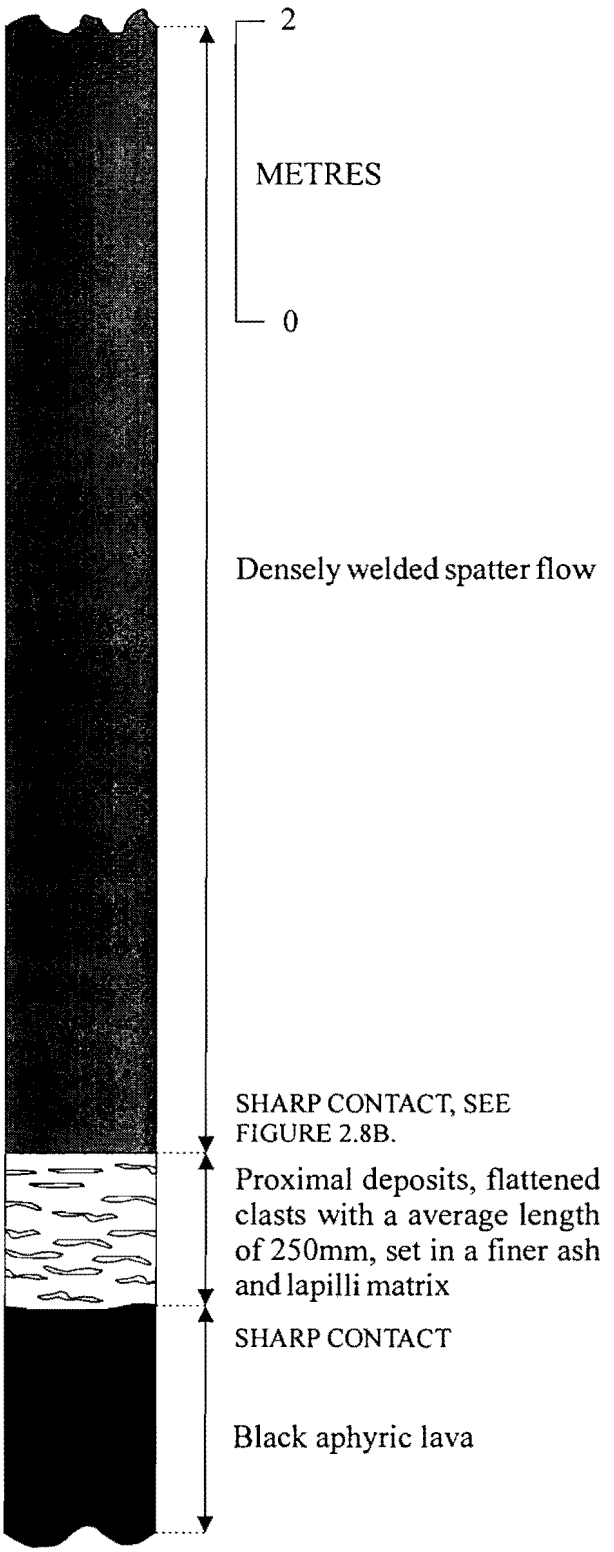

APPENDIX 2D: WITCH HILL SCENIC RESERVE (see Figure 2.9 for location)

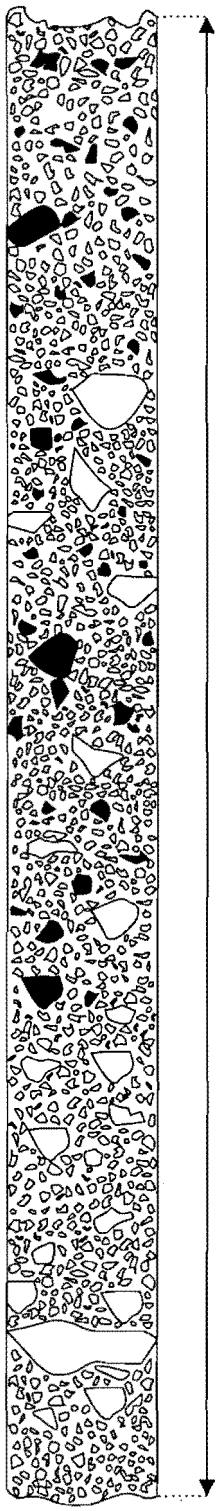

Medial deposits, dominated by blocks and bombs. Average clast size decreases from 200mm to 100mm. Rare large bombs and blocks (300mm) found near the top of the section. All bombs and blocks are set in a fine lapilli and ash matrix.

APPENDIX 2E: HOON HAY PARK (see Figure 2.11 for location)

HOON HAY PARK 1

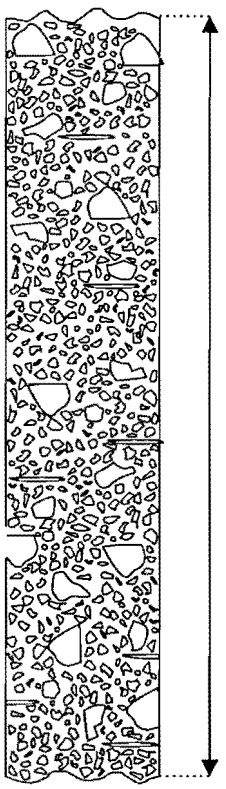

2

METRES

0

Medial deposits, dominated with bombs, that have an average length of ~250mm. Occasional flattened bombs are also found, with all clasts set in a lapilli rich matrix.

SEE FIGURE 2.12B FOR DETAIL

HOON HAY PARK 2

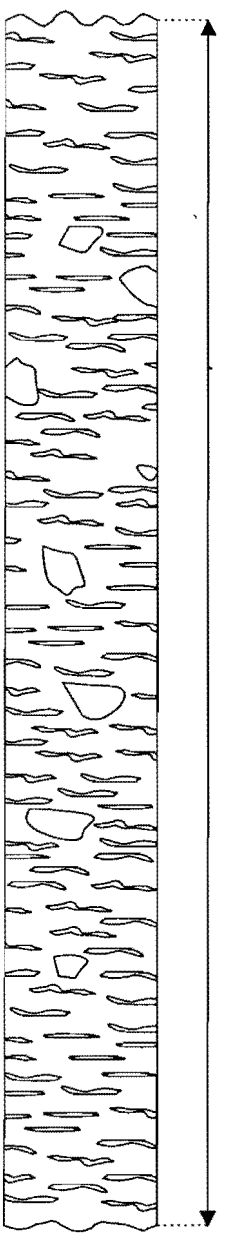

2

METRES

0

Welded proximal deposits, with dominant flattened clasts and occasional round clasts. Average clast length is ~300mm. Clasts are set in a fine grained matrix that is well sorted and consists of lapilli and ash.

APPENDIX 2F: NORTHERN GIBRALTAR ROCK (see Figure 2.13 for location)

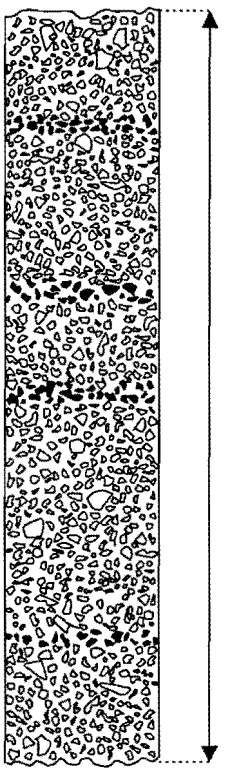

2

METRES

0

Outer medial deposits, consisting of dominantly well sorted, small bombs, blocks and lapilli. Dense layers of lapilli define bedding, and are ~120mm thick, consisting of clasts ranging in size from 40 - 80mm.

SEE FIGURE 2.14A&B FOR DETAIL

APPENDIX 2G: SOUTHERN GIBRALTAR ROCK (see Figure 2.15 for location)

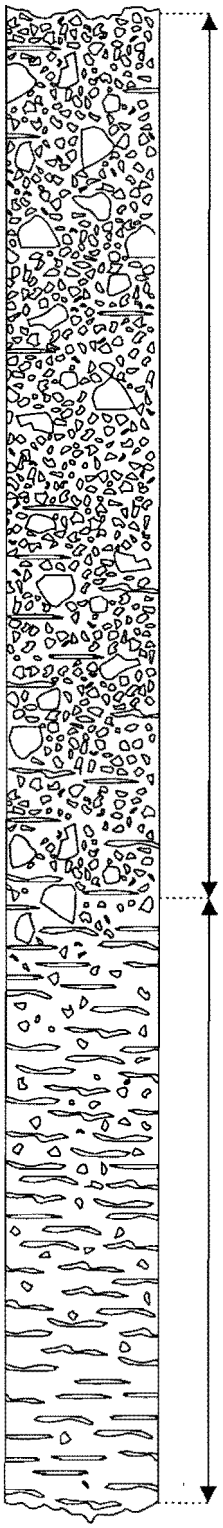

2

METRES

0

Medial deposits, dominated by bombs. Average bomb size increases up the section from 100mm to 300mm. Only rare large bombs (500mm) found near the top of the section. Occasional flattened bombs found in section (~350mm in length).

SEE FIGURE 2.16B FOR DETAIL

GRADATIONAL BOUNDARY

Welded proximal deposits, flattened clasts dominant with occasional round clasts. Average clast length is ~300mm. Clasts are set in a fine grained matrix that is well sorted and consists of lapilli and ash. Round bombs increase up the section, with welding decreasing.

APPENDIX 2H: SOUTHERN MOUNT EVANS (see Figure 2.17 for location)

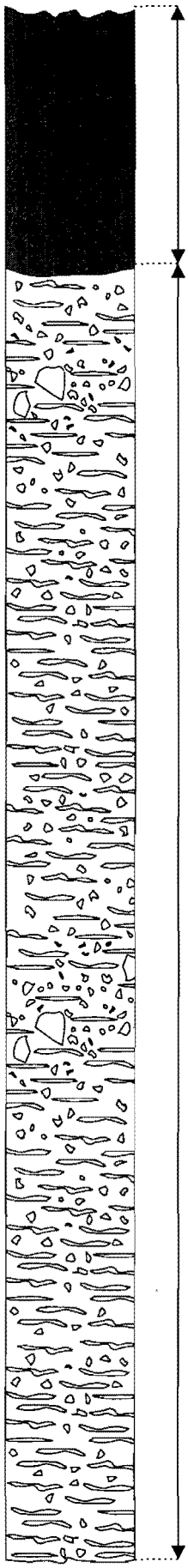

Densely welded spatter flow

SEE FIGURE 2.18C&D FOR DETAIL

SHARP CONTACT

Welded proximal deposits, flattened clasts dominant with well shaped bombs common (eg fusiform, round, and ribbon). Average clast length is ~400mm. Clasts are set in a fine grained matrix that is well sorted and consists of lapilli and ash.

SEE FIGURE 2.18A FOR DETAIL

2

METRES

0

APPENDIX 2I: NORTHERN MOUNT EVANS 1 (see Figure 2.19 for location)

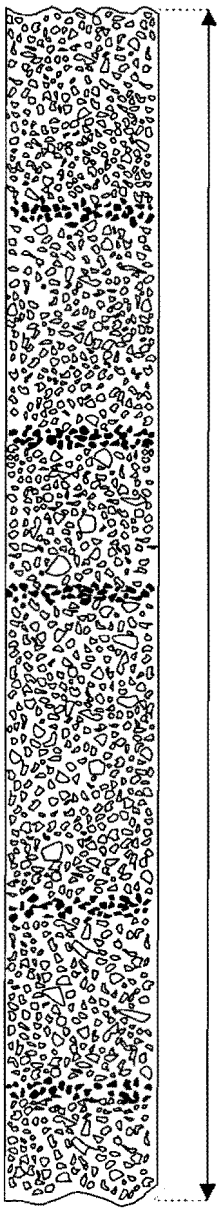

Outer medial deposits, consisting of dominantly well sorted, small bombs, blocks and lapilli. Dense layers of lapilli define bedding, and are ~150mm thick, consisting of clasts ranging in size from 40 - 80mm.

APPENDIX 2J: NORTHERN MOUNT EVANS 2 (see Figure 2.21 for location)

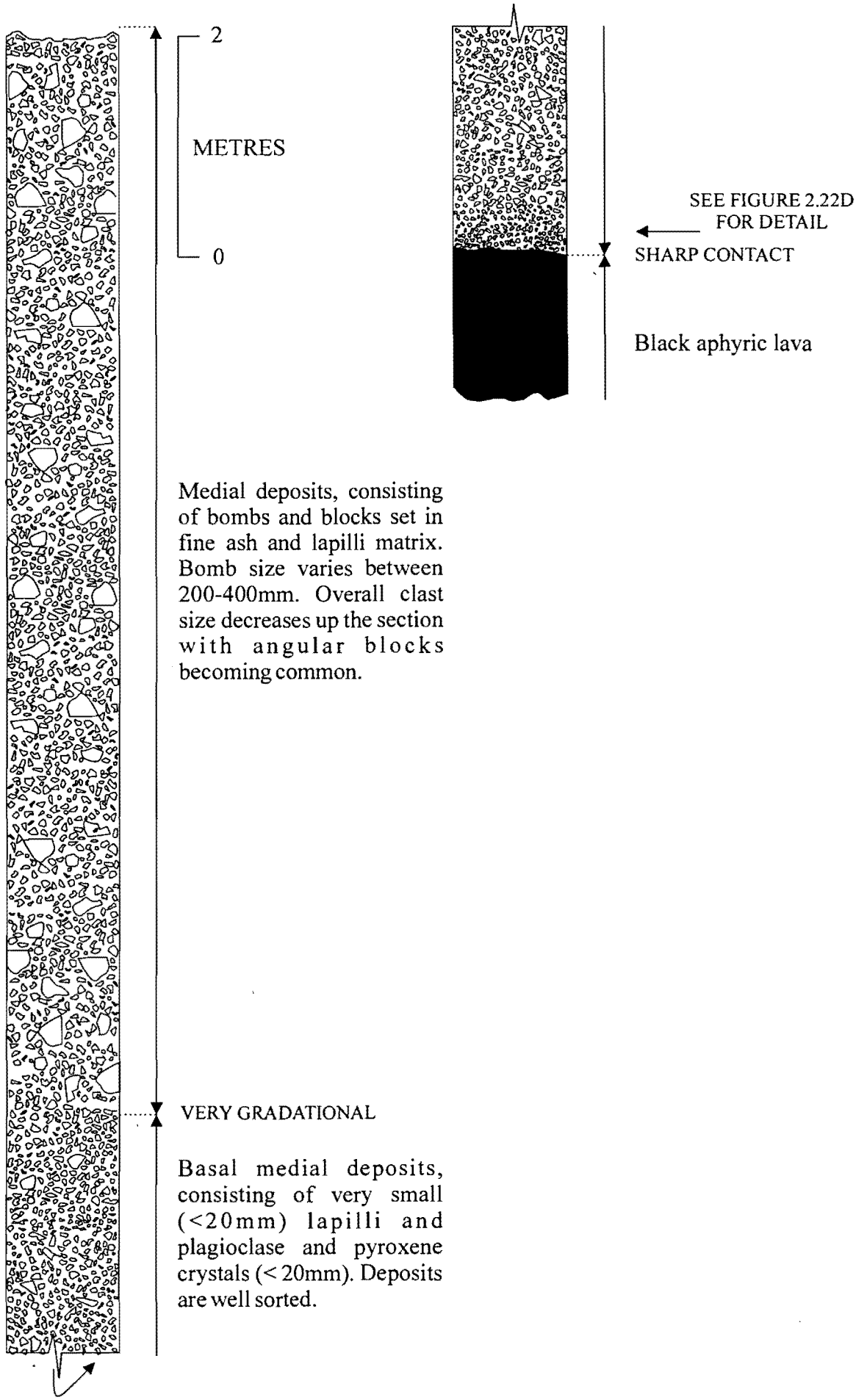

APPENDIX 2K: NORTHERN MOUNT EVANS 3 (see Figure 2.23 for location)

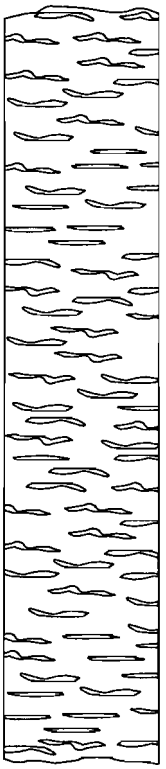

Welded proximal deposits, flattened clasts dominant with occasional round clasts. Average clast length is ~200mm. Clasts are set in a fine grained matrix that is well sorted and consists of lapilli, ash and pyroxene crystals. See Figure 2.21 for location of measured section.

APPENDIX 3A: SAMPLE ANALYSIS LIST

Map Ref.	Location		Sample	Thin Section	Geochem No.
M36 875352	SOUTHERN MOUNT CAVENDISH (see page 176 for location map)				
		1	Bomb	SMC131a	31036
		2	Bomb	SMC131b	
		3	Bomb	SMC331a	31037
		4	Bomb	SMC331b	
		5	Bomb		31038
		6	Bomb		31039
		7	Bomb		31040
		8	Bomb		31041
		9	Bomb		31042
		10	Bomb		31043
		11	Bomb		31051
		12	Bomb	SMC830a	31052
		13	Bomb	SMC830b	
		14	Proximal Deposit	SMC1126	31053
		15	Proximal Deposit	SMC21	31054
		16	Proximal Deposit		31055
		17	Distal Deposit	SMC930	31056
		18	Distal Deposit	SMC9301	
		19	Distal Deposit	SMC9302	
		20	Vent Deposit	SMC212	
		21	Vent Deposit	MC1226	
		22	Lava		31045
		23	Lava		31046
		24	Lava		31047
		25	Lava		31048
		26	Lava		31049
		27	Lava		31050
		28	Dike		31044
		29	Dike		31057
		30	Vent Deposit	MC99	31524
M36 869354	NORTHERN MOUNT CAVENDISH (see page 177 for location map)				
		1	Dike		31505
		2	Dike		31506
		3	Dike		31507
		7	Dike		31508
		8	Dike		31510
		9	Bomb		31511
		10	Spatter Flow	DNS3	31512
		11	Vent Deposit		31513
		12	Bomb	MC12	31514
		13	Dike		31515
		14	Proximal Deposit	MC14	31516
		16	Spatter Flow	MC16	31518

17	Spatter Flow		31519
18	Bomb	MC18	31520
19	Bomb	MC19	31521
20	Bomb		31522
21	Distal Deposit	MC21	
22	Bomb	MC22	31523
23	Spatter Flow	FE1	
24	Spatter Flow	DNS1	

M36 855354 CASTLE ROCK (see page 178 for location map)

1	Bomb	CR1	31525
2	Proximal Deposit	CR2	31526
3	Basal Lava		31527
4	Spatter Flow	CR4	31528
5	Proximal Deposit	CR5	31529
7	Proximal Deposit		31530
8	Proximal Deposit	CR8 a&b	31531

M36 844355 WITCH HILL SCENIC RESERVE (see page 179 for location map)

1	Spatter Flow	WH1	
3	Distal Deposit	WH3a	
4	Bomb	WH4	31532
5	Bomb		31534
6	Bomb	WH6	31533
8	Vent Deposit		31535
9	Dike		31536
11	Bomb	WH11	31537

M36 808315 HOON HAY PARK (see page 180 for location map)

1	Medial Material	HH1a&b	
2	Bomb	HH2	31538
3	Spatter Flow		31539
5	Proximal Deposit	HH5	
6	Dike		31540
8	Bomb		31541
9	Bomb	HH9	
10	Proximal Deposit	HH10	
12	Bomb	HH12	31542
13	Bomb	HH13	31543
14	Dike		31544
15	Bomb		31545
16	Bomb		31546
17	Medial Material	HH17 a&b	

M36 780282 NORTHERN GIBRALTAR ROCK (see page 181 for location map)

1	Medial Material	GR11a	
2	Bomb	GR11b	31552
3	Bomb		31553
4	Bomb	GR13	

5	Vent Deposit		31554
7	Proximal Deposit	GR16	
8	Spatter Flow		31555
11	Bomb	GR20	
12	Proximal Deposit	GR21	31556
13	Vent Deposit	GR22	31557
15	Bomb	GR24	31558
17	Dike		31559
181	Dike		26319
238	Bomb		26321

M36 787267 SOUTHERN GIBRALTAR ROCK (see page 182 for location map)

1	Bomb	GR1	31547
3	Vent Deposit	GR3	31548
4	Dike		31549
6	Dike		31550
8	Bomb	GR8	
10	Vent Deposit		31551

N36 914267 SOUTHERN MOUNT EVANS (see page 183 for location map)

1	Bomb		31560
2	Bomb	ES2	
4	Bomb		31561
5	Bomb	ES5	31562
7	Medial Material	ES7 a&b	
8	Spatter Flow		31563
10	Dike		31564
11	Dike		31565
12	Proximal Deposit	ES12	
13	Dike		31566
14	Dike		31567
15	Spatter Flow	ES15a	31568
43	Dike		27043
32	Dike		27037
18	Spatter Flow		27039

N36 914313 NORTHERN MOUNT EVANS 1 (see page 184 for location map)

1	Medial Material	EN16	
2	Proximal Deposit	EN17	31579
3	Vent Deposit	EN18	31580
4	Proximal Deposit	EN19	31581
5	Bomb	EN20	31582
6	Proximal Deposit	EN21	
7	Spatter Flow		31583
8	Bomb		31584
9	Dike		31585
10	Proximal Deposit	EN25	31586
11	Vent Deposit	EN26	31587
12	Distal Deposit	EN27	

99	Dike		26976

N36 925305 NORTHERN MOUNT EVANS 2 (see page 185 for location map)

1	Dike		31569
2	Bomb	EN2	31570
3	Distal Bomb		31571
4	Distal Deposit	EN4	
5	Bomb	EN5	31572
6	Proximal Deposit	EN6	31572
8	Basal Lava		31574
10	Lava		31575
11	Distal Bomb	EN11	31576
14	Dike		31577
15	Dike		31578

N36 915298 NORTHERN MOUNT EVANS 3 (see page 186 for location map)

1	Bomb	EN29	31588
2	Dike		31589
3	Bomb	EN31	31590
4	Dike		31591
5	Dike		31592
6	Bomb	EN34	
7	Bomb	EN35	31593
8	Vent Deposit		31594
9	Dike		31595

APPENDIX 3B: SAMPLE LOCALITIES

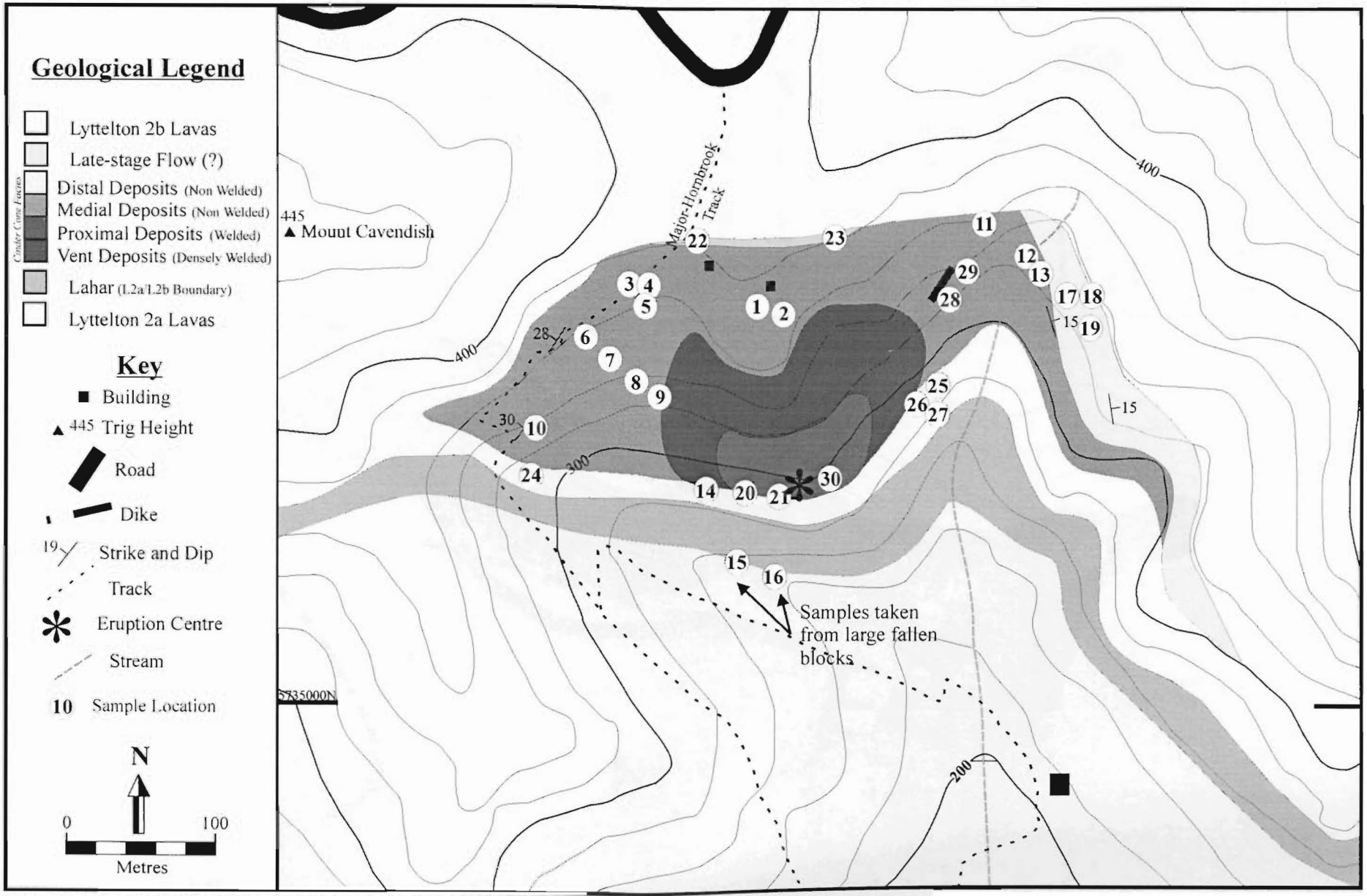

APPENDIX 3B: Sample localities for Southern Mount Cavendish (see Appendix 3A for sample numbers).

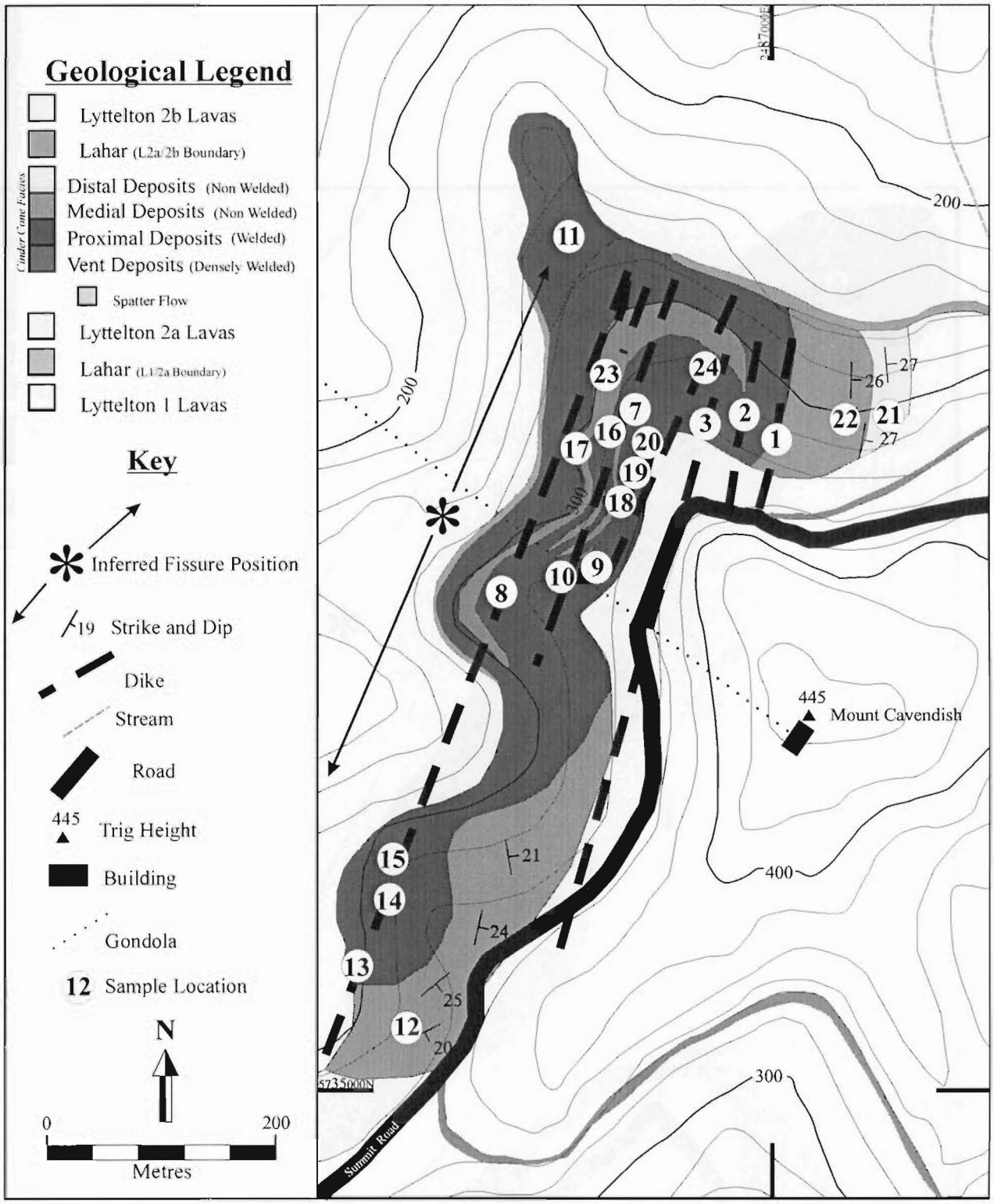

APPENDIX 3B: Sample location for Northern Mount Cavendish (see Appendix 3A for sample numbers).

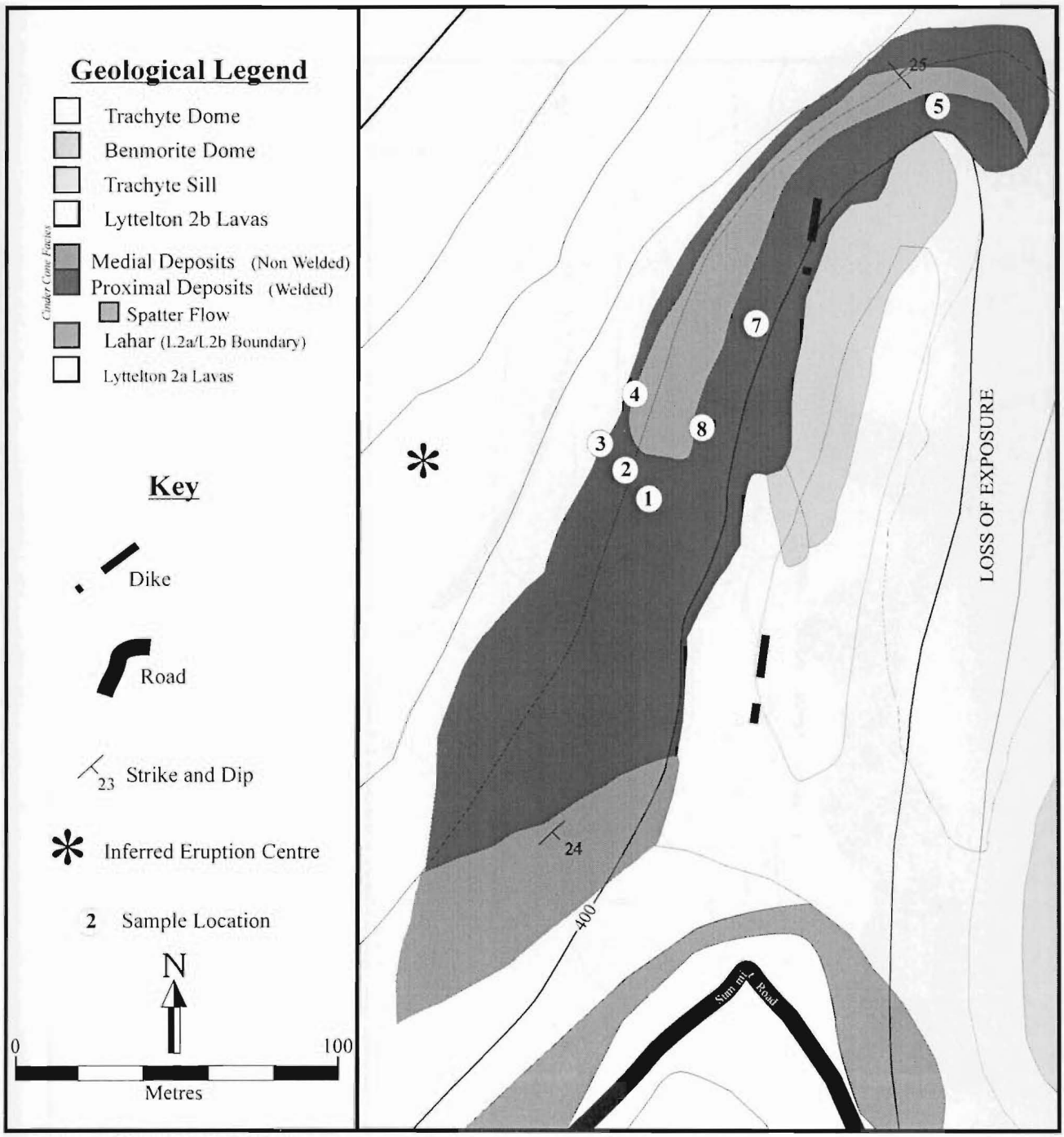

APPENDIX 3B: Sample location for Castle Rock (see Appendix 3A for sample numbers).

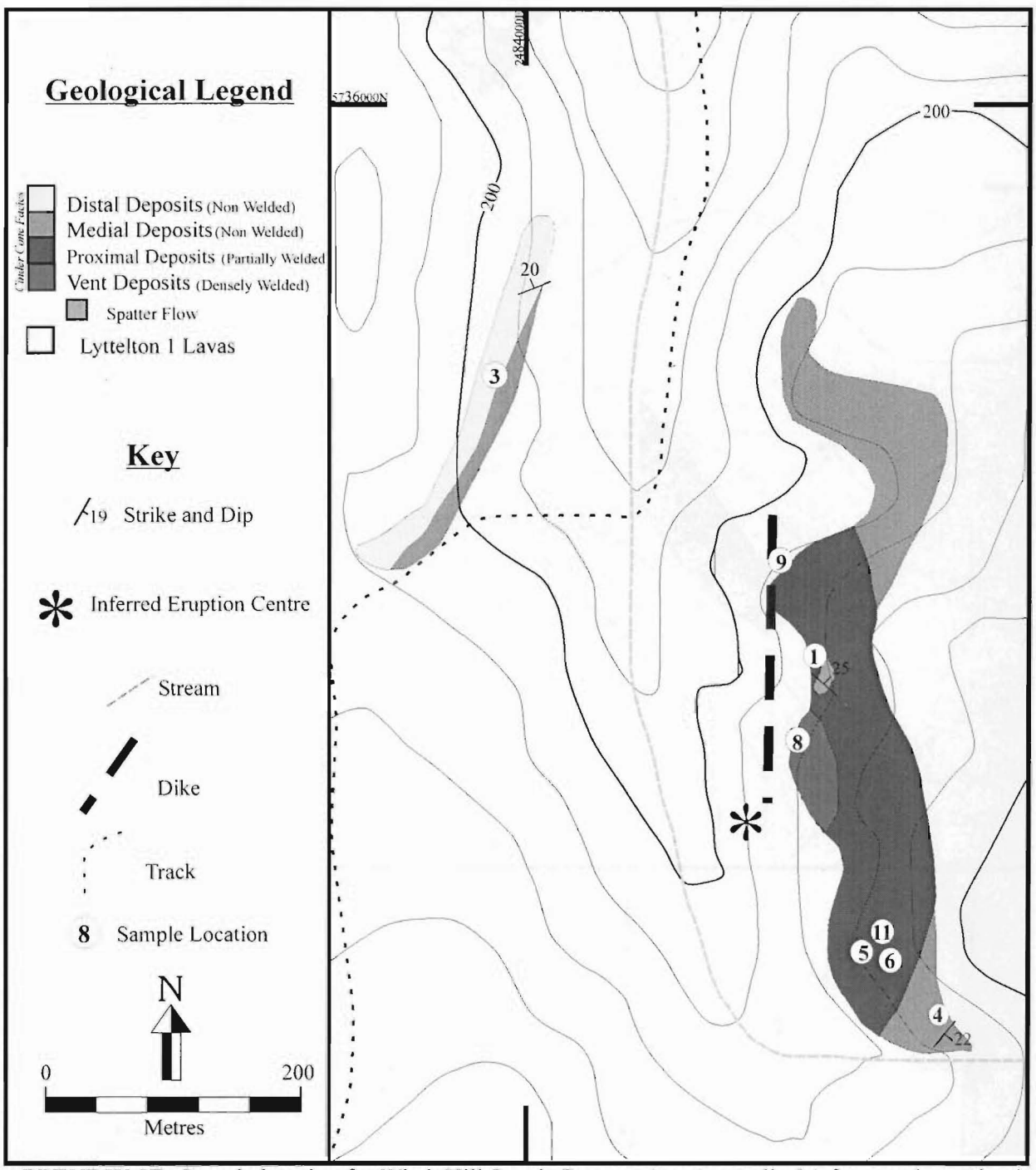

APPENDIX 3B: Sample location for Witch Hill Scenic Reserve (see Appendix 3A for sample numbers).

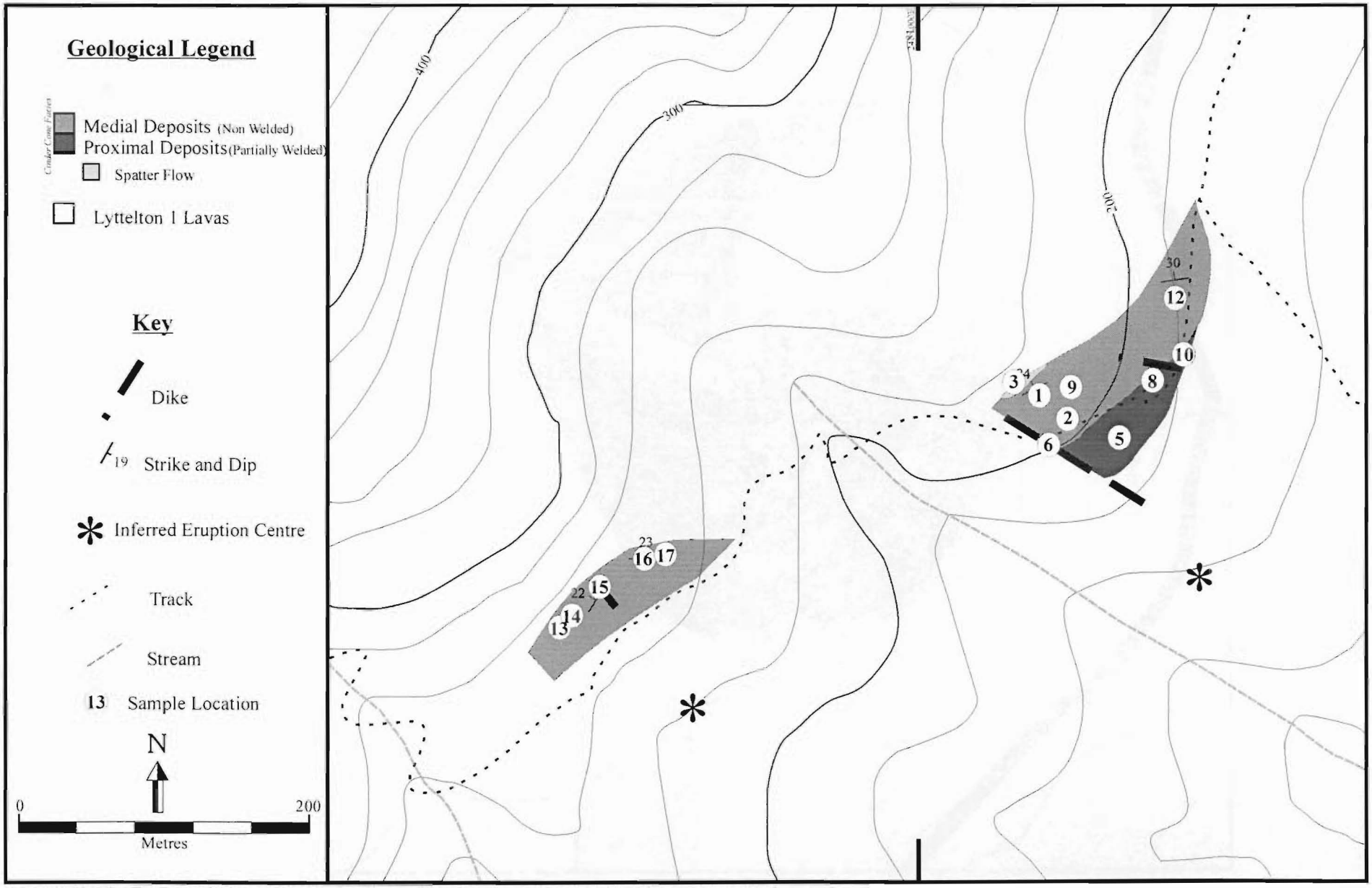

APPENDIX 3B: Sample location for the Hoon Hay Park area (see Appendix 3A for sample numbers).

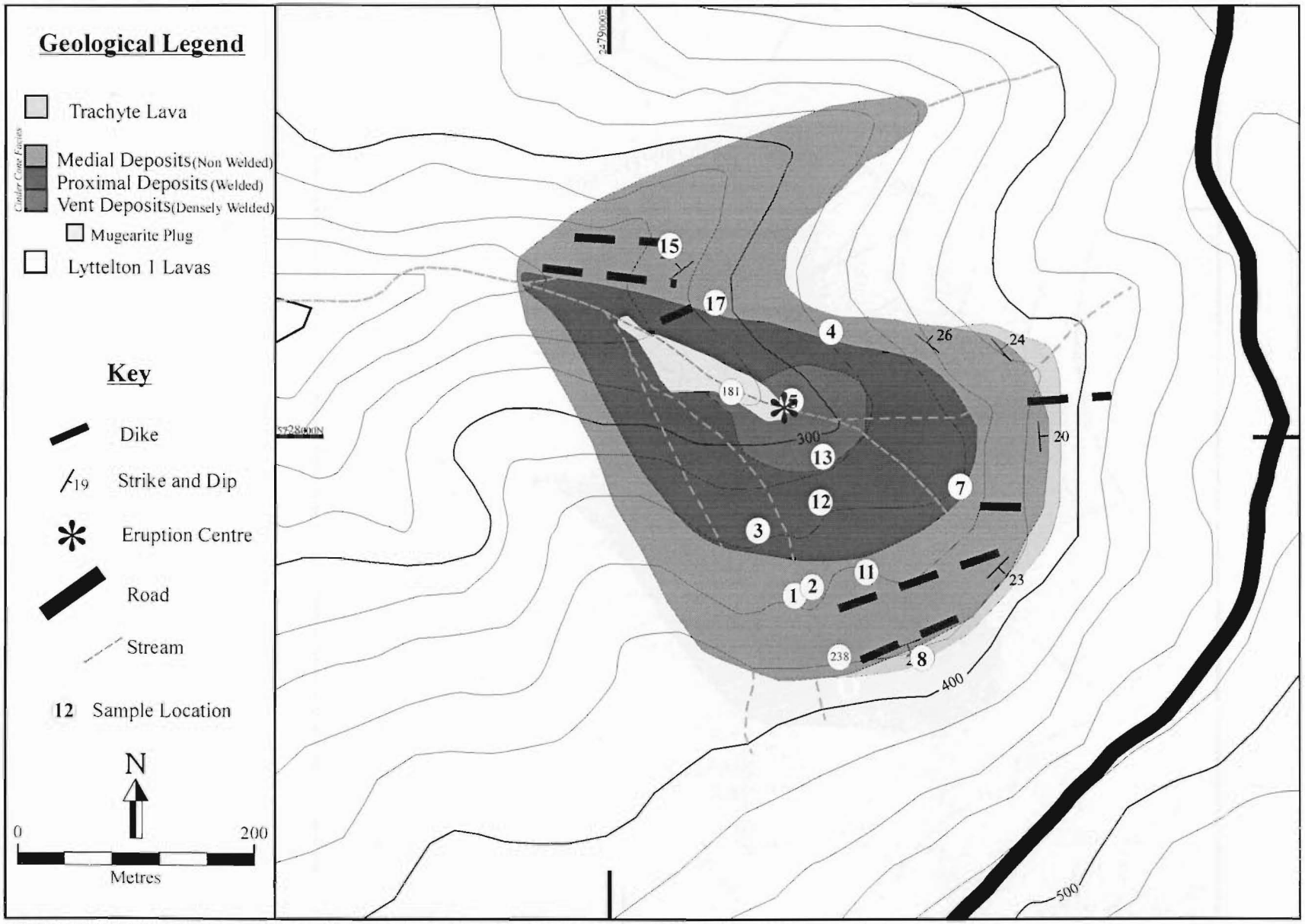

APPENDIX 3B: Sample location for Northern Gibraltar Rock area (see Appendix 3A for sample numbers).

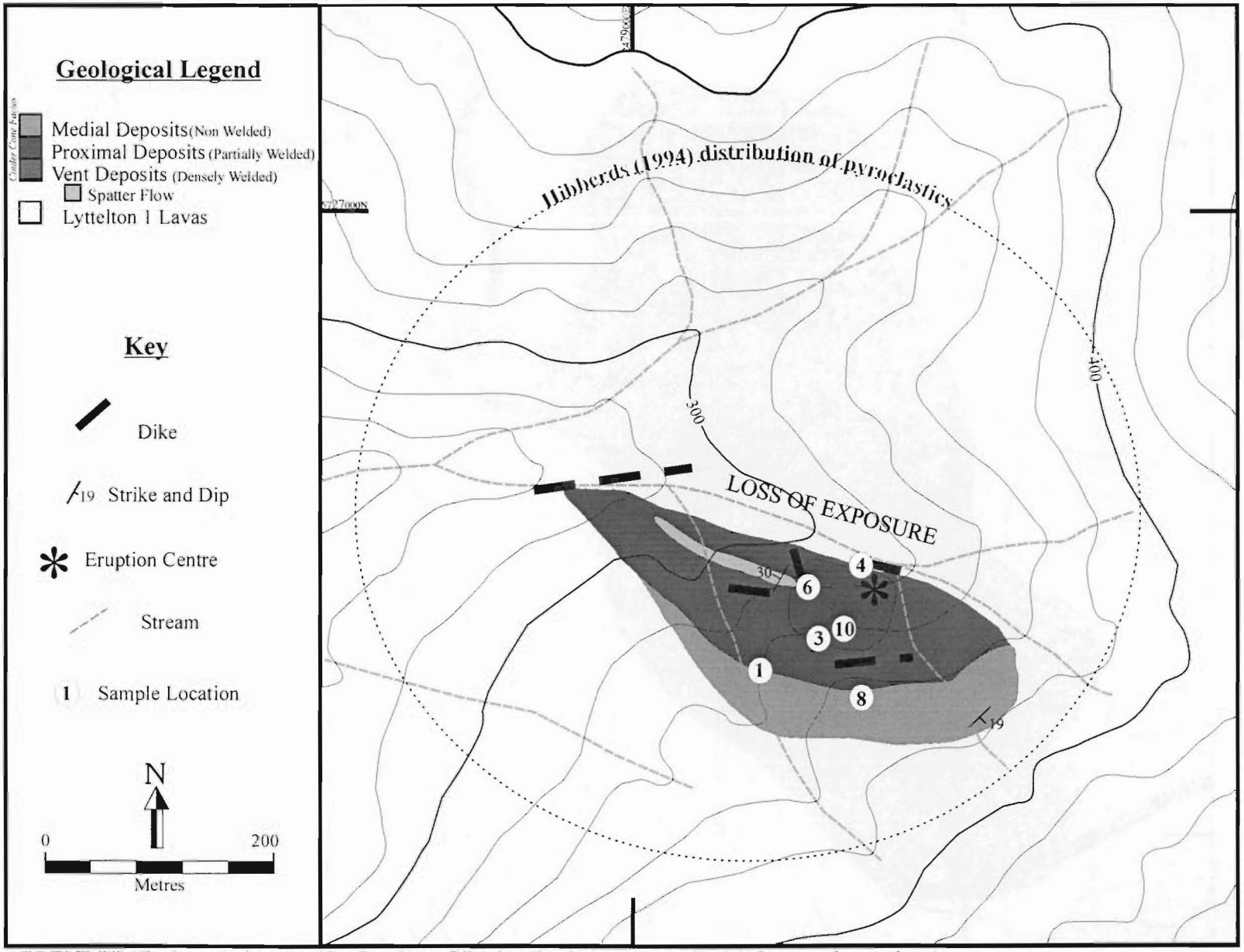

APPENDIX 3B: Sample location for Southern Gibraltar Rock (see Appendix 3A for sample numbers).

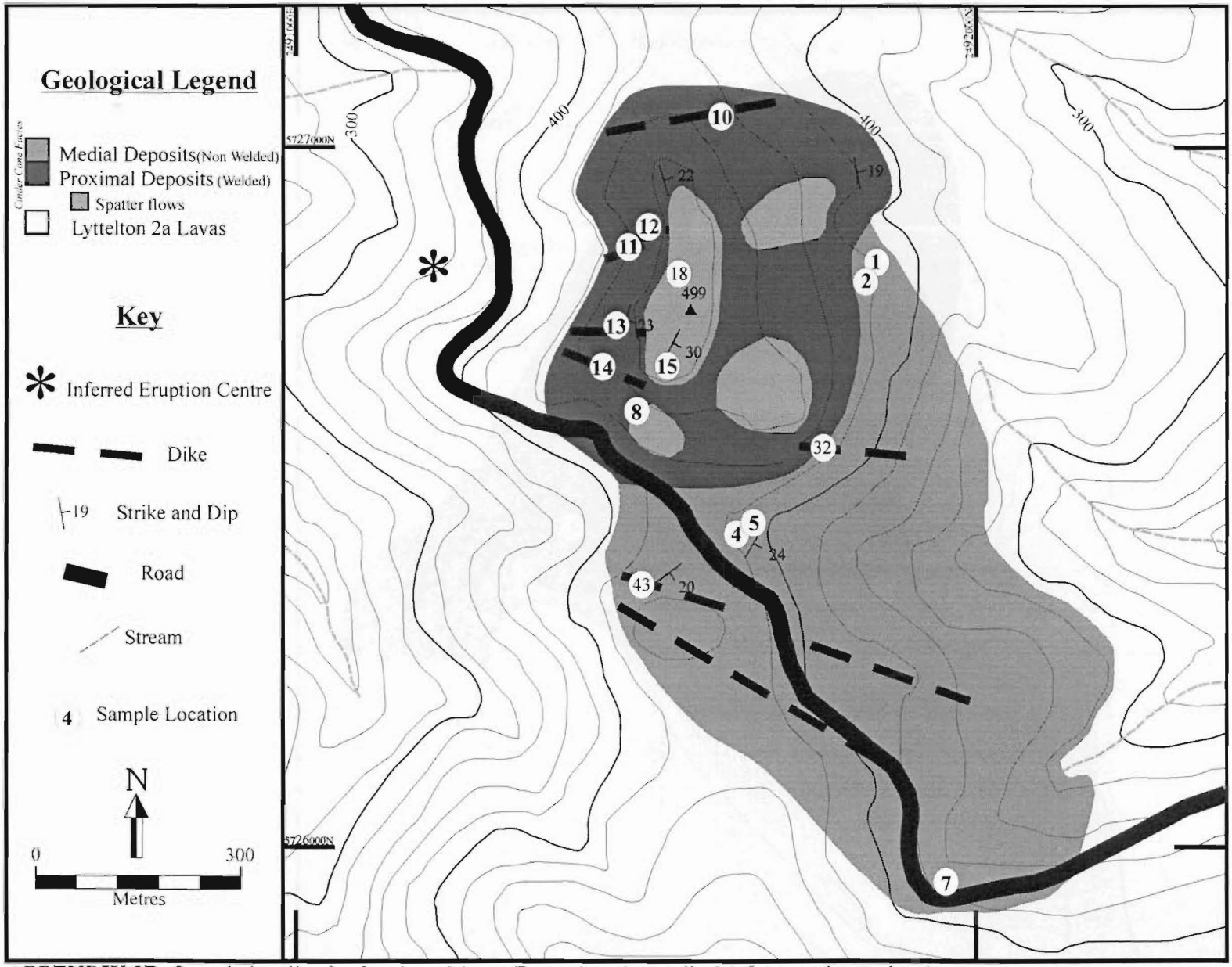

APPENDIX 3B: Sample locality for Southern Mount Evans (see Appendix 3A for sample numbers).

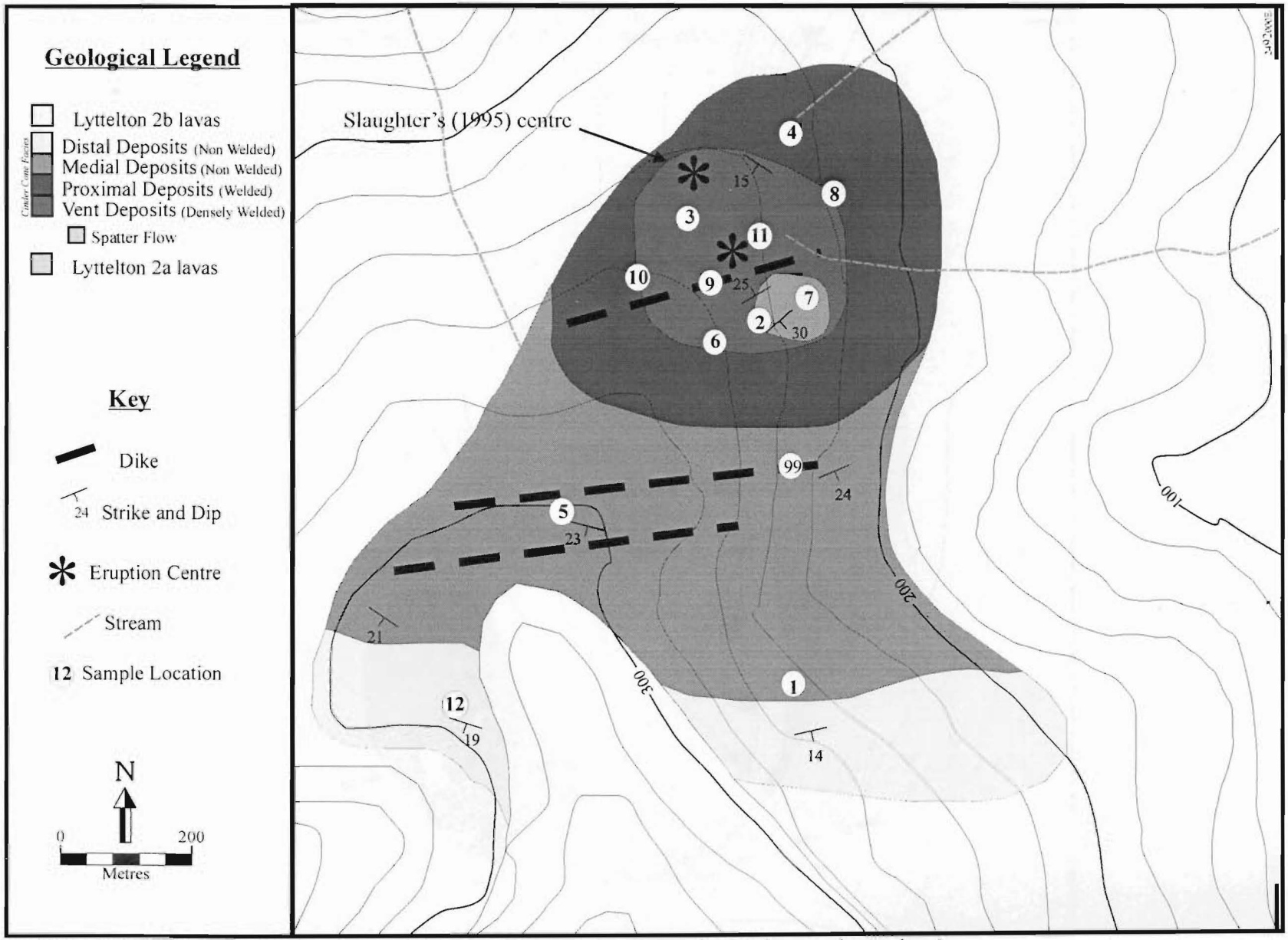

APPENDIX 3B: Sample locations for Northern Mount Evans 1 (see Appendix 3A for sample numbers).

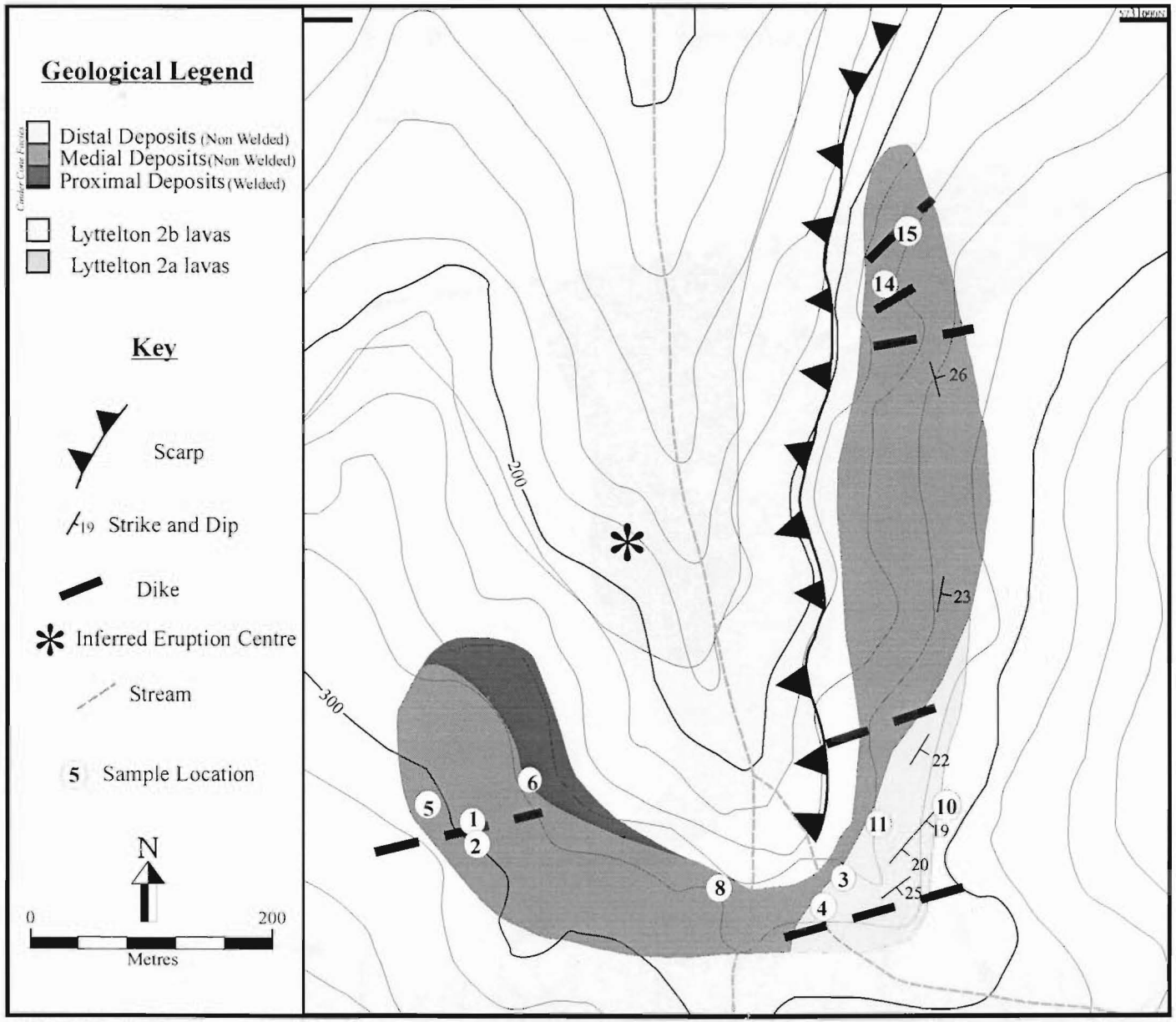

APPENDIX 3B: Sample locality for Northern Mount Evans 2 (see Appendix 3A for sample numbers).

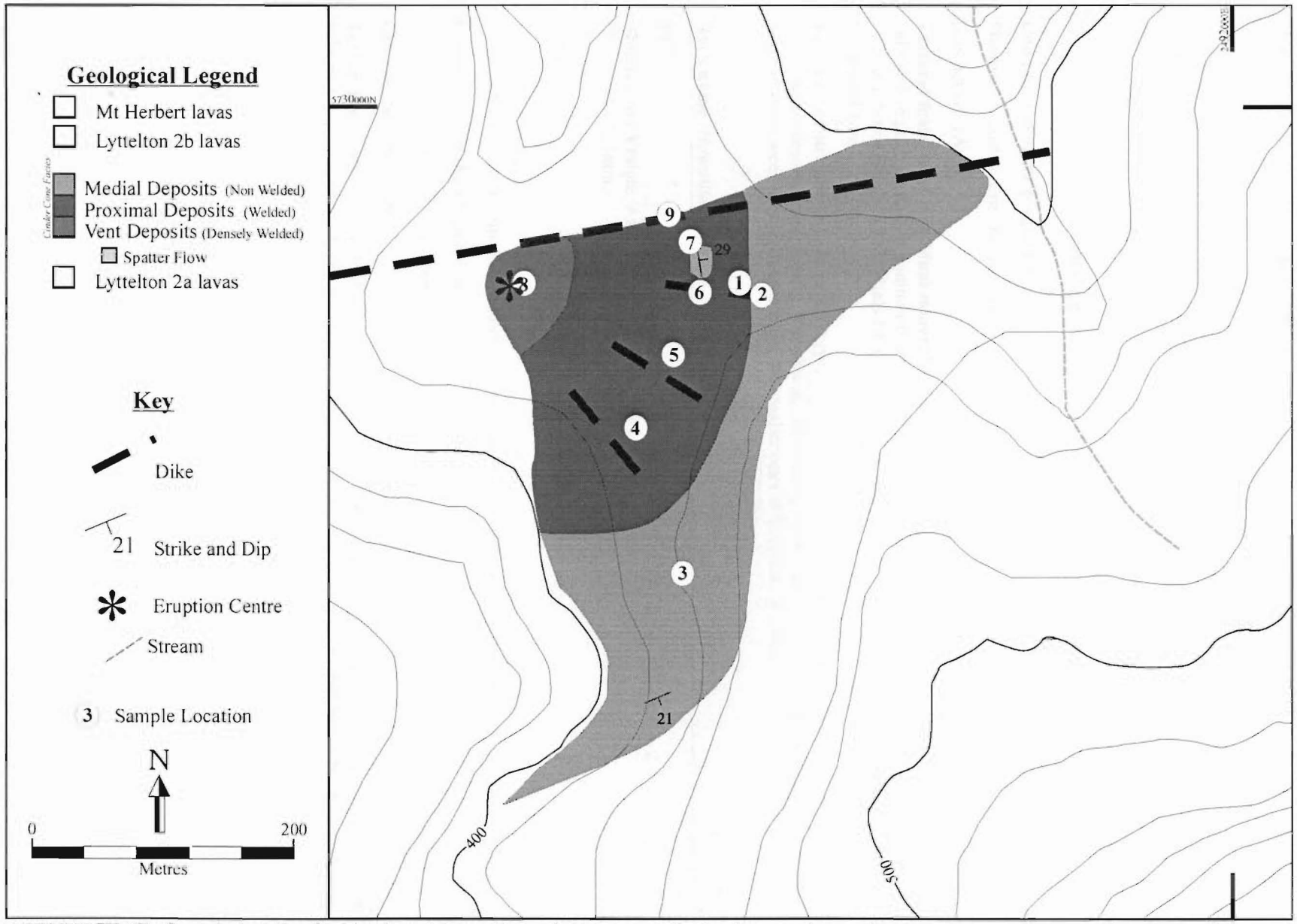

APPENDIX 3B: Sample locality for Northern Mount Evans 3 (see Appendix 3A for sample numbers).

APPENDIX 4A: THINSECTION DESCRIPTIONS

Southern Mount Cavendish

SMC131a

Mineral and Vesicle, Abundance (% of volume), Average size:

Plagioclase: 6, 1mm.

Olivine: --

Clinopyroxene: --

Iron oxide: --

Vesicles: 45, Core 2mm, Rim 1mm.

Groundmass (% of volume): Cryptocrystalline (plagioclase>magnetite>olivine>clinopyroxene)

Composition of the plagioclase:

Phenocryst (An%): Core 80, Rim 70

Groundmass (An%): 45

Textural features of individual minerals: Plagioclase is the only phenocryst present, occurring as euhedral laths and angular crystals. It commonly shows oscillatory zoning, and some crystals are embayed and slightly corroded. Some plagioclase crystals have more sodic overgrowths. Swallow tailed plagioclase is common in the groundmass.

Textural features of the rock: Holocrystalline, porphyritic, pilotaxtic, intergranular, with occasional sub-trachytic patches occurring locally. Vesicles are dominantly spherical in the inner core, moving outwards the larger ones between more irregular while the smaller ones still remain spherical.

Rock name: *Hawaiite Bomb*

SMC131b

Mineral and Vesicle, Abundance (% of volume), Average size:
Plagioclase: 6, 1mm.
Olivine: --
Clinopyroxene: --
Iron oxide: --
Vesicles: 40, 0.5mm.
Groundmass (% of volume): Cryptocrystalline (plagioclase>magnetite>olivine>clinopyroxene)

Composition of the plagioclase:

Phenocryst (An%): Core 80, Rim 70

Groundmass (An%): 49

Textural features of individual minerals: Plagioclase is the only phenocryst present, occurring as euhedral laths and angular crystals. It commonly shows oscillatory zoning, and some crystals are embayed and slightly corroded. Some plagioclase crystals have more sodic overgrowths. Swallow tailed plagioclase is common in the groundmass.

Textural features of the rock: Holocrystalline, porphyritic, pilotaxtic, intergranular, with occasional sub-trachytic patches occurring locally especially nearer the outer rim. Large vesicles are irregular in shape while the smaller ones remain more spherical.

Rock name: *Hawaiite Bomb*

SMC331a

Mineral and Vesicle, Abundance (% of volume), Average size:

Plagioclase: 10, 2mm.

Olivine: --

Clinopyroxene: --

Iron oxide: --

Vesicles: 30, 0.5mm.

Groundmass (% of volume): Cryptocrystalline (plagioclase>magnetite>olivine>clinopyroxene)

Composition of the plagioclase:

Phenocryst (An%): 68

Groundmass (An%): 49

Textural features of individual minerals: Plagioclase forms euhedral laths and angular fragments, it is commonly embayed and corroded and usually has oscillatory zoning. Inclusions of apatite and magnetite are found in some plagioclase crystals. Olivine is seen to have cores of iddingsite overgrown by fresher olivine. Clinopyroxene forms euhedral crystals, of which some have inclusions of iron oxides. Swallow tailed plagioclase is present in groundmass.

Textural features of the rock: Holocrystalline, porphyritic, pilotaxtic, intergranular, with occasional sub-trachytic patches occurring locally. Vesicles are dominantly spherical, with only a few larger ones being irregular. Some vesicles appear to be infilled or lined by a identified clay mineral.

Rock name: *Hawaiite Bomb*

SMC331b

Mineral and Vesicle, Abundance (% of volume), Average size:
Plagioclase: 10, 1.5mm.

Olivine: Trace, 0.8mm.

Clinopyroxene: --

Iron oxide: Trace, 0.6mm.

Vesicles: 30, 0.5mm.

Groundmass (% of volume): Cryptocrystalline (plagioclase>magnetite>olivine>clinopyroxene)

Composition of the plagioclase:

Phenocryst (An%): Core 78, Rim 66

Groundmass (An%): 45

Textural features of individual minerals: Plagioclase forms euhedral laths and angular fragments, it is commonly embayed and corroded and usually has oscillatory zoning. Some of the olivine is seen to have an unaltered core with an iddingsitised middle and a unaltered rim. Tiny clinopyroxene crystals are seen to mantle a sieved magnetite crystal. Clinopyroxene occurs as small subhedral crystals. Swallow tailed plagioclase is present in the groundmass.

Textural features of the rock: Holocrystalline, porphyritic, pilotaxtic, intergranular, with local trachytic patches. Vesicles are dominantly irregular with only the very small ones being more spherical.

Rock name: *Hawaiite Bomb*

SMC830a

Mineral and Vesicle, Abundance (% of volume), Average size:

Plagioclase: 5, 1mm.

Olivine: --

Clinopyroxene: 2, 1mm.

Iron Oxide: --

Vesicles: 45 (*IT = 40%*), 1mm.

Groundmass (% of volume): Cryptocrystalline (plagioclase>magnetite>olivine>clinopyroxene)

Composition of the plagioclase:

Phenocryst (An%): 70

Groundmass (An%): 50

Textural features of individual minerals: Plagioclase is corroded and embayed and displays no zoning. Clinopyroxene and magnetite are also embayed and corroded.

Textural features of the rock: Holocrystalline, porphyritic, pilotaxtic, intergranular. Rare small glass blebs can be found in some vesicles. Vesicles are irregular in shape except for some of the smaller ones. Small mafic areas that are less crystalline also may represent magma mingling.

Rock name: *Hawaiite Bomb*

SMC830b

Mineral and Vesicle, Abundance (% of volume), Average size:
Plagioclase: 1, 1mm.

Olivine: 1, 2mm.

Clinopyroxene: --

Iron oxide: 2, 2mm.

Vesicles: 35 (*IT = 40%*), 1mm.

Groundmass (% of volume): Cryptocrystalline (plagioclase>magnetite>olivine>clinopyroxene)

Composition of the plagioclase:

Phenocryst (An%): 68

Groundmass (An%): 40

Textural features of individual minerals: Plagioclase is corroded and embayed. Olivine is heavily altered to iddingsite and in places is also replaced by iron oxides (probably magnetite and/or hematite) making a thin reaction rim. Clinopyroxenes are embayed and corroded and some have iron oxide inclusions and some are also twinned. Iron oxides are embayed, possibly by vesicle action.

Textural features of the rock: Holocrystalline, porphyritic, pilotaxtic, intergranular. Some of the vesicles are stretched out but most are round.

Rock name: *Hawaiite Bomb*

SMC1126

Mineral and Vesicle, Abundance (% of volume), Average size:

Plagioclase: 5, 3mm.

Olivine: Trace, 2mm.

Clinopyroxene: Trace, 2.5mm.

Iron oxide: Trace, 1mm.

Vesicles: 60 (*IT = 65%*), 2mm.

Groundmass (% of volume): Cryptocrystalline (too fine to be accurate, plagioclase>magnetite>olivine)

Composition of the plagioclase:

Phenocryst (An%): 60

Groundmass (An%): 45

Textural features of individual minerals: Plagioclase is corroded and embayed, with cracking extensive in places. Plagioclase crystals are not zoned. Olivines have a iddingsite reaction rim, with smaller crystals completely pseudomorphed. One clinopyroxene is zoned, with a iron rich core, and paler rim. Iron oxides are euhedral.

Textural features of the rock: Holocrystalline, porphyritic, pilotaxtic, intergranular. Vesicles are dominantly round, with only very large ones being deformed.

Rock name: *Hawaiite Bomb (Proximal)*

SMC21

Mineral and Vesicle, Abundance (% of volume), Average size:
Plagioclase: 10, 2mm.

Olivine: 3, 1.5mm.

Clinopyroxene: Trace, 1.5mm.

Iron oxide: --

Vesicles: 30, 0.7mm.

Groundmass (% of volume): Plagioclase 34, Magnetite 15, Olivine 7, Apatite 1.

Composition of the plagioclase:

Phenocryst (An%): 70

Groundmass (An%): 50

Textural features of individual minerals: Plagioclase has oscillatory zoning and is embayed in places by vesicles. Apatite inclusions are also found in plagioclase crystals, which in places are also sieved. Olivine is completely iddingsitised with only pseudomorphs remaining. Clinopyroxenes have corroded edges, are embayed and some also have iron oxide inclusions. Glass is found to completely fill some small vesicles.

Textural features of the rock: Holocrystalline, intergranular, porphyritic, pilotaxtic with trachytic patches occurring locally. Glass is also found in small patches in some of the larger vesicles. Vesicles are dominantly irregular. Some areas of the slide have the appearance of magma mingling between more mafic and felsic magmas.

Rock name: *Proximal Deposits (Hawaiite)*

SMC9300

Mineral and Vesicle, Abundance (% of volume), Average size:

Plagioclase: 2, 1mm.

Olivine: 1, 1mm.

Clinopyroxene: 1, 1mm.

Iron oxide: 1, 1.5mm.

Vesicles: 40, 0.5mm.

Groundmass (% of volume): Plagioclase 24, Magnetite 10, Glass 20 (devitrified).

Composition of the plagioclase:

Phenocryst (An%): 65

Groundmass (An%): 30

Textural features of individual minerals: Plagioclase is corroded with no crystals displaying any zoning. Olivine (Fo85) is corroded with iddingsite rims. The smaller olivine crystals are completely iddingsitised with only pseudomorphs remaining. Clinopyroxenes are embayed and corroded. Iron oxides are embayed.

Textural features of the rock: Probably initially holocrystalline (holohyaline) but altered and iron stained. Large dark areas are tachylite lapilli, distinctively unaltered and filled with tiny crystals of plagioclase. Vesicles are spherical in shape and are commonly filled with chabazite. In some areas vesicles are broken and shards only remain.

Rock name: *Distal Lapilli Tuff.*

SMC9301

Mineral and Vesicle, Abundance (% of volume), Average size:

Plagioclase: 5, 1.5mm.

Olivine: 2, 1mm.

Clinopyroxene: 2, 1mm.

Iron oxide: 1, 1mm.

Vesicles: 40, 0.3mm.

Groundmass (% of volume): Plagioclase 30, Magnetite 10, Glass 20 (devitrified).

Composition of the plagioclase:

Phenocryst (An%): 70

Groundmass (An%): 40

Textural features of individual minerals: Plagioclase is embayed with oscillatory zoning. Olivine is corroded with iddingsite alteration rims. Clinopyroxene is twinned in places and corroded and embayed. Iron oxides are only corroded.

Textural features of the rock: Probably initially holocrystalline (holohyaline) but altered and iron stained. Large dark areas are tachylite lapilli, distinctively unaltered and filled with tiny crystals of plagioclase. Vesicles are spherical in shape and are commonly filled with chabazite. In some areas vesicles are broken and shards only remain. Natrolite found in some vesicles.

Rock name: *Distal Lapilli Tuff.*

SMC9302

Mineral and Vesicle, Abundance (% of volume), Average size:

Plagioclase: 4, 1.5mm.

Olivine: 2, 1mm.

Clinopyroxene: 1, 1mm.

Iron oxide: 2, 1mm.

Vesicles: 40, 0.3mm.

Groundmass (% of volume): Plagioclase 25, Magnetite 10, Glass 16 (devitrified).

Composition of the plagioclase:

Phenocryst (An%): 65

Groundmass (An%): 40

Textural features of individual minerals: Plagioclase has a interesting sieve texture in one phenocryst, with all other crystals embayed and displaying oscillatory zoning. Olivine is corroded, embayed and has alteration rims of iddingsite. Good example of a iron rich (green) augite. Iron oxides are only corroded.

Textural features of the rock: Probably initially holocrystalline (holohyaline) but altered and iron stained. Large dark areas are tachylite lapilli, distinctively unaltered and filled with tiny crystals of plagioclase. Vesicles are spherical in shape and are commonly filled with chabazite. In some areas vesicles are broken and shards only remain. Natrolite found in some vesicles.

***Rock name:** Distal Lapilli Tuff.*

SMC212

Mineral and Vesicle, Abundance (% of volume), Average size:

Plagioclase: 8, 2mm.

Olivine: 4, 1mm.

Clinopyroxene: 5, 1mm.

Iron oxide: 2, 1mm.

Vesicles: 20, 0.5mm.

Groundmass (% of volume): Plagioclase 32, Magnetite 22, Olivine 7, Clinopyroxene 5, Apatite 2.

Composition of the plagioclase:

Phenocryst (An%): Core 80, Rim 60

Groundmass (An%): 40

Textural features of individual minerals: Plagioclase is embayed and corroded and commonly shows oscillatory zoning. Some plagioclase phenocrysts also show sieve textures. Olivine is embayed and corroded with iddingsite alteration rims, smaller crystals are completely pseudomorphed and more euhedral. Clinopyroxene is embayed and corroded and one crystal is a distinct pale green (iron rich). Iron oxides form euhedral crystals that are probably magnetite.

Textural features of the rock: Holocrystalline, porphyritic, pilotaxtic, intergranular, with local trachytic patches. All vesicles are irregular in shape. Possibly more evidence of magma mingling between felsic and mafic magmas, felsic magma is more vesicular. Natrolite is also found lining some vesicles; it is stained an orange colour.

Rock name: *Vent Deposit (Hawaiite)*

SMC1226

Mineral and Vesicle, Abundance (% of volume), Average size:

Plagioclase: 8, 1.5mm.

Olivine: 4, 1mm.

Clinopyroxene: 4, 1mm

Iron oxide: 2, 1mm.

Vesicles: 20, 0.5mm.

Groundmass (% of volume): Plagioclase 30, Magnetite 20, Olivine 5, Clinopyroxene 5, Apatite 2.

Composition of the plagioclase:

Phenocryst (An%): 70

Groundmass (An%): 48

Textural features of individual minerals: Plagioclase is corroded and has oscillatory zoning. Olivine is strongly altered with reaction rims of mostly iddingsite and some bowlingite. Smaller olivine crystals are complete pseudomorphs. Clinopyroxene is corroded and embayed with some crystal displaying a fine sieving around their edges. Iron oxides are only corroded but one crystal displays a skeletal texture.

Textural features of the rock: Holocrystalline, porphyritic, pilotaxtic, intergranular, with local trachytic patches. All vesicles are irregular in shape.

Rock name: *Vent Deposit (Hawaiite)*

MC99

Mineral and Vesicle, Abundance (% of volume), Average size:

Plagioclase: 10, 1.5mm.

Olivine: 1, 1mm.

Clinopyroxene: 2, 0.8mm.

Iron oxide: 1, 0.7mm.

Vesicles: 20, 0.4mm.

Groundmass (% of volume): Plagioclase 32, Magnetite 22, Olivine 5, Clinopyroxene 4, Apatite 3.

Composition of the plagioclase:

Phenocryst (An%): 70

Groundmass (An%): 50

Textural features of individual minerals: Plagioclase has oscillatory zoning and overgrows some smaller phenocrysts. Some of plagioclase crystals are corroded while others are euhedral. Olivine is strongly altered to iddingsite with mostly only pseudomorphs present. Clinopyroxene is twinned and corroded while the iron oxides are only corroded.

Textural features of the rock: Holocrystalline, porphyritic, pilotaxtic, intergranular, with local trachytic patches. All vesicles are irregular in shape.

Rock name: *Vent Deposit (Hawaiite)*

Northern Mount Cavendish

MC12

Mineral and Vesicle, Abundance (% of volume), Average size:

Plagioclase: 7, 1mm.

Olivine: 1, 0.5mm.

Clinopyroxene: 4, 0.8mm.

Iron oxide: Trace, 0.6mm.

Vesicles: 35, 0.8mm.

Groundmass (% of volume): Cryptocrystalline (plag/alkali feldspar>magnetite>clinopyroxene>apatite).

Composition of the plagioclase:

Phenocryst (An%): 70

Groundmass (An%): 45

Textural features of individual minerals: Plagioclase is euhedral and also forms angular fragments, some crystals display oscillatory zoning. Swallow tailed plagioclase is common in the groundmass. Sieve textures are also present in some crystals of plagioclase. Olivine is completely replaced by iddingsite. Clinopyroxene is corroded and embayed with iron oxide inclusions. Some clinopyroxene crystals have a greenish colour indicating that they are more iron rich and some also display simple twinning. Iron oxides are mostly found as inclusions, with the crystals found outside in the groundmass being mostly corroded.

Textural features of the rock: Holocrystalline, porphyritic, pilotaxtic, intergranular. Glass is found to be infilling some vesicles along with chabazite. There is also another unidentified mineraloid filling some vesicles it is most probably a smectite clay of some sort.

Rock name: *Mugearite Bomb*

MC14

Mineral and Vesicle, Abundance (% of volume), Average size:

Plagioclase: 8, 1.5mm.

Olivine: 4, 0.6mm.

Clinopyroxene: 3, 0.7mm.

Iron oxide: 1, 1mm.

Vesicles: 40, 0.7mm.

Groundmass (% of volume): Cryptocrystalline (plagioclase/alkali feldspar>magnetite>clinopyroxene).

Composition of the plagioclase:

Phenocryst (An%): 65

Groundmass (An%): 32

Textural features of individual minerals: Plagioclase crystals are embayed, corroded and sieved, with swallow tailed examples common in the groundmass. Normal zoning in plagioclase is common. Olivine displays iron oxide alteration, and is completely pseudomorphed by hematite and/or magnetite. Clinopyroxenes are embayed, and corroded with iron oxide inclusions. Iron oxides are typically corroded.

Textural features of the rock: Holocrystalline, porphyritic, pilotaxtic, intergranular. Vesicles are dominantly spherical with larger ones showing more deformation. Vesicles can be seen to be filled in with glass in places.

Rock name: *Proximal Deposit (Mugearite)*

MC15

Mineral and Vesicle, Abundance (% of volume), Average size:

Plagioclase: 10, 2mm.

Olivine: Trace, 0.5mm.

Clinopyroxene: 8, 1mm.

Iron oxide: 2, 1mm.

Vesicles: 30, 0.5mm.

Groundmass (% of volume): Cryptocrystalline (plag/alkali feldspar>magnetite>clinopyroxene>apatite).

Composition of the plagioclase:

Phenocryst (An%): 65

Groundmass (An%): 32

Textural features of individual minerals: Plagioclase is extensively embayed and corroded with oscillatory zoning shown by some phenocrysts. Some plagioclase crystals though are quite euhedral, with swallow tailed examples common in the groundmass. Larger crystals of olivine have been completely replaced by iron oxides, probably hematite and/or magnetite. Some crystals are also replaced by bowlingite. Clinopyroxenes are altered in places in fibrous mineral, and are embayed and corroded. Iron oxides are embayed and corroded. A orthopyroxene crystal is also found in is subhedral in shape. Apatite phenocrysts rare, commoner in groundmass.

Textural features of the rock: Holocrystalline, porphyritic, pilotaxtic, intergranular. Vesicles are irregular in shape. Possible evidence of mixing of more felsic and mafic magmas. Chabazite in vesicles is common.

Rock name: *Proximal deposit (Mugearite)*

MC16

Mineral and Vesicle, Abundance (% of volume), Average size:

Plagioclase: 1, 0.7mm.

Olivine: --

Clinopyroxene: 5, 0.8mm.

Iron oxide: 1, 0.5mm.

Vesicles: 35, 0.3mm.

Groundmass (% of volume): Cryptocrystalline (plag/alkali feldspar>magnetite>clinopyroxene>apatite)

Composition of the plagioclase:

Phenocryst (An%): 70

Groundmass (An%): 50

Textural features of individual minerals: Plagioclase crystals are sieved with embayments, and corroded edges common. Some crystals display oscillatory zoning while others are unzoned. Swallow tails in groundmass. Clinopyroxenes display thin red to black reaction rims. Iron oxides are embayed and corroded.

Textural features of the rock: Holocrystalline, porphyritic, pilotaxtic, intergranular, with subtrachytic to trachytic patches. Vesicles are dominantly irregular in shape and are also seen in some areas to be lined with smectite clays.

Rock name: *Spatter Flow (Mugearite)*

MC18

Mineral and Vesicle, Abundance (% of volume), Average size:

Plagioclase: 10, 1.5mm.

Olivine: Trace, 0.9mm.

Clinopyroxene: 5, 1mm.

Iron oxide: 1, 0.5mm.

Vesicles: 40, 0.8mm.

Groundmass (% of volume): Cryptocrystalline (plag/alkali feldspar>magnetite>clinopyroxene>apatite)

Composition of the plagioclase:

Phenocryst (An%): 65

Groundmass (An%): 40

Textural features of individual minerals: Plagioclase is unzoned, and is corroded and embayed. Swallow tailed plagioclase is common in the groundmass. Olivine is altered to hematite and/or magnetite. Clinopyroxene are embayed and corroded. One clinopyroxene crystal has a thick red reaction rim, while others display a thinner rim. A few of the clinopyroxene crystals are zoned, ie darker rims. Iron oxides are corroded and some are skeletal.

Textural features of the rock: Holocrystalline, porphyritic, pilotaxtic, intergranular. Vesicles are mostly spherical but some of the larger ones are irregular in shape.

Rock name: *Mugearite Bomb*

MC19

Mineral and Vesicle, Abundance (% of volume), Average size:

Plagioclase: 15, 1.5mm.

Olivine: --

Clinopyroxene: 7, 1mm.

Iron oxide: 2, 1mm.

Vesicles: 35, 0.5mm.

Groundmass (% of volume): Cryptocrystalline (plag/alkali feldspar>magnetite>clinopyroxene>apatite)

Composition of the plagioclase:

Phenocryst (An%): 65

Groundmass (An%): 30

Textural features of individual minerals: Plagioclase is dominantly euhedral with large crystals extensively crack and corroded. Some of the crystals also display reverse zoning. Clinopyroxene is embayed and corroded, with thin reaction rims. Some clinopyroxene crystals are also twinned. Iron oxides are usually corroded and embayed. There is one large magnetite crystal that has an excellent skeletal texture.

Textural features of the rock: Holocrystalline, porphyritic, pilotaxtic, intergranular with sub-trachytic areas. Vesicles are dominantly spherical in smaller sizes and irregular in larger sizes. Chabazite also lines most of the vesicles.

Rock name: *Mugearite Bomb*

MC21

Mineral and Vesicle, Abundance (% of volume), Average size:

Plagioclase: 15, 1.5mm.

Olivine: --

Clinopyroxene: 3, 1mm.

Iron oxide: 2, 1mm.

Vesicles: 25, 0.5mm.

Groundmass (% of volume): Plagioclase 15, Magnetite 5, Glass 35 (devitrified).

Composition of the plagioclase:

Phenocryst (An%): 65

Groundmass (An%): 49

Textural features of individual minerals: Large plagioclase crystals are corroded and embayed with some crystals displaying oscillatory zoning. Some crystals display no zoning while others are only overgrown with thin sodic rims. Clinopyroxene is typically corroded and embayed. Iron oxides are embayed and corroded. Crystals generally appear to be broken.

Textural features of the rock: Hypocrystalline (glass rich 20-50%), vitrophyric, intersertal. Glass infilling some vesicles and in other areas occurs as long stretched out segments. Chabazite is seen in most of the spherical vesicles. Vesicles are also seen to be responsible for causing embayments in some of the crystals. Smectite clays line some of the vesicles.

Rock name: *Distal Lapilli Tuff*

MC22

Mineral and Vesicle, Abundance (% of volume), Average size:

Plagioclase: 10, 1mm.

Olivine: Trace, 0.5mm.

Clinopyroxene: 5, 0.5mm.

Iron oxide: --

Vesicles: 40, 0.5mm

Groundmass (% of volume): Cryptocrystalline (plagioclase/alkali feldspar>magnetite>clinopyroxene)

Composition of the plagioclase:

Phenocryst (An%): 68

Groundmass (An%): 49

Textural features of individual minerals: Plagioclase is corroded and embayed with some crystals displaying oscillatory and reverse zoning. Plagioclase crystals are also seen in places to have iron oxide and clinopyroxene inclusions. Swallow tailed plagioclase can be found in the groundmass. Olivine in the groundmass forms tiny iddingsite pseudomorphs. Clinopyroxene is typically corroded and embayed. Apatite microphenocrysts are rare, with apatite more common in the groundmass.

Textural features of the rock: Holocrystalline, porphyritic, pilotaxtic, intergranular, sub-trachytic areas. Natrolite can be found in some of the vesicles, which are mostly round with a few irregular.

Rock name: *Mugearite Bomb*

FE1

Mineral and Vesicle, Abundance (% of volume), Average size:

Plagioclase: 7, 1.2mm.

Olivine: --

Clinopyroxene: 4, 0.7mm.

Iron oxide: 7, 0.5mm.

Vesicles: 35 (*IT = 32%*), 0.5mm.

Groundmass (% of volume): Cryptocrystalline (plagioclase/alkali feldspar>magnetite>clinopyroxene)

Composition of the plagioclase:

Phenocryst (An%): 72

Groundmass (An%): 42

Textural features of individual minerals: Plagioclase is sieved, but not zoned, with corrosion rare. Swallow tailed plagioclase can be found in the groundmass. Clinopyroxene is commonly twinned with orange reaction rims. Clinopyroxene is also found to be corroded and embayed. Iron oxides are corroded and embayed.

Textural features of the rock: Holocrystalline, porphyritic, pilotaxtic, intergranular, with sub-trachytic areas. Bands of larger spherical vesicles inbetween finer irregular ones. Chabazite can be found in some vesicles.

Rock name: *Spatter Flow (Mugearite)*

DNS1

Mineral and Vesicle, Abundance (% of volume), Average size:

Plagioclase: 10, 2mm.

Olivine: 1, 0.9mm.

Clinopyroxene: 5, 0.5mm.

Iron oxide: 1, 0.8mm.

Vesicles: 35.0.5mm.

Groundmass (% of volume): Cryptocrystalline (plagioclase/alkali feldspar>magnetite>clinopyroxene)

Composition of the plagioclase:

Phenocryst (An%): 65

Groundmass (An%): 48

Textural features of individual minerals: Plagioclase is embayed and corroded (some euhedral), displays no zoning, with rare crystals that are sieved. Olivine is only present as pseudomorphs of iddingsite. Clinopyroxenes are well shaped, with larger crystals embayed and twinned. Iron oxides are corroded and embayed.

Textural features of the rock: Holocrystalline, porphyritic, pilotaxtic, intergranular, with sub-trachytic areas. Bands of larger spherical vesicles inbetween finer irregular ones. Chabazite can be found in some vesicles.

Rock name: *Mugearite Spatter Flow*

DNS3

Mineral and Vesicle, Abundance (% of volume), Average size:

Plagioclase: 10, 2mm

Olivine: Trace, 0.8mm.

Clinopyroxene: 7, 1.5mm.

Iron oxide: 4, 0.8mm.

Vesicles: 25, 0.3mm.

Groundmass (% of volume): Cryptocrystalline (plag/alkali feldspar>magnetite>clinopyroxene>apatite)

Composition of the plagioclase:

Phenocryst (An%): 75

Groundmass (An%): 45

Textural features of individual minerals: Some plagioclase crystals are oscillatory zoned, some are also sieved, with corrosion, and embayments common. Some crystals however are more euhedral and unzoned. Olivine is completely replaced by iddingsite. Clinopyroxene is embayed, corroded, zoned and in some areas ophitic. Iron oxides are embayed and corroded. Large rounded clinopyroxene crystal.

Textural features of the rock: Holocrystalline, porphyritic, pilotaxtic, intergranular. Local areas of mafic and trachytic felsic patches. Biotite and chabazite are seen in the vesicles, which are irregular.

Rock name: *Mugearite Spatter Flow*

Castle Rock

CR2

Mineral and Vesicle, Abundance (% of volume), Average size:

Plagioclase: 2, 1.1mm.

Olivine: 1, 0.9mm.

Clinopyroxene: Trace, 0.8mm.

Iron oxide: --

Vesicles: 40, 0.6mm.

Groundmass (% of volume): Cryptocrystalline (plagio/alkali feldspar>magnetite>clinopyroxene>apatite)

Composition of the plagioclase:

Phenocryst (An%): 67

Groundmass (An%): 44

Textural features of individual minerals: Plagioclase crystals are corroded, embayed and overgrown by more sodic plagioclase. Swallow tails are commonly found in the groundmass. Olivine is altered to a iddingsite and bowlingite, varying in amounts from rims to complete pseudomorphs. Some olivine crystals are also have more opaque areas that appear to be either hematite and/or magnetite. One crystal of clinopyroxene is zoned most are subhedral though and unzoned. Iron oxides are corroded with most subhedral in shape. Apatite needles common.

Textural features of the rock: Holocrystalline, porphyritic, pilotaxtic, intergranular, more felsic areas have a trachytic texture. Vesicles vary in shape and size with larger ones more deformed and smaller ones more spherical. Large ones can be seen in some areas to be stretched parallel to the trachytic texture. Chabazite and natrolite are found in some vesicles.

Rock name: Proximal Deposit (Mugearite)

CR4

Mineral and Vesicle, Abundance (% of volume), Average size:

Plagioclase: 6, 1mm.

Olivine: Trace, 2mm.

Clinopyroxene: 1, 0.9mm.

Iron oxide: Trace, 0.8mm.

Vesicles: 0 (dense flow).

Groundmass (% of volume): Cryptocrystalline (plagioclase/alkali feldspar>magnetite>clinopyroxene)

Composition of the plagioclase:

Phenocryst (An%): 75

Groundmass (An%): 45

Textural features of individual minerals: Plagioclase is corroded and embayed, some crystals are euhedral. None of crystals are zoned, but some have small opaque inclusions. Olivine is corroded with iddingsite pseudomorphs common in the groundmass. Clinopyroxene is corroded, as are iron oxides.

Textural features of the rock: Holocrystalline, porphyritic, intergranular, pilotaxtic, with trachytic textures common in some areas. Some areas have a strong LPO developed. Biotite is rarely found in the groundmass.

Rock name: *Hawaiite Spatter Flow*

CR5

Mineral and Vesicle, Abundance (% of volume), Average size:

Plagioclase: 3, 1mm.

Olivine: --

Clinopyroxene: 1, 0.7mm.

Iron oxide: 2, 0.6mm.

Vesicles: 30, 0.3mm.

Groundmass (% of volume): Cryptocrystalline (plagio/alkali feldspar>magnetite>clinopyroxene>apatite)

Composition of the plagioclase:

Phenocryst (An%): 60

Groundmass (An%): N/A (Alkali Feldspar)

Textural features of individual minerals: Plagioclase sieved, corroded, embayed with some crystals also displaying overgrowths of more sodic plagioclase. One crystal displays oscillatory zoning. Clinopyroxene is corroded with a thin reddy orange alteration rim common. There is also one example of a iron rich crystal. Iron oxides are corroded. Apatite microphenocrysts occur occasionally on the edges of the plagioclase crystals.

Textural features of the rock: Holocrystalline, porphyritic, sub-trachytic. Vesicles are dominantly irregular.

Rock name: *Proximal Deposit (Benmoreite)*

CR8a

Mineral and Vesicle, Abundance (% of volume), Average size:

Plagioclase: 3, 1.2mm.

Olivine: 1, 1mm.

Clinopyroxene: 1, 0.8mm.

Iron oxide: 1, 0.6mm.

Vesicles: 25, 0.8mm.

Groundmass (% of volume): Cryptocrystalline (plagioclase>magnetite>clinopyroxene, apatite trace)

Composition of the plagioclase:

Phenocryst (An%): 65

Groundmass (An%): 48

Textural features of individual minerals: Plagioclase is normally zoned, and also displays corrosion and embayments. Olivine is completely altered (pseudomorphs) to iddingsite and iron oxides. Clinopyroxene is subhedral and commonly has iron oxide inclusions and some display ophitic textures. There is one example of clinopyroxene displaying zoning. Iron oxides are usually corroded.

Textural features of the rock: Holocrystalline, porphyritic, pilotaxtic, intergranular, with sub-trachytic textures occurring nearer the edge of the slide. Vesicles are very irregular, although some of the smaller ones are more spherical.

Rock name: *Proximal Deposit (Hawaiite)*

CR8b

Mineral and Vesicle, Abundance (% of volume), Average size:

Plagioclase: 3, 2.5mm.

Olivine: 1, 0.9mm.

Clinopyroxene: 1, 1mm.

Iron oxide: 1, 0.8mm.

Vesicles: 25, 0.6mm.

Groundmass (% of volume): Cryptocrystalline (plagioclase>magnetite>clinopyroxene, apatite trace)

Composition of the plagioclase:

Phenocryst (An%): 68

Groundmass (An%): 42

Textural features of individual minerals: Plagioclase crystals are corroded, embayed, with some displaying oscillatory zoning. Swallow tails can also be seen in the groundmass. Olivine is completely altered (pseudomorphs) to iddingsite and iron oxides. Clinopyroxene commonly have iron oxide inclusions and some display ophitic textures. There are some examples of clinopyroxene displaying zoning. Iron oxides are usually corroded and embayed.

Textural features of the rock: Holocrystalline, porphyritic, pilotaxtic. Vesicles are very irregular, although some of the smaller ones are more spherical. Chabazite also occurs in some vesicles.

Rock name: *Proximal Deposit (Hawaiite)*

Witch Hill Scenic Reserve

WH1

Mineral and Vesicle, Abundance (% of volume), Average size:

Plagioclase: 5, 1mm.

Olivine: 2, 1mm.

Clinopyroxene: 3, 0.5mm.

Iron oxide --

Vesicles: 35, 0.4mm.

Groundmass (% of volume): Cryptocrystalline (plagioclase>magnetite>clinopyroxene, apatite trace)

Composition of the plagioclase:

Phenocryst (An%): 60

Groundmass (An%): 50

Textural features of individual minerals: Plagioclase phenocrysts show no zoning, with most being corroded and sieved. Plagioclase in the groundmass commonly has swallow tail textures. Olivine is completely altered to iddingsite with only pseudomorphs remaining. Clinopyroxene is corroded and embayed and has a orange reaction rim.

Textural features of the rock: Holocrystalline, porphyritic, pilotaxtic, intergranular. Darker patches have a trachytic texture and are vesicle poor. Vesicles are generally irregular in shape.

Rock name: *Spatter Flow (Hawaiite)*

WH3a

Mineral and Vesicle, Abundance (% of volume), Average size:

Plagioclase: 8, 1.5mm.

Olivine --

Clinopyroxene: 4, 1mm.

Iron oxide --

Vesicles: 33, 0.5mm.

Groundmass (% of volume): Plagioclase 10, Magnetite 3, Clinopyroxene 2, Glass 40 (devitrified).

Composition of the plagioclase:

Phenocryst (An%): 70

Groundmass (An%): 45

Textural features of individual minerals: Plagioclase is heavily cracked with most crystals corroded, embayed and some are also sieved. Plagioclase crystals in the groundmass display swallow tail textures. Clinopyroxene phenocrysts have a orange reaction rim and some display zoning and fresher overgrowths. Iron oxides are corroded and embayed.

Textural features of the rock: Hypocrystalline (glass rich), vitrophyric, intersertal. Shards of glass in the matrix. Some vesicles completely filled with glass (amygdales). Vesicles are dominantly spherical in shape.

Rock name: *Distal Lapilli Tuff*

WH4

Mineral and Vesicle, Abundance (% of volume), Average size:

Plagioclase: 6, 2mm.

Olivine --

Clinopyroxene: 3, 1mm.

Iron oxide: Trace, 1mm.

Vesicles: 40, 1.5mm (core), 0.4mm (rim).

Groundmass (% of volume): Cryptocrystalline (plagioclase>magnetite>clinopyroxene, apatite trace)

Composition of the plagioclase:

Phenocryst (An%): 70

Groundmass (An%): 58

Textural features of individual minerals: Plagioclase is corroded, embayed and with some crystals displaying oscillatory zoning and sieving. Some crystals however are more euhedral and some are unzoned. Clinopyroxene is corroded and altered. Plagioclase in the groundmass displays swallow tail textures.

Textural features of the rock: Holocrystalline, porphyritic, pilotaxtic, intergranular. Vesicles are seen in places to be causing the embayments. Black/reddy blebs, opaque, occur in some vesicles (maybe hematite). Large vesicles are irregular in shape while smaller ones are more spherical.

Rock name: *Hawaiite Bomb*

WH6

Mineral and Vesicle, Abundance (% of volume), Average size:

Plagioclase: 7, 1.5mm.

Olivine 1, 0.9mm.

Clinopyroxene: 3, 1mm.

Iron oxide: 1, 1mm.

Vesicles: 40 (*IT = 37%*), 1mm.

Groundmass (% of volume): Cryptocrystalline (plagioclase>magnetite>clinopyroxene, apatite trace)

Composition of the plagioclase:

Phenocryst (An%): 75

Groundmass (An%): 45

Textural features of individual minerals: Plagioclase phenocrysts are mostly corroded, however some are euhedral. Olivines are altered to iron oxides (hematite and/or magnetite), and are still euhedral in shape. Clinopyroxene has a orange alteration rim and is corroded. Iron oxides are only corroded.

Textural features of the rock: Holocrystalline, porphyritic, pilotaxtic, intergranular, sub-trachytic in places. Glass occurs in some vesicles (amygdales). Vesicles are spherical in smaller sizes and become more irregular in larger sizes.

Rock name: *Hawaiite Bomb*

WH11

Mineral and Vesicle, Abundance (% of volume), Average size:

Plagioclase: 7, 2mm.

Olivine 1, 1mm.

Clinopyroxene: 1, 1mm.

Iron oxide: 1, 1mm.

Vesicles: 40 (*IT = 36%*), 0.9mm.

Groundmass (% of volume): Cryptocrystalline (plagioclase>magnetite>clinopyroxene, apatite trace)

Composition of the plagioclase:

Phenocryst (An%): 75

Groundmass (An%): 45

Textural features of individual minerals: Plagioclase phenocrysts are mostly corroded, embayed and sieved, some however show wavy oscillatory zoning. Swallow tailed texture is common in the groundmass. Olivine is completely replaced by iron oxide products (hematite and/or magnetite) with euhedral pseudomorphs only remaining. Clinopyroxene is corroded with alteration rims. Iron oxides are only corroded.

Textural features of the rock: Holocrystalline, porphyritic, pilotaxtic, intergranular, sub-trachytic in places. Vesicles are dominantly spherical, appearing in bands in places. Large vesicles are more deformed and irregular in shape.

Rock name: *Hawaiite Bomb*

Hoon Hay Park

HH1

Mineral and Vesicle, Abundance (% of volume), Average size:

Plagioclase: Trace, 0.8mm.

Olivine: --

Clinopyroxene: --

Iron oxide: --

Vesicles: 30, 0.6mm.

Groundmass (% of volume): Plagioclase 25, Magnetite 5, Glass 40 (devitrified).

Composition of the plagioclase:

Phenocryst (An%): N/A

Groundmass (An%): 42

Textural features of individual minerals: Plagioclase only occurs as small microlites. Iron oxides form small euhedral to subhedral crystals. There are no other minerals present.

Textural features of the rock: Highly altered, probably hypocrystalline and intersertal but difficult to tell with so much alteration. Plagioclase is not altered though. Chabazite lines vesicles of which they are dominantly spherical in shape.

Rock name: *Distal Lapilli Tuff*

HH2

Mineral and Vesicle, Abundance (% of volume), Average size:

Plagioclase: 15, 1.1mm.

Olivine: 2, 0.7mm.

Clinopyroxene: 2, 0.6mm.

Iron oxide: --

Vesicles: 15, 0.7mm.

Groundmass (% of volume): Cryptocrystalline (plagio/alkali feldspar>magnetite>clinopyroxene>apatite)

Composition of the plagioclase:

Phenocryst (An%): 46

Groundmass (An%): 34

Textural features of individual minerals: Plagioclase is euhedral to subhedral in shape, with minor corrosion. Some crystals display normal and oscillatory zoning. Olivine has been completely replaced by iddingsite with pseudomorphs only remaining. Clinopyroxene, is subhedral in shape and one crystal is twinned. Iron oxides show signs of corrosion but most are euhedral. Round apatite crystals found as small inclusions in plagioclase.

Textural features of the rock: Holocrystalline, porphyritic, pilotaxtic, intergranular. Phenocrysts of dominant euhedral shapes occur in more mafic patches with a sweeping trachytic texture. Natrolite can be seen radiating in some vesicles. Vesicles are dominantly spherical in shape, although irregulars one do rarely occur.

Rock name: *Mugearite Bomb*

HH5

Mineral and Vesicle, Abundance (% of volume), Average size:

Plagioclase: 7, 1.2mm.

Olivine: 1, 0.8mm.

Clinopyroxene: 2, 0.9mm.

Iron oxide: 2, 0.7mm.

Vesicles: 25, 0.4mm.

Groundmass (% of volume): Plagioclase 35, Magnetite 20, Amphibole 3, Orange mineraloid 5.

Composition of the plagioclase:

Phenocryst (An%): 48

Groundmass (An%): 38

Textural features of individual minerals: Plagioclase is corroded and embayed, with some crystals displaying oscillatory zoning. Some crystals are also euhedral and unzoned. Only iddingsite pseudomorphs of olivine remain. Clinopyroxene crystals have iron oxide inclusions, and some also display simple twinning.. Iron oxides are commonly corroded. Amphibole is also occurs in trace amounts.

Textural features of the rock: Holocrystalline, porphyritic, pilotaxtic, sub-trachytic. Signs of mingling, with denser felsic and more vesicular mafic ares. Glomeroporphyritic texture common. Vesicles are irregular in shape.

Rock name: *Proximal Deposit (Mugearite)*

HH9

Mineral and Vesicle, Abundance (% of volume), Average size:

Plagioclase: 6, 1mm.

Olivine: 1, 0.6m.

Clinopyroxene: --

Iron oxide: 2, 0.5mm.

Vesicles: 20, 0.3mm (felsic), 15, 0.4mm (mafic).

Groundmass (% of volume): Cryptocrystalline (plagioclase/alkali feldspar>magnetite>clinopyroxene)

Composition of the plagioclase:

Phenocryst (An%): 45

Groundmass (An%): 37

Textural features of individual minerals: Plagioclase is embayed and corroded with oscillatory zoning present in some phenocrysts. Swallow tails are common in the groundmass. Olivine is totally replaced by iddingsite with only pseudomorphs remaining. Occasionally olivine is also altered to iron oxides. Iron oxides occur as euhedral angular crystals.

Textural features of the rock: Holocrystalline, porphyritic, pilotaxtic, intergranular, with felsic areas displaying a trachytic texture. Vesicles are mostly spherical in felsic areas, with overall larger ones becoming more deformed. Magma mingling evident. Natrolite and chabazite present in some vesicles.

Rock name: *Mugearite Bomb*

HH10

Mineral and Vesicle, Abundance (% of volume), Average size:

Plagioclase: 11, 1mm.

Olivine: --

Clinopyroxene: 1, 0.7mm.

Iron oxide: 1, 0.5mm.

Vesicles: 28, 0.6mm.

Groundmass (% of volume): Cryptocrystalline (plagioclase/alkali feldspar>magnetite>clinopyroxene)

Composition of the plagioclase:

Phenocryst (An%): N/A

Groundmass (An%): N/A

Textural features of individual minerals: Plagioclase margins are sieved, with some crystals displaying oscillatory zoning. Overgrowths of more sodic plagioclase are common and some crystals also appear to have been broken. Clinopyroxene is twinned in some crystals and have orange alteration rims. Clinopyroxene has inclusions of iron oxide and plagioclase (ophitic). Iron oxides are subhedral in shape.

Textural features of the rock: Holocrystalline, porphyritic, pilotaxtic, intergranular. Crystals appear broken. Some occur in glomeroporphyritic clusters. Vesicles are dominantly spherical with only the larger ones being more deformed.

Rock name: *Proximal Deposit (Mugearite)*

HH12

Mineral and Vesicle, Abundance (% of volume), Average size:

Plagioclase: 6, 1mm.

Olivine: --

Clinopyroxene: Trace, 0.5mm.

Iron oxide: 4, 0.6mm.

Vesicles: 25, 0.4mm.

Groundmass (% of volume): Cryptocrystalline (plagioclase/alkali feldspar>magnetite>clinopyroxene)

Composition of the plagioclase:

Phenocryst (An%): 45

Groundmass (An%): 34

Textural features of individual minerals: Plagioclase are slightly deformed and are even broken in places. Some crystals are euhedral while others are sieved. Normal zoning appears commonly. Some clinopyroxene crystals display a iron oxide rim (?). Iron oxides are generally sub-euhedral and there are also examples of corrosion and embayments.

Textural features of the rock: Holocrystalline, porphyritic, pilotaxtic, intergranular. Vesicles are very irregular.

Rock name: *Mugearite Bomb*

HH13

Mineral and Vesicle, Abundance (% of volume), Average size:

Plagioclase: 10, 1.6mm.

Olivine: 2, 1.5mm.

Clinopyroxene: 3, 1.3mm.

Iron oxide: 1, 0.6mm.

Vesicles: 35, 0.6mm.

Groundmass (% of volume): Cryptocrystalline (plagioclase/alkali feldspar>magnetite>clinopyroxene)

Composition of the plagioclase:

Phenocryst (An%): 65

Groundmass (An%): 47

Textural features of individual minerals: Plagioclase is embayed and corroded with lesser amounts of euhedral crystals. Oscillatory is common along with sieving in plagioclase. Olivine is altered to iddingsite with only pseudomorphs remaining. Clinopyroxene is corroded and embayed and some crystals are twinned. Less common is sieving of the clinopyroxene crystal face, and iron oxide inclusions.

Textural features of the rock: Holocrystalline, porphyritic, pilotaxtic, intergranular. This sample is very crystalline. Orange material lining some vesicles is possibly a clay mineral or stained zeolite (low RI). Vesicles are spherical in shape.

Rock name: *Hawaiite Bomb*

HH17a

Mineral and Vesicle, Abundance (% of volume), Average size:

Plagioclase: 10, 1.1mm.

Olivine: 2, 1.1mm.

Clinopyroxene: 6, 1.2mm.

Iron oxide: 1, 0.4mm.

Vesicles: 25, 0.5mm.

Groundmass (% of volume): Cryptocrystalline (Glass (devitrified)>plagioclase>iron oxides)

Composition of the plagioclase:

Phenocryst (An%): 72

Groundmass (An%): 46

Textural features of individual minerals: Plagioclase is sieved, overgrown by sodic plagioclase, with some crystals displaying oscillatory zoning. Some crystals also appear to be broken (?) and many display embayments. Olivine is highly altered with pseudomorphs of iddingsite common, some crystals also appear as if they are sieved. Clinopyroxene crystals are sieved, corroded, overgrown, embayed, and some have reaction rims. Many clinopyroxene crystals also display iron oxide inclusions and ophitic textures. Iron oxides crystals are dominantly euhedral but some are corroded and embayed.

Textural features of the rock: Hypocrystalline (glass-rich), vitrophyric, intersertal. Vesicles are dominantly spherical.

Rock name: *Medial Matrix Tuff*

Northern Gibraltar Rock

GR11a

Mineral and Vesicle, Abundance (% of volume), Average size:

Plagioclase: --

Olivine: --

Clinopyroxene: --

Iron oxide: -- (No phenocrysts)

Vesicles: 45, 0.5mm.

Groundmass (% of volume): Cryptocrystalline (Glass (devitrified)>plagioclase>iron oxides)

Composition of the plagioclase:

Phenocryst (An%): N/A

Groundmass (An%): 46

Textural features of individual minerals: Plagioclase crystals in the groundmass commonly have swallow tailed shapes. Olivine and clinopyroxene are heavily altered and stained by iron. Iron oxides occur as small angular fragments.

Textural features of the rock: Hypocrystalline (glass-rich) which is very altered, intersertal, hyalopilitic. Vesicles are dominantly circular and infilled with unidentified zeolites and smectite clays.

Rock name: *Medial Matrix Tuff*

GR13

Mineral and Vesicle, Abundance (% of volume), Average size:

Plagioclase: Trace, 1.2mm.

Olivine: --

Clinopyroxene: --

Iron oxide: --

Vesicles: 25, 0.3mm.

Groundmass (% of volume): Cryptocrystalline (plag/alkali feldspar>magnetite>clinopyroxene, apatite tr)

Composition of the plagioclase:

Phenocryst (An%): N/A

Groundmass (An%): 40

Textural features of individual minerals: Plagioclase crystals are unzoned and in the groundmass displays swallow tailed forms. Overall this slide is very fine grained

Textural features of the rock: Holocrystalline, pilotaxtic, intergranular, sub trachytic patches. Magma mingling is evident with denser and more vesicular patches mixed together. Glass is found in some of the vesicles along with chabazite. Large vesicles are more deformed with smaller ones being more spherical.

Rock name: *Mugearite Bomb*

GR16

Mineral and Vesicle, Abundance (% of volume), Average size:

Plagioclase: 2, 1.2mm.

Olivine: 1, 0.8mm.

Clinopyroxene: --

Iron oxide: 1, 0.6mm.

Vesicles: 30, 0.3mm.

Groundmass (% of volume): Cryptocrystalline (plagioclase>magnetite>clinopyroxene, apatite trace)

Composition of the plagioclase:

Phenocryst (An%): 68

Groundmass (An%): 49

Textural features of individual minerals: Plagioclase is corroded and embayed, with swallow tail textures common in the groundmass. Olivine is completely replaced by iddingsite and or bowlingite and iron oxides with pseudomorphs only remaining. Iron oxides are euhedral and some have small embayments.

Textural features of the rock: Holocrystalline, porphyritic, pilotaxtic, intergranular, sub-trachytic in places. Magma mingling is evident with areas of felsic mixed with more vesicular mafic areas. Glass infills some vesicles, as does chabazite. Vesicles varying shape with large ones being more deformed and smaller ones being more spherical.

Rock name: *Hawaiite Bomb*

GR20

Mineral and Vesicle, Abundance (% of volume), Average size:

Plagioclase: --

Olivine: --

Clinopyroxene: --

Iron oxide: --

Vesicles: 30, 0.4mm.

Groundmass (% of volume): Cryptocrystalline (plagio/alkali feldspar>magnetite>clinopyroxene, apatite tr)

Composition of the plagioclase:

Phenocryst (An%): N/A

Groundmass (An%): 48

Textural features of individual minerals: Plagioclase crystals are unzoned, while in the groundmass commonly show swallow tail textures.

Textural features of the rock: Holocrystalline, pilotaxtic, strong trachytic textures in areas. Magma mingling with mafic finely vesicular areas and more felsic trachytic crystalline areas. Natrolite is seen to occur in some areas.

Rock name: *Mugearite Bomb*

GR21

Mineral and Vesicle, Abundance (% of volume), Average size:

Plagioclase: 6, 1mm.

Olivine: --

Clinopyroxene: Trace, 1mm.

Iron oxide: 1, 0.6mm.

Vesicles: 15 (*IT = 22%*), 0.2mm.

Groundmass (% of volume): Cryptocrystalline (plagioclase>magnetite>clinopyroxene)

Composition of the plagioclase:

Phenocryst (An%): 73

Groundmass (An%): 43

Textural features of individual minerals: Plagioclase is corroded, embayed, sieved, with some larger crystals having oscillatory zoning. Swallow tailed plagioclase is common in the groundmass. Clinopyroxene is subhedral in shape and has iron oxide inclusions. Iron oxides are sieved and corroded.

Textural features of the rock: Holocrystalline, porphyritic, pilotaxtic, intergranular, with trachytic areas. Magma mingling with mixing between mafic and felsic areas. Vesicles are irregular in shape.

Rock name: *Proximal Deposit (Hawaiite)*

GR22

Mineral and Vesicle, Abundance (% of volume), Average size:

Plagioclase: 12, 1mm.

Olivine: 3, 1mm.

Clinopyroxene: --

Iron oxide: 4, 0.5mm.

Vesicles: 10, 0.mm.

Groundmass (% of volume): Cryptocrystalline (plagioclase>magnetite>clinopyroxene)

Composition of the plagioclase:

Phenocryst (An%): 78

Groundmass (An%): 47

Textural features of individual minerals: Plagioclase is sieved, embayed, corroded with some crystals more euhedral in shape. Some crystals also exhibit oscillatory zoning. Olivine is completely altered being replaced by iddingsite and bowlingite. Iron oxides are embayed.

Textural features of the rock: Holocrystalline, porphyritic, pilotaxtic, intergranular, very altered. Swallow tails in groundmass. Vesicles lined with orange identified mineraloid (possibly a stained zeolite but more likely to be smectite clay).

Rock name: *Vent Deposit (Hawaiite)*

Southern Gibraltar Rock

GR1

Mineral and Vesicle, Abundance (% of volume), Average size:

Plagioclase: 15, 1.9mm.

Olivine: 5, 1.2mm.

Clinopyroxene: 4, 0.9mm.

Iron oxide: 1, 0.8mm.

Vesicles: 20, 0.8mm.

Groundmass (% of volume): Cryptocrystalline (plagioclase>magnetite>olivine>clinopyroxene)

Composition of the plagioclase:

Phenocryst (An%): 82

Groundmass (An%): 55

Textural features of individual minerals: Plagioclase crystals are embayed and corroded, with one large crystal also displaying oscillatory zoning. Olivine is completely replaced by iddingsite and also hematite in places. Clinopyroxenes are twinned, ophitic and sub-ophitic with iron oxide inclusions, and corrosion and embayments common. Iron oxides are typically corroded.

Textural features of the rock: Holocrystalline, pilotaxtic, porphyritic, intergranular. Large vesicles are deformed with smaller ones more spherical. Calcite is found completely infilling some vesicles (amygdales).

Rock name: *Basalt Bomb*

GR3

Mineral and Vesicle, Abundance (% of volume), Average size:

Plagioclase: 15, 1mm.

Olivine: 5, 1mm.

Clinopyroxene: 6, 0.8mm.

Iron oxide: 3, 0.6mm.

Vesicles: 4, 0.2mm.

Groundmass (% of volume): Cryptocrystalline (plagioclase>magnetite>clinopyroxene>olivine)

Composition of the plagioclase:

Phenocryst (An%): 73

Groundmass (An%): 51

Textural features of individual minerals: Plagioclase is corroded, sieved and has some crystals displaying oscillatory zoning. Olivine has been totally replaced by bowlingite and iddingsite. Clinopyroxene crystals are commonly twinned, and corroded with iron oxide inclusions also occurring. Some clinopyroxene crystals also have an ophitic texture. Iron oxides are subhedral to euhedral, showing signs of corrosion.

Textural features of the rock: Holocrystalline, porphyritic, intergranular and has three xenocrysts. Xenocrysts appear as if they are made up of feldspars. The groundmass also displays a sub-trachytic-trachytic texture. Vesicles are infilled with a unidentifiable mixture of clays and zeolites. Very unusual alteration product, appears to affect olivine, it is probably just bowlingite but occurs in great massed and appears almost opaque.

Rock name: *Vent Deposit (Hawaiite)*

GR8

Mineral and Vesicle, Abundance (% of volume), Average size:

Plagioclase: 13, 1.8mm.

Olivine: 4, 1.9mm.

Clinopyroxene: 3, 0.6mm.

Iron oxide: 2, 1.2mm.

Vesicles: 30, 0.6mm.

Groundmass (% of volume): Cryptocrystalline (plagioclase>magnetite>olivine>clinopyroxene)

Composition of the plagioclase:

Phenocryst (An%): 82

Groundmass (An%): 52

Textural features of individual minerals: Plagioclase is corroded, with smaller crystals more euhedral in shape, there is one example of oscillatory zoning. Olivine is totally replaced by iddingsite and/or bowlingite, with some crystals displaying opaque rims. Clinopyroxenes are twinned, some are zoned, with most showing signs of corrosion and orange reaction rims. Iron oxides are corroded and subhedral.

Textural features of the rock: Holocrystalline, porphyritic, pilotaxtic, intergranular. Large vesicles are deformed with smaller vesicles isolated and more spherical.

Rock name: *Basalt Bomb*

Southern Mount Evans

ES2

Mineral and Vesicle, Abundance (% of volume), Average size:

Plagioclase: 6, 1.2mm.

Olivine: Trace, 1.4mm.

Clinopyroxene: Trace, 0.6mm.

Iron oxide: 1, 0.7mm.

Vesicles: 35, 0.6mm.

Groundmass (% of volume): Cryptocrystalline (plag/alkali feldspar>magnetite>olivine>clinopyroxene)

Composition of the plagioclase:

Phenocryst (An%): 67

Groundmass (An%): 45

Textural features of individual minerals: Plagioclase crystals are mostly corroded with a few more euhedral. Some crystals also display oscillatory zoning with most normally zoned. Olivine is completely altered to iron oxides (probably hematite and/or magnetite). Clinopyroxenes are corroded and some are also twinned. Iron oxides are twinned.

Textural features of the rock: Holocrystalline, porphyritic, pilotaxtic, intergranular. Shows signs of magma mingling with very spherical areas of vesicles and more irregular areas. Chabazite also occurs in some vesicles and others are filled with glass.

Rock name: *Mugearite Bomb*

ES5

Mineral and Vesicle, Abundance (% of volume), Average size:

Plagioclase: --

Olivine: --

Clinopyroxene: --

Iron oxide: --

Vesicles: 40, 0.5mm.

Groundmass (% of volume): Cryptocrystalline (plagioclase/alkali feldspar>magnetite>olivine>apatite)

Composition of the plagioclase:

Phenocryst (An%): N/A

Groundmass (An%): 48

Textural features of individual minerals: Very fined grained, no phenocrysts (aphyric). Occasional swallow tailed plagioclase can be seen in the groundmass.

Textural features of the rock: Holocrystalline, with possibly magma mixing of felsic trachytic areas and more mafic non-vesicular areas. At the very edge of the slide is a quartz xenolith. Large vesicles are deformed while smaller vesicles remain more spherical.

Rock name: *Mugearite Bomb*

ES7a+b

Mineral and Vesicle, Abundance (% of volume), Average size:

Plagioclase: 2, 1.5mm.

Olivine: 1, 0.8mm.

Clinopyroxene: 2, 0.7mm.

Iron oxide: 1, 1.1mm.

Vesicles: 40, 0.3mm.

Groundmass (% of volume): Plagioclase 20, Magnetite 12, Glass (devitrified) 22.

Composition of the plagioclase:

Phenocryst (An%): 75

Groundmass (An%): 49

Textural features of individual minerals: One plagioclase crystal has inclusions of iron oxides, augite, and apatite and others also display oscillatory zoning. Some plagioclase crystals also appear as if they are broken. Olivine is totally replaced by iddingsite. Clinopyroxene crystals have rounded edges, some are twinned, some have iron oxides parallel to cleavage, and some have a ophitic texture. Some clinopyroxene crystals are embayed have some have a greenish colouration suggesting iron enrichment. Iron oxides are embayed, and some show evidence that nearby vesicles may have been responsible.

Textural features of the rock: Hypocrystalline, vitrophyric, intersertal, with angular shards representing broken vesicles common. The whole slide appears as if it has been stained by iron discolouration. Vesicles are spherical, and commonly infilled with chabazite.

Rock name: *Medial Matrix Tuff*

ES12

Mineral and Vesicle, Abundance (% of volume), Average size:

Plagioclase: --

Olivine: --

Clinopyroxene: --

Iron oxide: --

Vesicles: 20, 0.4mm.

Groundmass (% of volume): Cryptocrystalline (plagioclase/alkali feldspar>magnetite>olivine>apatite tr)

Composition of the plagioclase:

Phenocryst (An%): N/A

Groundmass (An%): 47

Textural features of individual minerals: Very fine grained, small crystals of plagioclase in the groundmass have swallow tailed texture.

Textural features of the rock: Holocrystalline, porphyritic, very fine grained.

Rock name: *Proximal Deposit (Mugearite)*

ES15a

Mineral and Vesicle, Abundance (% of volume), Average size:

Plagioclase: 1, 1.4mm.

Olivine: Trace, 2mm.

Clinopyroxene: --

Iron oxide: 1, 0.6mm.

Vesicles: 2, 0.4mm.

Groundmass (% of volume): Cryptocrystalline (plagioclase/alkali feldspar>magnetite>olivine>apatite)

Composition of the plagioclase:

Phenocryst (An%): 78

Groundmass (An%): 50

Textural features of individual minerals: Plagioclase crystals are euhedral to subhedral and show no zoning. Swallow tailed plagioclase is common in the groundmass. Olivine is completely replaced by iddingsite. Iron oxides are euhedral to subhedral.

Textural features of the rock: Holocrystalline, porphyritic, intergranular, with fine-grained trachytic texture well developed.

Rock name: *Spatter Flow (Mugearite)*

Northern Mount Evans 1

EN16

Mineral and Vesicle, Abundance (% of volume), Average size:

Plagioclase: 4, 1.4mm.

Olivine: 0.5, 1.7mm.

Clinopyroxene: --

Iron oxide: 1, 1.1mm.

Vesicles: 35, 0.5mm.

Groundmass (% of volume): Plagioclase 16, Magnetite 8, Glass (devitrified) 35.

Composition of the plagioclase:

Phenocryst (An%): 65

Groundmass (An%): 50

Textural features of individual minerals: Plagioclase crystals are broken, corroded, overgrown, and one crystal displays oscillatory zoning. Complete replacement of olivine or clinopyroxene by a fibrous creamy brown mineral. It is most likely to be olivine since it is so susceptible to weathering. Iron oxides are generally corroded.

Textural features of the rock: Hypocrystalline (glass rich), intersertal, vitrophyric, with a sub-trachytic texture developed locally. Glassy groundmass, lots of broken shards, and chabazite dominating in the infilling of vesicles, (amygdales). Vesicles are dominantly spherical in shape.

Rock name: *Medial Matrix Tuff*

EN17

Mineral and Vesicle, Abundance (% of volume), Average size:

Plagioclase: 10, 1.9mm.

Olivine: Trace, 1.1mm.

Clinopyroxene: Trace, 0.6mm.

Iron oxide: 3, 0.3mm.

Vesicles: 20 (*IT = 28%*), 0.4mm.

Groundmass (% of volume): Cryptocrystalline (plagioclase/alkali feldspar>magnetite>olivine>apatite)

Composition of the plagioclase:

Phenocryst (An%): 75

Groundmass (An%): 50

Textural features of individual minerals: Plagioclase crystals are embayed and some display oscillatory zoning. Other crystals are overgrown by more sodic rims, and some small euhedral crystals have no zoning at all. Olivine is totally altered to iddingsite with pseudomorphs only remaining. Clinopyroxene crystals are corroded and some have developed thin reaction rims. Iron oxides are corroded and some appear to have been embayed by vesicles.

Textural features of the rock: Holocrystalline, porphyritic, pilotaxtic, intergranular. Vesicles are irregular in shape.

Rock name: *Spatter Flow (Hawaiite)*

EN18

Mineral and Vesicle, Abundance (% of volume), Average size:

Plagioclase: 10, 1.1mm.

Olivine: 2, 1mm.

Clinopyroxene: 2, 0.5mm.

Iron oxide: 1, 0.5mm.

Vesicles: 20, 0.3mm.

Groundmass (% of volume): Cryptocrystalline (plag>magnetite>olivine>clinopyroxene, apatite trace)

Composition of the plagioclase:

Phenocryst (An%): 75

Groundmass (An%): (Felsic) 40, (Mafic) 50

Textural features of individual minerals: Plagioclase is embayed and some crystals display oscillatory zoning. Swallow tails can also be seen in the matrix. Olivine is totally replaced by iddingsite with fibrous pseudomorphs only remaining. Clinopyroxene is embayed and corroded. Iron oxide crystals are corroded. Small round orthopyroxene crystals can also be seen.

Textural features of the rock: Holocrystalline, porphyritic, pilotaxtic, intergranular. Vesicles are irregular and small. Darker more mafic areas have a better defined trachytic texture suggesting possibly magma mixing.

Rock name: *Vent Deposit (Hawaiite)*

EN19

Mineral and Vesicle, Abundance (% of volume), Average size:

Plagioclase: 10, 1.3mm.

Olivine: 1, 1mm.

Clinopyroxene: Trace, 2.5mm.

Iron oxide: 1, 0.8mm.

Vesicles: 30, 0.5mm.

Groundmass (% of volume): Cryptocrystalline (plag>magnetite>olivine>clinopyroxene, apatite trace)

Composition of the plagioclase:

Phenocryst (An%): 70

Groundmass (An%): 50

Textural features of individual minerals: Plagioclase crystals are corroded and embayed, sieved and have swallow tails in the groundmass. Olivine is altered to hematite and/or magnetite with euhedral crystals remaining Clinopyroxene crystals are corroded as are iron oxide crystals.

Textural features of the rock: Holocrystalline, porphyritic, pilotaxtic, intergranular, with strong trachytic areas in one half of the slide. Vesicles are irregular in larger sizes and more spherical in smaller sizes. Chabazite is commonly seen to infill most vesicles.

Rock name: *Hawaiite Bomb*

EN20

Mineral and Vesicle, Abundance (% of volume), Average size:

Plagioclase: 10, 1.2mm.

Olivine: Trace, 0.8mm.

Clinopyroxene: Trace, 0.7mm.

Iron oxide: Trace, 0.6mm.

Vesicles: 35 (*IT = 49%*), 0.6mm.

Groundmass (% of volume): Cryptocrystalline (plag>magnetite>olivine>clinopyroxene, apatite trace)

Composition of the plagioclase:

Phenocryst (An%): 72

Groundmass (An%): 48

Textural features of individual minerals: Plagioclase is corroded and embayed (some evidence by vesicles), with some crystals showing oscillatory zoning. Groundmass plagioclase commonly shows swallow tailed textures. Olivine is completely replaced by hematite and magnetite and clinopyroxene crystals commonly have a thin red reaction rim. Iron oxides are rare.

Textural features of the rock: Holocrystalline, porphyritic, pilotaxtic, intergranular, local trachytic areas. Vesicles are dominantly spherical, and are commonly infilled with chabazite.

Rock name: *Hawaiite Bomb*

EN25

Mineral and Vesicle, Abundance (% of volume), Average size:

Plagioclase: 6, 1.8mm.

Olivine: Trace, 0.9mm.

Clinopyroxene: 1, 1mm.

Iron oxide: 2, 1.5mm.

Vesicles: 30 (*IT = 26%*), 0.6mm.

Groundmass (% of volume): Plagioclase 30, Magnetite 20, Clinopyroxene 11.

Composition of the plagioclase:

Phenocryst (An%): 75

Groundmass (An%): 49

Textural features of individual minerals: Plagioclase crystals are embayed, overgrown and some display oscillatory zoning. Olivine is replaced by hematite and magnetite. Clinopyroxene crystals commonly have reddy orange reaction rims present.

Textural features of the rock: Holocrystalline, porphyritic, pilotaxtic, intergranular. Vesicles are dominantly irregular in shape. Signs of magma mixing between felsic les vesicular magma and more vesicular mafic magmas.

Rock name: *Proximal Deposit (Hawaiite)*

EN26

Mineral and Vesicle, Abundance (% of volume), Average size:

Plagioclase: 5, 1.5mm.

Olivine: 2, 1mm.

Clinopyroxene: 1, 0.5mm.

Iron oxide: 1, 0.4mm.

Vesicles: 5, 0.1mm.

Groundmass (% of volume): Plagioclase 35, Magnetite 25, Olivine 8, Clinopyroxene 8, Apatite 10.

Composition of the plagioclase:

Phenocryst (An%): 75

Groundmass (An%): 45

Textural features of individual minerals: Plagioclase is commonly corroded and emabyed, however there are examples of more euhedral crystals. Some plagioclase crystals also display oscillatory zoning. Olivine is totally replaced by iddingsite, with pseudomorphs only remaining. Clinopyroxene is embayed and corroded, as are most iron oxide crystals. Some iron oxides also display sieving. Amphibole also occurs in a trace amount.

Textural features of the rock: Holocrystalline, porphyritic, pilotaxtic, intergranular. Biotite is commonly seen infilling some of the vesicles and there is some evidence for magma mingling.

Rock name: *Vent Deposit (Hawaiite)*

EN27

Mineral and Vesicle, Abundance (% of volume), Average size:

Plagioclase: 4, 0.8mm.

Olivine: 2, 1mm.

Clinopyroxene: --

Iron oxide: --

Vesicles: 35, 0.3mm.

Groundmass (% of volume): Plagioclase 15, Magnetite 5, Clinopyroxene 1, Glass 40 (devitrified).

Composition of the plagioclase:

Phenocryst (An%): 66

Groundmass (An%): 43

Textural features of individual minerals: Plagioclase is commonly corroded and embayed, with a few crystals displaying oscillatory zoning. Swallow tails are common in plagioclase in the groundmass. Olivine is totally replaced by iddingsite with pseudomorphs only remaining, some are also corroded.

Textural features of the rock: Hypocrystalline (glass rich), vitrophyric, intersertal, hyalopilitic, with glass also commonly seen to infill some vesicles. Tachylite lapilli fragments are also easily seen that contain small microlites.

Rock name: *Distal Lapilli Tuff*

Northern Mount Evans 2

EN2

Mineral and Vesicle, Abundance (% of volume), Average size:

Plagioclase: 7, 0.9mm.

Olivine: Trace, 0.6mm.

Clinopyroxene: 2, 0.8mm.

Iron oxide: 1, 0.4mm.

Vesicles: 50, 0.1mm, 0.8mm (Bimodal)

Groundmass (% of volume): Cryptocrystalline (plag>magnetite>olivine>clinopyroxene, apatite trace)

Composition of the plagioclase:

Phenocryst (An%): 79

Groundmass (An%): 51

Textural features of individual minerals: Plagioclase is embayed by vesicles and some crystals are corroded while others are euhedral. Swallow tailed plagioclase is common in the groundmass. Plagioclase crystals are unzoned. Olivine is completely altered to iddingsite, with pseudomorphs common. Clinopyroxene is commonly corroded with twinned crystals rare. Iron oxides are corroded. Orthopyroxene occurs as a small rounded crystal.

Textural features of the rock: Holocrystalline, porphyritic, pilotaxtic, intergranular. Mingling evident between high vesicular and low vesicular areas.

Rock name: *Basalt Bomb*

EN5

Mineral and Vesicle, Abundance (% of volume), Average size:

Plagioclase: 15, 1.2mm.

Olivine: 4, 0.8mm.

Clinopyroxene: 6, 1.0mm.

Iron oxide: 2, 0.6mm.

Vesicles: 10, 0.2mm.

Groundmass (% of volume): Cryptocrystalline (plagioclase/alkali feldspar>magnetite>olivine>apatite)

Composition of the plagioclase:

Phenocryst (An%): 72

Groundmass (An%): 48

Textural features of individual minerals: Plagioclase crystals are mostly corroded, although some are a lot more euhedral. One very large plagioclase crystal has oscillatory zoning. Swallow tailed plagioclase is common in the groundmass. Olivine is completely replaced by iddingsite. Clinopyroxene is seen to be embayed by vesicles, and is corroded with rare ophitic textures. Iron oxides are corroded and embayed.

Textural features of the rock: Holocrystalline, porphyritic, pilotaxtic, intergranular. Vesicles are very small and therefore are all spherical.

Rock name: *Shoshonite Bomb*

EN6

Mineral and Vesicle, Abundance (% of volume), Average size:

Plagioclase: 3, 0.4mm.

Olivine: Trace, 0.2mm.

Clinopyroxene: 4, 0.6mm.

Iron oxide: 1, 0.4mm.

Vesicles: 10, 0.2mm.

Groundmass (% of volume): Cryptocrystalline (plagioclase/alkali feldspar>magnetite>olivine>apatite)

Composition of the plagioclase:

Phenocryst (An%): 65

Groundmass (An%): 47

Textural features of individual minerals: Plagioclase is euhedral in shape commonly and normally zoned. Olivine is totally replaced by iddingsite and pseudomorphs only remain. Clinopyroxene is twinned in some examples and has inclusions of magnetite and plagioclase (ophitic) in others. Iron oxides are corroded. Apatite microphenocrysts are also found as round inclusions in plagioclase.

Textural features of the rock: Holocrystalline, porphyritic, pilotaxtic, intergranular. Reddy ares a lot more vesicular than more mafic areas. Glass infilling some vesicles along with chabazite in others. Vesicle are irregular in shape.

Rock name: *Shoshonite Bomb*

EN11

Mineral and Vesicle, Abundance (% of volume), Average size:

Plagioclase: 8, 1mm.

Olivine: Trace, 0.4mm.

Clinopyroxene: 2, 0.9mm.

Iron oxide: 1, 0.6mm.

Vesicles: 25, 0.2mm (tuff), 10, 0.7mm (bomb).

Groundmass (% of volume): Cryptocrystalline (plagioclase/alkali feldspar>magnetite>olivine>apatite)

Composition of the plagioclase:

Phenocryst (An%): 71

Groundmass (An%): 49

Textural features of individual minerals: Plagioclase crystals are corroded and embayed, although some crystals are more euhedral. Some crystals are zoned and swallow tailed textures are common in the groundmass. Olivine is completely replaced by iddingsite. Clinopyroxene crystals are corroded and embayed, some are twinned and most have a thin brown reaction rim. Iron oxides are corroded. Apatite inclusions in plagioclase.

Textural features of the rock: This slide has been cut at the boundary between a bomb and a distal lapilli tuff. The tuff contains tachylite lapilli fragments set in a devitrified groundmass. The bomb is holocrystalline, porphyritic, pilotaxtic, intergranular. Smectite clays are seen to line some vesicles. Large vesicles are deformed, smaller ones are spherical.

Rock name: *Distal Lapilli Tuff/ Latite Bomb*

Northern Mount Evans 3

EN29

Mineral and Vesicle, Abundance (% of volume), Average size:

Plagioclase: 3, 1.5mm.

Olivine: Trace, 0.5mm.

Clinopyroxene: 1, 1mm.

Iron oxide: 1, 0.9mm.

Vesicles: 45, 1.1mm.

Groundmass (% of volume): Cryptocrystalline (plagioclase>magnetite>olivine>clinopyroxene, apatite trace)

Composition of the plagioclase:

Phenocryst (An%): 67

Groundmass (An%): 49

Textural features of individual minerals: Plagioclase is corroded and embayed and some crystals have overgrowths of more sodic plagioclase. Olivine is replaced by hematite and magnetite. Clinopyroxene is commonly corroded, embayed, and has a orange alteration rim. Iron oxides are corroded.

Textural features of the rock: Holocrystalline porphyritic, pilotaxtic, intergranular. Large vesicles are more irregular in shape and smaller ones are more spherical. Vesicles are commonly infilled with chabazite..

Rock name: *Hawaiite Bomb*

EN31

Mineral and Vesicle, Abundance (% of volume), Average size:

Plagioclase: 2, 1.1mm.

Olivine: --

Clinopyroxene: 1, 1mm.

Iron oxide: Trace, 2,mm.

Vesicles: 35, 1mm.

Groundmass (% of volume): Cryptocrystalline (plagioclase>magnetite>olivine>clinopyroxene, apatite trace)

Composition of the plagioclase:

Phenocryst (An%): 68

Groundmass (An%): 43

Textural features of individual minerals: Plagioclase crystals are commonly corroded and embayed, with smaller crystals commonly more euhedral. Plagioclase crystals are not zoned. Clinopyroxene is embayed and corroded along with iron oxides.

Textural features of the rock: Holocrystalline, porphyritic, pilotaxtic, intergranular, with local trachytic areas. Vesicles are dominantly spherical but are more flattened near edge of the slide (rim of the bomb). Chabazite is commonly found infilling some of the vesicles.

Rock name: *Hawaiite Bomb*

EN34

Mineral and Vesicle, Abundance (% of volume), Average size:

Plagioclase: 2, 2mm.

Olivine: --

Clinopyroxene: --

Iron oxide: --

Vesicles: 60, 0.9mm.

Groundmass (% of volume): Cryptocrystalline (plagioclase>magnetite>olivine, apatite trace)

Composition of the plagioclase:

Phenocryst (An%): 70

Groundmass (An%): 48

Textural features of individual minerals: Plagioclase is the only phenocryst phase. One large crystal is seen to have oscillatory zoning, with most crystals being corroded.

Textural features of the rock: Holocrystalline, porphyritic, pilotaxtic, intergranular. Vesicles are irregular in shape when large and more spherical when smaller. Chabazite is commonly seen to infill most of the vesicles.

Rock name: *Hawaiite Bomb*

EN35

Mineral and Vesicle, Abundance (% of volume), Average size:

Plagioclase: 5, 2.7mm.

Olivine: 3, 0.7mm.

Clinopyroxene: 2, 0.8mm.

Iron oxide: 1, 1mm.

Vesicles: 20, 0.6mm.

Groundmass (% of volume): Plagioclase 30, Magnetite 20, Olivine 10, Clinopyroxene 9.

Composition of the plagioclase:

Phenocryst (An%): 52

Groundmass (An%): 45

Textural features of individual minerals: Plagioclase is sieved, embayed and corroded and commonly shows normal zoning. Olivine is sieved, embayed and corroded and commonly has a iddingsite alteration rim, along with complete pseudomorphs. Clinopyroxene is embayed and also has a strong alteration rim. Iron oxides are sieved. There is one plagioclase crystal that displays hourglass/sector zoning.

Textural features of the rock: Holocrystalline, porphyritic, pilotaxtic, intergranular. Note the closeness of the groundmass and phenocryst An%, this is reflected in the slide with most of the phenocrysts sieved extensively. Chabazite commonly infills most of the vesicle. Vesicles are dominantly circular.

Rock name: *Hawaiite Bomb*

APPENDIX 4B: VESICLE PERCENTAGES

Vesicle estimates were initially done visually, and then 9 slides were selected to be stained with a blue dye. Stained slides were then scanned in at 300dpi using a slide scanner, and saved as a bitmap image (jpg format). Slide images were then imported into "Corel Photopaint" and cropped to remove any areas where vesicles had not been stained (eg air bubbles). Images were then exported in a tiff format. The digitised image was analysed with the 'UTHSCSA Image Tool' program[1]. The colour image (Appendix Figure 1) was converted to a grey scale image and manually thresholded to find that grey-scale range corresponding to a certain colour. This threshold was used to obtain a black/white image (Appendix Figure 2) at which a black white pixel count resulted in a percentage of the investigated thin section object (Appendix Table 1). The results are given in Appendix 4D.

[1] Image Tool' was developed at the University of Texas Health Science Centre at Sat Antonio, Texas and is available from the Internet by anonymous FTP fttp://maxrad6.uthscsa.edu.

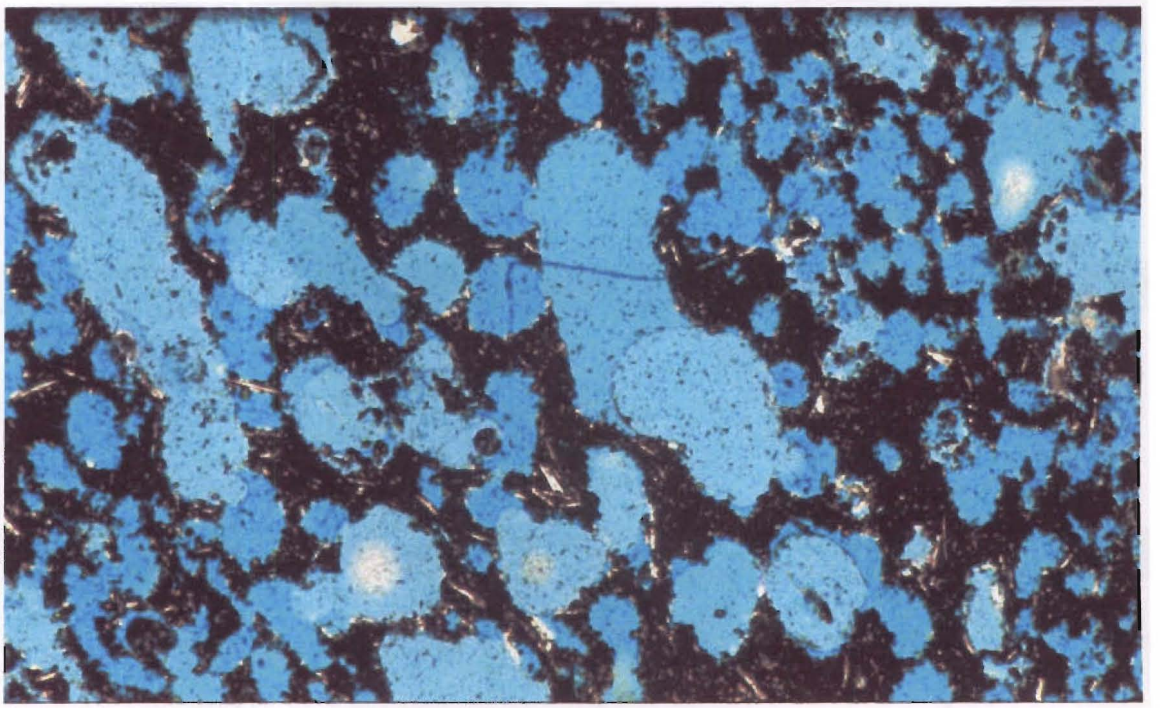

Appendix Figure 1. Slide EN 20, showing vesicles stained blue.

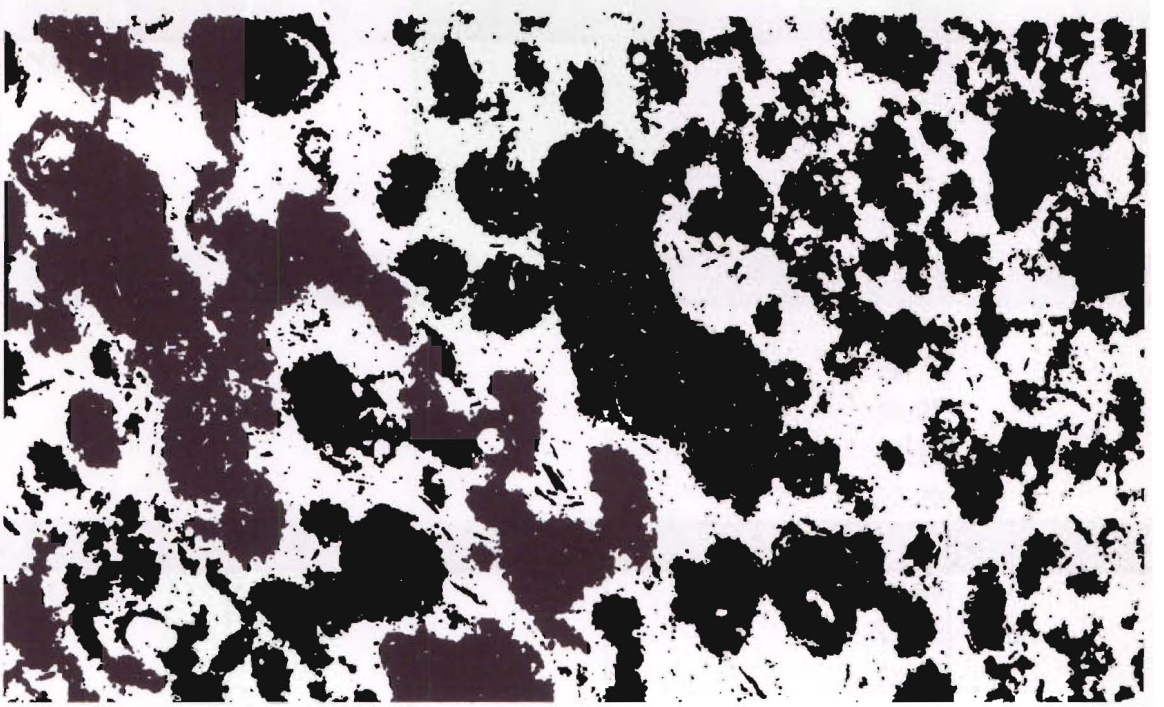

Appendix Figure 2. Black and white pixel image after threshold.

Appendix Table 1. Results of black and white pixel counts from 'Image Tool'.

	Black count	White Count	Black %	White %
Mean	975216.00	950947.00	50.63	49.37

APPENDIX 4C: VESICLE PERCENTAGES

Sample Number	Sample Type	Visual Estimate	Image Analyser Estimates	Difference
EN25			36.93	
			18.85	
			20.58	
			27.67	
			28.64	
	Proximal	30	Average = 26.5	3.5 Over
GR21			23.46	
			20.67	
			22.32	
			19.6	
			26.33	
	Proximal	15	Average = 22.5	7.5 Under
SMC1126			64.11	
			66.7	
			57.2	
			68.66	
			71.05	
	Proximal	60	Average = 65.5	5.5 Under
EN17			29.21	
			26.55	
			25.98	
			29.87	
			30.21	
	Spatter Flow	20	Average = 28.3	8.3 Under
FE1			31.79	
			31.79	
			38.05	
			27.13	
			32.29	
	Spatter Flow	35	Average = 32.2	2.8 Over
WH11			40.89	
			33.73	
			32.12	
			36.47	
			38.9	
	Bomb	40	Average = 36.4	3.6 Over
			41.48	

WH6			37.88 33.13 36.18 35.78	
	Bomb	40	Average = 36.9	3.1 Over
EN20			50.63 55.06 43.67 49.74 47	
	Bomb	35	Average = 49.2	14.2 Under
SMC830			38.35 38.52 32.61 48.52 40.77	
	Bomb	40	Average = 39.8	0.2 Over

APPENDIX 5A: GEOCHEMICAL METHODS

Sample Preparation

112 samples were selected for geochemical analysis from over 150 collected samples from all sites and facies. Each sample was described in the field and allocated a field number. Samples were then cut with a diamond saw into 5-8 cm cubes. All signs of alteration were removed and samples were also cleaned using a diamond lap, to remove any tungsten carbide that may have become embedded in the samples. Each sample was then thoroughly cleaned under running tap water to remove any loose material. Samples where then placed on clean paper and left to dry overnight. Some of the more porous samples had to be placed in an oven at ~108 °C and left overnight. Samples were then crushed in a hydraulic crusher into angular fragments ranging in size from 20-2 mm. The crushed sample was then placed into a tungsten carbide ring mill (Tema Mill) and ground into a powder. The powder was then placed in a clean labelled plastic bag. After each sample was crushed and milled both machines were thoroughly cleaned using convectional methods.

Pressed powder pellets, for trace analysis were made by mixing 11 g of ground rock powder with ~18 drops of 7% Mowiol solution. The mixture for each sample was then hydraulically pressed into 40 mm pellets and allowed to dry overnight. Samples were labelled and placed into sealed individual bags, that were also labelled. All equipment was cleaned thoroughly between each sample.

Fusion beads for major element analysis were produced using a Fusilux fusion bead casting furnace. The furnace was heated to 1030 °C, upon which four platinum crucibles were placed into and agitated for 30 seconds. The crucibles were then removed and allowed to cool to room temperature (about six minutes). All four crucibles were then weighed separately before adding 6.98 g of flux to each crucible and reweighing. Three of the crucibles then had 1.3 g of dried rock powder added to them and were then again reweighed. Three micro-spatulas of ammonium nitrate were then added to three crucibles which had the rock powder in them. Three drops of ammonium iodide solution was then added to each of the rock samples before all samples were placed back into the furnace. The crucibles were then agitated for 15 minutes before being removed and allowed to cool down to room temperature (~ 20 minutes). Samples were then reweighed to calculate loss

on ignition, with all crucibles then placed back into the furnace for a further 10 minutes. After 6 minutes the crucible with only flux was removed and turned on it side to allow the molten flux to chill against the side of the crucible (for easier removal). After 10 minutes each crucible is removed and poured into a mould that has been heating in the furnace for ten minutes. Moulds were then air cooled for 8 minutes, inverted to release each sample, with samples then being placed in labelled self-seal plastic bags. All samples were stored in an airtight container until analysis. Crucibles were cleaned by placing then in an ultrasonic bath for 10 minutes, before being washed in tap water to remove any fragments. Crucibles and moulds were then placed in a beaker of simmering 15% citric acid for 30 minutes. Crucibles and moulds were then removed and washed in tap water again, and thoroughly dried with paper towels. Once this had been done the whole process was repeated for the next batch.

Sample Analysis

Samples were analysed by technician Stephen Brown using a Philips PW2400 X-ray Fluorescence spectrometer. The spectrometer is calibrated using sets of international standards that have been certified. Fusion beads (major elements) and pressed powder pellets (trace elements) were irradiated with a rhodium end window tube operating at 50kV/55mA and 60kV/46mA, respectively. Measurement programs and calibration details were accessed via a computer linked to the spectrometer.

Data Presentation

The data in Appendices 5B & 5C is raw data, with total iron given as Fe_2O_3. Some values are less than values (eg < 3) and this indicates that these quantities are falling below the detection limit of the spectrometer. Major elements were recalculated so that totals added up to 100.00 without loss on ignition before being plotted in Figures 4.1, 4.2, 4.5, 4.6, 4.11. Total iron (eg Fe_2O_3) was also recalculated to FeO and Fe_2O_3 before being plotted on the AFM diagram (Figure 4.3).

APPENDIX 5B: GEOCHEMISTRY

Sample No.	31036	31037	31038	31039	31040	31041	31042	31043	31044	31045	31046	31047
Sample Type	Bomb	Bomb	Bomb	Bomb	Bomb	Bomb	Bomb	Bomb	Dike	Lava	Lava	Lava
Name	Hawaiite	Hawaiite	Hawaiite	Hawaiite	Hawaiite	Hawaiite	Hawaiite	Hawaiite	Hawaiite	Mugearite	Mugearite	Trachyte
Location	SMC	SMC	SMC	SMC	SMC	SMC	SMC	SMC	SMC	SMC	SMC	SMC
SiO2	47.77	49.49	49.72	48.92	50	49.69	48.85	50.07	49.97	51.83	51.71	64.36
TiO2	3.19	2.85	2.8	2.92	2.83	2.8	2.9	2.79	2.99	2.26	2.28	0.94
Al2O3	16.66	15.44	15.43	15.88	15.66	15.6	16.23	15.53	15.56	15.64	15.88	16.53
Fe2O3	14.69	13.53	13.42	14.02	13.47	13.77	14.27	13.53	13.69	12.97	13.15	5.23
MnO	0.24	0.21	0.21	0.2	0.17	0.19	0.19	0.18	0.21	0.15	0.17	0.04
MgO	2.68	3.85	3.88	3.6	3.05	3.59	3.02	3.25	3.11	2.85	2.62	0.57
CaO	7.25	8.13	8.06	7.96	7.79	7.89	6.86	7.6	7.41	6.75	6.46	3.02
Na2O	3.6	3.95	3.92	3.92	4.31	3.9	3.81	4.2	4.41	4.29	4.35	4.3
K2O	1.31	1.51	1.61	1.34	1.61	1.39	1.67	1.72	1.78	2.11	2.14	4.05
P2O5	0.85	0.83	0.83	0.8	0.84	0.78	0.85	0.82	0.86	0.88	0.89	0.25
LOI	1.94	0.22	0.08	0.5	1.31	0.56	1.49	0.33	0.22	0.29	0.4	0.69
Total	100.18	100.02	99.95	100.05	100.03	110.14	100.14	100.01	100.19	100	100.06	99.98
V	119	120	119	122	131	119	114	118	132	79	86	49
Cr	4	24	26	17	39	32	30	28	8	16	40	6
Ni	10	16	18	16	16	19	32	21	9	14	13	4
Zn	145	143	140	143	133	133	134	127	127	145	158	82
Zr	363	325	319	335	320	323	333	322	335	366	377	458
Nb	82	73	72	75	72	72	75	72	74	66	68	42
Ba	426	380	365	423	376	410	382	360	377	1002	743	770
La	55	52	47	58	46	48	42	50	48	59	59	63
Ce	112	88	87	96	99	93	97	93	96	115	112	108
Nd	54	41	32	31	44	44	42	38	51	48	48	49
Ga	26	25	25	26	25	25	25	24	26	26	27	26
Pb	1	4	3	4	3	2	4	2	3	7	5	19
Rb	13	25	28	17	26	16	35	36	36	49	48	155
Sr	547	562	557	569	565	569	511	556	529	495	499	314
Th	4	4	6	3	7	6	5	5	7	8	8	17
Y	48	42	44	44	47	43	39	42	41	48	51	34

31048 Lava Hawaiite	31049 Lava Hawaiite	31050 Lava Trachyte	31051 Bomb Hawaiite	31052 Bomb Hawaiite	31053 Proximal Mugearite	31054 Proximal Hawaiite	31055 Proximal Hawaiite	31056 Distal Basalt	31057 Dike Hawaiite	31524 Vent Hawaiite	31505 Dike Mugearite	31506 Dike Mugearite
SMC	SMC	SMC	SMC	SMC	SMC	SMC	SMC	SMC	SMC	SMC	MC	MC
49.48	50.7	65.25	49.52	49.38	50.67	50.64	50.13	48.15	50.22	50.04	52.9	53.41
2.63	2.78	0.91	2.86	2.78	2.74	2.74	2.85	2.91	2.96	2.75	2.06	2.57
19.08	15.68	16.25	15.33	15.49	15.78	15.48	15.48	14.88	15.24	15.78	16.67	17.73
11.65	12.97	5.05	13.51	13.91	12.76	13.41	13.41	15.15	13.54	13.49	10.07	8.55
0.14	0.16	0.04	0.21	0.21	0.15	0.2	0.21	0.19	0.2	0.19	0.15	0.11
2.3	2.71	0.37	3.86	3.12	2.9	3.5	3.76	4.29	3.26	3.31	3.06	1.75
7.51	7.27	2.85	8.14	7.71	7.51	7.21	7.98	5.23	7.63	7.47	6.64	6.93
4.02	4.67	4.38	3.83	4.3	4.3	4.61	4.51	3.02	4.45	4.61	4.72	4.97
1.42	1.82	4.02	1.57	1.69	1.71	1.73	1.62	1.14	1.73	1.64	2.41	2.04
0.64	0.86	0.24	0.82	0.85	0.78	0.81	0.82	0.61	0.84	0.81	0.66	0.98
1.25	0.39	0.75	0.31	0.58	0.73	-0.1	-0.71	4.62	0.07	0.04	0.69	1.27
100.1	99.98	100.11	99.94	100	100.03	100.22	100.04	100.17	100.13	100.14	100.03	100.29
139	119	47	129	108	103	132	120	100	129	136	79	77
9	27	6	21	28	35	31	22	33	6	31	37	13
13	13	3	17	27	25	24	15	34	10	23	36	13
109	146	87	143	131	135	143	136	143	138	133	102	135
248	344	457	324	332	336	343	318	331	331	325	401	395
55	76	41	73	74	74	76	71	72	74	72	88	87
328	372	766	426	385	348	355	352	253	371	419	636	562
36	48	63	45	49	42	50	44	49	44	44	58	54
79	108	107	99	94	97	97	95	106	102	82	114	113
40	46	61	52	65	63	70	55	59	44	48	45	50
25	25	25	24	24	24	24	24	22	26	24	24	28
2	1	19	1	1	1	1	4	2	5	1	6	3
23	41	153	26	33	36	38	32	24	35	30	51	45
619	543	309	561	552	532	531	542	507	530	549	636	705
3	5	20	5	4	4	5	6	6	4	7	9	9
27	43	38	43	44	44	43	42	45	42	43	38	42

31507 Dike Benmoreite	31508 Dike Mugearite	31510 Dike Mugearite	31511 Bomb Mugearite	31512 Spatter Mugearite	31513 Vent Mugearite	31514 Bomb Mugearite	31515 Dike Hawaiite	31516 Proximal Mugearite	31517 Proximal Mugearite	31518 Spatter Mugearite	31519 Spatter Mugearite
MC	MC	MC	MC	MC	MC	MC	MC	MC	MC	MC	MC
58.12	51.32	53.81	55.05	53.19	51.07	52.14	49.56	50.21	53.24	52.86	54.41
0.78	2.31	2.24	1.86	2.19	2.28	2.13	2.7	2.37	2.19	2.07	2.07
20.07	17.74	15.23	14.83	15.63	17.31	15.97	15.44	17.4	16.25	15.94	15.88
5.47	10.16	12.53	12.86	12.07	12.17	9.93	13.43	12.92	12.33	12.15	11.39
0.09	0.11	0.13	0.18	0.14	0.15	0.21	0.22	0.2	0.17	0.26	0.15
0.94	2.59	1.78	1.47	2.43	2.56	2.08	3.9	1.96	1.88	2.29	1.95
4.02	7.63	6.1	5.36	6.7	6.71	8.59	7.55	6.3	5.55	6.26	5.78
6.09	4.4	4.58	4.38	4.35	4.2	3.79	4.19	3.91	4.4	4.51	4.65
3.11	1.9	2.09	2.17	1.97	1.73	1.79	1.66	2.03	2.3	2.26	2.27
0.31	0.82	0.77	0.65	0.77	0.59	2.02	0.79	0.86	0.83	0.82	0.71
1.44	1.29	1	1.51	0.84	1.63	1.55	1.01	2.25	1.27	0.87	1.12
100.44	100.26	100.24	100.32	100.28	100.4	100.19	100.44	100.41	100.4	100.29	100.36
12	112	73	20	113	133	110	138	105	84	58	88
6	16	3	3	27	17	13	28	17	14	12	11
5	23	3	5	16	26	9	25	28	18	21	10
125	107	145	180	140	125	143	132	149	146	164	144
579	291	414	469	352	351	385	314	363	374	402	394
93	69	75	85	65	63	71	69	67	70	69	72
703	567	576	637	481	469	546	421	579	534	656	574
90	51	47	46	41	48	50	40	53	52	63	43
129	95	109	124	88	97	104	81	99	94	96	94
46	38	49	54	46	48	53	40	56	52	64	46
28	25	26	28	26	28	26	24	27	27	27	26
10	4	5	6	7	6	8	2	6	7	7	9
96	36	43	39	42	19	44	29	53	68	44	63
837	676	459	441	483	482	510	636	474	440	465	453
1	8	7	10	6	10	7	3	8	9	10	8
39	37	52	57	44	47	50	42	51	47	73	44

31520 Bomb Mugearite	31521 Bomb Mugearite	31522 Bomb Mugearite	31523 Bomb Mugearite	31525 Bomb Mugearite	31526 Proximal Mugearite	31527 Lava Mugearite	31528 Spatter Hawaiite	31529 Proximal Benmoreite	31530 Proximal Basalt	31531 Proximal Hawaiite	31532 Bomb Basanite	31533 Bomb Hawaiite
MC	MC	MC	MC	CASTLE	CASTLE	CASTLE	CASTLE	CASTLE	CASTLE	CASTLE	WITCH	WITCH
52.18	51.89	52.42	53.7	50.58	51.92	51.32	50.3	56.5	48.43	49	42.82	49.5
2.31	2.33	2.13	2.12	3.01	2.58	2.57	3.01	1.41	3.02	2.99	2.33	3.15
16.21	16.58	15.66	15.77	15.7	15.03	14.87	15.35	16.22	17.43	16.33	12.69	16.57
12.17	12.41	12.27	11.36	14.19	13.55	13.99	14.04	11.26	13.89	13.77	25.64	13.82
0.23	0.19	0.19	0.17	0.22	0.14	0.32	0.16	0.24	0.2	0.19	0.29	0.17
2.26	2.21	2.31	2.44	2.12	2.09	2.07	3.07	0.98	2.82	3	2.47	2.49
6.94	6.94	6.18	6.71	5.94	6.04	6.22	7.74	3.95	8.35	7.95	6.15	7.18
4.17	4.32	4.38	4.11	4.03	4.28	4.25	3.99	5.25	3.49	3.7	2.75	4.09
1.88	1.92	2.18	1.88	1.91	2.03	2.05	1.56	3.08	1.11	1.48	1.05	1.57
0.79	0.73	0.87	0.77	0.75	1	0.98	0.63	0.53	0.59	0.6	0.6	0.69
1.12	0.78	1.74	1.19	1.84	1.32	1.71	0.51	0.75	1.03	1.4	3.44	1.16
100.26	100.29	100.32	100.22	100.28	99.98	100.34	100.35	100.17	100.37	100.4	100.25	100.39
120	103	71	105	174	107	114	201	13	121	216	261	171
24	22	10	12	3	3	3	5	3	33	22	29	32
22	19	13	7	3	3	3	9	3	39	26	16	21
135	140	146	155	151	159	164	135	148	132	135	133	135
331	333	380	384	355	388	383	301	407	283	290	253	317
62	63	72	72	68	73	70	58	72	54	56	53	66
559	489	583	544	493	538	639	449	1173	398	403	362	420
48	43	42	53	42	49	50	37	62	40	38	28	50
85	89	98	97	80	98	105	70	108	68	75	58	86
50	48	39	47	37	51	52	37	49	45	37	32	47
25	27	26	25	26	26	26	24	28	25	24	21	24
8	7	7	7	5	7	7	6	12	1	6	3	2
48	46	41	48	41	45	52	31	35	13	38	17	29
500	518	449	469	474	464	466	501	381	550	518	427	522
6	7	8	8	5	5	6	5	8	4	3	3	5
51	48	47	50	41	53	52	42	64	44	38	38	66

31534	31535	31536	31537	31538	31539	31540	31541	31542	31543	31544	31545	31546
Bomb	Vent	Dike	Bomb	Bomb	Spatter	Dike	Bomb	Bomb	Bomb	Dike	Bomb	Bomb
B-Andesite	Mugearite	Trachyte	Hawaiite	Mugearite	Benmoreite	Rhyolite	Benmoreite	Mugearite	Basalt	Basalt	Basalt	Basalt
WITCH	WITCH	WITCH	WITCH	HOON	HOON	HOON	HOON	HOON	HOON	HOON	HOON	HOON
52.23	51.3	66.04	48.72	53.98	58.75	70.57	58.76	50.08	48	48.67	47.42	48.63
2.8	2.69	0.98	3.13	2.39	1.33	0.25	1.37	2.15	2.73	2.76	3.19	2.98
16.12	15.51	17.28	16.24	17.04	16.21	14.49	16.24	17.14	15.47	16.04	16.48	16.68
14.04	12.85	2.89	13.75	10.16	9.23	3.78	8.97	12.24	12.8	12.51	13.05	11.78
0.07	0.2	0.01	0.2	0.1	0.08	<0.01	0.1	0.21	0.14	0.16	0.18	0.16
0.92	3.35	0.12	3.09	2.46	0.83	<0.05	0.98	2.6	5.7	4.96	4.43	4.71
6.36	7.6	2.34	7.71	6.68	4.22	0.56	4.46	6.33	9.23	9.55	9.92	10.73
2.58	4.27	5.3	4.07	3.95	5.05	4.97	5.03	4.86	2.68	2.94	3.3	3.06
2.04	1.7	3.81	1.35	2	2.91	4.76	2.85	1.76	0.66	0.8	1.03	0.63
1.25	0.64	0.3	0.7	0.57	0.55	0.05	0.56	1.02	0.41	0.4	0.49	0.39
1.66	0.11	1.19	1.27	0.72	1.26	1.01	1.16	2.02	2.66	1.41	0.85	0.58
100.06	100.21	100.26	100.24	100.04	100.42	100.43	100.48	100.42	100.48	100.19	100.33	100.33
163	165	3	124	202	25	4	24	62	241	254	255	283
3	20	3	31	23	3	3	3	3	126	140	39	148
19	26	3	19	13	3	3	3	5	104	94	32	78
126	128	156	152	97	143	52	153	162	114	114	101	108
382	325	590	313	333	480	558	473	454	156	160	217	170
79	66	73	66	59	77	88	77	83	33	33	47	35
500	438	927	483	478	596	610	570	609	214	224	289	252
49	39	71	39	33	54	83	61	58	15	20	22	15
89	77	137	80	81	112	144	111	117	36	40	48	41
52	40	62	40	46	60	65	48	56	26	26	34	36
26	24	29	26	25	28	28	28	28	21	21	23	22
5	5	20	4	8	12	20	10	6	1	1	4	1
45	39	115	10	51	97	165	91	13	4	9	14	5
525	504	349	538	546	405	86	416	563	482	505	570	549
6	6	16	4	10	11	23	12	10	2	1	2	3
49	43	47	50	32	53	61	48	50	25	29	31	28

31547	31548	31549	31550	31551	31552	31553	31554	31555	31556	31557	31558	31559
Bomb	Vent	Dike	Dike	Vent	Bomb	Bomb	Vent	Spatter	Proximal	Vent	Bomb	Dike
Basalt	Mugearite	Basalt	Mugearite	Basalt	Mugearite	Mugearite	Benmoreite	Trachyte	Mugearite	Hawaiite	Benmoreite	Hawaiite
STHGIB	STHGIB	STHGIB	STHGIB	STHGIB	NTHGIB	NTHGIB	NTHGIB	NTHGIB	NTHGIB	NTHGIB	NTHGIB	NTHGIB
47.34	51.46	48.13	51.39	48	53.33	51.95	54.48	67.21	50.35	49.45	55.37	48.34
3.41	2.77	2.57	3.29	3.57	2	1.96	1.76	0.69	2.77	2.74	1.78	2.92
17.14	15.71	16.96	16.11	16.25	17.16	18.2	17.48	15.48	16.96	16.92	17.95	17.26
13.07	12.88	11.98	10.65	13.01	10.1	12.58	10.74	4.63	11.41	12.61	9.42	12.97
0.46	0.14	0.32	0.19	0.21	0.17	0.25	0.15	0.06	0.13	0.17	0.07	0.17
2.33	3.36	4.97	2.64	3.65	1.85	1.11	1.27	0.26	2.46	3.03	0.82	3.39
9.02	7.23	9.35	8.17	9.48	6.53	4.25	4.58	2.34	7.91	7.67	4.37	7.25
3.34	4.02	3.13	4.35	3.42	4.5	4.42	5.3	4.88	4.41	4.01	4.74	3.51
1.09	1.65	0.84	1.84	1.27	2.15	2.58	2.64	3.69	1.68	1.58	2.62	1.58
0.46	0.57	0.45	0.82	0.52	0.89	0.83	0.73	0.13	0.8	0.7	0.7	0.62
2.53	0.5	1.66	0.9	1.01	1.7	1.63	1	0.72	1.06	1.18	2.43	2.37
100.2	100.27	100.36	100.35	100.39	100.37	99.77	100.12	100.1	99.94	100.06	100.27	100.38
317	220	197	193	295	86	48	56	3	162	175	47	177
130	3	96	3	46	3	3	3	3	8	14	3	37
308	11	122	26	49	3	6	3	3	32	29	3	39
154	130	94	151	114	156	135	139	138	142	130	111	115
194	280	168	356	236	424	469	451	645	326	296	455	272
39	51	34	74	50	77	84	79	83	67	62	84	57
735	443	229	513	417	619	648	583	768	504	473	817	380
24	32	26	52	28	56	47	53	51	50	41	67	34
44	75	47	92	61	124	128	117	94	83	72	126	67
32	38	32	50	34	44	43	38	38	51	46	58	46
22	24	22	26	22	26	28	27	29	25	24	29	24
3	3	1	2	1	3	5	5	21	1	1	3	1
18	26	10	41	29	56	66	68	86	31	27	62	37
618	554	553	587	639	574	450	510	234	619	606	521	510
5	8	3	5	3	9	10	10	17	4	4	8	3
29	37	29	54	33	49	43	40	42	57	44	43	32

31560 Bomb Basalt	31561 Bomb Mugearite	31562 Bomb Mugearite	31563 Spatter Basalt	31564 Dike Benmoreite	31565 Dike Hawaiite	31566 Dike Hawaiite	31567 Dike Hawaiite	31568 Spatter Mugearite	31569 Dike Hawaiite	31570 Bomb B-Andesite	31571 Bomb Hawaiite	31572 Bomb Shoshonite
STHEVN	STHEVN	STHEVN	STHEVN	STHEVN	STHEVN	STHEVN	STHEVN	STHEVN	NTHEV2	NTHEV2	NTHEV2	NTHEV2
48.55	52.33	52.72	49.09	54.58	49.14	48.87	49.3	51.57	46.74	52.05	49.89	52.91
2.58	2.28	2.27	2.56	1.26	3.37	3.15	2.94	2.62	2.43	2.31	2.21	2.12
17.73	14.46	14.31	18.39	16.68	16.07	16.23	17.37	14.42	14.01	16.33	18.61	16.6
12.59	14.35	14.39	11.94	11.63	13.23	12.75	11.49	14.55	13.21	11.59	11.03	11.07
0.16	0.24	0.17	0.16	0.21	0.14	0.17	0.21	0.19	0.18	0.15	0.17	0.15
3	1.88	2.25	2.7	1.79	3.06	3.57	3.3	3.05	8.24	3.57	3.39	3.11
9.29	6.05	6.15	8.47	4.45	8.14	8.88	9.22	6.84	8.72	7.76	8.81	7.18
3.73	4.01	4.06	3.47	5.43	3.82	3.74	3.74	4.07	3.96	3.24	3.81	3.59
0.89	1.99	1.86	1.24	2.76	1.41	1.26	1.27	1.63	1.77	1.52	1.11	1.78
0.7	1.04	0.9	0.57	0.66	0.66	0.58	0.58	0.85	0.61	0.64	0.65	0.56
1.43	1.52	0.84	1.75	1.01	1.41	1.12	0.82	0.4	0.55	1.15	0.68	1.28
100.35	100.14	99.94	100.34	100.45	100.44	100.32	100.23	100.19	100.41	100.3	100.35	100.35
152	99	103	171	3	230	217	184	154	206	178	147	155
79	4	3	8	3	15	22	34	11	232	43	29	20
92	6	4	14	3	18	21	32	11	210	38	33	24
125	171	165	115	135	132	123	111	172	137	115	122	122
256	334	328	226	466	281	241	244	300	342	282	255	332
58	62	61	45	95	63	52	54	59	80	50	47	56
493	442	416	418	689	360	329	387	404	554	688	467	494
36	44	33	27	58	29	22	32	36	43	32	35	37
70	85	90	72	131	77	78	65	87	99	72	74	85
58	43	45	38	53	34	44	43	45	48	39	34	37
26	26	26	25	26	25	25	24	25	22	26	25	24
1	4	3	2	7	2	2	1	3	1	2	3	7
2	43	42	14	70	29	47	31	34	36	23	13	36
662	472	454	747	513	567	560	643	474	766	522	644	498
3	6	7	2	8	3	4	2	3	6	5	5	5
35	50	49	38	50	39	38	37	48	27	38	35	38

31573 Proximal Shoshonite	31574 Lava Hawaiite	31575 Lava Hawaiite	31576 Bomb Latite	31577 Dike Hawaiite	31578 Dike Benmorite	31579 Spatter Hawaiite	31580 Vent Hawaiite	31581 Proximal Hawaiite	31582 Bomb Hawaiite	31583 Spatter Hawaiite	31584 Bomb Hawaiite	31585 Dike Trachyte
NTHEV2	NTHEV2	NTHEV2	NTHEV2	NTHEV2	NTHEV2	NTHEV1	NTHEV1	NTHEV1	NTHEV1	NTHEV1	NTHEV1	NTHEV1
54.19	49.03	49.5	57.28	50.25	57.7	47.84	49.91	47.95	48.69	50.03	49.89	61.17
2.03	2.4	2.36	1.28	2.18	1.21	3.16	2.97	3.25	3.06	2.98	3.16	0.48
16.11	18.23	18.5	15.62	19.69	17.1	16.5	16.45	16.92	16.6	16.39	16.29	18.38
12.15	10.86	10.85	10.24	9.64	9.38	13.42	12.9	13.78	13.29	12.57	13.33	5.44
0.15	0.15	0.18	0.16	0.14	0.14	0.2	0.17	0.18	0.18	0.18	0.16	0.15
1.72	4.01	3.71	1.19	2.88	1.01	3.47	3.07	2.92	3.02	2.95	2.85	0.48
4.94	9.03	8.93	4.72	9.24	3.43	8.61	7.64	7.55	8.36	7.58	7.63	1.18
4.32	4.02	4.13	4.62	4.2	6.13	4.31	4.23	3.89	4.28	4.19	4.18	6.17
2.6	1.23	1.29	2.9	1.34	3.14	1.26	1.52	1.37	1.51	1.45	1.5	4.87
0.74	0.73	0.73	0.43	0.64	0.35	0.7	0.63	0.72	0.69	0.6	0.64	0.11
1.39	0.36	-0.06	1.39	0.22	0.65	0.66	0.71	1.42	0.31	1.15	0.87	1.94
100.35	100.04	100.16	99.82	100.42	100.24	100.13	100.18	99.95	99.99	100.07	100.5	100.38
56	141	123	19	102	3	103	201	186	145	166	219	3
3	33	29	4	15	3	21	17	19	28	15	16	3
3	31	32	3	15	3	23	31	18	19	22	13	3
147	104	96	165	99	132	140	138	132	124	149	138	132
394	219	222	553	242	572	290	283	291	288	282	287	821
64	52	51	97	57	120	62	63	66	64	62	63	176
644	361	409	765	358	677	436	397	432	387	389	512	963
42	36	45	60	33	73	55	42	41	37	33	35	81
99	69	74	128	70	135	93	67	69	75	85	79	150
43	38	44	53	44	57	62	44	52	39	43	47	54
27	24	25	28	24	31	25	24	25	24	23	23	30
8	1	1	7	1	6	1	2	1	2	3	1	14
65	15	27	72	20	75	7	23	16	21	25	35	97
441	890	836	397	857	444	584	576	555	584	578	570	55
9	3	4	10	2	11	2	3	4	2	4	4	18
36	30	36	56	32	49	53	36	40	38	36	38	45

31586 Proximal Hawaiite	31587 Vent Hawaiite	31588 Bomb Basalt	31589 Dike Basalt	31590 Bomb Hawaiite	31591 Dike Mugearite	31592 Dike Hawaiite	31593 Bomb Hawaiite	31594 Vent Mugearite	31595 Dike Mugearite
NTHEV1	NTHEV1	NTHEV3	NTHEV3	NTHEV3	NTHEV3	NTHEV3	NTHEV3	NTHEV3	NTHEV3
47.59	49.75	48.89	46.57	49.4	50.13	47.67	46.87	52.01	50.66
3.22	3.04	2.72	2.78	2.88	3.1	2.92	2.87	2.33	2.5
16.66	16.01	15.99	15.93	16.94	16.55	17.22	15.45	15.69	16.75
14.03	12.59	12.76	13.91	13.58	11.94	13.79	14.33	12.73	11.89
0.2	0.16	0.19	0.17	0.15	0.2	0.22	0.17	0.22	0.16
3.32	3.46	3.08	6.59	2.06	2.28	2.34	5.74	2.64	3.77
8.22	8.23	7.84	8.66	6.7	7.6	6.89	7.95	6.56	7.43
4.27	4.19	3.96	3.26	3.87	4.48	4.21	3.22	5.06	4.3
1.17	1.48	1.69	0.95	1.75	1.71	1.95	1.15	2.08	1.71
0.67	0.65	0.91	0.8	0.9	1.16	0.91	0.84	0.99	0.6
0.46	0.38	2.39	0.77	1.79	1.28	1.96	1.78	0	0.7
99.8	99.93	100.41	100.39	100.02	100.42	100.07	100.36	100.31	100.46
109	213	130	187	125	144	102	182	69	132
19	20	28	75	19	3	22	71	3	29
29	19	26	98	24	8	25	78	3	42
139	128	99	102	146	147	130	177	152	103
294	275	322	145	349	332	355	181	393	341
65	61	72	39	76	75	78	46	85	69
390	340	400	400	795	478	538	986	544	438
25	26	38	23	49	49	37	29	49	44
85	72	83	54	94	118	105	62	109	82
52	44	51	37	48	46	44	41	48	48
26	24	23	18	26	25	26	19	26	27
1	2	2	1	2	2	1	1	3	2
7	27	30	12	31	36	32	13	53	31
582	548	601	864	598	601	580	838	529	539
3	3	3	1	3	5	6	1	5	4
39	37	42	26	51	42	42	35	53	39

APPENDIX 5C: PREVIOUS WORKERS GEOCHEMISTRY

Author	Slaughter (1995)	Hibberd (1994)	Hibberd (1994)	Mckenzie (1995)	Mckenzie (1995)	Mckenzie (1995)
Sample No.	26976A	26319A	26321A	27043A	27037A	27039A
Sample Type	Dike	Feeder Dike (?)	Bomb	Dike	Dike	Spatter
Name	Trachyte	Mugearite	Mugearite	Hawaiite	Hawaiite	Mugearite
Location	NthEvan1	NthGibRock	NthGibRock	SthEvan	SthEvan	SthEvan
SiO2	63.06	54.53	53.61	46.5	51.03	51.7
TiO2	0.39	1.77	1.94	2.64	2.75	2.68
Al2O3	17.28	16.64	16.61	14.56	14.26	14.46
Fe2O3	5.33	10.59	10.98	13.99	14.44	14.66
MnO	0.12	0.17	0.19	0.17	0.22	0.19
MgO	0.3	2.55	2.35	6.89	3.48	3
CaO	1.07	5.74	6.35	7.99	7.21	6.87
Na2O	7.26	5.17	4.5	4.15	4.11	4.08
K2O	4.72	2.42	2.23	1.5	1.02	1.63
P2O5	0.07	0.77	0.81	0.69	0.82	0.86
LOI	0.73	0.31	0.52	-0.4	-0.04	0.2
Total	100.33	100.66	100.09	99.04	99.91	100.33
V	4	No Traces Done		123	112	110
Cr	3			133	31	18
Ni	11			130	20	22
Zn	141			125	140	155
Zr	1328			321	263	271
Nb	293			70	56	58
Ba	660			385	361	376
La	88			56	47	48
Ce	136			117	88	105
Nd	59			42	50	50
Ga	27			33	25	26
Pb	15			5	8	2
Rb	131			34	42	41
Sr	75			795	465	468
Th	24			8	2	11
Y	38			21	40	38